DISSERTATION

# IMPACT OF IRON AND REDOX CHEMISTRY ON THE ENVIRONMENTAL FATE OF METALLOIDS AND RADIONUCLIDES

Submitted by

Lyndsay D. Troyer

Department of Chemistry

In partial fulfillment of the requirements

For the Degree of Doctor of Philosophy

Colorado State University

Fort Collins, Colorado

Spring 2014

Doctoral Committee:

Adviser: Thomas Borch

Branka M. Ladanyi
Nancy E. Levinger
Charles S. Henry
Eugene F. Kelly

ABSTRACT

IMPACT OF IRON AND REDOX CHEMISTRY ON THE ENVIRONMENTAL FATE OF METALLOIDS AND RADIONUCLIDES

Millions of cubic meters of uranium (U) mine tailings worldwide and millions of gallons of contaminated groundwater are the result of U mining and milling activity. Arsenic can occur at up to 10 weight percent in U ore, so both U and As can be released during U mining. Although these elements commonly occur together, little research into their redox behavior when present in the same environmental system has been performed. The goal of this research is to gain an improved understanding of how redox chemistry affects U and As speciation and complexation when the two elements are present together as co-contaminants.

The North Cave Hills in Harding County, South Dakota is an abandoned U mine where overburden has been left open to weathering and transport since mining began in 1955. The exposed overburden has resulted in above-background level concentrations of U and As in sediments and groundwater in the surrounding wetlands. We conducted a field-scale study to investigate U and As redox chemistry at the North Cave Hills by taking sediment samples from the tailings pile and the down gradient watershed in order to assess U and As fate and transport. As sediments pass through anoxic zones at the field site, U is immobilized as reduction takes place but As can simultaneously be released into surface waters as reductive dissolution of Fe minerals also occurs.

A laboratory-based study was conducted in order to examine the redox chemistry of U and As in North Cave Hills sediments under controlled conditions. Upon microbial reduction of sulfate and formation of mackinawite in batch systems, U(VI) and As(V) were reduced to nano-

$UO_2$ and a reduced As-sulfide mineral phase respectively during biostimulation by three different electron donors. When these systems were exposed to air for 24 hours, mackinawite protected U and As from oxidation and little change in their solid-phase speciation was observed. While mackinawite was shown to play a role in reduction, we could not determine if direct microbial reduction of U and As was also taking place in the systems.

In order to further explore the reduction of U(VI) and As(V) by mackinawite, an experiment was set up to determine if As(V) prevented U(VI) reduction, especially following the formation of uranyl arsenate precipitates. As(V) only had an impact on the extent of U reduction at concentrations higher than would occur in most environmental systems. When As(V) concentrations were high, U(VI) was shown to be resistant to reduction because of the precipitation of a uranyl arsenate mineral phase.

The findings in this dissertation contribute important information that will improve our current understanding of U and As redox behavior that will lead to improved remediation strategies to effectively prevent the mobilization of both elements in environmental systems.

ACKNOWLEDGEMENTS

Firstly, I would like to thank my adviser Dr. Thomas Borch who has provided invaluable guidance through the Ph.D. process. Without his advice, support, and friendship, my journey to this publication would not have been possible. I have grown in ways I could not have anticipated thanks to his mentoring and the many opportunities he has provided. I would especially like to thank Dr. Borch for his uninhibited passion for and love of science that has been a constant source of motivation and inspiration.

I would like to also thank Dr. James J. Stone who has been a close collaborator throughout my doctoral work and who helped with my understanding of the North Cave Hills field site and with field sampling. Special thanks goes to Dr. Juan S. Lezama-Pacheco for his mentoring in data fitting. His lessons and continual willingness to help during X-ray experiments have vastly improved my ability to collect and analyze X-ray absorbance spectroscopy (XAS) data. Additional collaborators I would like to thank include Dr. Yuanzhi Tang, Dr. John R. Bargar and Dr. Matthew Ginder-Vogel for their help with XAS data analysis.

I have met many fellow researchers and students throughout this processes that I consider both friends and colleagues. I would primarily like to thank Dr. Joshua J. Stratton for the daily help and advice. I would like to thank the other members of my graduate school support team—Dr. Leon van Eck, Dr. Jeffrey C. Shearer, and Nicole C. Escudé. I would also like to acknowledge Lance N. Larson, Dr. Rong Wei, and Dr. Michael S. Massey for their assistance with sample collection and for engaging conversation. All of the members of the Borch research group have offered me their help throughout my Ph.D. years. Several group members contributed directly to my work by offering advice and helping with laboratory work including Dr. Masayuki Shimizu, Andria J. Marsh, and Dr. Amrita Bhattacharyya. I would also like to thank Damaris L.

Roosendaal for her four years of assistance in the Borch research group and for always cheering me up.

I would like to acknowledge my committee members Dr. Eugene F. Kelly, Dr. Nancy E. Levinger, Dr. Charles S. Henry, and Dr. Branka M. Ladanyi for their feedback. I would like to recognize the financial assistance that made this work possible. My work was primarily supported by the US Environmental Protection Agency – Region 8 and the US Department of Agriculture/Forest Service – Northern Region. My work was also funded, in part, by a National Science Foundation CAREER Award to Dr. Thomas Borch (EAR0847683). In addition to the time spent carrying out research at the North Cave Hills, South Dakota and in the laboratory at Colorado State University, research was carried out at two synchrotron facilities, the Stanford Synchrotron Radiation Lightsource, a Directorate of SLAC National Accelerator Laboratory and an Office of Science User Facility operated for the U.S. Department of Energy Office of Science by Stanford University and at GeoSoilEnviroCARS at the Advanced Photon Source of the Argonne National Laboratory, which is supported by the National Science Federation, US DOE, and the state of Illinois. I would like to thank the beamline scientists at these facilities for their help including Joseph Rogers, Dr. Matthew Newville and Dr. Antonio Lanzirotti.

To my parents, Adonis H. Troyer and Carol L. Troyer, I would like thank you for always pushing me to the best of my abilities and for your love and encouragement. Last, but not least, I would like to thank my partner Eric R. Scott. Thank you for encouraging me to think scientifically, keeping me fed, making me laugh, and for supporting me unconditionally.

TABLE OF CONTENTS

LIST OF TABLES

LIST OF FIGURES

# CHAPTER 1

# INTRODUCTION

## Uranium Uses

Uranium is a radioactive, carcinogenic element and is the most abundant actinide. On average, U is present in the Earth's crust at a concentration of 2.7 mg/kg and in the oceans at a concentration of 3.3 μg/L. (*1*, *2*) The main use of U in the world is as a fuel source in nuclear reactors.

There are many steps in the process of making and using fuel for nuclear reactors. While radioactive waste is produced in each of these steps, the greatest volume of waste is present as U mine and mill tailings. Uranium mining has generated 938 million cubic meters of tailings worldwide and 10,000,000 gallons of contaminated freshwater. (*3*, *4*) Uranium can be mined by three different methods including open pit mining, underground mining, and in situ recovery or in situ leaching. During the Cold War era, the United States focused on the production of nuclear weapons and power plants and there was a boom in open-pit mining. Mining left surface-exposed U ore and tailings and released U to the environment at greater rates than those typically found in nature. (*5*) Most mining sites were not reclaimed, leaving many open to continued erosion and leaching resulting in the release of heavy metals to the environment.

Uranium is most commonly found in the environment in the +4 and +6 oxidation states referred to as uranous U(IV) and uranyl U(VI) oxidation states. Of the two oxidation states, U(IV) is the primary state found in U ore. The most common U ore mineral is uraninite ($UO_2$), followed by pitchblende (amorphous $UO_2$) and coffinite ($USiO_4$). While most of the U mining during the Cold War was open-pit mining, the majority of U mining in the United States is now

done by in situ leaching. (*6*) With in situ leaching, solutions are pumped into the ground, often containing carbonate and synthetic oxidants, in order to dissolve and oxidize U and then brought to the surface for processing. (*3*) This method avoids the surface disturbance of open pit mining and produces a smaller volume of tailings.

Due to its radioactivity and carcinogenicity, the U.S. EPA has defined a Maximum Contaminant Level (MCL) of 30 μg U/L, or 0.126 μM. The transport of U largely depends on its oxidation state and complexation with natural ligands. In order to stay below these levels and prevent further U mobilization, continuing U research aims improve our understanding of U redox and complexation chemistry.

**Uranium chemistry in the environment**

While the most common U oxidation states found in natural aqueous environments are +4 and +6, U can exist in four different oxidation states—+3, +4, +5, and +6. In aqueous environments, U(III) is oxidized by water to U(IV) and, because of its transient nature, U(V) easily disproportionates to become U(VI) or U(IV). The standard oxidation potential for the following half reaction

$$U^{4+} + H_2O \rightarrow UO_2^{2+} + 4H^+ + 2e^-$$

is $E_H° = 0.273 \pm 0.005$ V, indicating that U(VI) is the more stable of the two dominant oxidation states. (*7*) Because the $UO_2^{2+}$ complex is highly soluble, this species along with its complexed forms is most commonly found in surface waters. In a system free of dissolved carbonate, the dominant forms of U are $UO_2^{2+}$ at pH less than 5.5, $UO_2OH^+$ at pH=5.5-7, and $UO_2(OH)_2^0$ at pH greater than 7. Most environmental systems contain dissolved carbonate so U carbonate complexes will be predominant rather than U hydroxyl complexes in naturally occurring systems. At pH less than 6, $UO_2^{2+}$ remains to be dominant in solution, but at higher pH

values, $UO_2CO_3$, $UO_2(CO_3)_2^{2-}$, and $UO_2(CO_3)_3^{4-}$ are the dominant U(VI) species. When U carbonate complexes are present, U(VI) solubility is increased from carbonate-free systems. At pH values greater than 5, the boundary between the formation of solid $UO_2$ and aqueous forms of U(VI) occurs at a lower $E_H$ in a system including dissolved carbonate than a system without. The presence of carbonate can also limit U(VI) adsorption to mineral surfaces at pH above 5. (*1*)

The presence of calcite ($CaCO_3$) in natural environments can also affect U mobility. When both calcium and carbonate are present in a system, the two dominant aqueous species are $Ca_2UO_2(CO_3)_3^0$ at pH less than 8.5 and $UO_3(CO_3)_3^{4-}$ at pH greater than 8.5. (*8*) A calcite saturated system exhibits low U(VI) adsorption onto natural sediments in comparison to a $Ca^{2+}$ free system at pH less than 8.5 due to the presence of the $Ca_2UO_2(CO_3)_3^0$ complex. (*9*) At pH greater than 8.5, $Ca_2UO_2(CO_3)_3^0$ is no longer the dominant U species, so solubility of U does not differ from a $Ca^{2+}$ free system.

Iron is the fourth most abundant element in the earth's crust and is responsible for controlling the fate and transport of environmental contaminants including metalloids and radionuclides. (*10*) Depending upon the pH of a system, a high percentage of dissolved U can be immobilized through adsorption onto Fe oxy(hydr)oxides. At pH greater than 5, a significant percentage of U was adsorbed to the surface of Fe oxy(hydr)oxides. (*11*) In a system free of carbonate, the major surface site reactions taking place are

$$\equiv FeOH + UO_2^{2+} + H_2O \rightarrow \equiv FeO^-—UO_2OH^+ + 2H^+$$

$$\equiv FeOH + 3UO_2^{2+} + 5H_2O \rightarrow \equiv FeO^-—(UO_2)_3(OH)_5^+ + 6H^+$$

where $UO_2OH^+$ and $(UO_2)_3(OH)_5^+$ are the dominant aqueous forms of U(VI). (*11*) Inner-sphere, bidentate surface complexes that are stable at pH >5 could also be formed by the following reaction:

$2(\equiv FeOH) + 3UO_2^{2+} + 5H_2O \rightarrow 2(\equiv FeO^-)—(UO_2)_3(OH)_5^+ + 7H^+$ (*12*)

In the presence of dissolved $CO_2$ under alkaline pH conditions, carbonate will form ternary complexes with surface-associated U, such as $(\equiv FeO_2)UO_2CO_3^{2-}$. The formation of these complexes results in the desorption of U(VI) from the Fe oxide surface, increasing U mobility. (*12*) The optimal pH range for U adsorption onto Fe oxy(hydr)oxides is from 5.5-7.5, where adsorption is at a maximum but desorption due to carbonate will not occur. (*13*) Environmental pH is most commonly in this optimal range.

Redox chemistry is an important consideration when determining the mobility of U. Traditionally, remediation strategies for U immobilization aim to reduce U(VI) to mineralized $UO_2$. The reduction of U(VI) can be coupled to the oxidation of Fe(II) to Fe(III).(*13*) This reaction is enhanced when Fe(II) is associated with a mineral surface to form the complex $\equiv FeOFeOH^0$. U(VI) reduction by Fe(II) is also enhanced if Fe(II) is present within a mineral crystal structure such as in the mineral magnetite ($Fe_3O_4$). (*14*) In addition to Fe, the oxidation of aqueous or structural sulfide can be coupled with the reduction of U(VI) (*15*, *16*). Direct enzymatic reduction of U has also been shown to take place by both Fe and sulfate reducing bacteria. (*17-19*)

While traditional studies have stimulated U(VI) reduction to $UO_2$ in order to immobilize U, recent research has shown that $UO_2$ is not the only product of U reduction. Nano-uraninite and molecular U(IV) have been identified in biostimulated systems using X-ray absorption spectroscopy. (*20-22*) These species are thought to be unstable and reactive, but have also been shown to be transported as colloids, meaning that U(IV) is not necessarily immobile as has long been assumed. (*23*) Another strategy for U(VI) immobilization has been the addition of phosphate to oxic contaminated systems. U(VI)-phosphate precipitates, including uranium

hydrogen phosphate [$UO_2HPO_4 \cdot 3H_2O$], chernikovite [$UO_2HPO_4 \cdot 4H_2O$], and autunite [$Ca(UO_2)_2(PO_4)_2 \cdot 11H_2O$], can form at high phosphate concentrations and U(VI) adsorption to Fe oxy (hydr)oxides is enhanced at low phosphate concentrations. (*24-26*) While U(VI)-phosphate minerals have low solubility and are not subject to remobilization by oxidation, their long-term stability is still not well understood.

**Arsenic chemistry in the environment**

Arsenic is a naturally occurring element that is toxic to humans and also carcinogenic. Arsenic poses a global human health concern as prolonged exposure can result in As toxicosis, a summation of diseases causing skin lesions and a variety of cancers. (*27*) The high levels of As in drinking water in Southeast Asia have resulted in the largest mass poisoning in history. (*28*) Because of this epidemic, the World Health Organization has set the recommended As concentration in drinking water at 10 μg/L. (*29*) The combination of U and As in soils is not uncommon at mining sites. Arsenic is often found in U ore deposits at concentrations as high as 10 weight percent. (*30*)

The predominant oxidation states of As are +3 and +5. In solution, As tends to be present as oxyanionic acids including $AsO_3^{3-}$ and $AsO_4^{3-}$. Arsenic can also be found in the environment as As(III)-sulfide mineral phases including arsenopyrite (FeAsS), realgar ($As_4S_4$), orpiment ($As_2S_3$), or scorodite ($FeAsO_4 \cdot 2H_2O$). (*31*, *32*) Unlike U, both oxidation states of As are soluble and do not readily complex with other ions in solution. Similar to U, redox chemistry plays an important role in the mobility of As. In contrast to U whole reduce form is commonly mineralized, the reduced form of As, As(III), is the more toxic and more mobile form in comparison to oxidized form, As(V). As with U, As reduction can be coupled with the oxidation of aqueous or structural sulfide.(*33*, *34*) Microbes have been shown to directly reduce As(V)

either for respiration or as a detoxification mechanism. (*29*) Reduction of As(V) can also result in the formation of As(III)-sulfide mineral phases depending upon the concentration of sulfide present in a system.(*34-36*)

As with U, Fe minerals can control the mobility of As by surface adsorption. (*37*, *38*) As(V) readily adsorbs to Fe minerals under most environmental conditions, while As(III) adsorption behavior varies with pH. If Fe(III) minerals undergo reductive dissolution, desorption and subsequent release of As from these minerals occurs, but sequestration through sorption or co-precipitation can also take place as new Fe mineral phases form. (*38*, *39*)

**North Cave Hills**

The site under investigation for this dissertation is in the Cave Hills area of Harding County, South Dakota. This area contains uraniferous lignite beds that underwent open pit U mining from 1955 to 1967 with no erosion controls or reclamation according to the General Mining Laws and Public Law 357. Uranium was discovered in the Cave Hills when the US Atomic Energy Commission did airborne surveys for radiation anomalies in 1954. (*40*) Uranium and other heavy metals were released to the surrounding watersheds through physical erosion and geochemical processes during this time period. Since then, the abandoned mine wastes have remained exposed to wind and water erosion. Heavy metals from the site migrated to down gradient watersheds, contaminating surface water, soil, and groundwater. (*41*) The major drainages of the site lead to both the North and South Fork of the Grand River that form the Shadehill Reservoir, the major reservoir in northwestern South Dakota.

**Research objectives**

Uranium and As are two toxic, redox-active elements that can occur as co-contaminants. (*42*, *43*) Their differences in behavior under similar redox conditions makes their simultaneous remediation challenging. Previous research has focused on the chemical behavior of U and As separately in model systems containing synthesized Fe minerals rather than in the presence of a complex mixture of Fe minerals such as that found in natural soil and sediment. (*4*, *37*, *44*) While some studies have characterized either U or As redox chemistry in U mine and mill sediments, the behavior of the two contaminants together has not been thoroughly explored. (*45-47*)

The overall goal of this research was to obtain a better understanding of chemical mechanisms controlling the fate and transport of both U and As by elucidating the interactions between these contaminants and Fe minerals. By determining these mechanisms, insight will be provided into the types of remediation technologies necessary, if any, to prevent the mobilization and transport of U and As at sites of mine and mill tailings worldwide.

The first objective was to characterize the mechanisms governing the fate and transport of U and As at the North Cave Hills mine tailings site. Previous studies have looked into physical controls on U and As transport at the North Cave Hills, but a detailed study into the chemical species of U and As present in sediments has not been previously conducted. (*40*, *48*) Many studies also limit their sampling to the U tailings pile and do not include down gradient sampling sites. Chapter 2 focuses on the speciation of U and As at oxic and anoxic zones surrounding the tailings pile including the nearby impacted watershed.

The characterization of sediments collected in the field could only provide limited information about U and As behavior in anoxic environments and could not show what would occur during seasonal changes at the site. The second objective was to examine the effects of

redox chemistry on U and As speciation and chemical behavior in natural North Cave Hills sediments under controlled laboratory conditions. In addition, differences in As and U redox behavior during biostimulation with a specific electron donor was studied. Again, previous studies have not examined the effects of the presence of As(V) on the behavior of U during biostimulation nor have they examined how the use of different electron donors affects the extent of U(VI) reduction. This work is described in Chapter 3.

Two unexpected observations in the work in Chapter 3 brought about the work described in Chapter 4. In the batch experiments, mackinawite played a role in the reduction of U(VI) and As(V) and uranyl arsenate precipitation was observed. The third objective was to look at the effect of As(V) on the extent of U(VI) reduction in the presence of mackinawite and to examine the redox stability of uranyl arsenate minerals. Again, the effect of As(V) on U redox chemistry has not been previously studied in a controlled laboratory experiment. All previous work into uranyl arsenate formation in the presence of mineral surfaces has used non-redox active minerals, so this work aims to explore the susceptibility of U to redox changes when present as uranyl arsenate.

In addition to the three chapters mentioned above, two published papers to which I contributed are included in the appendix. The first paper determined of changes in Fe mineralogy following microbial incubation with hydrocarbons and the second paper characterized Fe mineralogy at an acid mine drainage site.

CHAPTER 2

# EFFECT OF BIOGEOCHEMICAL REDOX PROCESSES ON THE FATE AND TRANSPORT OF AS AND U AT AN ABANDONED URANIUM MINE SITE: AN X-RAY ABSORBTION SPECTROSCOPY STUDY[1]

## Introduction

With the Cold War came a boom in U mining that left behind a legacy of environmental problems. (*3*) At that time, no government requirements for mine tailing reclamation were in place. Unreclaimed tailings left U ore exposed to weathering, resulting in the spread of U and other metals to surface water, groundwater, and sediments surrounding mine sites.

The North Cave Hills in Harding Country, South Dakota is one of those unreclaimed U mine tailings sites. Open-pit mining began at this site in 1955 after U-containing lignite seams were discovered and continued through 1967. (*41*) Because of the lack of reclamation requirements, loose piles of overburden and ashed material were left behind, allowing for the release of heavy metals, metalloids, and radionuclides into the surrounding watershed. Previous work at the site identified the major metals in sediments in the surrounding watershed to include Cu, Pb, Se, Th, As, U, and V. (*40*) Of these elements, U and As have the greatest potential to

[1] The work presented in Chapter 2 was modified from a manuscript published in Environmental Chemistry with permission from CSIRO Publishing (http://dx.doi.org/10.1071/EN13129). Special thanks to co-authors on the manuscript—Dr. Thomas Borch and Dr. James J. Stone. With the exception of assistance with soil sampling by Lance N. Larson and Dr. James J. Stone, laser ablation inductively coupled plasma mass spectrometry (ICP-MS), and sequential extractions performed by Dr. Rong Wei, all work described here was performed myself. Laser ablation ICP-MS performed by M. Lizabeth Alexander at the Pacific Northwest National Laboratory's Environmental Molecular Sciences Laboratory operated for the Department of Energy by Battelle Memorial Institute. Standards used for linear combination fitting of X-ray absorption spectra were provided by Dr. John R. Bargar, Dr. Juan S. Lezama-Pacheco, and Dr. Peggy A. O'Day and by Robert T. Downs and the RRUFF library.

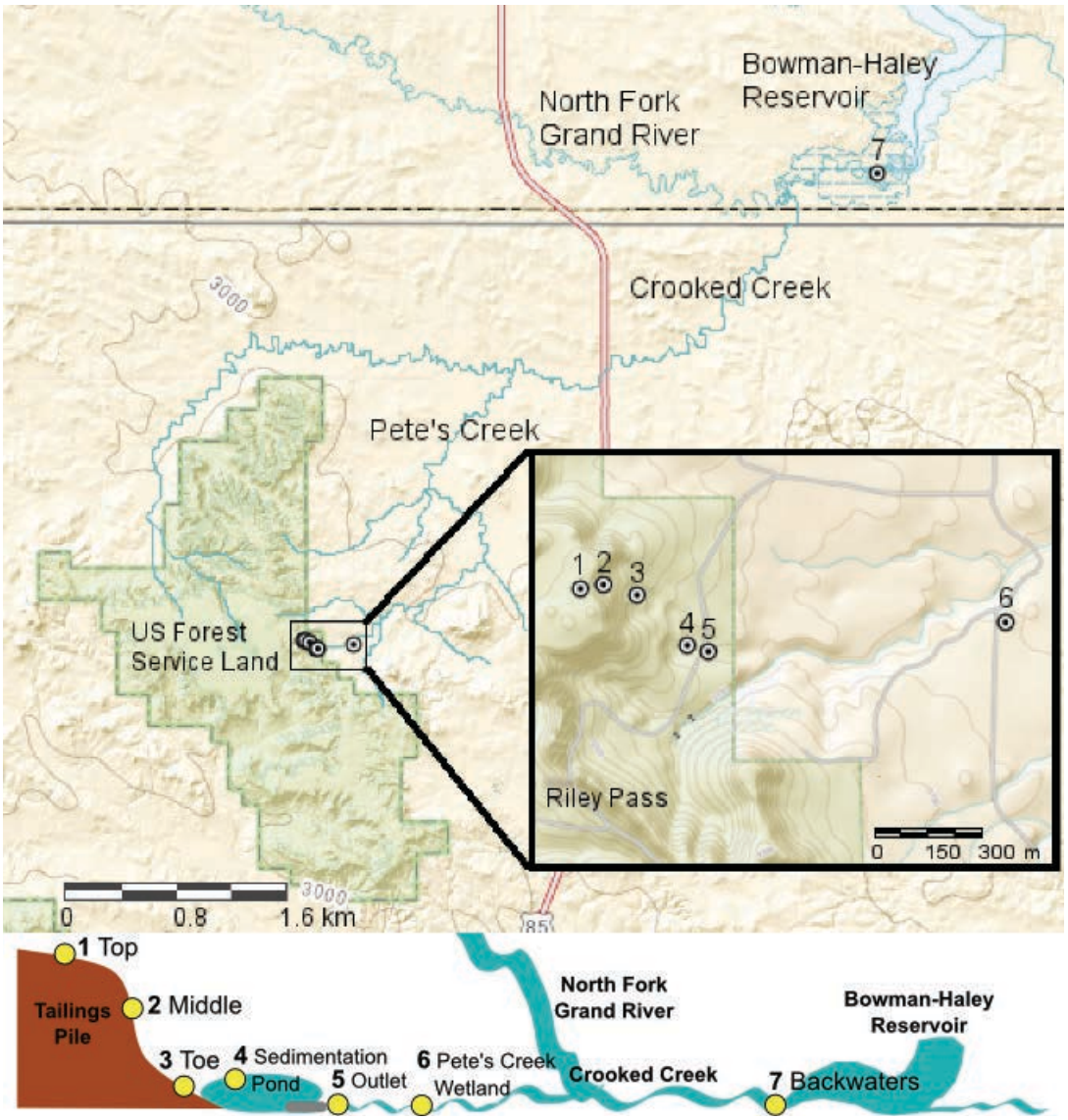


**Figure 2.1.** Map of sampling locations. Shaded green areas correspond to the US Forest Service land. Black circles indicate sampling locations and numbers correspond to labels in the drawing and in Table 1. The drawing is not to scale. Sampling locations are marked with yellow circles. The base map was provided by the United States Geological Survey and the National Map.

threaten the local water supply because of their redox-sensitivity, solubility, and their concentration levels at the North Cave Hills. Uranium and As were previously found in near-source and watershed sediments at levels above their respective background concentrations of 4 mg/kg and 27 mg/kg. (*41*) Near-source surface water U and As concentrations as measured by Larson, et al. were above the Environmental Protection Agency (EPA)'s maximum contaminant levels (MCL) which are 30 ppb and 10 ppb for U and As respectively. (*48*) Down gradient of the tailings is a wetland followed by Crooked Creek that flows to the Bowman Haley Reservoir, which is open to the public for recreation (Figure 2.1). Larson, et al. have previously shown that heavy metal accumulation in the reservoir is the result of local U mining activity. (*49*)

U and As have differences in mobility under similar redox conditions. Under oxic conditions and environmentally relevant pHs, U is present as aqueous U(VI) species, including $UO_2(OH)_2^0$ and $UO_2(OH)_3^-$. (*12*) When carbonate and/or calcium is also present, U(VI) can form uranyl-carbonato and/or uranyl-calcium-carbonato complexes including $(UO_2)_2CO_3(OH)^{3-}$, $UO_2(CO_3)_2^{2-}$, $UO_2(CO_3)_3^{4-}$, $Ca_2UO_2(CO_3)_3^0$ and $CaUO_2(CO_3)_3^{2-}$. (*3*, *50*) These complexes have high solubility, limiting U(VI) adsorption to Fe oxy(hydr)oxides and sediments when calcium and carbonate are present. (*3*, *8*, *12*, *51*) Under anoxic conditions, U can be present as molecular U(IV), nano-uraninite, or the most stable and least soluble of the reduced forms, crystalline uraninite ($UO_2$). (*20*, *21*, *52*, *53*) While U is less mobile in its reduced forms than in its oxidized forms, As is generally more mobile in its reduced form as As(III). (*41*, *54-56*) Arsenic can adsorb to iron oxides under environmental pH as both As(III) ($H_2AsO_3^0$) and As (V) ($H_2AsO_4^-$). (*37*, *40*) Although As(III) has a greater sorption affinity to iron oxides than does As(V) at pH 7, As(V) binds more strongly to iron oxides and is not as easily desorbed and released into surface waters as As(III). (*37*, *38*, *41*) In addition to having greater mobility, As(III) is more toxic to

humans than As(V). (*43*, *49*) As(III)-sulfide mineral phases with low solubility, such as realgar ($As_4S_4$) and orpiment ($As_2S_3$), can also form under anoxic conditions, but because Fe-sulfide mineral formation is favored, As(III) is most commonly found in its dissolved form. (*12*, *36*, *57*)

Iron and sulfate biogeochemical cycling can control the mobility of U and As. Studies of abiotic reduction of U(VI) by Fe(II) in soils have shown that U(VI) can be reduced by adsorbed Fe(II) and by structural Fe(II), to a limited extent. (*3*, *50*, *58*, *59*) Uranium can also be reduced by biogenically produced or synthetic Fe-sulfide and by aqueous sulfide under anoxic conditions. (*15*, *16*, *55*, *60*, *61*) Enzymatic reduction of U(VI) has been observed by iron and sulfate reducing bacteria. (*17*, *62*) While both As(III) and As(V) can be adsorbed to iron minerals, As can be released, not only by desorption, but by microbial reduction of iron mineral phases, resulting in mineral dissolution. (*63*) Arsenic has been shown to be released during microbial reduction of sulfate to sulfide, resulting in thioarsenate formation.(*45*) In addition, As(V) can be reduced by dissimilatory metal reducing bacteria or by bacteria as a detoxification mechanism to form less toxic methylated As(III). (*29*, *64*, *65*) Thermodynamically, As(V) reduction is favored over Fe(III) and sulfate reduction. (*66*) Uranium and As may also control the solubility of each other in the environment. Recently, U and As have also been found to form uranyl arsenate surface complexes with aluminum oxide at pH 5-12 and uranyl arsenate aqueous complexes and precipitates under acidic conditions in the laboratory. (*67*, *68*) Little is known about the formation of uranyl arsenates in the environment, but their effect on mobility of U and As should be considered in environments where both elements are present.

Previous studies at the North Cave Hills have tried to determine major mechanisms controlling U and As transport and fate at the site. Kipp, et al. found that both aerobic and anaerobic processes in sediments play a role in U and As transport by comparing their

concentrations to that of thorium—a metal that is not sensitive to environmental redox changes. (*40*) While U and As concentrations fluctuated with distance from the tailings pile, thorium, which was used as a naturally occurring conservative tracer, steadily decreased suggesting that, in addition to erosion, redox-promoted transport may be significant. (*40*) The study also determined that U and As were primarily associated with the Fe oxide fraction of collected soils, further emphasizing the need for a better understanding of Fe controls on U and As fate at this site. Larson et al. looked at the seasonal variation of U and As speciation in North Cave Hills sediment pore waters, concluding that seasonal changes in redox conditions will continue to promote release of U and As as a result of reductive Fe oxide dissolution. (*48*) Aqueous surface water and pore water Fe, U, and As concentrations measured by Larson et al. complement sediment concentrations measured in our study.

Although As can occur in U ore at concentrations up to 10 weight%, (*30*) the fate and transport of both U and As at U mine tailings has not been previously investigated at any other field sites. However, U geochemistry has been studied extensively in Rifle, Colorado and other mill tailing sites. (*3, 5, 55, 69*) At these sites, U immobilization can occur with reduction to U(IV) or when U(VI) forms stable precipitates with e.g., dissolved phosphate. (*3, 52, 70, 71*) Stucker, et al. discovered that As was released to Rifle, CO groundwater during bioremeditation of U. (*45*) Donahue and Hendry studied As transport at a U mill tailing in Canada and found that As is primarily present as calcium arsenates, which could dissolve into site pore water resulting in concentrations of up to 126 ppm As. (*30, 46*) Arsenic was also found to be adsorbed to ferrihydrite resulting in long-term stability under site conditions, preventing aqueous As transport. (*30, 47, 72*) The majority of these studies have focused on the geochemistry and stability of U or As in tailings piles rather than physical and chemical controls on down gradient

**Table 2.1.** Sampling location information including latitude and longitude coordinates, soil redox measurements (mV), and surface water pH.

| Site Number (see Figure 1) | Location Name | Latitude/Longitude | Redox (mV) | pH |
|---|---|---|---|---|
| 1 | Top of the Tailings | 45.84642°, -103.47553° | 328 | — |
| 2 | Middle of the Tailings | 45.84650°, -103.47467° | 237 | — |
| 3 | Toe of the Tailings | 45.84625°, -103.47325° | 408 | — |
| 4 | Sedimentation Pond | 45.84481°, -103.47119° | -25 | 7.1 |
| 5 | Pond Outlet | 45.84472°, -103.47064° | 160 | — |
| 6 | Pete's Creek Wetland | 45.84547°, -103.45875° | -79 | 7.3 |
| 7 | Bowman-Haley Backwaters | 45.95331°, -103.28758° | -153 | 8.6 |

transport of both elements in the same study.

Due to the dissimilarity of these co-contaminant metal redox pairs, and due to negative health effects associated with both U and As, it is essential to understand the processes that promote the retention and redox transformation of U and As within mining-impacted watersheds such as the North Cave Hills, South Dakota. (*73*, *74*) Thus, the goal of this work is to determine how sorption and redox processes within various sites (e.g., tailings pile, sedimentation pond, wetlands, reservoir) control the down-gradient transport of U and As at an unreclaimed uranium mine tailing site.

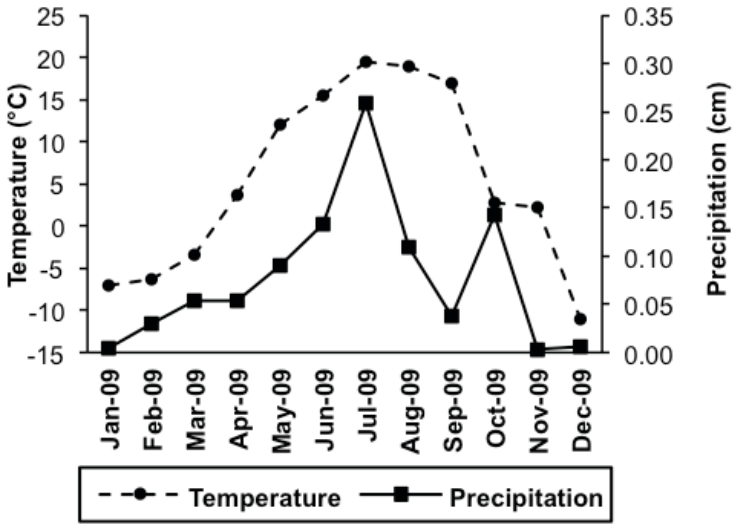


**Figure 2.2.** Average monthly climate data for the year of 2009 collected at Antelope Range from the South Dakota Climate and Weather's Automatic Weather Data Network. The left axis corresponds to temperature (dashed line) and the right axis corresponds to precipitation (solid line).

## Materials and Methods

### *Study Site and Sample Collection*

Samples were collected from nine previously established locations including the North Cave Hills mine tailings and the surrounding down gradient watershed. (*40, 41*, *48*) Locations were selected based upon variation in redox conditions and U and As concentrations in sediments and pore water from past studies (Figure 2.1, Table 2.1). (*41*) All samples were collected in late June of 2009, at the beginning of the rainy season (Figure 2.2). Three samples were collected from the tailings pile, including the top of the pile (1), the middle of the pile's eastern slope (2), and the toe of the pile (3) prior to entering a sedimentation pond. The collection site at the base of the pile was selected because of evidence of recent erosion and rainwater transport. The fourth sampling site is at the inlet to the sedimentation pond located

about 0.7 km downstream of the tailings pile (4). The pond is intended to capture sediment from the tailings pile to prevent physical transport (erosion) into Pete's Creek. The fifth sampling site is at the sedimentation pond's outlet pipe draining into Pete's Creek (5). The next sampling location is within the sediment deposition zone surrounding Pete's Creek referred to as Pete's Creek Wetland (6), approximately 2 km from the tailings pile. Pete's Creek then connects to Crooked Creek, which leads into the Bowman-Haley Reservoir, 45 km down gradient of the tailings pile. The final sampling location is at the inlet to the reservoir, referred to as Bowman-Haley Backwaters (7).

At the time of sample collection, the oxidation-reduction potential (ORP) was measured using a handheld meter and ORP probe (Hanna Instruments 9025) by inserting the probe into the moist soil. The pH of surface waters was measured at sampling locations where soils were submerged. Two cores were collected at each sampling location, one preserved anoxically for determination of metal speciation and one collected for determination of total metal content. Soil cores were collected using a stainless steel soil corer lined with a polyethylene tube approximately 30 cm long. Both soil cores were preserved by immediately capping the tubes and sealing the caps with wax. The soil cores were then stored on ice for up to 2 days and transported to an anaerobic chamber in the laboratory. Because of the loose sediment material at the Bowman-Haley reservoir, an anoxic soil core was not preserved. Anoxic cores were divided into 5 cm sections by depth and allowed to dry in the anaerobic chamber. Once dry, soil samples were ground by mortar and pestle and passed through a 2 mm sieve. For long-term storage, samples were transferred into 125 mL airtight crimp-sealed bottles. For some analyses, samples were homogenized by taking equal masses of soil from each of the 5 cm sections of each core.

Samples were combined using a mortar and pestle. For the majority of analyses, the top 5 cm of the soil core were used.

***Laboratory methods***

Soil texture analysis for homogenized dry samples was performed by Colorado State University's Soil Testing Laboratory. The clay-sized fraction of the homogenized dried soils was separated and prepared for analysis by X-ray diffraction (XRD) with a Scintag X2 theta-theta powder diffractometer with a Peltier detector and Cu X-ray tube at Colorado State University Department of Chemistry's Central Instrument Facility. The X-ray source was operated at 40 kV and 40 mA. Soluble salts and carbonates were removed from soils by washing with 1 M HCl. (*75*) Soils were washed and centrifuged and the solution was decanted. This process was repeated several times until the soil was no longer suspended in solution. Soil was then transferred into a beaker and 30% $H_2O_2$ was added to remove organic material. (*76*) The solution was covered with a watch glass and heated to 70 °C until bubbling had subsided. Soils were then passed through a 63 μm sieve (mesh size #230) to remove the sand fraction. The clay fraction was separated from the silt fraction by centrifuging repeatedly with sodium hexametaphosphate at 2 minutes at 600 rev/min at 20 °C until the solution remained clear. (*77*) Upon isolating the clay-sized fraction, each sample was treated in three different ways, Mg-saturated air-dried, (*78*) Mg-saturated glycerol solvated, (*79*) and K-saturated air-dried (*78*) and then filtered onto Isopore membrane filters (5.0 μm TMTP, Millipore) and transferred to microscope slides, (*80*) allowing for the identification of smectite, vermiculite, chlorite, mica, gibbsite, and kaolinite.

Total sediment metal concentrations were determined by total digestion of a 1.0 g sample from the top 5 cm of soil cores by the method described by Soltanpour, et al. (*81*) The resulting digestions were analyzed by Inductively Coupled Plasma Mass Spectrometry (ICP-MS) (Perkin

Elmer Elan DRC II) for U and As concentrations and Inductively Coupled Plasma Optical Emission Spectroscopy (ICP-OES) (Thermo Scientific Iris Intrepid II) for Fe at Colorado State University's Soil Testing Laboratory. Sequential extractions were performed separately for analysis of U and As. Extraction procedures for As were based upon Huang and Kretzschmar.(*82*) Steps 1, 3, 5, 6, and 7 were performed to extract soluble and exchangeable, manganese oxide associated, poorly crystalline Fe and Al (hydr)oxide associated, sulfide associated, and crystalline Fe and Al (hydr)oxide associated As, respectively. To measure concentrations in the residual fraction, 5 mL of concentrated $HNO_3$ was added to the remaining sediment and heated at 85 °C for 3 hours, rather than using X-ray fluorescence. (*71*, *83*) Sequential U and As extractions were also performed based upon a modified method from Tessier et al. as described in Salome et al. (*71*, *84*) Extracts were also analyzed for both U and As by ICP-MS. Total carbon measurements were also performed on a Shimadzu TOC-L at Colorado State University's EcoCore Analytical Laboratory.

***X-Ray Absorption Spectroscopy (XAS)***

All XAS samples were taken from the homogenized top 5 cm of the dried soil cores. Samples were analyzed at the Stanford Synchrotron Radiation Lightsource (SSRL) in Menlo Park, CA. All anoxic soil preparations occurred within an anaerobic chamber containing 95% $N_2$, 5% $H_2$. Samples were placed into a Teflon holder sealed by a Kapton polyimide film to prevent oxidation while minimizing X-ray absorption as previously described. (*85*) X-ray absorption fine structure (EXAFS) spectroscopy was used to characterize Fe mineralogy. X-ray absorption near-edge fine structure (XANES) spectroscopy was performed to determine the valence state of U and As. XAS was performed at beamline 11-2 (26-pole wiggler), 10-2 (30-pole wiggler), and 7-3 (20-pole wiggler) at SSRL. The ring operates at 3 GeV with a current of 450 mA. During data

collection, As samples were maintained at a temperature of 5 K to prevent beam-induced redox reactions using an Oxford Instruments CF1208 continuous flow liquid helium cryostat. (*86*) Energy selection was accomplished with a Si (220) monochromator. All Fe EXAFS spectra were collected in fluorescence mode with a wide-angle collection ionization chamber (Lytle detector). U and As XANES spectra were collected in fluorescence mode with a 30-channel Ge detector. EXAFS spectra are collected from -200 to +1000 eV around the K-edge of Fe (7111 eV). For U and As, XANES spectra were collected from -150 to 450 eV around the $L_{III}$-edge of U (17176 eV) and the K-edge of As (11876 eV). Between 2 and 3 spectra were averaged for each sample. U and As spectra were fit by linear combination fitting of normalized XANES spectra in Athena between -20 and +25 eV from 17178 eV for U and -20 and +35 eV from 11873 eV for As. (*87*) Uranium reference compounds included uranyl acetate and uraninite. (*88*) Arsenic reference compounds included As(III) adsorbed to goethite, As(V) adsorbed to goethite, (*86*) and orpiment ($As_2S_3$). Standards of As adsorbed to goethite were prepared according to Amstaetter, et al. by adding 1.2 mg/L of sodium arsenite and sodium arsenate to a 5.4 g/L suspension of goethite (Bayferrox 920 Z, LANXESS Deutschland GmbH).(*86*) Orpiment was obtained from the RRUFF database at University of Arizona Mineral Museum and was originally from Mercur, Utah. Linear combination fitting of $k^3$-weighted Fe EXAFS spectra was performed from 3 to 12 k ($Å^{-1}$) using Athena. (*87*) All references were chosen based on their likelihood of being a soil component. The Fe EXAFS spectrum of smectite (SAZ-1) was obtained from Dr. Peggy O'Day at University of California, Merced. (*89*) Compounds were only included in the fit if the contribution was a fraction greater than 0.05. Fits are approximately within ±5% of the mole percentages. (*85*)

## Results and Discussion

### *Geochemical Characterization of Field Site*

Soil redox measurements were taken at each of the sampling locations (Table 2.1). The redox potential varies from site to site, with the tailings pile and the pond outlet being oxic to suboxic. All of the sites that were under surface water were anoxic: the sedimentation pond, Pete's Creek wetland, and Bowman-Haley backwaters. pH measurements were only taken at locations where surface water was present above the sampled soil core (Table 2.1). pH readings were 7.1 and 7.3 for near-source sampling locations and 8.6 at the Bowman-Haley backwaters sites. Total carbon measurements and elemental analysis for each sampling site are shown in Table 2.2. Previous work at the North Cave Hills has found surface waters around the area to be between pH 7 and 10 and to have high alkalinity with $CaCO_3$ concentrations up to 300 mg/L. (*41*)

Iron is redox sensitive, abundant in soils, and known to influence U and As mobility in soil and sediments. (*54*) Total Fe concentrations in the top 5 cm of soil from each sampling site are shown in Figure 2.3. The concentration of solid phase Fe was greater at sites downstream of the sedimentation pond. The top, middle, and bottom of the tailings pile and the sedimentation pond ranged from 8,180 to 9,780 mg/kg total Fe, while the samples collected from the pond outlet, Pete's Creek Wetland, and Bowman-Haley Backwaters contained 14,100 to 17,700 mg/kg total Fe. The highest concentration of Fe was measured at the sedimentation pond's outlet at

**Table 2.2.** Total elemental analysis of soils from each sampling site as determined by X-ray fluorescence spectroscopy and total carbon measured for each site.

| Number (see Figure 1) | Location Name | Total C (ppm) | Mo (ppm) | Pb (ppm) | Ba (ppm) | Cr (ppm) | Mn (ppm) | Ni (ppm) | Rb (ppm) | Sr (ppm) | Ti (ppm) | Zn (ppm) |
|---|---|---|---|---|---|---|---|---|---|---|---|---|
| 1 | Top of the Tailings | 6100 | 12.7 | 9.52 | 142 | 59.0 | 124 | 44.2 | 49.7 | 69.8 | 1350 | 59.2 |
| 2 | Middle of the Tailings | 11100 | 14.5 | 8.50 | 121 | 37.4 | 72.2 | — | 41.6 | 65.1 | 988 | 23.1 |
| 3 | Toe of the Tailings | 48500 | 73.0 | 11.0 | 113 | 35.6 | 55.4 | 30.6 | 37.1 | 96.9 | 1280 | 41.8 |
| 4 | Sedimentation Pond | 25400 | 24.3 | 8.81 | 93.1 | 27.3 | 81.4 | — | 34.4 | 88.5 | 930 | 37.0 |
| 5 | Pond Outlet | 29100 | 15.4 | 12.4 | 169 | 47.9 | 144 | 61.3 | 52.1 | 88.3 | 1660 | 208 |
| 6 | Pete’s Creek Wetland | 16200 | — | 12.3 | 138 | 54.1 | 152 | 34.1 | 56.1 | 72.8 | 1610 | 43.7 |
| 7 | Bowman-Haley Backwaters | 16300 | — | 4.91 | 47 | 25.3 | 184 | 18.4 | 22.6 | 49.5 | 580 | 15.0 |

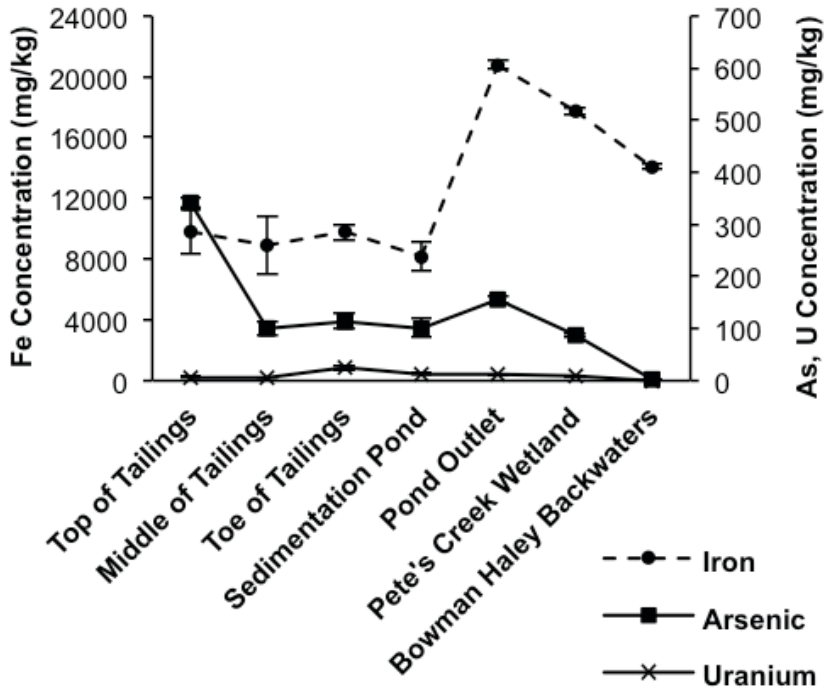


**Figure 2.3.** Total concentrations of solid phase iron, arsenic, and uranium in the top 0-5 cm of sediment cores as determined by total soil digestion followed by ICP-MS. The left axis corresponds with iron, indicated by the dashed line. The right axis corresponds with arsenic and uranium, indicated by solid lines. Error bars indicate one standard deviation from the average of triplicate digests.

20,800 mg/kg. The high concentration at the pond outlet indicates that dissolved Fe(II) and suspended iron oxides are accumulating in the pond water and are then carried downstream through the pond outlet. Although relatively low aqueous Fe(II) concentrations (2 mg/L) were measured in the pond by Larson, et al., oxidative precipitation of dissolved Fe(II) may, in part, be responsible for accumulation of Fe(III) oxides at this sampling location, Pete's Creek wetland, and Bowman-Haley backwaters sites. (*48*) Of the total extracted Fe, only 55% was in crystalline form at the pond outlet compared to 75% in the pond (Figure 2.4). The greater fraction of amorphous and exchangeable Fe at the outlet compared to that at the pond suggests that precipitation of amorphous iron oxides such as ferrihydrite occurs at the outlet (Figure 2.4).

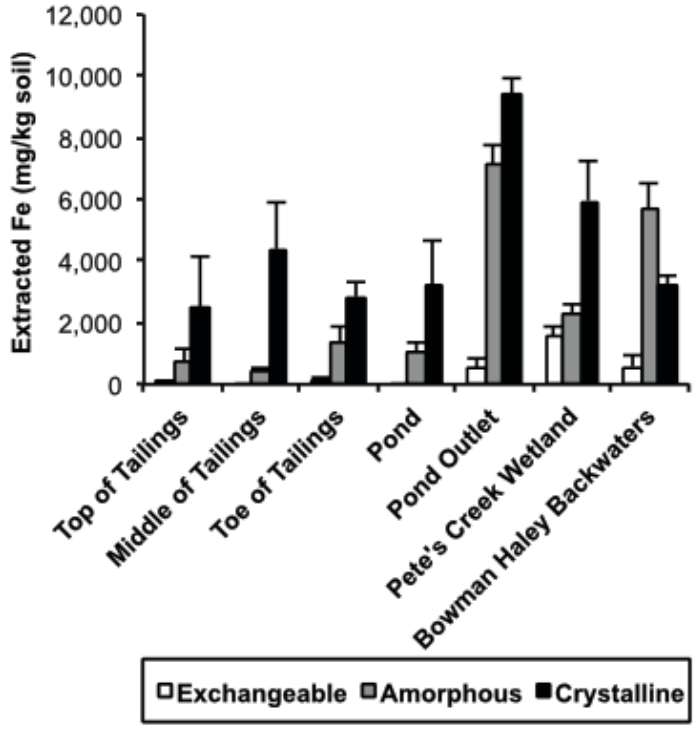


**Figure 2.4.** Sequential extractions of sediment-associated iron. Bars indicate percent exchangeable (white), amorphous (dashed), and crystalline (gray) iron of the total extracted iron. Error bars indicate one standard deviation from the mean of triplicate extractions.

The distribution of soil iron minerals was determined by linear combination fitting (LCF) of EXAFS data in k-space (Figure 2.5, Figure 2.6, Table 2.3). Based on LCF-EXAFS, the iron mineral composition at the site is primarily made up of iron-bearing silicates including smectite and augite. At all three of the tailings pile sampling locations, the dominant Fe-bearing mineral was smectite (35-54%), while at the down gradient locations the dominant Fe-bearing mineral was augite (31-86%). All of the spectra were fit including ferrosmectite and goethite as standards, in addition to using smectite and augite. Goethite, an iron oxy(hydr)oxide, could form by precipitation at the pond outlet (30%) following dissolution of amorphous iron hydroxides like ferrihydrite which can occur in the reducing environment of the sedimentation pond. (*90*)

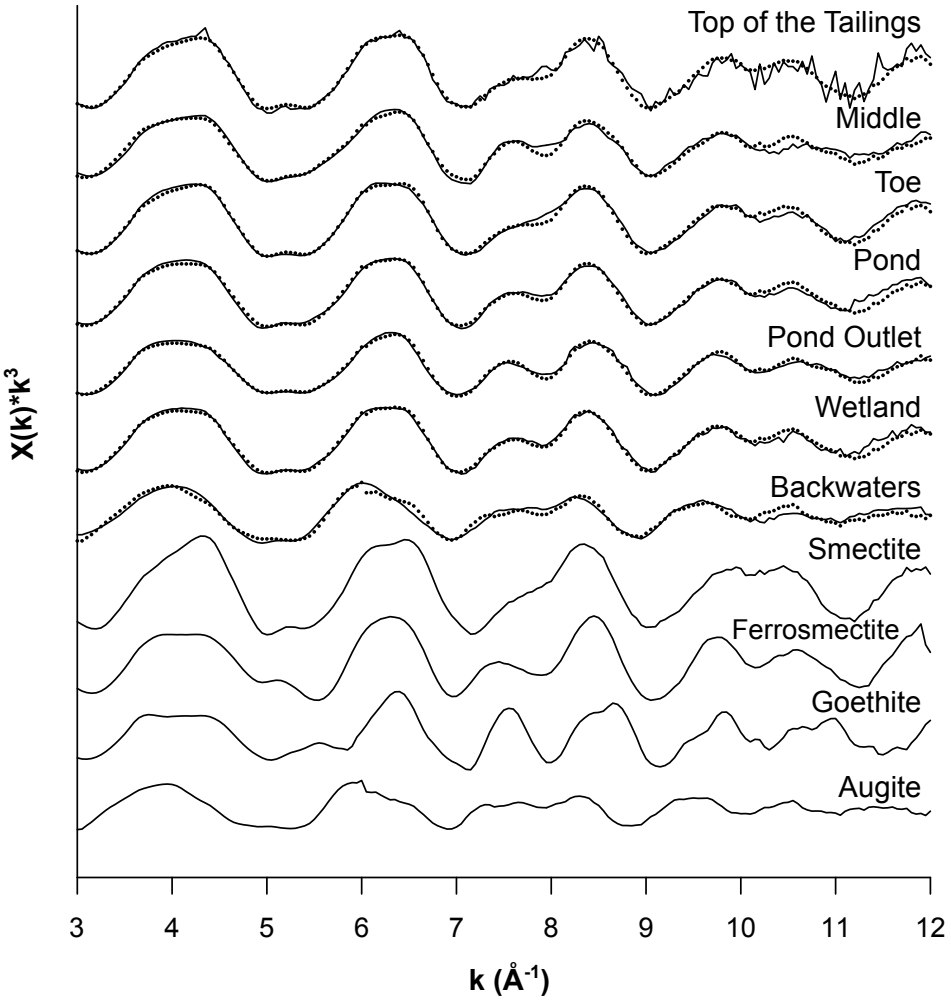


**Figure 2.5.** Linear-combination fits (dots) of iron EXAFS spectra (solid lines) from all of the sampling locations. The reference compounds used in fitting are plotted at the bottom for comparison.

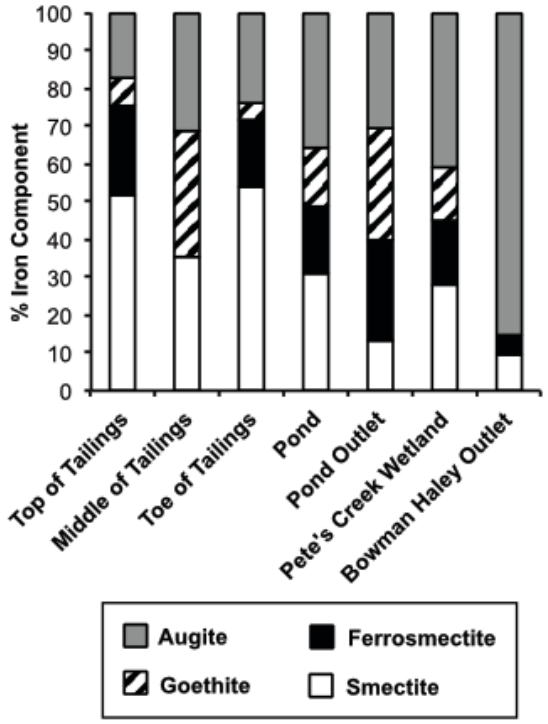


**Figure 2.6.** Distribution of Fe minerals in sediments as determined by linear-combination fitting of $k^3$ Fe EXAFS. Stacked bars represent reference compounds including augite (gray), goethite (dashed), ferrosmectite (black), and smectite (white). Components are plotted as percent of the total, with approximately 5% error.

**Table 2.3.** Summary of Fe EXAFS linear-combination fitting.

| Location Name | % Smectite | % Ferrosmectite | % Goethite | % Augite | R factor |
|---|---|---|---|---|---|
| Top of the Tailings | 51.6 | 23.9 | 7.1 | 17.4 | 0.068693 |
| Middle of the Tailings | 35.3 | 0 | 33.1 | 31.5 | 0.041328 |
| Toe of the Tailings | 54.3 | 17.4 | 4.6 | 23.7 | 0.020924 |
| Sedimentation Pond | 31.0 | 17.9 | 15.5 | 35.6 | 0.029843 |
| Pond Outlet | 13.0 | 27.0 | 29.5 | 30.5 | 0.018432 |
| Pete's Creek Wetland | 27.9 | 17.0 | 14.4 | 40.7 | 0.023450 |
| Bowman-Haley Backwaters | 9.7 | 4.8 | 0 | 85.5 | 0.065118 |

Clay X-ray diffraction resulted in similar diffraction patterns for all of the sampling sites, confirming the presence of smectite and goethite in site sediments. Analysis of the clay XRD patterns identified mica, kaolinite, and gibbsite at all of the sampling locations (Figure 2.7).

***Geochemical Controls on U Transport***

Uranium surface sediment concentrations vary, based on our limited number of sampling sites, within the tailings pile, but are consistently low at all other sampling locations. The highest concentration of total U among the sampling sites, as determined by total digestion, was found at the toe of the tailings (25 mg/kg). High concentrations may be found there because of the deposition of sediment resulting from weathering of the tailings pile. All sites downstream of the toe of the tailings have total U concentrations between 0 and 15 mg/kg in surface sediments as determined by total digestion (Figure 2.2). In addition to being determined by digestion, total sediment concentrations for uranium were determined by laser-ablation ICP-MS (Figure 2.8a). Sediment U concentrations determined by total digestion follow the same trend by site as by laser ablation with the exception of the top of the tailings (7 and 64 mg/kg respectively) and the pond outlet (12 and 33 mg/kg respectively), which were both determined to be greater by laser ablation. Laser-ablation ICP-MS determines concentration by ablation of a spot 50 μm in diameter of the sediment sample, so concentrations may be greater if an area containing mineralized U was analyzed. (*91*) With the inhomogeneity of the sediment at the top of the tailings pile, this result is not unexpected. Background level U sediment concentrations were previously determined to be 4 mg/kg. (*41*) The Bowman-Haley backwaters site was the only site with U concentrations below background level as measured by total digestion.

Low sediment concentrations down gradient of the tailings pile may be the result of the sedimentation pond, either by serving its purpose to prevent down gradient sediment transport or

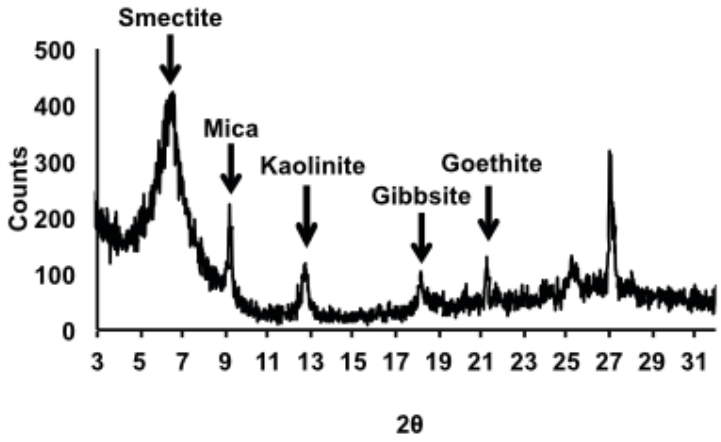


**Figure 2.7.** X-ray diffraction pattern of clay sediment fraction from the sedimentation pond sampling site. Diffraction peaks are labeled with their corresponding clays and minerals.

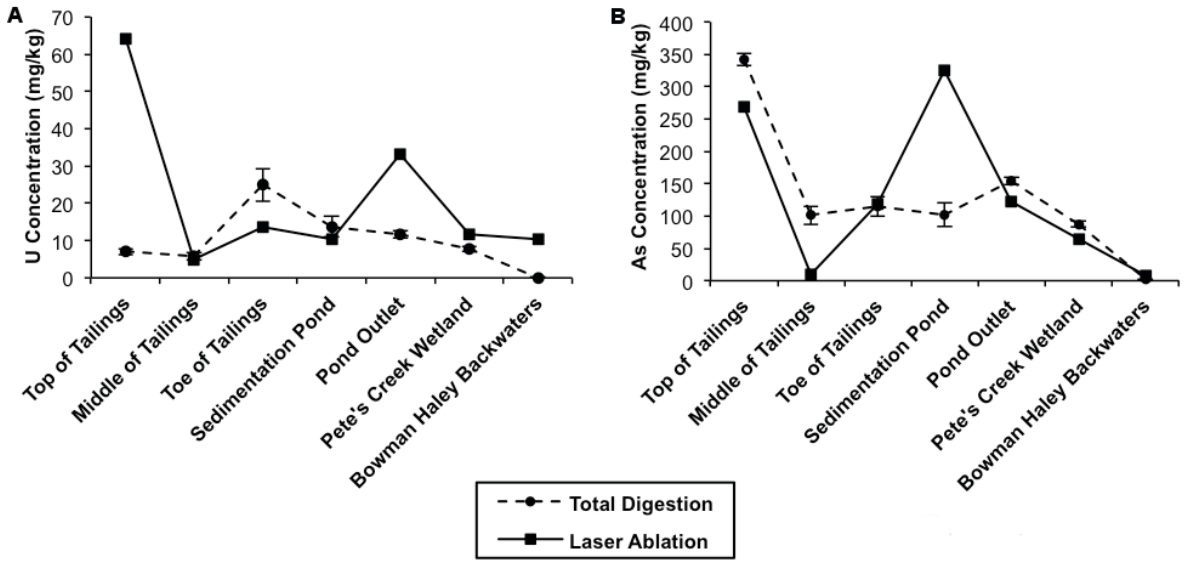


**Figure 2.8.** Total concentrations of solid phase uranium (a) and arsenic (b) in the top 0-5 cm of sediment cores as determined by total digestions analyzed by ICP-MS (dotted lines) and by laser ablation ICP-MS (solid lines). Error bars on the total digest values indicate one standard deviation from the average of triplicate digests.

by promoting U reduction of dissolved U(VI) species to insoluble uraninite or to biomass-associated molecular U(IV) (Figure 2). (*53*, *55*) The redox conditions of the pond promote microbial reduction of uranyl to insoluble uraninite that would settle to the bottom of the pond and not be transported. (*19*) Alternatively molecular U(IV) associated with biomass may form on sediments which would also settle to the bottom of the pond. (*53*) Sediment sulfur concentrations (measured by Larson, et al.) and sediment Fe concentrations in the pond could allow for the precipitation of amorphous FeS, following microbial reduction of sulfate and Fe(III) oxy (hydr)oxides, which can abiotically reduce uranyl to uraninite or non-uraninite U(IV). (*48*, *53*, *55*, *61*, *92*) Because of the low environmental sediment U concentrations, U XANES spectra were only obtained for the top of the tailings, toe of the tailings, pond, and pond outlet (Figure 2.9, Figure 2.10, Table 2.4). Of the collected spectra, the U XANES spectrum from the pond outlet was fit with the greatest percentage of U(IV) (45.1%). Similar to the reduced Fe observed at the outlet, the presence of U(IV) at the outlet supports that uranium reduction is occurring in the pond and uraninite or biomass-associated molecular U(IV) is settling out at the outlet. The greater concentration of sediment U determined by laser-ablation ICP-MS than by total digestion at the pond outlet also supports the presence of heterogeneously distributed mineralized U(IV) or mineral associated U(VI). Although U(IV) forms can be oxidized to soluble U(VI) with exposure to oxygen, U(IV) is likely to remain stable in the pond because oxygen exposure would not occur without significant mixing of the pond water.

The distribution of uranium in soils as determined by sequential extractions (Figure 2.11) shows little difference between sites of differing redox conditions, indicating that uranium may be transported down gradient of the sedimentation pond mainly as sediment-associated uranium rather than as dissolved U(VI). Sequential extractions show that U is primarily associated with

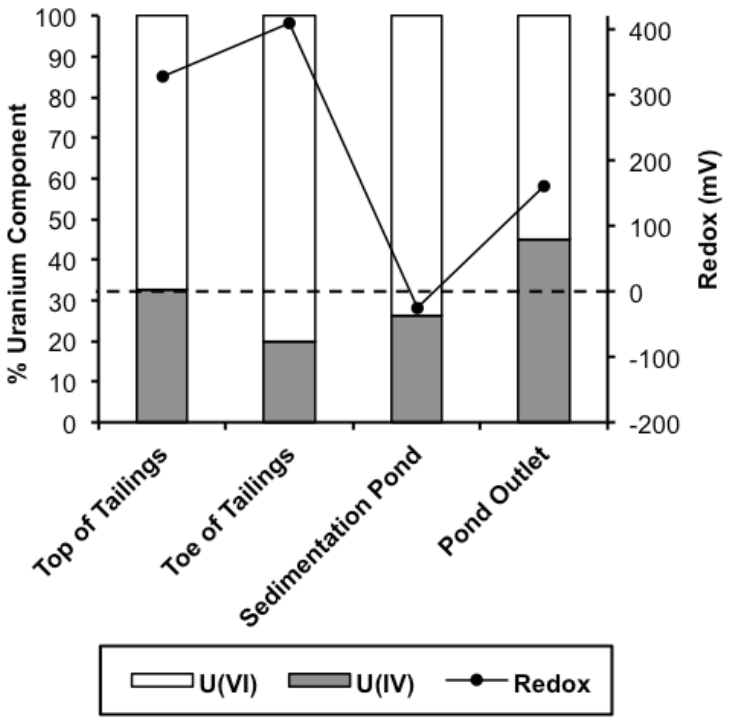


**Figure 2.9.** Uranium speciation as determined by linear-combination fitting of uranium XANES spectra of sediments collected 0-5 cm from the surface. Spectra were fit with the following 2 reference compounds—uranyl acetate (white) and uraninite (gray). Components are plotted as percent of the total, with approximately 5% error. The line indicates field ORP measurements taken at a depth of 0-5 cm from the surface during field sampling

**Table 2.4.** Summary of U XANES linear-combination fitting.

| Location Name | % Uraninite* | % Uranyl Acetate* | R factor |
|---|---|---|---|
| Top of the Tailings | 32.5 | 67.5 | 0.003771 |
| Middle of the Tailings | — | — | — |
| Toe of the Tailings | 19.7 | 80.3 | 0.001874 |
| Sedimentation Pond | 26.4 | 73.6 | 0.001293 |
| Pond Outlet | 45.1 | 54.9 | 0.000481 |
| Pete's Creek Wetland | — | — | — |
| Bowman-Haley Backwaters | — | — | — |

*Components represent reference compounds used for linear-combination fitting, not exact identification of U(IV) and U(VI) forms present.

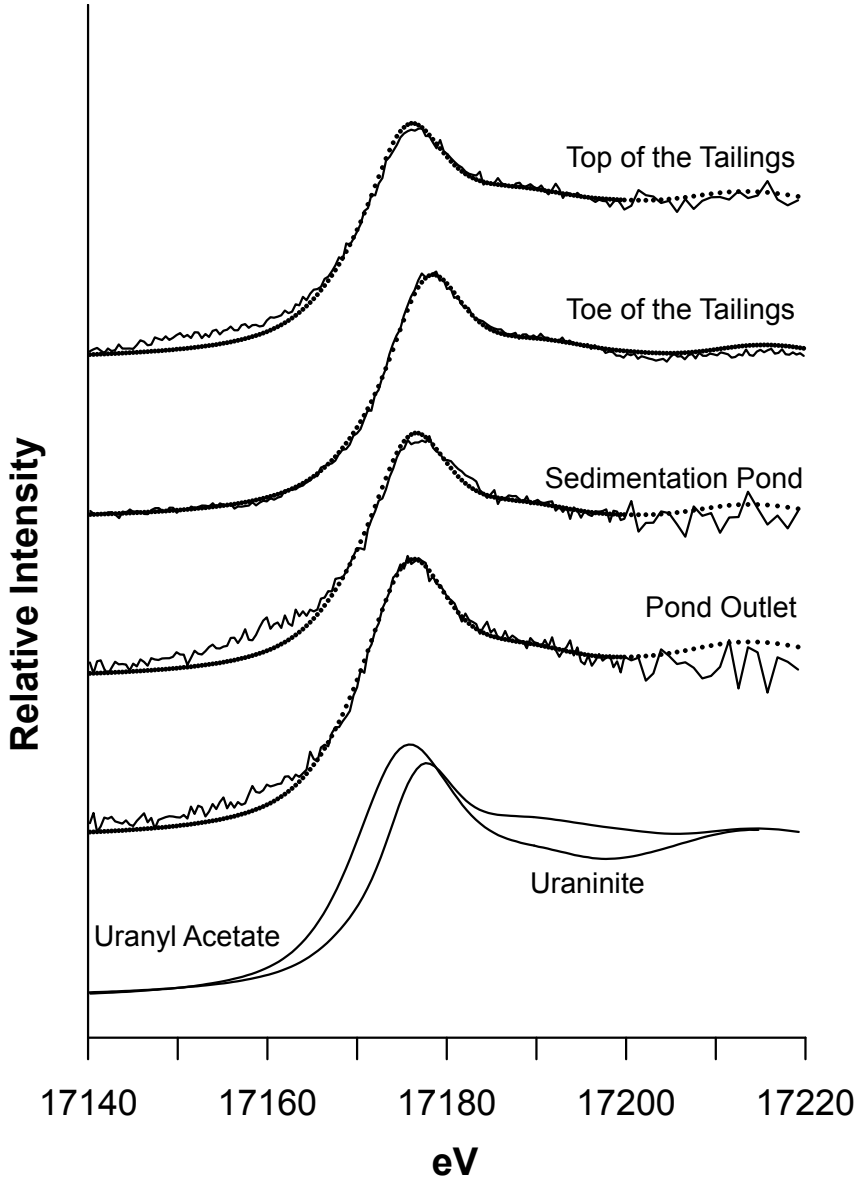


**Figure 2.10.** Linear-combination fits (dots) of uranium XANES spectra (solid lines) from the top of the tailings pile, toe of the tailings, sedimentation pond, and the pond outlet. The reference compounds used in fitting are plotted at the bottom for comparison.

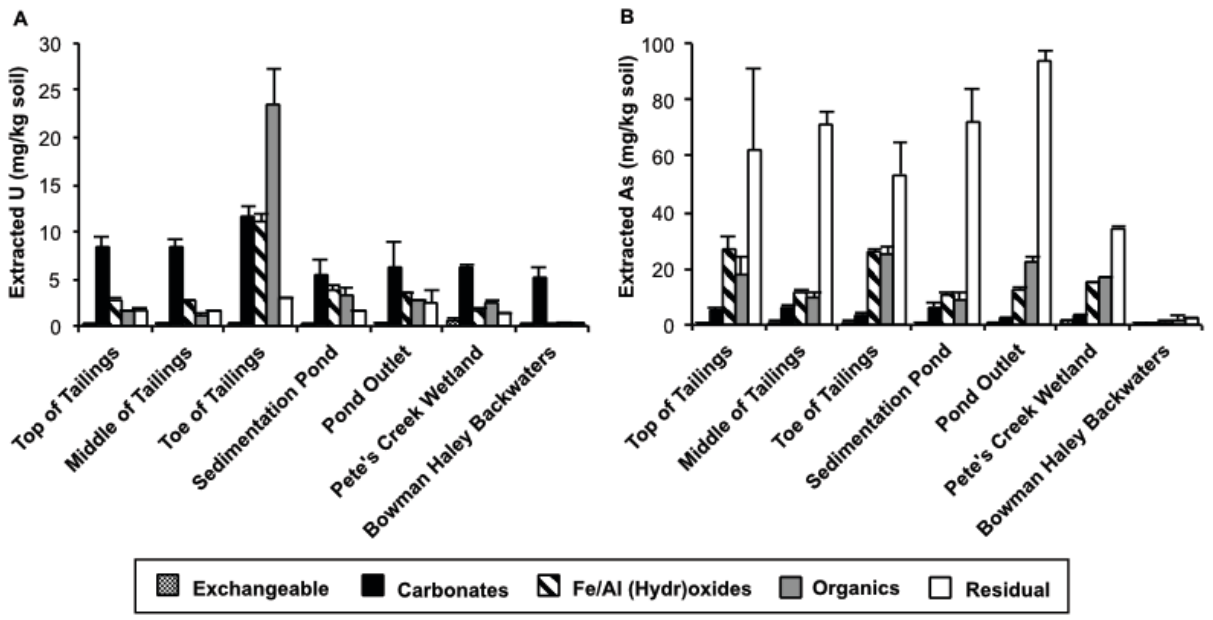


**Figure 2.11.** Sequential extractions of sediment-associated A) uranium and B) arsenic determined by the method described in Salome et al., 2013. Bars indicate concentration of uranium and arsenic associated with each fraction. Error bars indicate one standard deviation from the mean of triplicate extractions.

the carbonate and phosphate mineral (acid extractable) fraction of sediment at all of the sampling locations except for the toe of the tailings (Figure 2.11a). Based on the carbonate concentration and pH of North Cave Hills surface waters, U is most likely associated with carbonate rather than phosphate, including carbonate minerals such as calcite and aragonite. (*84*) U in the carbonate mineral fraction is likely incorporated into carbonate minerals in source materials and would not be released down gradient of the pond because calcite and aragonite have low solubility under the neutral to basic pH conditions of the sampling locations. (*1, 93*) Aqueous U concentrations in surface waters (in Larson, et al.) support the lack of solubilized U at down gradient sites, with a U concentration 2 times background level (32.7 µg/L) measured at Pete's Creek wetland and a below background level concentration (5.14 µg/L) measured at the

Bowman-Haley backwaters during summer sampling.(*48*) Aqueous U(VI) is expected to adsorb preferentially to amorphous iron oxides in sediments rather than to carbonate minerals.(*1*) At the top of the tailings, the pond, and the pond outlet, the amount of U associated with the iron mineral fraction increases from the top and middle of the tailings pile which could indicate that aqueous U(VI) is adsorbed to iron oxy(hydr)oxides at those sites. (*8, 94*) The sodium acetate fraction (iron mineral-associated fraction) of the Tessier et al. method has also been shown to extract U(IV), so increased U extracted in iron mineral fraction may also support the presence of U(IV) in the pond and at its outlet. (*84, 95*)

***Geochemical Controls on As Transport***

Total As in sediments at the site does not simply decrease with distance from the tailings pile, indicating that As transport is controlled by chemical processes in addition to physical processes (Figure 2.3). Sediment As concentrations measured by total digestion are similar for near-source sites including the tailings pile, the pond, and its outlet, ranging between 101 and 155 mg/kg, with the exception of the top of the tailings pile (Figure 2.3). The sediment As concentration at the top of the tailings pile was 346 mg/kg. Surface sediment concentrations are likely high at this sampling site because of the presence of As-containing minerals that were brought to the surface during mining activity. The second highest As sediment concentration of the sampling locations as measured by total digestion is at the pond outlet (155 mg/kg). Similar to the U sediment concentrations, As sediment concentrations were measured by both total digestion and laser ablation. Sediment As concentrations measured by the two methods follow the same trend by sampling location with the exception of the sedimentation pond (Figure 2.8b). The As concentration in the pond was greater when measured by laser ablation (324 mg/kg) than by total digestion (102 mg/kg). This is likely due to heterogeneous distribution of As in the pond.

Of the sites sampled in Larson, et al., surface water As concentrations were highest in the pond (1260 µg/L). (*48*)

Reductive dissolution of Fe oxy (hydr)oxides promotes the release of adsorbed As and likely occurs under the reducing conditions of the sedimentation pond, resulting in high aqueous As concentrations in the pond and high sediment As concentrations at the outlet. (*38*, *66*, *96*) The high fraction of amorphous Fe measured at the pond outlet (Figure 2.4) supports that reductive dissolution occurs in the pond. Because As(III) is more readily desorbed from Fe oxides than As(V), release of As may also occur upon microbial reduction of As(V) to As(III) under the reducing conditions of the pond. (*29*, *38*, *66*) Larson, et al. found the As in sediment pore water at the sedimentation pond to be 55-93% As(III) during summer sampling, supporting that microbial reduction and release from sediment is taking place. (*48*) Arsenic mobilized in the pond is transported to down gradient locations where it is immobilized in oxic zones as As(III) is oxidized to As(V) and adsorption to soil minerals occurs. (*29*) Downstream of the tailings pile by 2 km, the Pete's Creek wetland site has an As concentration of 87 mg/kg, suggesting that transport is limited past the pond. Surface water As concentrations are also lower at the Pete's Creek wetland site than at the pond (577 µg/L). (*48*) At the Bowman-Haley backwaters site, the sediment As concentration is 2 mg/kg which is below the mean background level of 26 mg/kg established by Stone, et al. (*41*) In addition, no detectable As was measured in surface water samples at the backwaters site. (*48*)

The results of the Huang and Kretschzmar sequential extraction method indicate that As is primarily found associated with the poorly crystalline Fe and Al oxide fraction (ligand-promoted dissolution fraction) for all of the sampling sites with 45 to 80% of total As present in that fraction (Figure 2.12). (*82*) This fraction may also include amorphous clay minerals, but

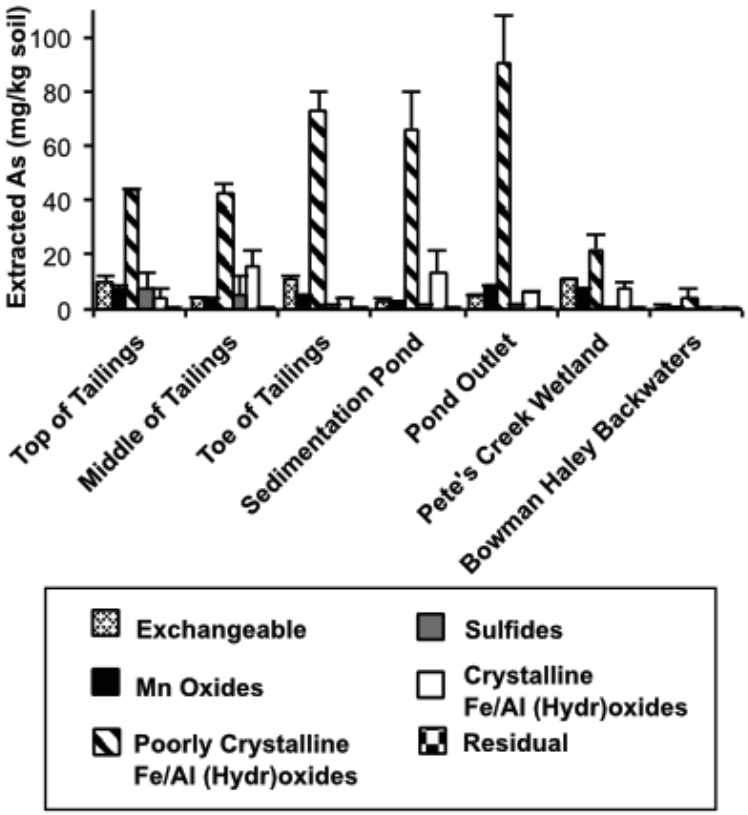


**Figure 2.12.** Sequential extractions of sediment-associated arsenic obtained according to the methodology developed by Huang and Kretzschmar, 2010. Bars indicate concentration of arsenic associated with each fraction. Error bars indicate one standard deviation from the mean of triplicate extractions.

XRD of the material remaining after each extraction step would need to be performed in order to determine with certainty if clay minerals were dissolved. (*82*) The other method of extraction based on Tessier et al. shows that As is primarily associated with the residual fraction (38-80%), which includes phyllosilicates (clays) and inosilicates (Figure 2.11b). (*84*) This result indicates that As may be present at the sampling sites associated with clay minerals. While clay minerals have a lower affinity for As(III) and As(V) than Fe oxy(hydr)oxides, they are the dominant Fe-bearing minerals present in North Cave Hills soils according to linear combination fitting of Fe

EXAFS spectra (Figure 2.6, Figure 2.5, Table 2.3). (*97*) Adsorption of As to clays at the pond outlet may prevent down gradient As transport because complete desorption of As from clay minerals is not shown to occur under the pH conditions of the North Cave Hills. (*97*)

An As-sulfide mineral phase (orpiment) was found to be present at the top of the tailings pile as determined by As XANES linear-combination fitting, which implies that As minerals were brought to the surface during mining (Figure 2.13, Table 2.5). These As-bearing minerals release As to down gradient areas during weathering or oxidative dissolution at the site's near-neutral pH conditions. (*98, 99*) In addition to the top of the tailings, fits of As XANES spectra from Pete's Creek wetland and Bowman-Haley backwaters, both reduced sampling sites, were improved when orpiment ($As_2S_3$) was included as a reference compound (Figure 2.13, Table 2.4). Larson, et al. determined that formation of orpiment is thermodynamically favorable at the reduced areas surrounding the North Cave Hills based on dissolved As(III) and $SO_4^{2-}$ concentrations at the Bowman-Haley outlet. (*48*) Newman, et al. found that precipitation of As(III)-sulfides occurs following As(V) and $SO_4^{2-}$ reduction, both of which are likely to take place under the redox conditions of the sites. (*100*) As(III)-sulfides can also form after adsorbed As(III) is incorporated into the structure of precipitated metal-sulfides. (*101*) Pete's Creek wetland and Bowman-Haley backwaters have the highest percentage of As(III) of the sampling sites (60-70%), so incorporation may take place (Figure 2.13, Figure 2.14, Table 2.4). There is no direct evidence for the presence of metal sulfides at the sites, but the sediment sulfur concentrations in Larson, et al. were highest at the Bowman-Haley backwaters site. (*48*) Although the As XANES spectra were best fit with an orpiment reference, the specific As(III)-sulfide mineral could not be identified conclusively without EXAFS information. However,

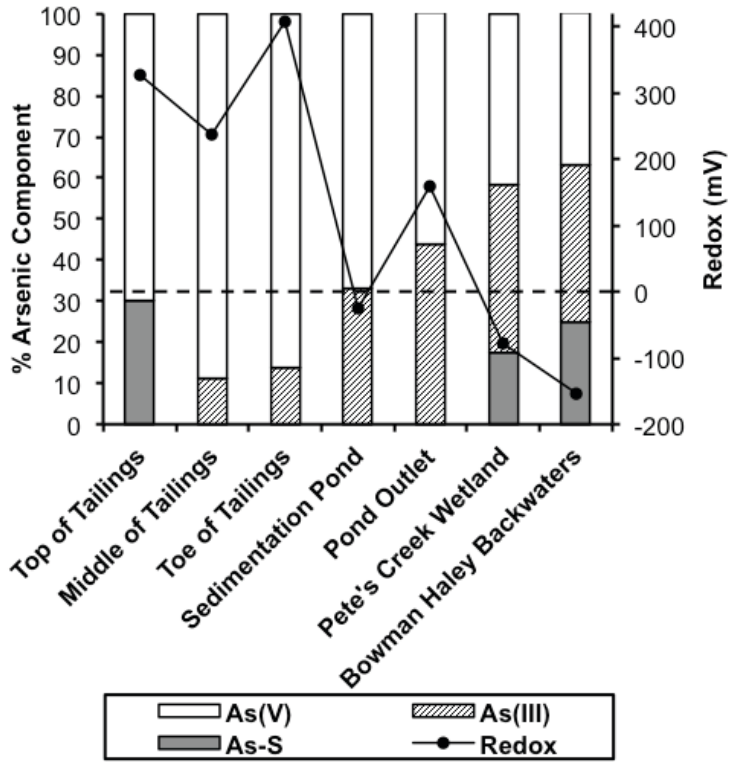


**Figure 2.13.** Arsenic speciation as determined by linear-combination fitting of arsenic XANES spectra of sediments collected 0-5 cm from the surface. Spectra were fit with the following 3 reference compounds—arsenate adsorbed to ferrihydrite, arsenite adsorbed to ferrihydrite, and orpiment. The line indicates field ORP measurements taken at a depth of 0-5 cm from the surface during field sampling.

**Table 2.5.** Summary of As XANES linear-combination fitting. The R factor is the normalized sum of the difference between the model and the fit.

| Location Name | % Orpiment* | % As(III) adsorbed to goethite* | % As(V) adsorbed to goethite* | R factor |
|---|---|---|---|---|
| Top of the Tailings | 30.1 | 0 | 69.9 | 0.014789 |
| Middle of the Tailings | 0 | 11.3 | 88.7 | 0.003969 |
| Toe of the Tailings | 0 | 13.8 | 86.2 | 0.002586 |
| Sedimentation Pond | 0 | 33.0 | 67.0 | 0.001037 |
| Pond Outlet | 0 | 43.8 | 56.3 | 0.001209 |
| Pete's Creek Wetland | 17.6 | 40.8 | 41.6 | 0.000903 |
| Bowman-Haley Backwaters | 25.0 | 38.3 | 36.8 | 0.006110 |

*Components represent reference compounds used for linear-combination fitting, not exact identification of As-S mineral, As(III), and As(V) forms present.

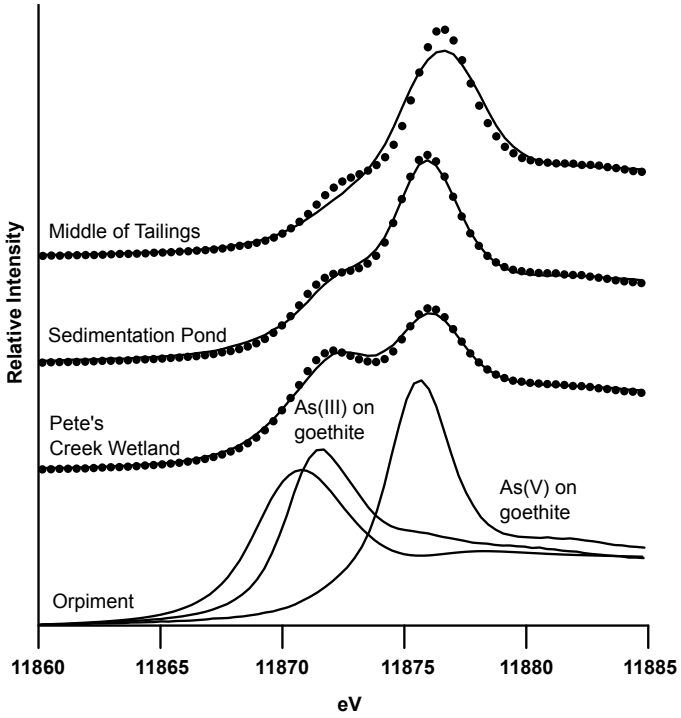


**Figure 2.14.** Linear-combination fits (dots) of arsenic XANES spectra (solid lines) from the middle of the tailings pile, sedimentation pond, and Pete's Creek wetland. The reference compounds used in fitting are plotted at the bottom for comparison.

EXAFS spectra could not be collected for these samples due to low environmental concentrations. Examples of As XANES data and fits can be seen in Figure 2.10.

**Environmental Implications**

The results of this study illustrate that a combination of wet chemical analysis, XRD, and X-ray absorption spectroscopy can be successfully applied to help elucidate major mechanisms controlling the fate and transport of U and As in complex natural systems such as abandoned mining sites. Here we show that sedimentation ponds used to prevent physical transport of U and As from mine tailings are likely to also result in reduction of U(VI) and As(V). Reduction of U(VI) to U(IV) will further limit down gradient transport of aqueous U. On the other hand,

As(V) reduction in the pond is clearly shown to promote aqueous transport of As(III) due to either reductive dissolution of Fe oxy(hydr)oxides, an important sorbent for As, or direct reduction of sorbed As(V) resulting in formation of aqueous As(III). Although As is mobilized within the sedimentation pond and accumulating at the pond outlet, sediment and surface water concentrations at the furthest (45 km) down gradient sampling site, the Bowman-Haley backwaters, are below background levels. (*48*) Our findings suggest that As was immobilized due to As(V) adsorption to clays or Fe oxy(hydr)oxides in oxic zones or mineralization of As(III) to As(III)-sulfides in anoxic zones such as within Pete's Creek wetland. In contrast, the U concentration did not vary much between the sedimentation pond and the down gradient sites. Although U was measured in sediments at two times background levels at the Bowman-Haley backwaters site by laser ablation ICP-MS, U does not pose a risk to human health at that level by any type of acute or chronic exposure. (*42*) In order to better elucidate the molecular structure and interactions between U and As, and with soil minerals, high quality EXAFS spectra are needed. However, this study shows that it can be very challenging to obtain bulk EXAFS spectra due to low (<100 ppm) environmental concentrations indicating that future studies should include micro-focused XAS techniques in order to obtain an improved understanding to further advance best managing practices or reclamation strategies for mine tailings. (*102*)

# CHAPTER 3

# IMPACT OF BIOSTIMULATION ON AS AND U REDOX CHEMISTRY IN MINE TAILINGS SEDIMENTS

[2]

## Introduction

Because reclamation was not required when U mining began, the transport of heavy metals and radionuclides from unreclaimed U mine and mill sites has resulted in contaminated surface and groundwater in addition to millions of cubic meters of contaminated tailings worldwide. (*3*) Stimulation of microbial activity in contaminated sediments has been used to immobilize heavy metals and radionuclides in order to prevent their transport. (*103*) For U in particular, biostimulation is used to reduce soluble U(VI) and immobilize it as uraninite ($U^{IV}O_2$). Uraninite formation can occur by direct enzymatic reduction of U(VI) by iron and sulfate-reducing bacteria (*19, 62, 104-106*) or by indirect reduction by sulfide (*15, 107*) or adsorbed or structural Fe(II) (*13, 14, 59, 92, 108-115*). Reactive Fe(II) sulfide mineral phases such as pyrite ($Fe_2S$) and mackinawite (FeS) can form in biostimulated systems and abiotically reduce U(VI). (*16, 55, 60, 61, 116-119*) The reduction of U(VI) has been widely studied in natural U-contaminated sediments in microcosms (*120-126*), column systems (*53, 127-129*), and in field studies. (*130-133*) In order to stimulate microbial activity, electron donors (i.e. ethanol, acetate, lactate, glucose) are added to sediments, often promoting the growth of a specific microbial community depending on the selected donor. While studies have examined the shifts in microbial

[2] Standards used for linear combination fitting of X-ray absorption spectra were provided by Dr. John R. Bargar, Dr. Juan S. Lezama-Pacheco, and by Robert T. Downs and the RRUFF library. All work presented in this chapter was carried out by primarily by me with the exception of sequential extractions performed by Dr. Rong Wei. Special thanks to collaborators—Dr. James J. Stone, Dr. Juan S. Lezama-Pacheco, and Dr. John R. Bargar.

communities upon electron donor addition, few have studied how specific electron donors affect the extent of U(VI) reduction in biostimulated sediments. (*134-137*)

Uranium and As are commonly found together at sites of historic U mining or milling because As occurs naturally in U ore up to 10 weight percent. (*3*) The simultaneous remediation of U and As poses a challenge because of the difference in U and As mobility under similar redox conditions. As previously discussed, U can be immobilized as uraninite—a reduced form of U. In addition to producing long-range ordered, crystalline uraninite, some biostimulation experiments have observed that reduction of U(VI) can result in nanocrystalline $UO_2$ and molecular U(IV) which may have different implications for the mobility of reduced U. (*23*, *53*, *138*) While U(IV) is the less mobile form of U, As tends to be more mobile as its reduced form (As(III)). When present in its oxidized form (As(V)), As readily absorbs to mineral surfaces under environmental pH. (*37*, *38*) Although U and As are common co-contaminants, no laboratory studies have examined both As and U redox behavior together in sediments. When the aqueous or sediment concentrations of As have been measured over time in biostimulation experiments, studies suggest that As release may occur during U bioremediation. (*45*, *124*)

When present together, U and As can also interact with one another in their oxidized forms. Arsenate (As(V)), which can serve as an analog for phosphate, may form ternary complexes with uranyl (U(VI)) on the surface of Fe oxy(hydr)oxides present in soils. (*24*, *25*, *139*) Arsenic and U can also form uranyl arsenate aqueous complexes or mineral precipitates, such as trögerite ($UO_2HAsO_4 \cdot 4H_2O$), depending upon their concentrations and solution pH. (*67*, *68*, *140*) Little is known about how As and U affect the mobility of one another or how redox changes affect the stability of uranyl arsenate minerals.

The North Cave Hills in Harding County, South Dakota is a site of historic U open-pit

mining. Both physical and chemical transport of As and U at this site have been previously characterized. (*40, 48, 141*) Arsenic has been shown to be mobilized from sediments in anoxic zones down gradient from the tailings pile, while U transport from these anoxic zones is limited. In addition to these findings, Larson et al has shown that As and U mobility differs with seasonal changes in precipitation and environmental redox conditions. While previous studies have examined the behavior of As and U in the field, this work will examine their behavior in field sediments under a controlled laboratory environment. The goal of this work was to examine how changes in redox chemistry affect speciation of As and U present in North Cave Hills sediments in order to understand the mobility and fate of As and U when present in a system together. A secondary goal of the experiment was to compare the extent of As and U reduction in the presence ethanol, acetate, and lactate—three common electron donors used in the biostimulation of native bacteria in sediments.

## Materials and Methods

### *Field sample collection*

The sediment used in the batch experiments was collected from a sedimentation pond at the base of the North Cave Hills mine tailings. A soil core was collected using a stainless steel soil corer lined with a polyethylene tube approximately 30 cm long. The sediment core was then stored on ice and transported to an anaerobic chamber in the laboratory. The 30 cm sediment cores were homogenized and then frozen for long-term storage.

### *Batch experiments*

The composition of synthetic surface water (SSW) was based upon the average concentration of ions in North Cave Hills surface waters and prepared using a protocol described by Smith, et al. (*142*) The concentrations of each chemical in the final SSW are shown in Table

**Table 3.1.** The composition of the synthetic surface water used as the media in the batch experiments. Concentrations were based on concentrations of sampled surface water from locations surrounding the North Cave Hills.

| Chemical | mM |
|---|---|
| $MgSO_4$ | 1.07 |
| $CaCl_2 \cdot 2H_2O$ | 0.0257 |
| $Ca(NO_3)_2 \cdot 4H_2O$ | 0.00600 |
| $CaCO_3$ | 0.506 |
| $KHCO_3$ | 0.783 |
| $Na_2SO_4$ | 1.12 |
| $NaHCO_3$ | 1.76 |

3.1. All batch experiments were conducted in 125 mL crimp-sealed serum bottles. Individual stock solutions were prepared of 16.8 mM uranyl acetate, 16.8 mM sodium arsenate ($Na_2HAsO_4 \cdot 7H_2O$), 1 M sodium acetate, 1 M sodium lactate, 1 M ethanol, and 10 mM ammonium chloride ($NH_4Cl$) in DDI water. All stock solutions were filter sterilized (Nalgene 0.2 µm sterile Nylon) into autoclaved bottles and purged overnight with ultra high purity $N_2$ and then transferred into an anaerobic chamber. The concentration of ammonium chloride added to batch experiments was based on the concentration used in Jeon et al. (*143*) Prior to the set up of the individual serum bottles, the thawed sediment was incubated in four 500 mL bottles at a concentration of 100 g/L in an anaerobic chamber including three bottles containing 10 mM sodium lactate, sodium acetate, or ethanol each, and one bottle without added electron donor. Bottles were stirred continuously for 7 days in order to encourage growth of native bacteria. The resulting aqueous phase of the microbial incubations was decanted into a new bottle. Eight replicate serum bottles were prepared anoxically with final concentrations of 10 g/L of thawed

sediment, 10 mM sodium acetate, sodium lactate or ethanol, 5 mL of the appropriate microbial incubation, and 100 μM $NH_4Cl$. All bottles were filled with purged SSW to a total volume of 100 mL. Six replicate serum bottles were prepared anoxically for sterile systems containing 10 g/L autoclaved thawed sediment, 5 mL of autoclaved microbial incubation without electron donor, and 100 μM $NH_4Cl$. All serum bottles were crimp-sealed and removed from the anaerobic chamber in order to be placed on a table shaker. Bottles were returned to the anoxic chamber for sampling and were sampled upon initial setup and every four days (1 mL) by syringe and filtered (VWR 0.2 μm Nylon) in the anaerobic chamber. After 4 days of reaction time, sodium arsenate and uranyl acetate stock solutions were added to each bottle to a final concentration of 168 μM in order to allow the bacterial community time to acclimate before the As(V) and U(VI) additions. One mL samples were also taken immediately following the sodium arsenate and uranyl acetate additions. Bottles were vacuum filtered (Acetate Plus 5 μm) after 5 days of reaction immediately following U and As addition and after 44 days of reaction. The sediment from each bottle was dried in the anaerobic chamber. If replicate bottles were filtered at the same time, sediment was homogenized for analysis using a mortar and pestle. One bottle from the eight replicates was filtered on day five—24 hours after the sodium arsenate or uranyl acetate addition. Three bottles from each treatment were filtered after 44 days of reaction time. In systems that initially did not contain any uranyl acetate, 168 μM uranyl acetate was added to four bottles on day 44 and then allowed to react for an additional 48 hours before two of them were filtered. This additional experiment was performed because of the lack of change over the 44 day period observed in bottles that initially contained U(VI). Oxidation experiments were performed on the remaining two bottles by opening them up to air and placing them back on the shaker plugged with cotton stoppers. The final two bottles were then filtered following 24 hours open to

air. The batch sample used for Fe EXAFS was taken from three serum bottles containing ethanol as electron donor. These bottles was allowed to react for 60 days rather than the 44 day time period to ensure that changes in Fe mineralogy were detectable by bulk Fe K-edge EXAFS.

***Aqueous analysis***

The aqueous samples that were taken every 4 days were analyzed for several different analytes. Dissolved Fe(II) concentrations were measured using the ferrozine method and an Eon Biotek microplate reader. (*144*) Acetate and sulfate concentrations over time were determined by ion chromatography (Dionex ICS-2100). Total As and U concentrations were measured using an inductively coupled plasma mass spectrometer (ICP-MS) (Perkin Elmer Elan DRC II). Fe sequential extractions were also performed on selected filtered sediments based on the method described in Roden, et al. (*145*) Adsorbed Fe(II) and Fe(III) were extracted using 1 M sodium acetate. Amorphous Fe(II) and Fe(III) were extracted using a pH 3 ammonium oxalate solution. Total crystalline Fe was extracted using a pH 4.8 solution of sodium citrate with the addition of sodium dithionite. All extracts were analyzed for Fe using the Ferrozine method. (*144*)

***X-ray absorption spectroscopy***

Samples were analyzed at the Stanford Synchrotron Radiation Lightsource (SSRL) in Menlo Park, CA. All preparation of anoxic filtered sediment samples took place in an anaerobic chamber. Samples were placed into a Teflon holder surrounded by Kapton polyimide film to prevent oxidation while minimizing X-ray absorption. Extended X-ray absorption fine structure (EXAFS) spectroscopy was used to characterize Fe mineralogy before and after reaction. Fe EXAFS collection was performed at beamline 4-1 (20-pole wiggler) at SSRL. The ring operates at 3 GeV with a current of 450 mA. Energy selection is accomplished with a Si (220) monochromator with spectra recorded in fluorescence mode using a 13-channel Ge detector.

EXAFS spectra are collected from -200 to +1000 eV around the K-edge of Fe. EXAFS and X-ray absorption near-edge structure spectroscopy (XANES) were collected for As and U in order to determine As and U speciation and binding environment. As and U XAS were collected at beamline 13-BM-D at the Advanced Photon Source (APS) in Argonne, IL. The ring at APS operates at 7 GeV with a current of 100 mA. Energies were selected with a Si (111) monochromator. All spectra collected at the APS were collected in fluorescence mode using a 12-channel Ge detector. Arsenic K-edge spectra were collected from -200 to +1000 eV around edge energy (11,867 eV). Uranium $L_{III}$-edge spectra were collected from -250 to +1000 eV around the edge energy (17,167 eV). Between 2 and 3 spectra are averaged for each sample. Reference compounds are used to perform linear combination XANES and $k^3$-weighted EXAFS spectral fitting using Athena interface to IFEFFIT. (*87*, *146*) Iron reference compounds included unreacted sediment from the North Cave Hills sedimentation pond and synthesized mackinawite anoxically aged for three weeks and provided by Bostick. (*147*) Arsenic reference compounds included orpiment ($As_2S_3$) obtained from the RRUFF database at University of Arizona Mineral Museum and originally from Mercur, Utah and As(V) and As(III) adsorbed to goethite (Bayferrox 920 Z, LANXESS Deutschland GmbH, Leverkusen, Germany). (*86*) Uranium reference compounds included U(VI) adsorbed to ferrihydrite and biogenic nanoparticulate $UO_2$. (*88*) Compounds are only included in the fit if the contribution is a fraction greater than 0.05. Fits are within about ±5% of the mole percentages of fractions for As LCF of XANES and within about ±10% for U LCF of XANES and were fit from -20 to +30 eV from the edge. (*128*, *148*)

## Results

### *Aqueous concentrations*

#### *Fe(II) concentrations*

Aqueous Fe(II) concentrations were followed throughout the course of the experiment to serve as an indicator of when reductive dissolution of Fe(III) oxy(hydr)oxides began to take place. An increase in Fe(II) concentrations was observed in all treatments. In systems with As(V) (Figure 3.1a) and no added As(V) or U(VI) (Figure 3.2a), Fe(II) concentrations increased from 0 μM Fe(II) at the start of the experiment to 200-500 μM Fe(II) after 8-12 days of reaction. In these treatments, Fe(II) concentrations then began to decrease in the bottles containing acetate and lactate on day 16-20 and continued to decrease to below detection limits by day 20-24. No decrease in Fe(II) concentrations was observed in bottles containing ethanol. Instead, Fe(II) concentrations remained steady at ~200 μM in the As(V)-containing systems and at ~500 μM in the U(VI)-containing systems throughout the course of the experiment. In contrast to the systems without U(VI), systems containing U(VI) (Figure 3.3a and 3.4b) behaved similarly in the beginning of the experiment but no decrease in Fe(II) concentrations was observed until the end of the experiment at day 44. In comparing electron donors, the highest Fe(II) concentrations were observed in ethanol-containing systems with all combinations of As(V) and U(VI), while the lowest Fe(II) concentrations were consistently observed in the acetate-containing systems.

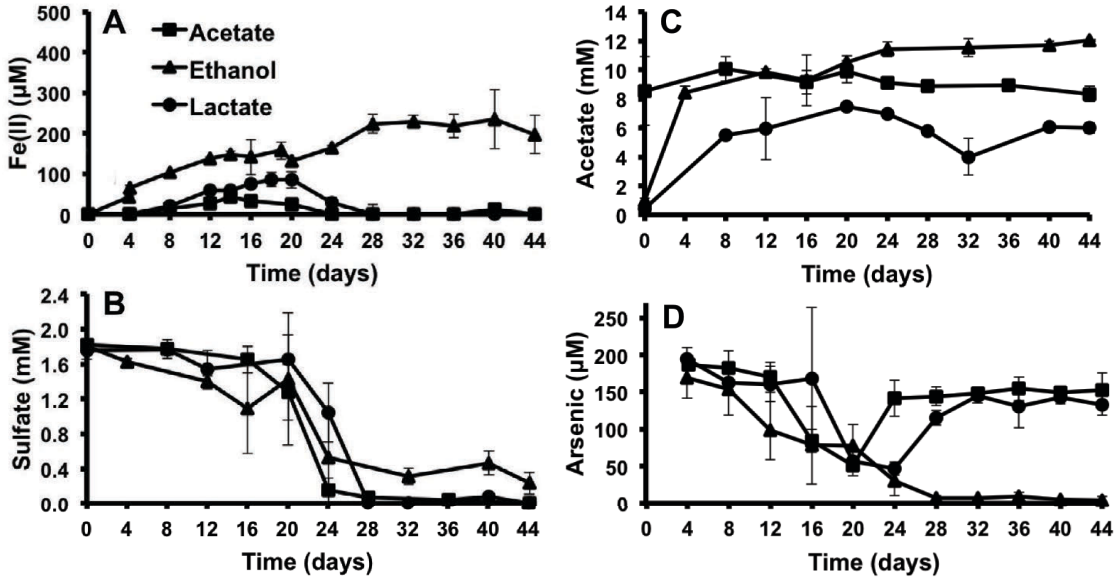


**Figure 3.1.** Aqueous concentrations of Fe(II) (a), sulfate (b), acetate (c), and As (d) in systems containing As. Bottles contained a synthetic surface water prepared to simulate the surface water composition at the North Cave Hills, 168 μM As(V), 10 mM of electron donor (ethanol, acetate, or lactate), and 10 g/L North Cave Hills soil. Aqueous concentrations of each analyte were measured every four days for 44 days. Error bars indicate one standard deviation from an average of a minimum of three replicates.

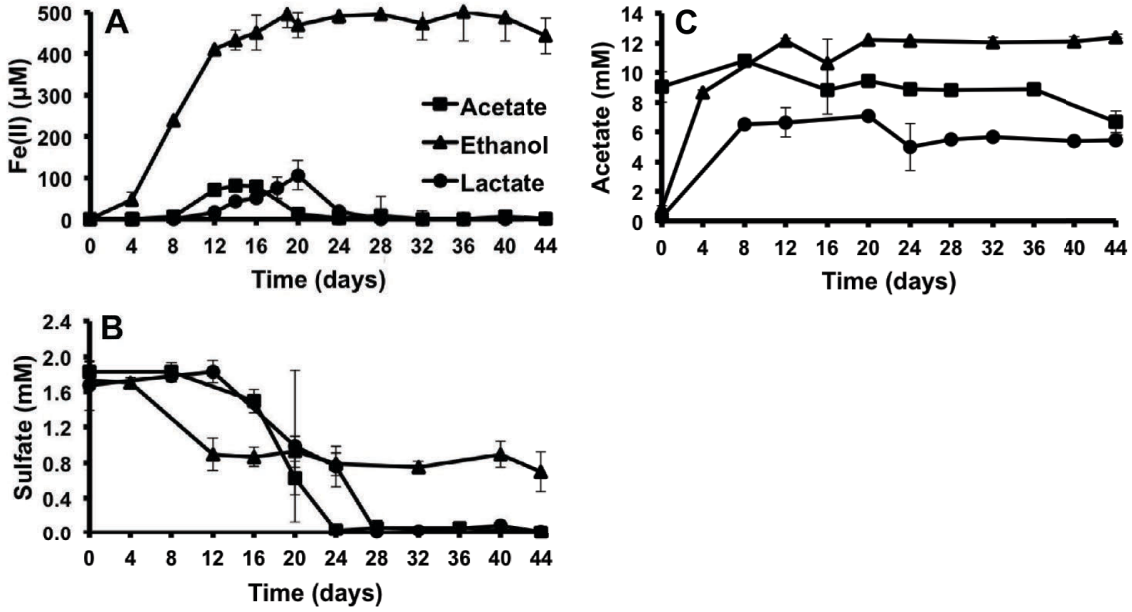


**Figure 3.2.** Aqueous concentrations of Fe(II) (a), sulfate (b), and acetate (c) in systems. Bottles contained synthetic surface water prepared to simulate the surface water composition at the North Cave Hills, 10 mM of electron donor (ethanol, acetate, or lactate), and 10 g/L North Cave Hills soil. Concentrations of aqueous analytes were measured every four days for 44 days. Error bars indicate one standard deviation from an average of a minimum of three replicates.

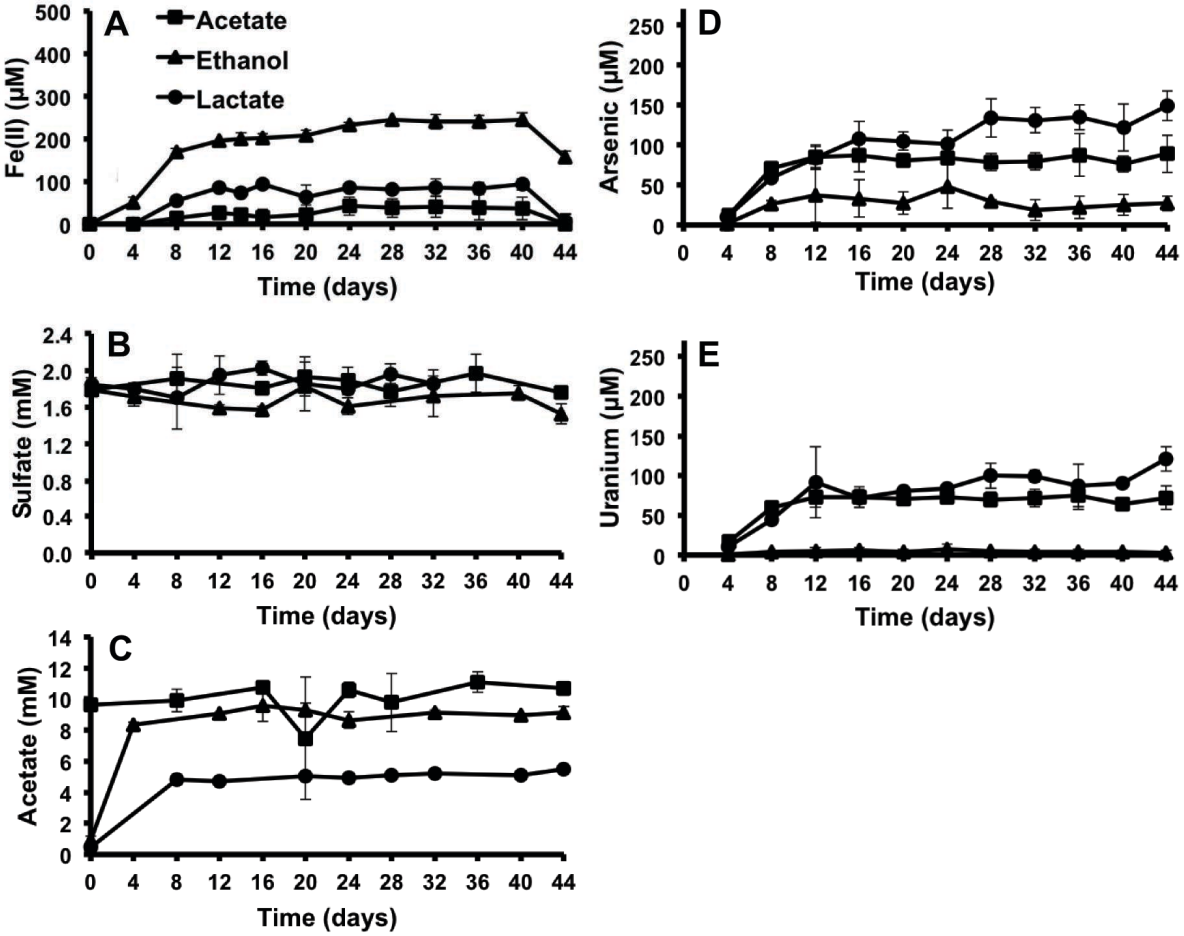


.

**Figure 3.3.** Aqueous concentrations of Fe(II) (a), sulfate (b), acetate (c), As (d), and D (e) in systems containing U and As. Bottles contained a synthetic surface water prepared to simulate the surface water composition at the North Cave Hills, 168 μM U(VI), 168 μM As(V), 10 mM of electron donor (ethanol, acetate, or lactate), and 10 g/L North Cave Hills soil. Concentrations of aqueous analytes were measured every four days for 44 days. Error bars indicate one standard deviation from an average of a minimum of three replicates.

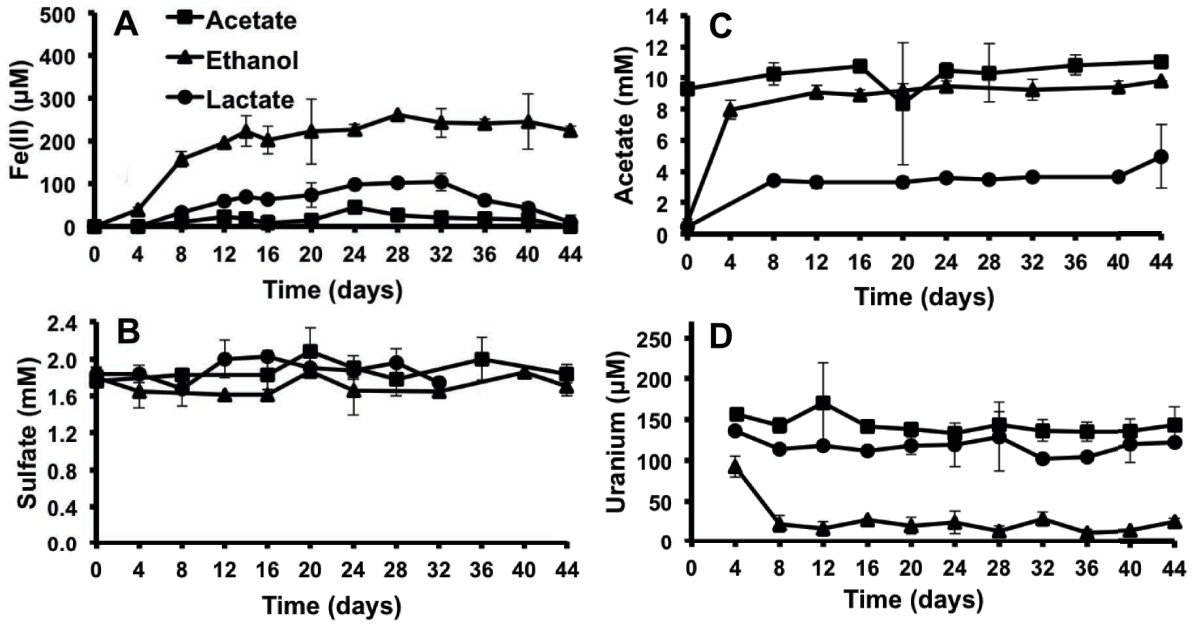


**Figure 3.4.** Aqueous concentrations of Fe(II) (a), sulfate (b), acetate (c), and As (d) in systems containing U. Bottles contained a synthetic surface water prepared to simulate the surface water composition at the North Cave Hills, 168 µM U(VI), 10 mM of electron donor (ethanol, acetate, or lactate), and 10 g/L North Cave Hills soil. Concentrations of each aqueous analyte were measured every four days for 44 days. Error bars indicate one standard deviation from an average of a minimum of three replicates

*Sulfate concentrations*

Aqueous sulfate concentrations were monitored throughout the course of the experiment to indicate microbial reduction of sulfate to sulfide. All systems initially contained 2.0 mM aqueous sulfate from the synthetic surface water medium. In systems without U(VI) (Figures 3.1b and 3.2b), sulfate concentrations began to sharply decrease around day 20 and continued to drop below detection limits by day 24-28. The only exception to this behavior was observed in the ethanol system without As(V) or U(VI) where the sulfate concentration remained at ~0.8 mM from day 12 to day 44. In all systems containing U(VI) (Figures 3.3b and 3.4b), the sharp decrease in sulfate concentrations was not observed. Instead, sulfate concentrations remained

around 1.8 mM throughout the experiment.

*Electron donor concentration*

The consumption of electron donors was monitored over time by measuring the concentration of acetate in each bottle. In all systems where acetate was used as an electron donor, acetate concentrations remained steady throughout the course of the experiment. The exception to this observation was the treatment without As(V) and U(VI) (Figure 3.2c) where a steady decrease in acetate concentration was observed from 10 mM to 6.7 mM by the end of the 44 day period. In systems containing ethanol as an electron donor, acetate concentrations increased from 0 mM to ~8 mM in the first 4 days of reaction and reached up to 12 mM by the end of the experiment. In all systems where lactate was provided as an electron donor, an increase in acetate concentration was also observed over time. In lactate-containing systems, acetate concentrations increased by day 8 and remained steady through the rest of the 44 day time period. In the systems containing As(V) (Figure 3.1c), a sharp decrease then increase in acetate concentrations was observed on day 28, while a similar dip was observed on day 24 in systems without As(V) or U(VI) (Figure 3.2c).

*Arsenic concentrations*

Total aqueous As concentrations were measured in treatments containing As(V). In systems without U(VI) (Figure 3.1d), aqueous As concentrations were measured to be 168 μM immediately following the As addition. Arsenic concentrations steadily decreased over the course of the 44 day period. In ethanol-containing treatments, As concentrations decreased below detection limits by day 28. While a decrease in As concentrations was observed in acetate and lactate-containing treatments from days 16-24, As concentrations decreased to 150 μM by day 44 in contrast to the ethanol treatments. In systems containing both As(V) and U(VI) (Figure

3.4d), As concentrations were below detection limits upon the initial addition of As(V) and U(VI), but increased to 27-150 μM over time depending upon the electron donor. The greatest increase was observed in acetate-containing systems and the smallest increase was observed in ethanol-containing systems. Following the 44 day time period, U(VI) was injected into bottles that had not previously contained U(VI). The aqueous As and U concentrations were monitored in these systems for 48 hours following the addition (46 days). In systems with As(V) and U(VI), As concentrations (Figure 3.5a) were observed to increase from day 44 to day 46 regardless of electron donor.

*Uranium concentrations*

Total aqueous U concentrations were measured in treatments that were injected with U(VI). In systems without As(V) (Figure 3.3d), each electron donor treatment had different measured initial U concentrations—156 μM in the acetate-containing systems, 136 μM in lactate-containing systems, and 92 μM in ethanol-containing systems. In the acetate and lactate containing systems, U concentrations remained constant during the 44 days, while the U concentration decreased to 22 μM in ethanol-containing systems. In systems containing both U(VI) and As(V) (Figure 3.4e), U concentrations were below detection for all electron donors following U(VI) and As(V) injection. Over time, U concentrations increased up to 91 μM in the lactate-containing systems and up to 73 μM in the acetate-containing systems, but remained below detection limit throughout the experiment in the ethanol-containing systems. In all systems where U(VI) was injected upon day 44, U concentrations (Figure 3.5b and 3.5c) decreased from day 44 to day 46. On day 46, bottles were opened to air and allowed to react for an additional 24 hours (47 total days). In bottles with both As(V) and U(VI), an increase in U concentration was observed in the lactate treatment, but not in with the other two electron

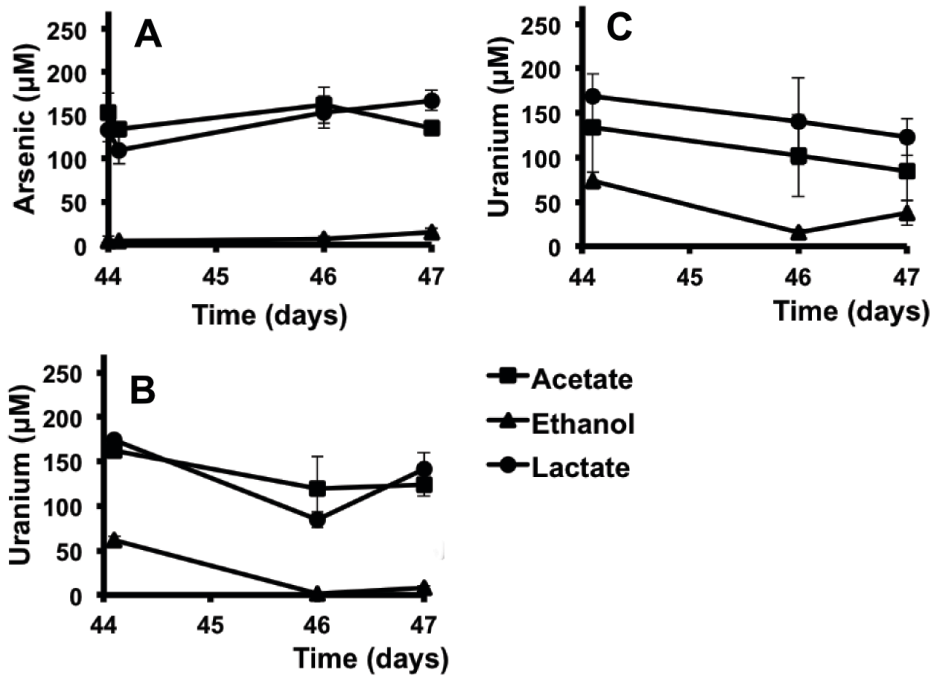


**Figure 3.5.** Aqueous concentrations of As and U in systems where U(VI) was added to As-containing system on day 44 (a and b) and in systems not containing either As or U where U(VI) was added on day 44 (c). Bottles contained a synthetic surface water prepared to simulate the surface water composition at the North Cave Hills, 168 µM As(V), 168 µM U(VI), 10 mM of electron donor (ethanol, acetate, or lactate), and 10 g/L North Cave Hills soil. Bottles were sampled immediately following the U addition on day 44 and then sampled again after 48 hours of reaction time (day 46). Bottles were then opened to air on day 46 and allowed to react for an additional 24 hours and were sampled after this time on day 47. Error bars represent one standard deviation from the mean of triplicates.

donors. In the bottles with only U(VI), an increase in U concentration was observed in the bottles containing ethanol, but a decrease was observed in the acetate and lactate-containing treatments.

***Solid phase speciation***

*Fe speciation and characterization*

Extractions were performed on filtered sediments collected on day 44 in order to determine distribution of Fe between operationally defined soil fractions and between Fe(II) and Fe(III) redox species. Total Fe values reported are for total moles of Fe in the 1 g of sediment in

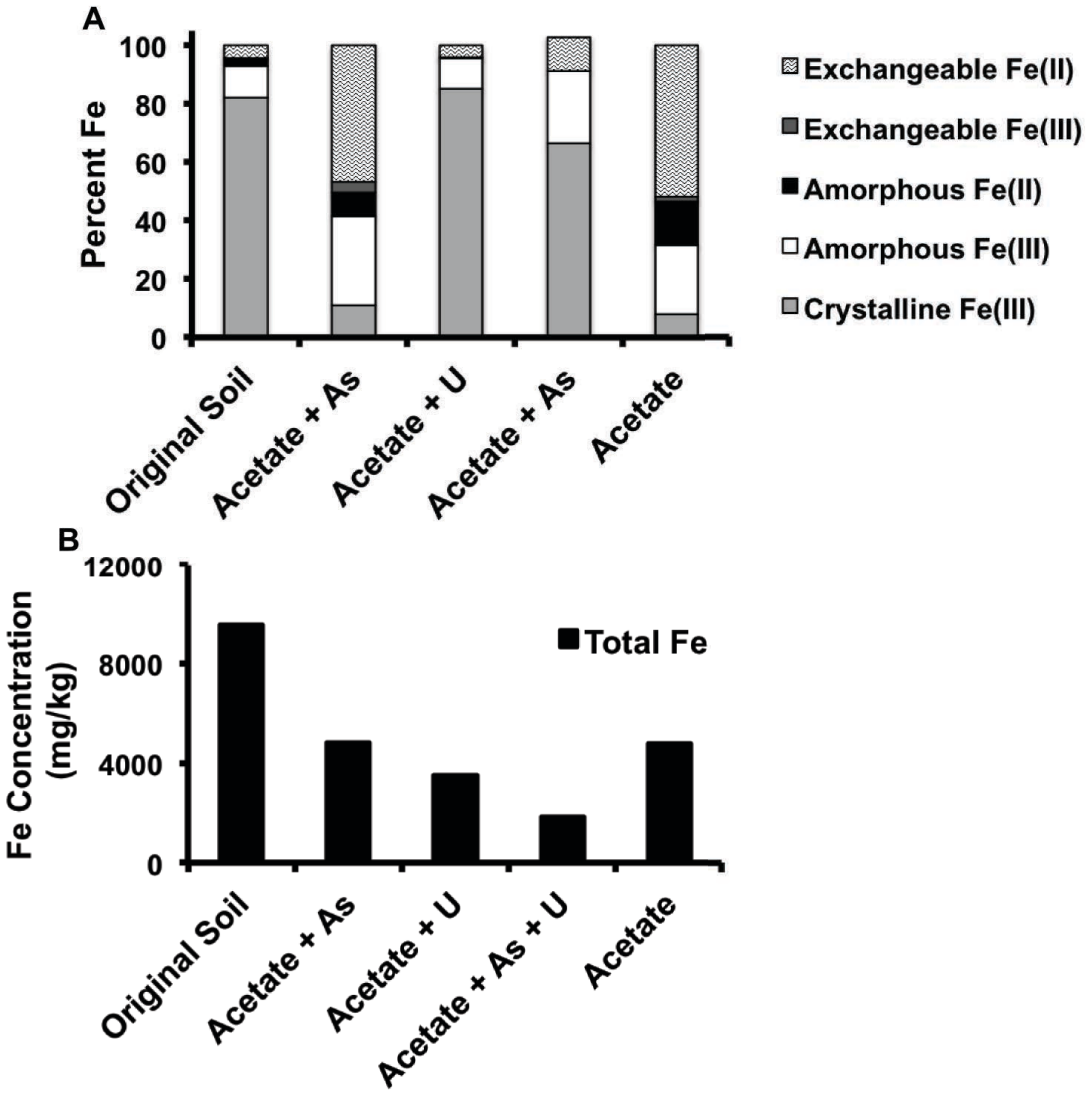


**Figure 3.6.** Results of the linear combination fitting of Fe K-edge extended X-ray absorption structure (EXAFS) spectra. The spectrum of reacted soil is indicated by the blue line and the fit is shown as a dotted line. The spectra of the two reference compounds used for fitting are plotted below, aged mackinawite and North Cave Hills sediment.

each reactor bottle (100 mL synthetic surface water) (Figure 3.6a). The North Cave Hills sediment contained 170 μmol of Fe before reaction. Total Fe decreased from 170 μmol/bottle to 33-86 μmol/bottle by the end of the experiment depending on the combination of As(V) and U(VI). The amount of Fe(II) and Fe(III) in the exchangeable, amorphous, and crystalline fractions of the sediment (Figure 3.6b) was also determined. Fe was primarily extracted as the crystalline fraction from sediment both before and after reaction in the U(VI)-containing treatments. In the unreacted sediment, 82% of the total extracted Fe was present in the crystalline fraction, while 67-85% was in the crystalline fraction of the U(VI)-containing treatments. In systems without U(VI), the primary Fe-containing fraction shifted from the crystalline fraction before reaction to the exchangeable Fe(II) fraction following reaction. In these systems, the Fe(II) exchangeable fraction accounted for 47-52% of the total Fe. The amorphous Fe(III) fraction also increased from 11% of the total extracted Fe in the unreacted sediment to 24-31% in the treatments without U(VI). Throughout the course of an experiment, visible color changes occurred in the solid-phase, going from brown to dark black. Fe EXAFS was collected on a sediment sample in order to determine if changes in mineralogy had occurred over the course of the experiment (Figure 3.7). LCF indicated that after 60 day of reaction, the Fe in the sample was 81.5% representative of the Fe minerals in the unreacted North Cave Hills sediment and 18.5 % representative of an aged mackinawite (FeS) reference compound.

*Uranium speciation*

The speciation of solid-associated U was determined using LCF of U $L_{III}$-edge XANES spectra. In all U(VI) containing systems, reduction of solid-phase U(VI) was not observed by day 44, regardless of the electron donor used (Table 3.2, Figure 3.8a). In the treatments where U(VI) was added upon day 44, reduced U was observed after the 48 hour reaction period (Table 3.2,

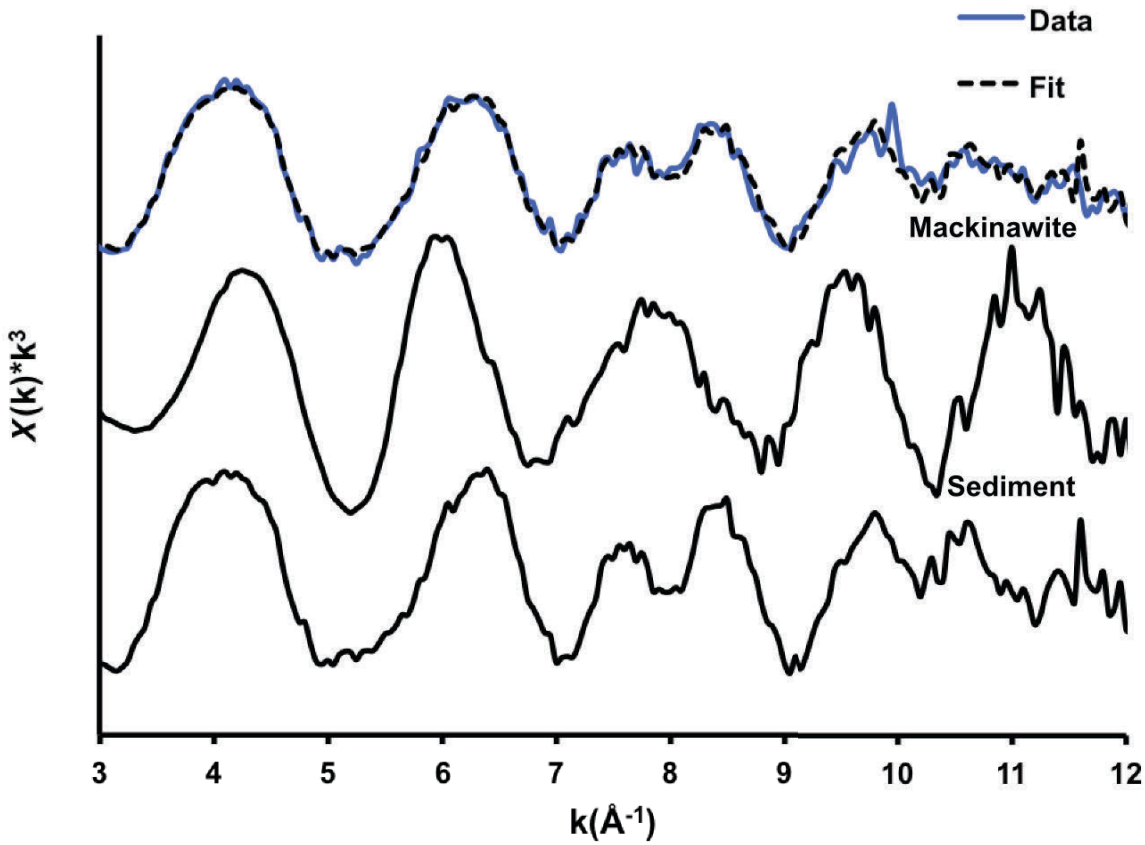


**Figure 3.7.** Results of the linear combination fitting of Fe K-edge extended X-ray absorption structure (EXAFS) spectra. The spectrum of reacted soil is indicated by the blue line and the fit is shown as a dotted line. The spectra of the two reference compounds used for fitting are plotted below, aged mackinawite and cave hills sediment.

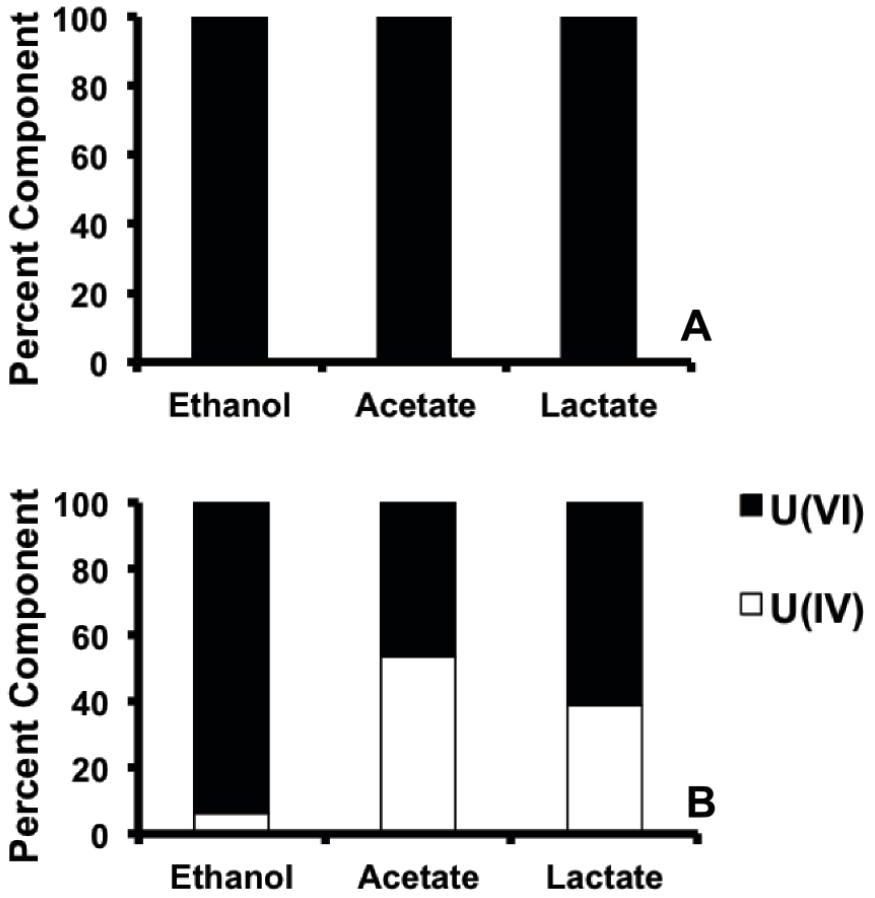


**Figure 3.8.** Speciation of soil-associated U as determined by LCF of XANES spectra. Bottles contain a synthetic surface water prepared to simulate the surface water composition at the North Cave Hills, 168 μM U(VI), 10 mM of electron donor (ethanol, acetate, or lactate), and 10 g/L North Cave Hills soil. Soils were collected on day 44 for analysis (A). In bottles that initially did not contain As(V) or U(VI), U(VI) was added on day 44 and soils were collected on day 46 for analysis (B). Soils from a minimum of 2 bottles were homogenized for XANES analysis.

**Table 3.2.** Summary of U XANES linear-combination fitting results in all U-containing batch systems. Treatments contain 168 μM U(VI) initially, 10 g/L soil, 10 mM of electron donor (ethanol, acetate, lactate) and 168 μM As(V) initially if As is included. The five day time point is after the initial addition of As(V) and U(VI) and the 44 day time point is at the end of the experiment. On day 44, U(VI) was added to any systems that did not initially contain U and samples were removed on day 46. Bottles were then opened to air for 24 hours and sampled on day 47 (oxidation). R factor is a measure of the misfit between the data and the fit.

| Time (days) | Treatment | % Nano-$UO_2$ | % U(VI) adsorbed to ferrihydrite | R factor |
|---|---|---|---|---|
| 44 (final) | Ethanol + U(VI) | 0.0% | 100% | 0.001408 |
| 44 (final) | Acetate + U(VI) | 0.0% | 100% | 0.000399 |
| 44 (final) | Lactate + U(VI) | 0.0% | 100% | 0.000182 |
| 44 (final) | Ethanol + U(VI) + As(V) | 0.0% | 100% | 0.000310 |
| 44 (final) | Acetate + U(VI) + As(V) | 0.0% | 100% | 0.000537 |
| 44 (final) | Lactate + U(VI) + As(V) | 0.0% | 100% | 0.000225 |
| 46 (after U(VI)) | Ethanol + U(VI) | 6.3% | 93.7% | 0.000391 |
| 46 (after U(VI)) | Acetate + U(VI) | 53.7% | 46.3% | 0.000102 |
| 46 (after U(VI)) | Lactate + U(VI) | 38.9% | 61.1% | 0.000050 |
| 46 (after U(VI)) | Ethanol + U(VI) + As(V) | 18.9% | 81.1% | 0.000425 |
| 46 (after U(VI)) | Acetate + U(VI) + As(V) | 0.0% | 100% | 0.001362 |
| 46 (after U(VI)) | Lactate + U(VI) + As(V) | 42.4% | 57.6% | 0.000180 |
| 47 (oxidation) | Ethanol + U(VI) | 27.8% | 72.2% | 0.000091 |
| 47 (oxidation) | Acetate + U(VI) | 66.1% | 33.9% | 0.000037 |
| 47 (oxidation) | Lactate + U(VI) | 25.9% | 74.1% | 0.000034 |
| 47 (oxidation) | Ethanol + U(VI) + As(V) | 11.5% | 88.5% | 0.000085 |
| 47 (oxidation) | Acetate + U(VI) + As(V) | 57.0% | 43.0% | 0.000154 |
| 47 (oxidation) | Lactate + U(VI) + As(V) | 39.0% | 61.0% | 0.000038 |

Figure 3.8b). The extent of U(VI) reduction was varied with the electron donor used. Of the different treatments, the most reduced solid-phase associated U was observed in the treatment without As(V) and with acetate as the electron donor. After the reoxidation experiment where bottles were open to air, some slight changes in distribution of U occurred but complete reoxidation of reduced U was not observed in any treatments. Examples of the quality of XANES LCF are shown in Figure 3.9.

*Arsenic speciation*

The solid-phase speciation of As was determined by LCF of As K-edge XANES spectra. Throughout the experiments, differences were observed in the speciation of As depending on whether U(VI) was present in the treatment. Upon the initial sampling following As(V) and U(VI) injection, solid-phase As was 33-43% reduced in systems without U(VI) (Table 3.3, Figure 3.10a), while only 0-6% of solid-phase As was found to be present in reduced forms in systems containing U(VI). Similar results were observed upon day 44 of the experiment where 69-95% of solid-phase As was reduced in systems without U(VI) (Figure 3.10b), while only 11-16% of solid-phase As was reduced in systems with U(VI) (Figure 3.10c). The reduced As component was fit with a combination of reference standards including As(III) adsorbed to goethite and orpiment. Following the reoxidation experiment, solid-phase As remained primarily reduced (85-89%). Examples of As K-edge XANES LCF are shown in Figure 3.11.

## Discussion

### *Mechanism of U reduction*

Based on previous work, U(VI) reduction could occur in our systems by three different mechanisms—by adsorbed or structural Fe(II), by aqueous or structural sulfide, and directly by bacteria. In systems that initially contained U(VI), microbial reduction of Fe(III)

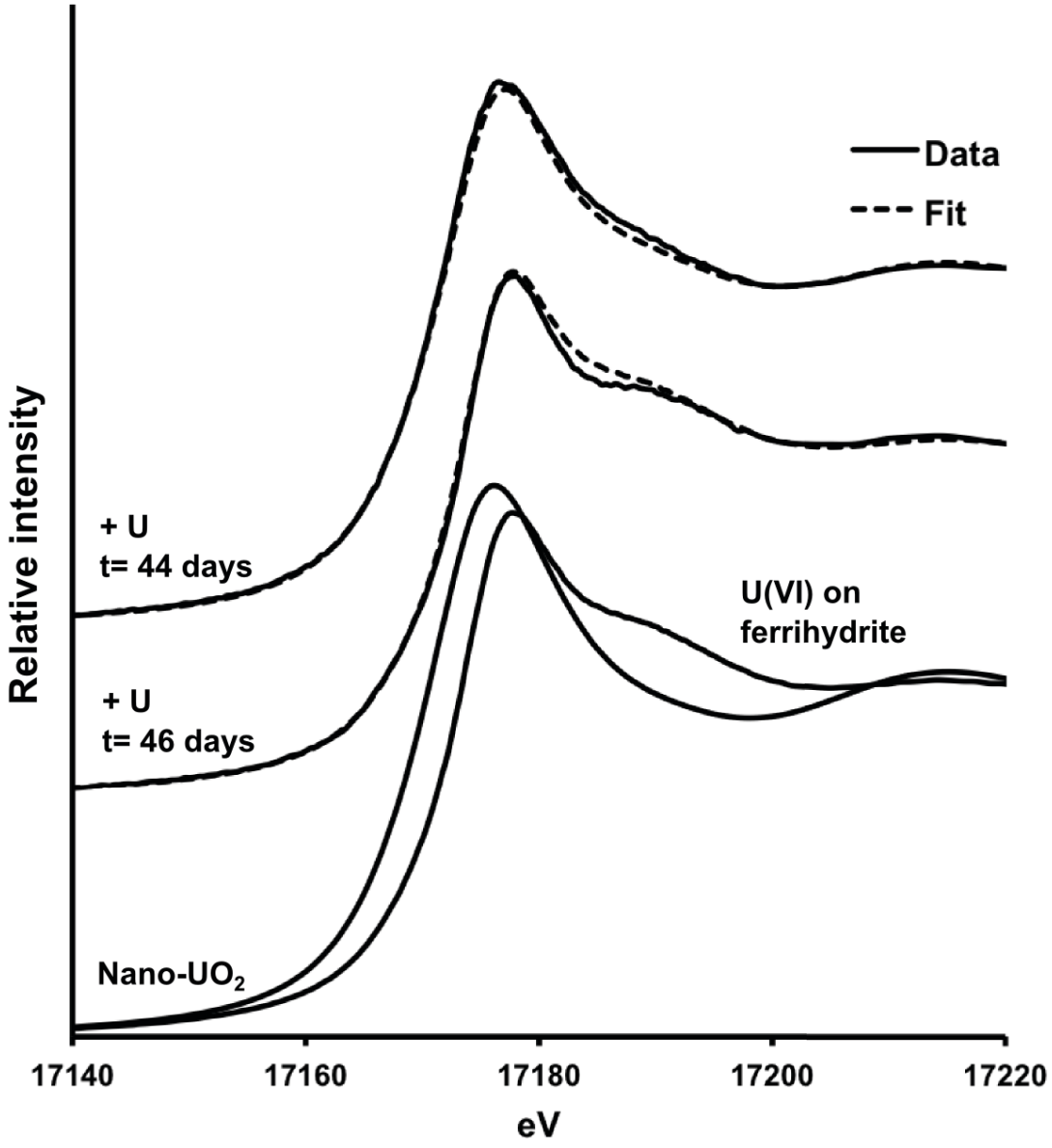


**Figure 3.9.** Examples of LCF of U $L_{III}$-edge XANES spectra. Data is indicated by solid lines and fits are indicated by dashed lines. Bottles contained synthetic surface water prepared to simulate the surface water composition at the North Cave Hills, 168 μM U(VI), 10 mM acetate, and 10 g/L North Cave Hills soil. The top spectrum is of filtered soil following 44 days of incubation and the second spectrum is of the soil from a bottle where U(VI) was added on day 44 of incubation and then filtered on day 46. Plotted on the bottom are the spectra of reference compounds used for fitting including nano-$UO_2$ (U(IV)) and U(VI) adsorbed to ferrihydrite.

**Table 3.3.** Summary of As XANES linear-combination fitting results in all As-containing batch systems. Treatments contain 168 µM As(V) initially, 10 g/L soil, 10 mM of electron donor (ethanol, acetate, lactate) and 168 µM U(VI) initially if U is included. The five day time point is after the initial addition of As(V) and U(VI) and the 44 day time point is at the end of the experiment. On day 44, U(VI) was added to any systems that did not initially contain U and samples were removed on day 46. Bottles were then opened to air for 24 hours and sampled on day 47 (oxidation). R factor is a measure of the misfit between the data and the fit.

| Time (days) | Treatment | % Orpiment | % As(III) adsorbed to goethite | % As(V) adsorbed to goethite | R factor |
|---|---|---|---|---|---|
| 5 (initial) | Ethanol + As(V) | 34.0% | 9.2% | 56.8% | 0.006127874 |
| 5 (initial) | Acetate + As(V) | 6.7% | 26.3% | 67.0% | 0.00848829 |
| 5 (initial) | Lactate + As(V) | 11.5% | 31.1% | 57.3% | 0.006528556 |
| 5 (initial) | Ethanol + As(V) + U(VI) | 0.0% | 0.0% | 100.0% | 0.005455967 |
| 5 (initial) | Acetate + As(V) + U(VI) | 0.0% | 0.0% | 100.0% | 0.005746193 |
| 5 (initial) | Lactate + As(V) + U(VI) | 0.0% | 6.3% | 93.7% | 0.005526309 |
| 44 (final) | Ethanol + As(V) | 95.2% | 0.0% | 4.8% | 0.016571746 |
| 44 (final) | Acetate + As(V) | 62.1% | 6.9% | 31.0% | 0.0044811 |
| 44 (final) | Lactate + As(V) | 84.0% | 0.0% | 16.0% | 0.012613576 |
| 44 (final) | Ethanol + As(V) + U(VI) | 0.0% | 10.8% | 88.2% | 0.003382109 |
| 44 (final) | Acetate + As(V) + U(VI) | 0.0% | 13.5% | 86.5% | 0.003090108 |
| 44 (final) | Lactate + As(V) + U(VI) | 6.9% | 18.9% | 74.2% | 0.002169092 |
| 46 (after U(VI)) | Ethanol + As(V) + U(VI) | 93.2% | 0.0% | 6.8% | 0.001532437 |
| 46 (after U(VI)) | Acetate + As(V) + U(VI) | 0.0% | 0.0% | 100% | 0.006189393 |
| 46 (after U(VI)) | Lactate + As(V) + U(VI) | 88.0% | 0.0% | 12.0% | 0.002256371 |
| 47 (oxidation) | Ethanol + As(V) + U(VI) | 88.7% | 0.0% | 11.3% | 0.001314616 |
| 47 (oxidation) | Acetate + As(V) + U(VI) | 75.0% | 10.8% | 14.2% | 0.001873528 |
| 47 (oxidation) | Lactate + As(V) + U(VI) | 85.8% | 0.0% | 14.2% | 0.002049405 |

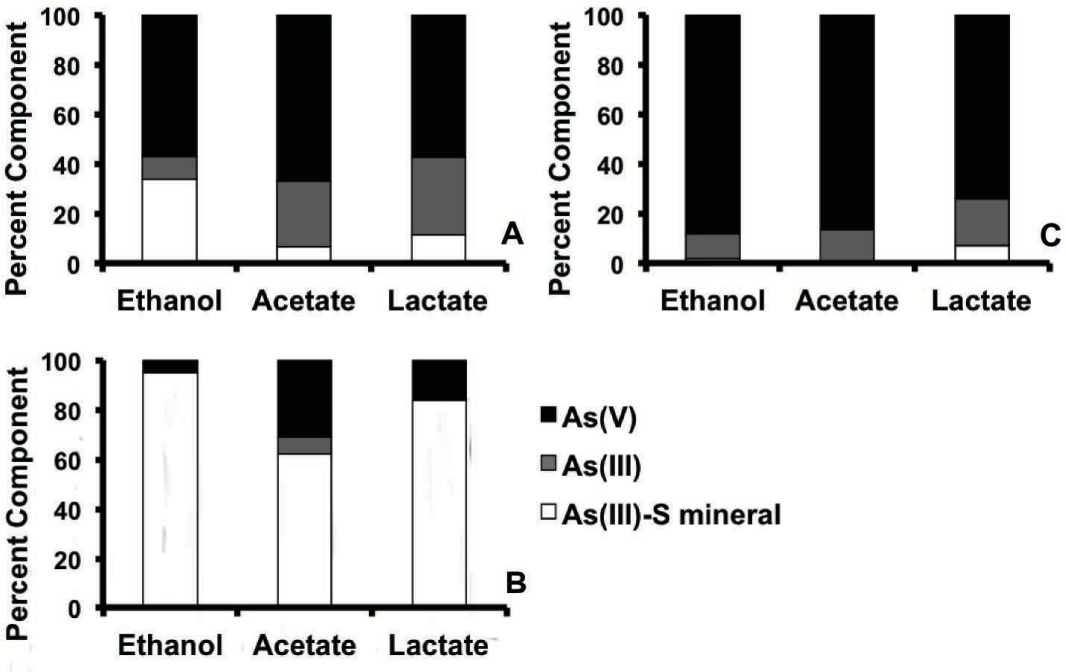


**Figure 3.10.** Speciation of soil-associated As as determined by LCF of XANES spectra. Bottles contain a synthetic surface water prepared to simulate the surface water composition at the North Cave Hills, 168 µM As(V), 10 mM of electron donor (ethanol, acetate, or lactate), and 10 g/L North Cave Hills soil. Soils were collected immediately after the addition of As(V) on day 5 for analysis (A) and then after 44 days of incubation (B). Soils were also incubated with 168 µM As(V) and 168 µM U(VI) and filtered after 44 days of incubation (C). Soils from a minimum of 2 bottles were homogenized for XANES analysis.

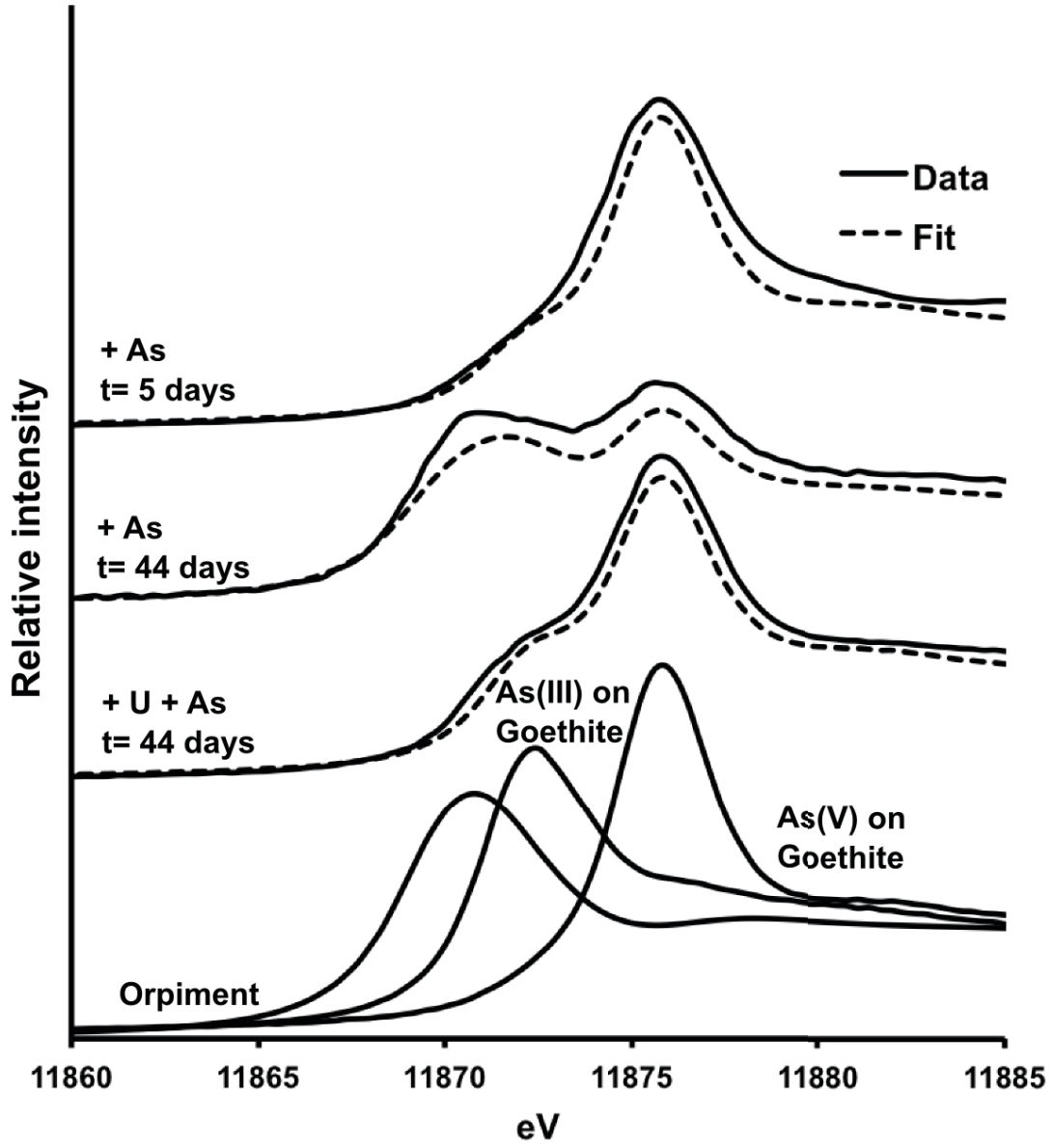


**Figure 3.11.** Examples of LCF of As K-edge XANES spectra. Data is indicated by solid lines and fits are indicated by dashed lines. Bottles contained synthetic surface water prepared to simulate the surface water composition at the North Cave Hills, 168 μM As(V), 168 μM U(VI), 10 mM acetate, and 10 g/L North Cave Hills soil. The first spectrum is of filtered soil following 5 days of incubation immediately following As(V) addition. The second spectrum is of filtered soil following 44 days of incubation. The third spectrum is of the soil from a bottle containing As(V) where U(VI) was added on day 44 of incubation and then filtered on day 46. Plotted on the bottom are the spectra of reference compounds used for fitting including orpiment ($As_2S_3$), As(III) adsorbed to goethite, and As(V) adsorbed to goethite.

oxy(hydr)oxides to aqueous Fe(II) occurred as evidenced by the increase in aqueous Fe(II) concentrations in U(VI)-containing systems and by the decrease in solid-phase Fe between unreacted and reacted sediment (Figure 3.6a). While reductive dissolution of Fe oxy(hydr)oxides took place, no U(VI) reduction occurred (Figure 3.8a) in the systems that initially contained U(VI). While Fe(II) was present in these systems, Fe(II) must be structurally incorporated or adsorbed to mineral surfaces in order to reduce U(VI). (*13*) The extent of Fe(II) remineralization or adsorption is limited in our systems as Fe sequential extractions (Figure 3.6b) did not indicate an increase in the exchangeable or amorphous Fe(II) fractions from the unreacted sediment. Additionally, most studies have examined U(VI) reduction by synthesized, pure Fe minerals, but when Latta, et al studied U(VI) reduction by Fe(II) adsorbed to natural sediments, little U(VI) reduction was observed. (*59, 110*) Therefore, Fe(II) can be ruled out as an effective reductant of U(VI) in our systems.

After 44 days of reaction, U(VI) reduction by aqueous sulfide could not be examined because reduction of sulfate to sulfide was not observed in any systems initially containing U(VI) (Figure 3.3b and 3.4b). In addition, no U(VI) reduction was observed in these systems. The lack of sulfate reduction in these treatments may be due to a toxic effect of U(VI) on the stimulated microbial communities. Although little research has been conducted on U(VI) toxicity to specific microbial communities such as sulfate-reducing bacteria, Tapia-Rodriguez, et al found that U(VI) concentrations as low at 160 μM could limit the activity of methanogenic bacteria. (*149*) Our systems contained 168 μM U(VI) initially, so U(VI) may have had a toxic effect on the bacteria. Konopka, et al observed that the toxicity of U(VI) to microbes was dependent on the composition of surface water or groundwater because positively charged U(VI) complexes such as $(UO_2)_3(OH)_5^+$ could interact with negatively charged cell surfaces, limiting

microbial activity. (*150*) Modeling our system conditions with Visual MINTEQ showed that $CaUO_2(CO_3)_3^{2-}$ and $Ca_2UO_2(CO_3)_3^{0}$ would be the dominant aqueous U(VI) species present, so the toxicity effect is not likely due to an abundance of positively charged U(VI) ionic complexes. While the species distribution does not explain the lack of sulfate reduction observed, the presence of $Ca^{2+}$ and $CO_3^{2-}$ may contribute to the lack of observed U(VI) reduction. Past research has shown that the formation of calcium-uranyl-carbonato complexes increase U solubility and also make U a less favorable electron acceptor. (*92*, *107*, *151*)

In systems that did not initially contain U(VI), sulfate reduction to sulfide was observed (Figure 3.1c and 3.2c). In addition, a visual color change from brown to black was observed, indicating that a precipitate was forming in these bottles. This precipitate was determined to be mackinawite (FeS) by LCF of an Fe K-edge EXAFS spectrum of reacted sediment. The spectrum was well fit with a mackinawite reference spectrum and a reference spectrum of unreacted North Cave Hills sediment (Figure 3.7). In addition, Fe sequential extractions indicate a decrease in the percent of total Fe present in the crystalline fraction and an increase in percent of total Fe in the exchangeable and amorphous fractions in systems without U(VI) (Figure 3.6a). Amorphous FeS or crystalline mackinawite would likely be extracted in the exchangeable or amorphous extraction steps because of the pH of the extraction solutions. (*145*, *152*) The precipitation of mackinawite is also supported by the trends in Fe(II) and sulfate aqueous concentrations in treatments where sulfate reduction was observed. In lactate and acetate-containing systems, a decrease in Fe(II) concentrations was observed at the same time period that sulfate concentrations decreased below detection limits (day 24-28). The observed simultaneous decrease supports that the precipitation of mackinawite from aqueous Fe(II) and sulfide took place at this time.

In order to study sulfide as an electron donor for U(VI) reduction, an additional experiment was performed where U(VI) was injected on day 44 into bottles that previously had not contained U(VI) and where mackinawite precipitation was observed. After U(VI) had been reacted for 48 hours, U(VI) reduction to U(IV) was observed in all treatments, indicating that sulfate reduction was necessary in order for U(VI) reduction to occur . Previous studies have shown that biogenic and synthetic mackinawite can reduce U(VI) to U(IV). (*16, 55, 60, 61*) While mackinawite has been shown to rapidly reduce U(VI) to nano-$UO_2$, enzymatic reduction of U(VI) may also be responsible for U(VI) reduction. In this study, we could not clearly distinguish between abiotic and microbial U(VI) reduction when U(VI) was in the presence of mackinawite. Of all available U(IV) reference compounds, nano-$UO_2$ produced the best fits to the collected XANES spectra indicating that nano-$UO_2$ is the most likely form of U(IV) present in the systems.

In a separate experiment (data not shown), Fe(II) and sulfide were injected into anoxic batch systems at the level of the aqueous concentrations observed in this experiment. Bottles also included sterilized North Cave Hills sediments. In these sterile treatments where the abiotic precipitation of mackinawite was promoted, U(VI) reduction was also observed. This additional experiment shows that U(VI) reduction can take place to a similar extent in the absence of bacteria. While these observations support that mackinawite acts as the primary electron donor in our systems, they do not rule out the possibility of a multiple reduction pathways, both abiotic and microbial, as were observed by Bargar, et al. (*55*)

**Effect of As on U behavior**

Arsenic had an effect on aqueous concentrations of U present in systems, but did not appear to have an effect on extent of U(VI) reduction. In systems containing both As(V) and

U(VI), As(V) and U(VI) concentrations were below detection limits upon initial injection (Figure 3.4d and e). In systems without both As(V) and U(VI), As(V) and U(VI) were initially measured at the concentrations that were injected in bottles that did not contain both analytes. When As(V) and U(VI) are present together in a system, they may precipitate as trögerite ($UO_2HAsO_4 \cdot 4H_2O$) either as a bulk mineral or as a surface precipitate. (*68*) Although As(V) has been shown to enhance uptake of U(VI) onto mineral surfaces, if adsorption was responsible for the lack of measured aqueous As(V) and U(VI) alone, we would expect to see similar low concentrations in the systems containing only As(V). (*25*, *140*) While the presence of As(V) with U(VI) may have caused trögerite precipitation, the presence of As(V) did not have an impact on the extent of U(VI) reduction. Because U reduction is less thermodynamically favorable when U is complexed with ions such as carbonate, we expected that the reduction potential of U may change when precipitated with As(V). If a change in U reduction potential did occur, mackinawite was still able to reduce U(VI). In systems where U(VI) was injected upon day 44, the extent of U(VI) reduction was similar in systems both with and without As(V) (Table 3.2).

***Mechanism of As reduction***

While mackinawite formation was required for U(VI) reduction to occur, As(V) reduction occurred without the formation of mackinawite. Upon the initial solid-phase sampling (5 days), some As(V) reduction to As(III) and a reduced As-sulfide mineral phase were detected in systems without U(VI) (Figure 3.10a). In systems containing U(VI), As(V) reduction was not observed at day 5 or day 44 (Figure 3.10c). As discussed earlier, U(VI) may be toxic to microbes that directly reduce As(V). Direct enzymatic reduction of As(V) may be responsible for the reduced As observed on day 5 because sulfate reduction to sulfide and mackinawite precipitation had not occurred that early in the experiment. Also, As(V) reduction by Fe(II) adsorbed to

goethite has been shown not to occur and Fe(II) is the only available electron donor present in the system on day 5. (*86*) As(V) reduction is more thermodynamically favorable than the reduction of Fe(III) in Fe oxy(hydr)oxides, so direct enzymatic reduction is likely to occur. (*29*, *66*) On day 44, solid-phase As is now 69-95% reduced (Figure 3.10b). In addition to microbial reduction of As(V), reduction of As(V) by precipitated mackinawite has likely occurred by day 44. Previous studies have observed the reduction of As(V) to realgar ($As_4S_4$) in systems containing As and mackinawite, which is why our XANES fits show an As-S mineral phase as the dominant solid-phase As species. (*34*, *153*) If all aqueous sulfate in our systems was reduced to sulfide, the excess aqueous sulfide present following mackinawite precipitation would favor the formation of realgar. (*36*, *154*) Similar to the mechanism of U reduction, we cannot distinguish between microbial and abiotic As(V) reduction, but it is likely that both mechanisms are occurring simultaneously in our systems.

***Differences in electron donors***

A secondary goal of this research was to compare extent of reduction of U(VI) and As(V) in the presence of different electron donors. Differences between the different electron donor treatments were observed both in the aqueous and solid-phase results. Overall, aqueous phase trends were similar among the lactate and acetate treatments and different for the ethanol treatments. The aqueous phase differences can be attributed largely to the change in pH of each treatment over the course of the experiment. While all bottles started at circumneutral pH, the final pH was 9.0-9.3 in the acetate and lactate systems and was 6.7 in the ethanol systems. These pH changes were expected due to the half reactions of the oxidation of each of the electron donors as follows for acetate, lactate, and ethanol respectively:

$CH_3COO^- + 4H_2O \rightarrow 2HCO_3^- + 9H^+ + 8e^-$

$C_3H_5O^- + 2H_2O \rightarrow CH_3COO^- + HCO_3^- + 5\ H^+ + 4e^-$

$CH_3CH_2OH + H_2O \rightarrow CH_3COO^-\ 5H^+ + 4e^-$

Acetate and lactate oxidation produce bicarbonate, which raises the pH in the system while ethanol oxidation produces acetic acid that lowers the pH. (*62*, *125*, *151*) The difference in pH explains why more aqueous Fe(II) is observed in the ethanol systems because of its increased solubility at acidic pH. U(VI) is also more soluble when present as uranyl-carbonato complexes resulting in higher aqueous concentrations in the basic lactate and acetate systems (Figure 3.3d) and uranyl-arsenate precipitate formation is favored under acidic conditions which is why As and U aqueous concentrations are lower in the ethanol treatments (Figure 3.4d and e). In the solid-phase, we observed the greatest extent of U(VI) reduction in the systems spiked with acetate, followed by lactate, followed by ethanol. We observed different trends in extent of As(V) reduction, with the most reduction observed in ethanol systems, followed by lactate, followed by acetate. The differences in extent of U(VI) and As(V) reduction with electron donor are likely due to the amount of mackinawite formed in each treatment. Differences can also be attributed to the stimulation of different microbial communities depending upon the electron donor used. For example, acetate is commonly used to stimulate sulfate-reducing bacteria that have been shown to directly reduce U(VI). (*17*, *137*)

***Sensitivity of oxygen***

Bottles containing U(VI) were opened to the air following 46 days of reaction without oxygen and were allowed to react for an additional 24 hours. Mackinawite has been shown to protect U(IV) from oxidation once exposed to oxygen. (*16*, *119*, *155*) The results of our experiments support that nano-$UO_2$ was protected by mackinawite from oxidation and that orpiment or As(III) was also protected from oxidation. The results of U XANES fitting shows

that overall more solid-phase U was present as U(IV) after oxidation than on day 46. An increase may be observed because of the variation between bottles or due to the fact that XANES analysis is not quantitative. Although more solid-phase U is reduced, an increase in aqueous concentrations of U between day 46 and 47 was observed (Figure 3.5b and 3.3c).

**Environmental Implications**

The goal of this study was to examine the speciation of both U and As under controlled conditions. Overall, we observed that both U and As were partially removed from the aqueous phase and were mineralized to a great extent by the end of the 46 day reaction period. Our results indicate that the activity of sulfate-reducing bacteria is necessary to observe U(VI) reduction to $UO_2$ either to promote the precipitation of mackinawite or to cause direct enzymatic reduction. Although toxicity effects were observed in U(VI)-containing treatments, added U(VI) and As(V) concentrations were above those naturally occurring at the North Cave Hills, so we do not expect a similar toxicity effect in the field. Overall, results show that biostimulation in the field would successfully remove As(V) and U(VI) from solution, preventing transport. We also observed that formation of mackinawite during biostimulation would protect reduced As and U from reoxidation if an anoxic zone became oxic upon seasonal weather variation. Further characterization of microbial communities in each bottle is required to better determine which electron donor would be the best choice for in-situ bioremediation.

CHAPTER 4

# SIMULTANEOUS REDUCTION OF ARSENIC(V) AND URANIUM(VI) BY MACKINAWITE (FeS): ROLE OF URANYL ARSENATE FORMATION[3]

## Introduction

Uranium ore can contain 1.2-10 weight percent As, resulting in U and As being found together in sediments at uranium mining or milling sites. (*3*, *30*) However, few studies have examined the redox behavior of both U and As under controlled laboratory settings. Under reducing conditions, the most common form of U(IV) is uraninite ($UO_2$) which is sparingly soluble and, therefore, less mobile than aqueous U(VI). (*3*) The mobility of As under reducing conditions is opposite that of U, with its reduced form, As(III), being more mobile because it is less likely to adsorb onto mineral surfaces under circumneutral pH ranges as comparing to its oxidized form, As(V). (*37*, *38*, *156*) The difference in mobility of these two toxic elements under similar redox conditions makes remediation of U and As-containing mine waters and sediments and of waste generated during U ore processing or from in-situ U mining challenging.

When present together, U(VI) and As(V) can also form uranyl arsenate aqueous complexes, ternary surface complexes on mineral surfaces, or mineral precipitates, such as trögerite ($UO_2HAsO_4 \cdot 4H_2O$), depending on their concentrations. (*67*, *68*, *157*, *158*) Although uranyl arsenate aqueous complexes and surface precipitates can form under laboratory conditions, their occurrence in natural systems has not been recorded. Even so, aqueous uranyl arsenate complexes are likely to form under low pH conditions consistent with acid mine

[3] All work presented here was performed by me with the exception of U $L_{III}$-edge EXAFS fitting performed by Dr. Yuanzhi Tang at the Georgia Institute of Technology. Special thanks to collaborator Dr. Yuanzhi Tang for providing U and As EXAFS and XANES standards.

drainage sites, but not under conditions typical of most historic U mining or mill tailings. (*67*) Arsenate can also serve as an analog for phosphate, as phosphate has similar behavior with uranyl precipitating as uranyl phosphates at high concentrations and forming ternary complexes on surfaces at low concentrations. (*24*, *26*, *139*) The formation of low solubility uranyl phosphate minerals has been studied in both laboratory and field-scale experiments as a method of U immobilization alternative to U(VI) reduction to $UO_2$. (*24*, *52*, *71*, *159-162*) Studies have also shown that the presence of aqueous phosphate impacts the reaction products of U bioreduction, (*21*, *22*, *52*, *163-165*) often leading to the formation of ningyoite-like phases [$CaU^{IV}(PO_4)_2 \cdot H_2O$]. Although studies have examined the effect of As pretreatment on U sorption to aluminum oxide, (*25*, *68*, *140*) no studies have examined the reactivity of U(VI) in the presence of As(V) and a redox active mineral such as an Fe(II) hydr(oxide) or sulfide.

Because of the redox behavior of U, microbially-mediated reduction of U(VI) to uraninite ($UO_2$) is often used as a remediation strategy for U immobilization. (*130*, *166*) During biostimulation, U(VI) can be reduced to $UO_2$ via direct enzymatic pathways, (*19*, *62*, *104*) or Fe(II)-mediated abiotic pathways, such as by mackinawite (FeS). Mackinawite forms when metal and sulfate-reducing microorganisms use Fe(III) and sulfate, respectively, as electron acceptors either in succession or simultaneously, (*124*, *132*, *167*) resulting in the precipitation of poorly crystalline mackinawite which ages over the course of a few days to crystalline mackinawite. (*152*, *168-170*) In laboratory studies, both synthetic and biogenic mackinawite have been shown to reduce U(VI) to nano-$UO_2$. (*16*, *55*, *60*, *61*) When formed in sediment systems during biostimulation, biomass-associated mackinawite has been shown to be the electron donor responsible for U(VI) reduction to nano-$UO_2$ and molecular U(IV). (*55*) Mackinawite can also act as a buffer, protecting $UO_2$ from reoxidation in biostimulated systems.

(*16*, *155*, *171*) In addition to reducing U(VI), mackinawite is capable of As reduction. As(III) was shown to be reduced to the arsenic sulfide mineral realgar (AsS) in the presence of mackinawite. (*34*, *153*) As(V) reduction to As(III) has also been shown to occur upon the formation of mackinawite in biostimulated sediment columns, but, because of low aqueous sulfide concentrations, realgar formation was not observed. (*36*, *172*)

Because of the common presence of As in U ore, the effect of As on U reduction by mackinawite must be considered for the design of U remediation strategies at mine-impacted sites and for the treatment of waste generated by ore processing and in-situ mining. While studies have examined the reduction of U(VI) and As(V) by mackinawite separately, the two elements have not been investigated together. As(V) pretreatment of aluminum oxide has been shown to increase the uptake of U(VI) due to precipitation of uranyl arsenates on the mineral surface, but little is known about the effect of As(V) on U(VI) reduction or uptake on a redox-active mineral such as mackinawite. (*68*) No previous studies have investigated the reduction of uranyl arsenate minerals such as trögerite. Thus, in this study, we examine the impact of As(V) on abiotic U(VI) reduction in the presence of mackinawite using complementary laboratory and spectroscopy analysis.

## Experimental Methods

### *Mackinawite Synthesis*

Mackinawite synthesis was carried out in an anoxic chamber containing 5% hydrogen and 95% nitrogen. All solutions used were purged with 99.99% pure nitrogen before use. Mackinawite was synthesized by mixing 100 mL of 0.57 M Fe(II) and 75 mL of 1.1 M $Na_2S•9H_2O$. (*16*, *173*) The Fe(II) stock solution was prepared by adding 3.63 g Fe(0) to 1M HCl according to Amstaetter et al in order to insure that no Fe(III) was present. (*86*) The mackinawite

was allowed to age for 3 days with constant stirring. After aging, the mackinawite was washed by alternating six times between centrifuging at 22095 *g* for 15 minutes and rinsing with DI water under anoxic conditions. After washing, the mackinawite was freeze-dried overnight under vacuum, ground, and stored anoxically until use.

***Batch Experiments***

A 5.0 g/L mackinawite suspension was prepared by adding the freeze-dried mackinawite to deoxygenated 0.1 M NaCl in an anoxic chamber. The suspension was allowed to equilibrate for 2 days while stirring. The suspensions were pH adjusted to 7.0 using 1.0 M HCl and allowed to stir for 24 hours until the pH had stabilized. The final mackinawite suspension concentration was determined to be 4.7 g/L by dissolving an aliquot of the suspension in 6 M HCl and analyzing for Fe(II) concentration using the Ferrozine method. (*144*) Stock solutions of 50 mM sodium arsenate and 50 mM uranyl acetate were prepared in DI water. Experiments were prepared by adding stock solutions of sodium arsenate and uranyl acetate to the mackinawite suspension to achieve final concentrations of 47 and 470 μM U(VI) and As(V) concentrations from 32 to 640 μM. The final concentration of mackinawite in each serum bottle was 4.6 g/L. An experiment was also set up where 3400 μM each of U(VI) and As(V) (15 μL) were combined prior to the addition of the mackinawite suspension (diluted to 10 mL) in order to encourage the precipitation of uranyl arsenate mineral(s). All samples were prepared in triplicate. Samples were shaken for 48 hours on a table shaker. 1 mL of the suspension was removed with a syringe after initial setup of the experiments and after 48 hours of reaction and was filtered through a 0.2 μm nylon filter. Total digestions were performed by combining 1 mL of sample with 1 mL of concentrated $HNO_3$. Reoxidation experiments were performed on two selected treatments (47 μM U(VI) only and 47 μM U(VI) + 32 μM As(V)) by injecting 10 mL of air into each bottle and

allowing the bottles to react for an additional 48 hours. 1 mL was sampled following this 24 hour reaction period and filtered as described above. Aqueous concentrations of uranium and arsenic in filtered samples and total digests were determined by using an inductively coupled-plasma mass spectrometer (ICP-MS; Perkin-Elmer Elan DRC-e). Sulfate concentrations in filtered samples were measured using a Dionex Ion Chromatograph. Aqueous Fe(II) concentrations were measured using the Ferrozine method. (*144*) pH was measured in all sample bottles at the beginning and the end of the experiment.

***X-ray Absorption Spectroscopy (XAS)***

Uranium and arsenic X-ray absorption spectroscopy (XAS) was performed at beamline 13-BM-D (GSE-CARS) at the Advanced Photon Source (APS) in Argonne, IL. Fe XAS was performed at beamline 4-1 (20-pole wiggler) at the Stanford Synchrotron Radiation Lightsource (SSRL) in Menlo Park, CA. From each triplicate, 5 mL of suspension was combined and vacuum filtered onto 13 mm (diameter) 0.2 μm cellulose acetate membrane filter in an anoxic chamber containing 5% hydrogen and 95% nitrogen. Membranes were enclosed in Kapton polyimide tape and were stored and transported in an anoxic jar (Remel, AnaeroPack® Rectangular Jar). Samples were kept in a $N_2$ environment during XAS analysis. The ring at APS runs at 7 GeV with a current of 100 mA. Energies were selected with a pair of Si (111) monochromator and spectra were collected in fluorescence mode using a 12-channel Ge detector. The ring at SSRL runs at 3 GeV with a current of 450 mA. Energies were selected with a pair of Si (220) monochromator and spectra were collected in fluorescence mode using a wide-angle collection ionization chamber (Lytle detector). For U, extended X-ray absorption fine structure (EXAFS) spectra were collected from -150 to 450 eV around the $L_{III}$-edge of U (17176 eV). For As, XANES spectra were collected from -150 to 450 eV around the K-edge of As (11876 eV). For

Fe, EXAFS spectra were collected from -200 to +1000 eV around the K-edge of Fe (7111 eV). Between 2 and 5 spectra were averaged for each sample.

Linear combination fitting (LCF) were conducted on the U $L_{III}$-edge and As K-edge X-ray absorption near edge structure (XANES) data to determine the speciation of U and As, and on the Fe K-edge EXAFS data to determine Fe mineralogy. The reference compounds used are (1) for U: trögerite ($U^{VI}O_2HAsO_4 \cdot 4H_2O$), U(VI) adsorbed to ferrihydrite, and nano-$U^{IV}O_2$; (2) for As: As(V) adsorbed to goethite, As(III) adsorbed to goethite, and orpiment ($As_2S_3$)(*86*); and (3) For Fe: fresh mackinawite and a mackinawite sample that had been anoxically aged for three weeks. LCF was performed with reference spectra using the software SixPACK (*174*) and Athena (*87*) interfaces to IFEFFIT. (*175*) Fits are within about ±5% of the mole percentages of fractions for As LCF and within about ±10% for U LCF. (*128*, *148*)

Detailed structure analysis of the U $L_{III}$-edge EXAFS data were performed with the programs WinXAS (*176*) and IFEFFIT. (*146*) Theoretical backscattering paths were calculated using FEFF7 (*177*) with $UO_2HAsO_4 \cdot 4H_2O$ and $UO_2$ as model structures. A global threshold energy value ($\Delta E_0$) was allowed to vary during fitting. The amplitude reduction factor, $S_0^2$, was determined from fitting of the model compounds and was fixed at $S_0^2 = 1$. For U EXAFS, a 4-leg axial multiple-scattering (MS) path was included in all samples. This MS path is composed of U-O-U-O with 180º scattering between the center U atom and the two axial O atoms. Errors for the fit parameters are estimated from fits of the model compounds. Error estimates are ±0.01 Å for the R value of the first oxygen shell, and ±0.05 Å for higher distance shells. For coordination number, which is heavily correlated to the Debye-Waller factor, the estimated errors are ±20% for the first oxygen shell and ±50% for shells at higher distance. Estimated errors for the Debye-

Waller factors are ±0.001 $Å^2$ for the first shell and ±0.005 $Å^2$ for higher shells. The goodness of fit values is evaluated by the residual value. (*176*)

### *Thermodynamic Modeling*

Visual MINTEQ (version 3.0) was used to model the saturation indices for possible uranyl arsenate precipitates such as trögerite ($UO_2HAsO_4 \cdot 4H_2O$) and $(UO_2)_3(AsO_4)_2 \cdot nH_2O$ under the range of U(VI) and As(V) concentrations examined. Due to the limited availability of stability constants of these mineral phases, calculations were carried out on the uranyl-phosphate system (e.g., the potential formation of solid phases bassettite ($Fe(UO_2)_2(PO_4)_2 \cdot 8H_2O$), autunite ($Ca(UO_2)_2(PO_4)_2 \cdot nH_2O$), chernikovite ($UO_2HPO_4 \cdot 4H_2O$) and $(UO_2)_3(PO_4)_2 \cdot nH_2O$) using phosphate as a chemical analog for arsenate. The presence of mackinawite was also included in the model. The thermodynamic constants used were from the visual MINTEQ 3.0 database.

## Results

### *Mackinawite characterization and aqueous chemistry*

Fe K-edge EXAFS spectra were collected on the mackinawite used for sorption experiments in order to confirm its structure. Fe EXAFS spectra were also collected on a mackinawite sample after 48 hours of reaction with 47 μM U(VI) and 32 μM As(V). Based on

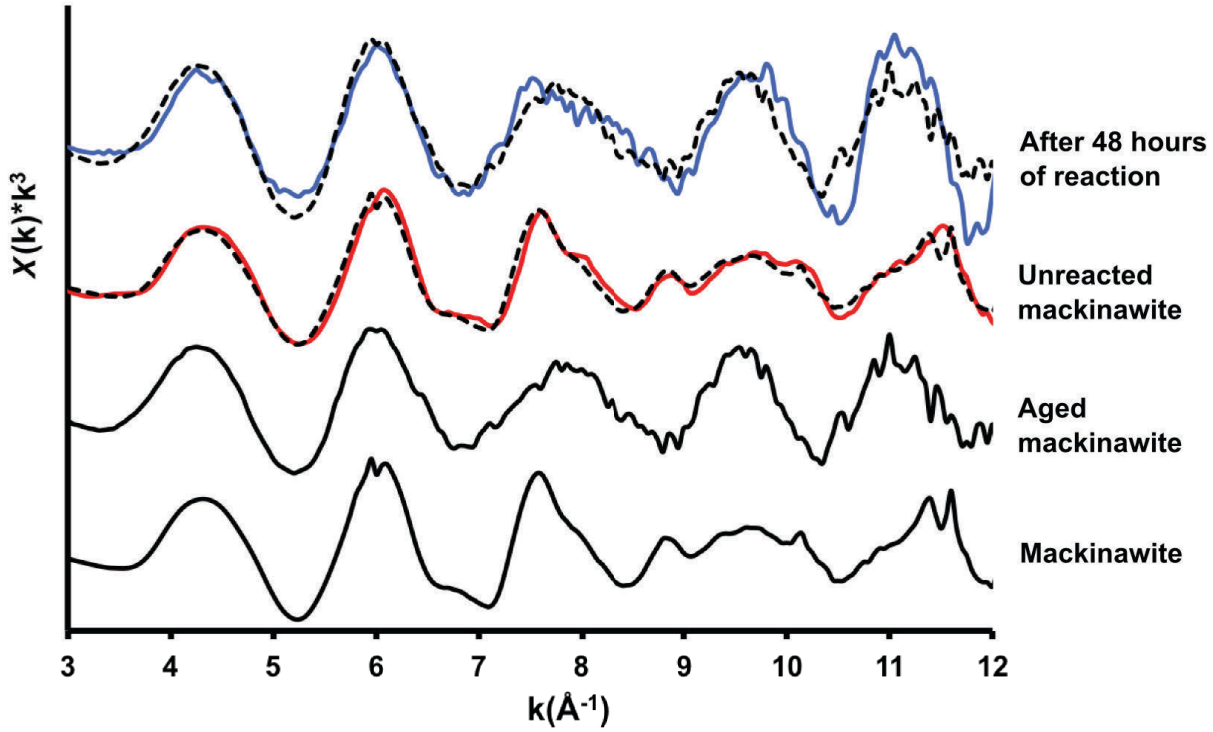


**Figure 4.1.** Fe K-edge $k^3$-weighted EXAFS spectra of synthesized mackinawite before (solid red line) and after (solid blue line) reaction with 47 µM U(VI) and 32 µM As(V). The solid black lines indicate reference spectra for freshly precipitated and aged mackinawite. The dotted lines indicate linear combination fitting results for the unreacted and reacted mackinawite.

LCF (Figure 4.1), mackinawite structure prior to reaction was similar to the freshly precipitated mackinawite reference sample. After 48 hours of reaction, the mackinawite structure changed and was fit with 17.7% of the freshly precipitated mackinawite standard and 82.3% of a mackinawite sample that had been aged anoxically for three weeks (Table 4.1). Aqueous concentrations of Fe(II) and sulfate were measured in all of the samples at the beginning and end of 48 hour reaction time, with Fe(II) concentrations decreased and sulfate concentrations increased over the time period for all treatments (Table 4.2).

**Table 4.1.** Summary of Fe K-edge $k^3$-weighted EXAFS linear-combination fitting results of mackinawite before and after reaction in batch experiments. The R factor is the normalized sum of the difference between the model and the fit.

| Location Name | % Mackinawite | % Aged Mackinawite | R factor |
|---|---|---|---|
| Mackinawite, before reaction | 92.8 | 7.2 | 0.055652 |
| Mackinawite, after reaction with 47 μM and 32 μM | 17.7 | 82.3 | 0.222485 |

**Table 4.2.** Summary of difference in aqueous Fe(II) and sulfate concentrations in batch systems before and after 48 hours of reaction.

| Sample Type | Initial U(VI) (μM) | Initial As(V) (μM) | Change in Fe(II) (μM) | Change in Sulfate (mM) |
|---|---|---|---|---|
| Added to mackinawite | 47 | — | -78 | 0.282±0.027 |
| | 47 | 32 | -2 | 0.283±0.021 |
| | 47 | 64 | -132 | 0.291±0.019 |
| | 47 | 320 | -44 | 0.292±0.033 |
| | 470 | — | -46 | 0.144±0.031 |
| | 470 | 32 | -110 | 0.126±0.004 |
| | 470 | 320 | -70 | 0.194±0.013 |
| | 470 | 640 | -16 | 0.173±0.029 |
| Combined before mackinawite addition | 340 | 340 | 4 | 0.023±0.032 |

### *U and As removal from solution*

Batch experiments were conducted to investigate U(VI) removal from solution at two concentration levels: 47 and 470 µM, hereafter referred to as low U and high U concentration experiments. As(V) was added to both the low and high U treatments over a range of concentrations, with 32–320 µM As(V) for the low U concentration treatments and 32–640 µM As(V) for the high U concentration treatments. The amount of U and As that was removed is summarized in Figure 4.2. Both in the absence and presence of As(V), 100% of U was removed from the aqueous phase at the end of the 48 hour reaction time. Arsenic removal varied by initial As(V) concentration, but was complete at the lowest concentration of As(V) (32 µM) with both low and high U(VI) concentration levels. In the low U concentration experiments, with increasing As(V) concentration, As(V) removal decreased from 100% at 32 µM As(V) to 92% at 320 µM As(V). As(V) removal also decreased in the high U concentration experiments from 100% at 32 µM As(V) to 93% at 640 µM As(V). To further examine the removal mechanism(s) for U(VI) and As(V) from solution, XANES and EXAFS spectroscopy was performed on filtered solids.

### *Extent of reduction of FeS-associated U(VI) and As(V)*

#### *Uranium speciation*

XANES spectroscopy was used to identify the distribution of U and As species associated with mackinawite. The results of LCF of U XANES data are summarized in Figure 4.3, Table 4.3, and Figure 4.4. In the absence of As(V), all solid-phase U is present as nano-$UO_2$ at both U concentrations. In low U concentration systems, As(V) had limited impact on the extent of U reduction. With the addition of 32 µM As(V), U(VI) was 100% reduced, similar to the As(V)-free system, indicating that As had no impact on U reduction at this concentration

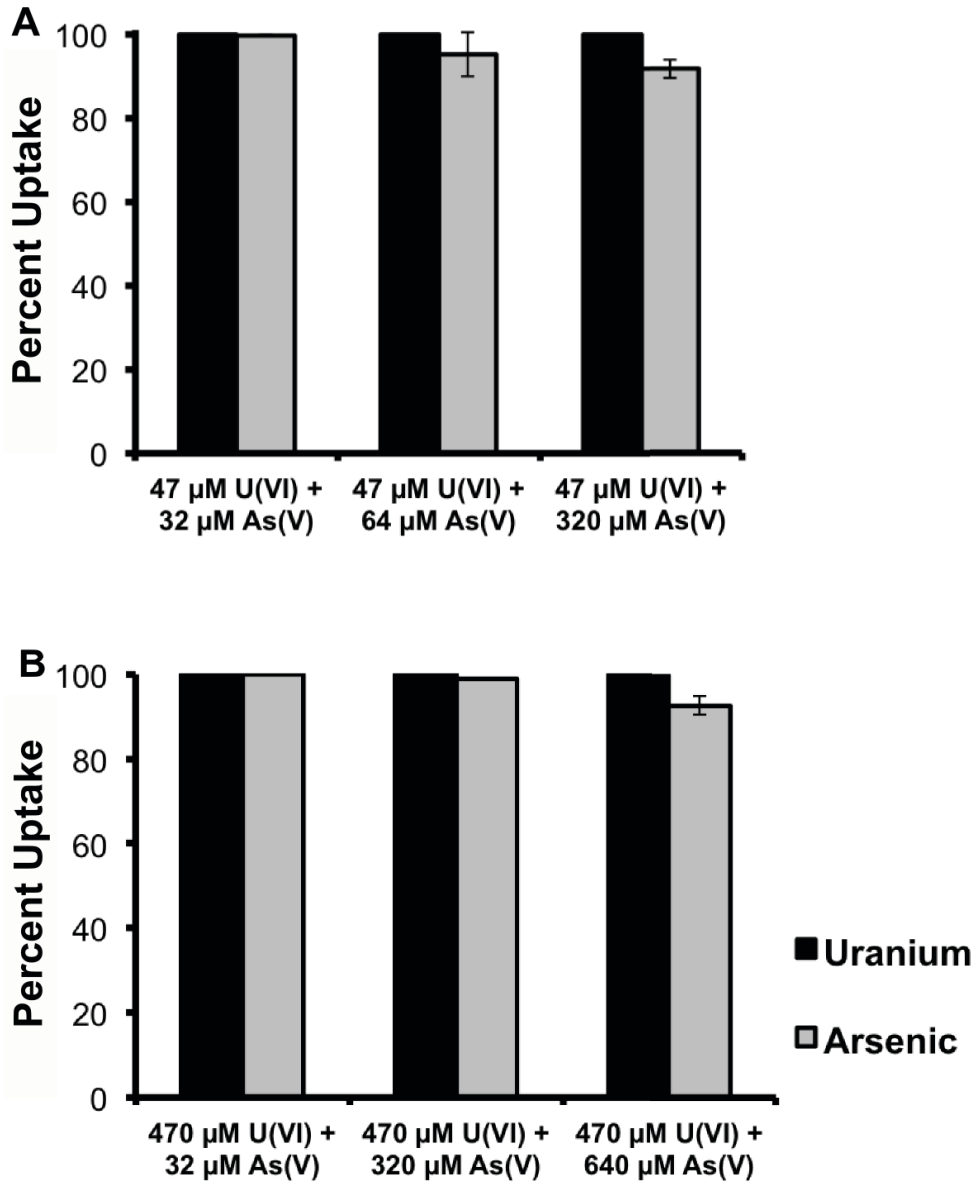


**Figure 4.2.** Percent uptake of U and As from the aqueous suspensions of batch experiments containing 4.6 g/L mackinawite and a) 47 µM U(VI) and b) 470 µM U(VI) with varying concentrations of As(V). Black bars indicate percent U uptake and gray bars indicate percent As uptake. Error bars indicate one standard deviation from the average of triplicates.

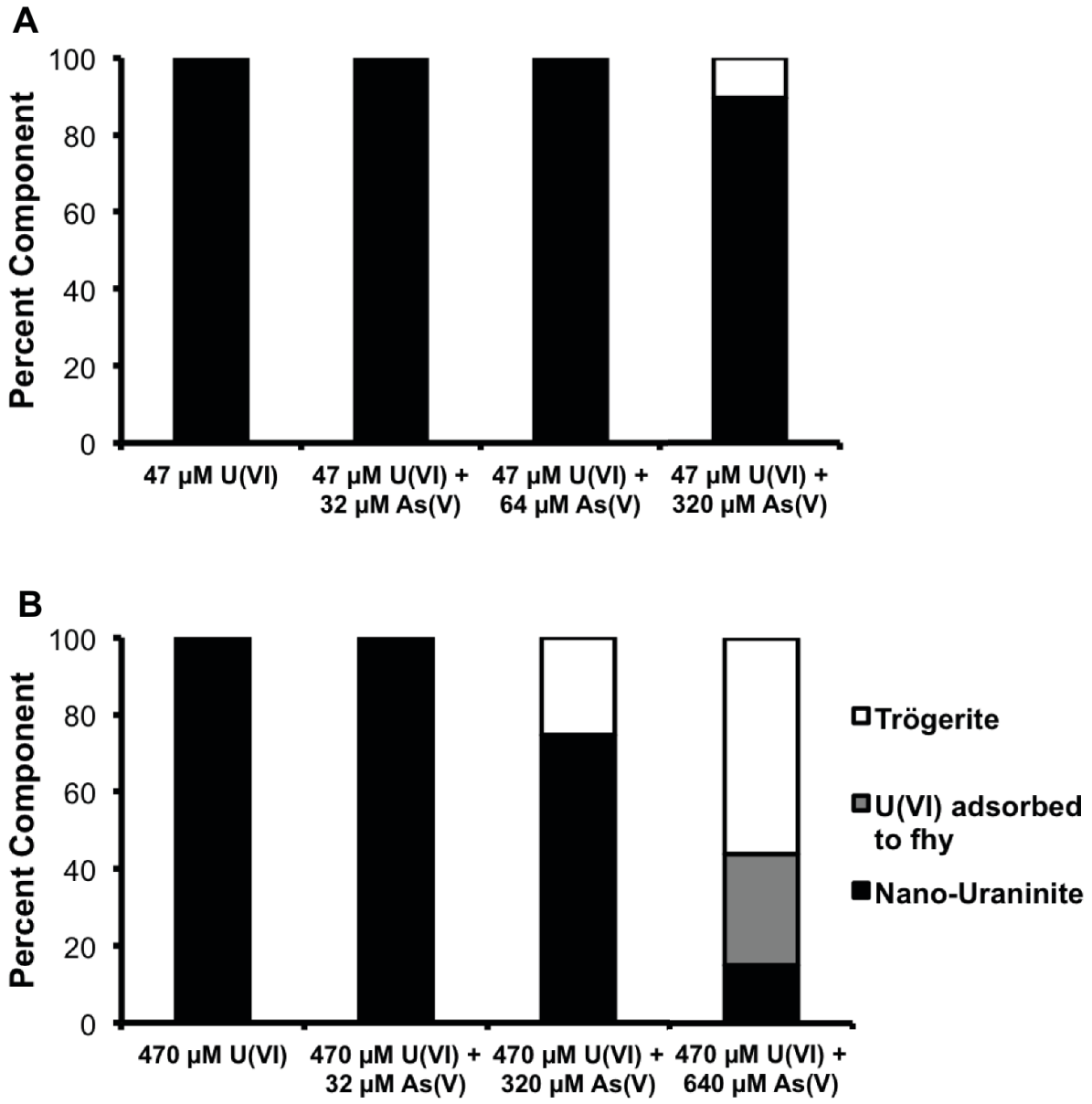


**Figure 4.3.** Percent U(IV) and U(VI) species in final reaction products as determined by linear-combination fitting of U $L_{III}$-edge XANES. Systems contained a) 47 µM U(VI) and b) 470 µM U(VI) with varying concentrations of As(V).

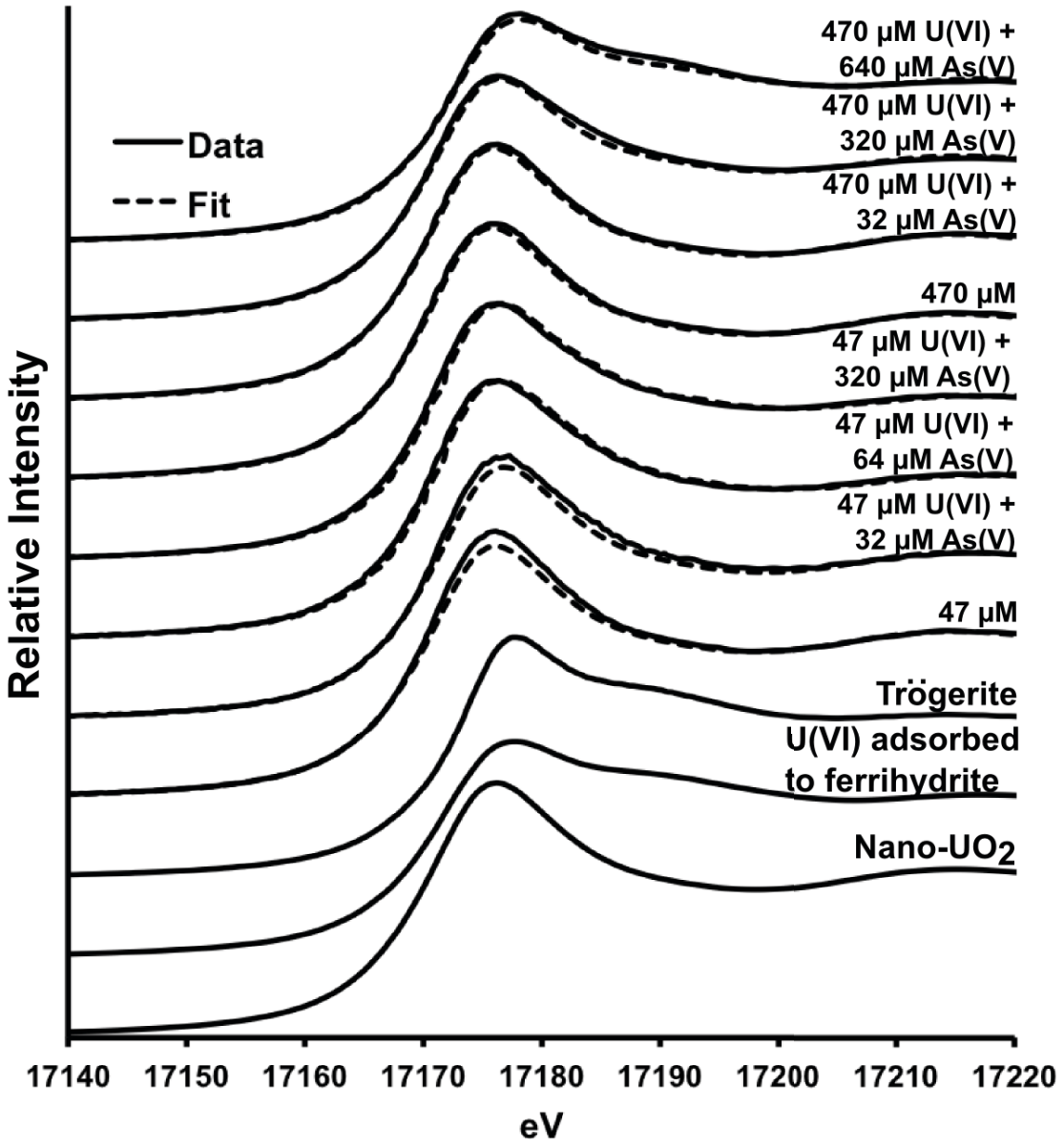


**Figure 4.4.** U $L_{III}$-edge XANES spectra of solid reaction products and reference compounds nano-$UO_2$ and trögerite.

**Table 4.3.** Summary of U XANES linear-combination fitting results for data shown in Figure SI3. The R factor is the normalized sum of the difference between the model and the fit.

| Sample Type | Initial U(VI) (μM) | Initial As(V) (μM) | % Nano-$UO_2$ | % U(VI) adsorbed to ferrihydrite | % Trögerite | R factor |
|---|---|---|---|---|---|---|
| Added to mackinawite | 47 | — | 100 | 0.00 | 0.00 | 0.0015220 |
| | 47 | 32 | 100 | 0.00 | 0.00 | 0.0016930 |
| | 47 | 64 | 100 | 0.00 | 0.00 | 0.0002760 |
| | 47 | 320 | 89.5 | 0.00 | 10.5 | 0.0002690 |
| | 470 | — | 100 | 0.00 | 0.00 | 0.0004878 |
| | 470 | 32 | 100 | 0.00 | 0.00 | 0.0003995 |
| | 470 | 320 | 74.7 | 0.00 | 25.3 | 0.0001437 |
| | 470 | 640 | 15.0 | 28.9 | 56.1 | 0.0000880 |
| Combined before mackinawite addition | 340 | 340 | 25.9 | 42.5 | 32.0 | 0.0014997 |

level. As As(V) concentrations increased, complete U(VI) reduction by mackinawite was prevented. The precipitation of nano-$UO_2$ phase decreased to 96% of the total solid-phase U with 64 μM As(V) addition and further to 90% with 320 μM As(V) addition. As(V) had a greater impact on the extent of U reduction in high U concentration systems. With the addition of 32 μM As(V), U reduction was complete, similar to the As(V)-free treatment. With the addition of 320 μM As, 75% of the solid-phase U present as reduced phase. The addition of 640 μM As had the greatest effect on U(VI) reduction where only 15.0% of the solid phase U was nano-$UO_2$. Three U standards (nano-$UO_2$, trögerite, and U(VI) adsorbed to ferrihydrite) were included in LCF to model the possible mechanism(s) of U(VI) removal from the suspension, namely reductive

precipitation, precipitation with As(V), and surface adsorption. In all systems, XANES fits were best represented by the combination of nano-$UO_2$ and trögerite standards, with the exception of the high U concentration treatment with 640 μM As(V) which was fit with 28.9% U(VI) adsorbed to ferrihydrite and 56.1% trögerite. In order to study the role of possible precipitation of uranyl arsenate mineral phase(s) (e.g. trögerite) on the reduction of U(VI), the extent of U(VI) reduction was also examined in an experiment where U(VI) and As(V) were combined prior to the addition of the mackinawite suspension. In this system, only 26% of U(VI) was reduced in comparison to 75% reduction in the system where U(VI) and As(V) were added directly to the mackinawite suspension. In this system, the U(VI) component was represented by 43% U(VI) adsorbed to ferrihydrite and by 32% trögerite. Reoxidation experiments were carried out on two of the low U concentration treatments: 47 μM U(VI) without As and 47 μM U(VI) with 32 μM As(V). Some reoxidation of U(IV) took place but was not complete (Figure 4.5 and Table 4.4). Prior to injection, the percent of U(VI) present was 0%, and increased to 27% and 44% after air injection in treatments without and with As(V), respectively.

*Arsenic speciation*

The percentage of reduced As species associated with solid phase was determined by LCF of As XANES spectra. The results of the fitting are summarized in Figure 4.6. In the low U concentration systems, 44–53% of the solid-phase associated As was reduced to As(III) at all added As(V) concentrations. In the high U concentration systems, less As(V) reduction occurred, with only 22–28% reduced to As(III) for all of the added As(V) concentrations. Complete reduction was not observed. To rule out the possibility that U(VI) may limit As(V) reduction, As(V) was combined with mackinawite at 32 and 320 μM concentrations without U(VI). Results are summarized in Figure 4.6, Table 4.5, and Figure 4.7. In systems containing 32 μM As(V),

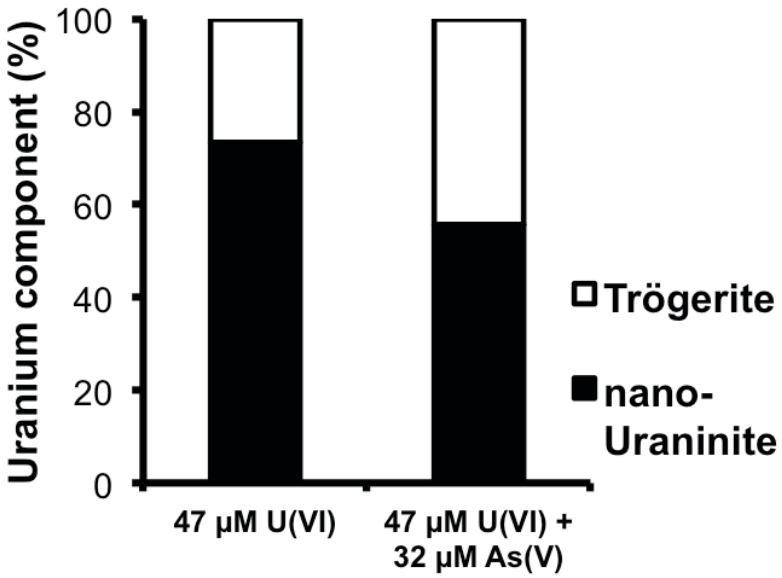


**Figure 4.5.** Percent U(IV) and percent U(VI) associated with mackinawite in batch systems as determined by linear-combination fitting of U $L_{III}$-edge XANES. Systems contained 47 µM U(VI) and 47 µM U(VI) with 32 µM As(V) and all systems contained 4.6 g/L of mackinawite. Data was collected after injection of 10 mL of air into each bottle followed by an additional 48 hours of reaction time. White bars indicate the U(VI) component fit with trögerite ($UO_2HAsO_4 \bullet 4H_2O$) as a reference compound and black bars indicate U(IV) fit using nano-$UO_2$ as a reference compound.

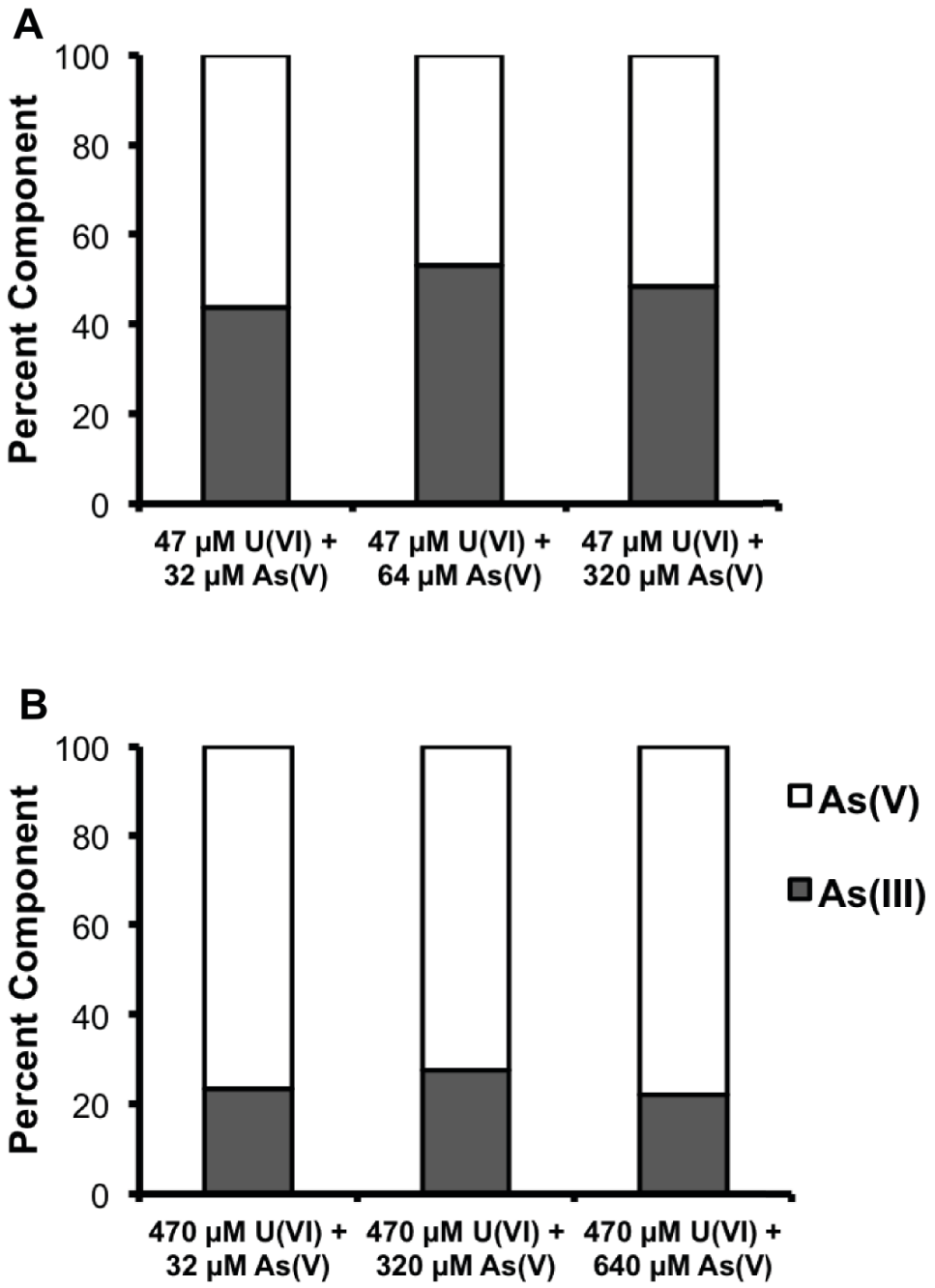


**Figure 4.6.** Arsenic redox speciation based on linear combination fitting of As K-edge XANES data for systems containing 47 µM U(VI) and 470 µM U(VI) with varying concentrations of As(V) and containing 4.6 g/L of mackinawite. White bars indicate As(V) and gray bars represent As(III). Reference compounds used in linear-combination fitting were As(V) and As(III) adsorbed to goethite.

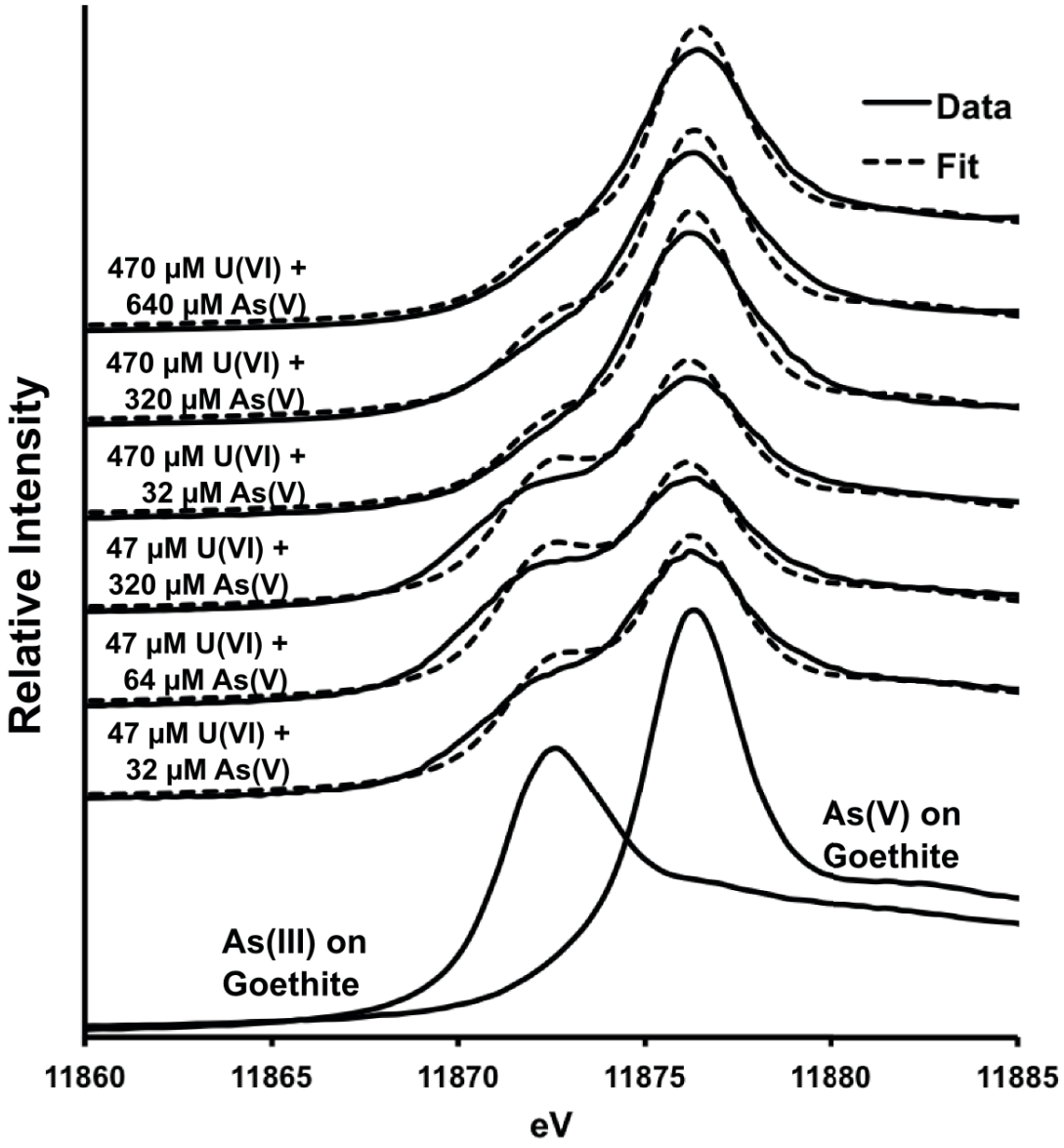


**Figure 4.7.** As K-edge XANES spectra from batch systems containing 470 µM U(VI) with varying concentrations of As(V) followed by spectra of batch systems containing 47 µM U(VI) with varying concentrations As(V). Standards used for linear combination fitting are As(III) adsorbed onto goethite and As(V) adsorbed onto goethite.

**Table 4.5.** Summary of As XANES linear-combination fitting results shown in Figure SI5. The R factor is the normalized sum of the difference between the model and the fit.

| Sample Type | Initial U(VI) (μM) | Initial As(V) (μM) | % As(III) adsorbed to goethite | % As(V) adsorbed to goethite | R factor |
|---|---|---|---|---|---|
| Added to mackinawite | 47 | 32 | 43.7 | 56.3 | 0.005370 |
| | 47 | 64 | 53.0 | 47.0 | 0.005591 |
| | 47 | 320 | 48.4 | 51.6 | 0.004117 |
| | 470 | 32 | 23.3 | 76.7 | 0.005235 |
| | 470 | 320 | 27.7 | 72.3 | 0.005745 |
| | 470 | 640 | 22.2 | 77.8 | 0.005114 |
| Combined before mackinawite addition | 340 | 340 | 14.7 | 85.3 | 0.004304 |

57.1% of solid-phase As was reduced, whereas in systems containing 320 μM, 63.5% of solid-phase As was reduced, demonstrating that complete reduction of As(V) did not occur even in the absence of U(VI). As(V) reduction was also investigated in the set-up where U(VI) and As(V) were combined prior to the addition of mackinawite. Similar to the case of U(VI), the percentage of As(V) reduction was lower (15%) than in the corresponding treatment where U(VI) and As(V) were added separately but simultaneously to the mackinawite suspension (28%). Thermodynamic modeling was performed to help determine the most likely aqueous complexes and mineral phases present at equilibrium for all of the As(V) treatments.

***Thermodynamic Modeling***

Thermodynamic modeling was performed using visual MINTEQ to determine if the conditions of each experimental treatment favored precipitation of uranyl arsenate mineral

phases. Limited information was available on the thermodynamic constants of uranyl arsenate aqueous complexes and solid phases. Rutsch et al (*157*) compared the formation constants of three uranyl arsenate aqueous complexes using time-resolved laser induced fluorescence spectroscopy (TR-LFS) and found their values to be similar to their uranyl phosphate analogs. Therefore we conducted speciation calculation using phosphate as a chemical analog for arsenate because of their similar stability constants. (*157*) The formation of four possible uranyl-phosphate minerals were considered including bassettite ($Fe(UO_2)_2(PO_4)_2 \cdot 8H_2O$), autunite ($Ca(UO_2)_2(PO_4)_2 \cdot nH_2O$), chernikovite ($UO_2HPO_4 \cdot 4H_2O$), and $(UO_2)_3(PO_4)_2 \cdot nH_2O$. However, $(UO_2)_3(AsO_4)_2 \bullet 12H_2O$ has never been found to occur in nature (*140*) and autunite formation would not be favored without the addition of calcium, so we will only report saturation indices for chernikovite, which is an analog for trögerite. In the low U concentration setups with all concentrations of As(V) (32-320 μM), systems were undersaturated for chernikovite. The high U concentration systems were also undersaturated for chernikovite at the all of the concentrations of As(V) (32 and 640 μM). The system containing 470 μM U(VI) and 640 μM As(V) was the closest to saturation for chernikovite with an index of -0.042. In the system where U(VI) and As(V) were combined prior to the addition of the mackinawite suspension, the saturation index for chernikovite was 0.860, indicating oversaturation prior to the mackinawite addition. We also observed a visible precipitate form in this treatment. The saturation indices for chernikovite support that trögerite is an appropriate reference compound to be used as the U(VI) standard in the LC fitting of U XANES data. Thus, EXAFS spectra were collected and interpreted in order to elucidate the potential role of trögerite.

**Table 4.6.** Summary of U $L_{III}$-edge EXAFS fitting results for selected U(VI) and As(V) treatments.

| Shell | CN [a] | R (Å) | $\sigma^2$ (Å$^2$) | $E_0$ (eV) | Residual (%) [b] |
|---|---|---|---|---|---|
| **3400 µM U + 3400 µM As before mackinawite addition** | | | | | |
| $O_{ax}$ | 2.4 | 1.83 | 0.008 | 6.78 | 7.5 |
| $O_{eq}$ | 6.3 | 2.29 | 0.009 | | |
| As | 1.2 | 3.72 | 0.002 | | |
| **470 µM U + 640 µM As added to mackinawite** | | | | | |
| $O_{ax}$ | 1.6 | 1.78 | 0.003 | 2.55 | 8.1 |
| $O_{eq}$ | 6.4 | 2.26 | 0.011 | | |
| 3400As | 1.8 | 3.68 | 0.008 | | |
| **470 µM U + 320 µM As added to mackinawite** | | | | | |
| $O_{ax}$ | 5.7 | 2.31 | 0.012 | 0.6 | 13.3 |
| U | 4.0 | 3.69 | 0.017 | | |

[a] coordination number

[b] $\text{Residual}(\%) = \sum_{i=1}^{N} | y_{\exp}(i) - y_{theo}(i) | \Big/ \sum_{i=1}^{N} | y_{\exp}(i) | \times 100$

***Characterization of solid-phase U***

The Fourier-transform of U $L_{III}$-edge EXAFS data was fit by shell-by-shell for selected samples in order to determine the local structure of U(VI) and U(IV) species in the final reaction products. The fitting parameters are summarized in Table 4.6. The three reported samples were chosen due to the differences in experimental setup and the observed distribution of U redox species as determined by LCF of XANES spectra. The three selected treatments contained (1) 470 µM U(VI) and 320 µM As(V) added simultaneously but separately to mackinawite, (2) 470 µM U(VI) and 640 µM As(V) added simultaneously but separately to mackinawite, and (3) 3400 µM U(VI) and 3400 µM As(V) combined prior to the addition of the mackinawite suspension. The data for each of these samples and their corresponding fits are shown in Figure 4.8. The

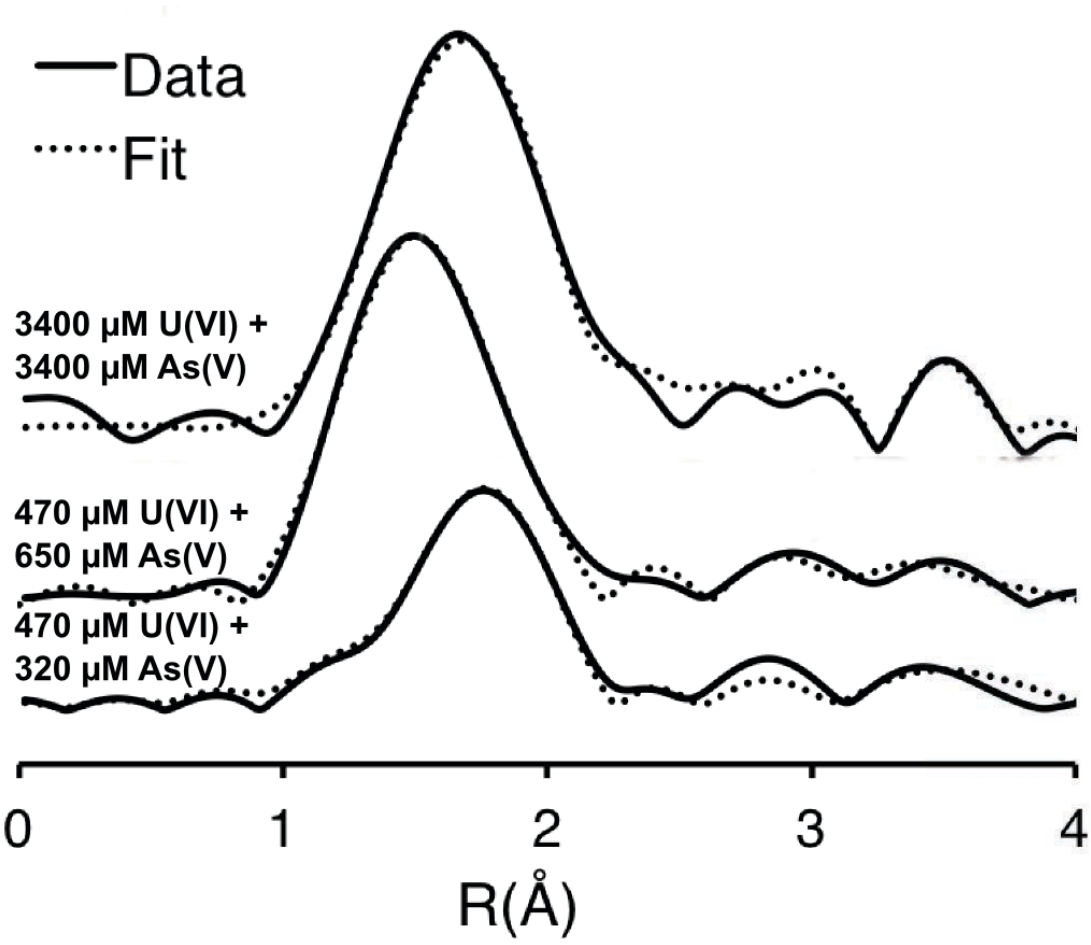


**FIGURE 4.8.** Shell by shell fitting of U $L_{III}$-edge EXAFS spectra for samples 3400 µM U + 3400 µM As combined prior to addition of the mackinawite suspension, 470 µM U + 650 µM As, and 470 µM U + 320 µM As added directly to the mackinawite suspension. The solid line indicates the collected data and the dotted line indicates the fit. Not corrected for phase shift.

spectra data were similar between the sample containing 470 µM U(VI) and 640 µM As(V) and the sample where U(VI) and As(V) were combined prior to the mackinawite addition. Of all of the treatments, these two treatments had the highest percentage of U(VI) in the solid reaction products as determined by LCF of U XANES. The overall fitting results indicated that both of these treatments contained a U(VI) form similar to the uranyl arsenate mineral trögerite. The first peak at ~1.4 Å in the Fourier Transform (without phase correction) is consistent with the

contribution from two axial oxygen atoms (~1.8 Å) and the equatorial oxygen atoms (~2.29-2.47 Å). The peak at ~3.7 Å indicates a backscattering contribution from the As atoms. In contrast to these two treatments, the sample containing 470 μM U(VI) and 320 μM As(V) was dominated by U(IV) species with a structure similar to nano-$UO_2$ as indicated by LCF of U XANES data, which is consistent with our shell-by-shell EXAFS fitting results. The peak at ~2.3 Å is indicative of the backscattering from the first O shell. An U shell is observed at ~3.7 Å with a coordination number of ~4, suggesting the dominant presence of nano sized $UO_2$, as no U-U correlation will be observed for monomeric U(IV) species (*21*, *22*) and a greater amplitude of this shell will be observed (coordination number of 12 as compared to 4 in our system) for highly crystalline or long-ranged ordered $UO_2$.

**Discussion**

While limited reduction of U(VI) to U(IV) in the presence of mackinawite was observed in early work, (*118*) two recent studies have observed complete reduction of U(VI) to U(IV). (*16*, *61*) These two studies also identified the reduced U(IV) as $UO_2$ and confirmed the presence of nano-$UO_2$ using a combination of shell-by-shell fitting of U $L_{III}$-edge EXAFS data and transmission electron microscopy. In our study, we also observed complete reduction of U(VI) to nano-$UO_2$ in the absence of As(V). We also observed complete removal of U(VI) from solution after 48 hours of reaction time in these systems (Figure 4.2). Earlier studies observed uptake of U(VI) onto the mackinawite surface within 15 minutes at pH 7, while reduction of U(VI) followed uptake and occurred on a longer time scale of 4 hours. (*60*) Although we did not conduct a time dependent study, U(VI) was fully reduced in samples without As(V) upon immediate mixing with mackinawite and filtering (results not shown) suggesting immediate reduction of U(VI) and precipitation as the cause of removal from solution. While complete

reduction of U(VI) was not observed with all concentrations of As(V), aqueous U(VI) was completely taken up by mackinawite in all treatments. (*16*, *60*, *61*, *118*) Based on previous research on the effect of arsenate and phosphate on U(VI) interactions with mineral surfaces (*24*, *26*, *68*) and at the U(VI) and As(V) concentration ranges and pH values (6.7–7.5) of our systems, we expect the primary form of solid-phase U(VI) to be uranyl arsenate surface precipitate(s) rather than adsorbed ternary uranyl arsenate surface complexes or U(VI) surface complexes. In addition, the number of reactive surface sites present on mackinawite, as estimated by the surface area and reactive site density measured by Wolthers et al., are not sufficient for all U(VI) and As(V) to be adsorbed by inner-sphere complexation in even the low concentration U systems. (*178*, *179*)

Two major mechanisms have been suggested for the reduction of U(VI) to $UO_2$ by mackinawite. Hua et al proposed that U(VI) could be reduced by either structural Fe(II) or $S^{2-}$ but could not distinguish between the two. (*60*) Hyun et al and Veeramani et al both suggest that U(VI) is reduced by structural $S^{2-}$ rather than Fe(II), but the two studies propose different oxidation products of $S^{2-}$ namely elemental sulfur and sulfate, respectively. (*16*, *61*) Our results are most consistent with the mechanism proposed by Veeramani et al because we observed an increase in aqueous sulfate concentrations in all systems (Table 4.2). In other studies, an increase in aqueous Fe(II) concentrations was observed following reaction, which indicated the exchange of structural Fe(II) for $UO_2^{2+}$ as U(VI) adsorption takes place. (*16*, *60*) We measured a decrease in aqueous Fe(II) concentrations over the reaction period, which rules out the possibility of exchange between Fe(II) and U(VI). We did not observe conversion of mackinawite to other mineral phases following the reaction period, suggesting that there was also no oxidation of structural Fe(II). Fe EXAFS data (Figure 4.1) show that the mackinawite structure was consistent

with nanoparticulate mackinawite at the start of the experiment and was dominated by crystalline mackinawite at the end of the experiment. Over the period of days, mackinawite can convert from nanoparticulate mackinawite to crystalline mackinawite. (*117*) Upon exposure to oxygen, mackinawite can also rapidly oxidize to goethite or lepidocrocite. (*16, 61*) Linear-combination fitting of the Fe XAS data did not indicate the presence of pyrite or any Fe(III) oxy(hydr)oxides, suggesting no changes in mineralogy in our system.

In this study, we examine the effect of As(V) on the reduction of U(VI) by mackinawite. Here, we observe that As(V) limits U(VI) reduction at high concentrations. The inhibition may be due to the formation of uranyl arsenate precipitates. Although thermodynamic calculations using Visual MINTEQ suggested undersaturation with regard to chernikovite (an analog for trögerite) at all experimental conditions where uranyl and arsenate were added simultaneously and separately, shell-by-shell fitting of the sample containing 470 μM U(VI) and 320 μM As(V) suggest the formation of a trögerite-like uranyl arsenate precipitate (Figure 4.8 and Table 4.6). This might be due to the variations in formation constants between uranyl phosphate and arsenate species (*158*) or the potential formation of poorly crystalline, highly disordered uranyl arsenate surface precipitates. Although the effect of As(V) on U(VI) reduction has not been previously studied, phosphate has been shown to affect the product of U(VI) reduction. Phosphate present in biomass is thought to promote the formation of molecular U(IV) rather than crystalline $UO_2$ (*21, 22, 52*), which was not detected in our study. However, due to the limited sensitivity of XAS, we can not rule out the possible existence of minor amounts of molecular U(IV) in our system, which could be masked by other more dominant U components. Studies have also found that microbially-mediated reduction of U(VI) in the presence of aqueous phosphate or as hydrogen uranyl phosphate ($UO_2HPO_4 \cdot 4H_2O$) results in the formation of the

U(IV) phosphate mineral ningyoite [$CaU(PO_4)_2$]. (*21*, *22*, *52*, *163-165*) Little research has discussed the existence of a similar U(IV) arsenate mineral phase (*180*) and LCF of our XANES and EXAFS did not indicate the presence of a reduced uranium arsenate mineral.

The ability for trögerite-like uranyl arsenate precipitates to be reduced by mackinawite was also investigated to elucidate if their formation prevents the reduction of both U(VI) and As(V). When U(VI) and As(V) were combined prior to the addition of mackinawite, the saturation index at that concentration level indicated that trögerite precipitation would be favored. The presence of a uranyl arsenate precipitate with a structure similar to trögerite was confirmed by shell-by-shell fitting of the U $L_{III}$-edge EXAFS spectrum for this treatment after reaction with mackinawite. The shell observed at ~3.7 Å is the indication of a backscattering contribution from the As atoms. $UO_2(HAsO_4)_2 \bullet H_2O$ was not present in our system based on U $L_{III}$ EXAFS data. (*68*, *140*) When uranyl arsenate precipitation occurred prior to the addition of the mackinawite suspension, less U(VI) reduction (39%) was observed as compared to the system where U(VI) and As(V) were added simultaneously and separately to mackinawite (75%). Rui et al showed that the bioreduction of hydrogen uranyl phosphate takes place following mineral dissolution. (*164*) With the presence of low solubility trögerite-like precipitates in our system, we expect decreased degree of U(VI) reduction where uranyl arsenate precipitates occurs, which was confirmed in our system.

In the presence of mackinawite, $UO_2$ was formed for all treatments. In the low U concentration systems, we observed that mackinawite protected $UO_2$ from complete reoxidation to U(VI) following air injections. Previous work has shown that mackinawite preferentially reacts with dissolved oxygen, preventing $UO_2$ oxidation. (*16*, *155*) In considering uranyl immobilization, both reduction to $UO_2$ and the formation of low solubility uranyl mineral

precipitates are environmentally relevant. Indeed, the stability of trögerite is similar to chernikovite and both are insoluble under groundwater conditions (*181*), allowing effective immobilization of uranyl contaminants.

Our system also examined the redox behavior of As because As(V) reduction was expected to occur in the presence of mackinawite. While some reduction of As(V) occurred, we did not observe complete reduction in any of the treatments (Figure 4.6 and Table 4.5). Based on the findings of Gallegos et al, As(V) can be reduced by structural $S^{2-}$ on mackinawite surface, which is the similar mechanism for U(VI) reduction. (*153*) With the formation of surface precipitates ($UO_2$ or uranyl arsenate precipitates), U(VI) may limit As(V) reduction by preventing As(V) interaction with surface $S^{2-}$ group. As previously discussed, the number of estimated reactive surface sites on mackinawite was not sufficient to adsorb all of the added As(V) in both low and high U concentration treatments. Studies have also found that in systems containing a mixture of Fe minerals, As has low affinity for mackinawite. (*36*, *182*) In addition, Widler and Seward found the point of zero charge of crystalline mackinawite to be 2.9, so the surface of mackinawite would be negatively charged in our system (pH 6.7-7.5) resulting in preferential adsorption of uranyl cations over arsenate anions. Based on XANES fitting, As(III) resulted from As(V) reduction, but no As-S mineral phases were formed. Past studies have observed that the reduction of As(V) by mackinawite results in the formation of the As-S mineral realgar ($As_2S_3$). (*34*, *153*) The formation of realgar in our study is not likely to occur because it is favored only under a narrow range of sulfide concentrations, where concentrations must be high enough to favor As-S mineral precipitation but not too high to favor formation of thioarsenite species. (*172*) Our results are consistent with other work where low aqueous sulfide concentration was observed to prevent realgar formation. (*36*, *172*)

**Environmental Implications**

Biogenic mackinawite has been shown to play an important role in the reduction of U(VI) in sediments at U mill tailings such as those in Rifle, CO. (*55*) Previous work and this study have also shown that mackinawite can prevent reoxidation of $UO_2$, subsequently preventing U remobilization. While studies have examined the ability for U(VI) to be reduced by synthetic and biogenic mackinawite, the effect of naturally occurring anions on U(VI) reduction has not been widely investigated. (*16*, *61*) An improved understanding on the influence of U-complexing anions (e.g., arsenate, vanadate, and phosphate) on U(VI) reduction will help us to better predict U(VI) reduction and retardation behavior in environmental systems. The high concentrations of As(V) and U(VI) used in this study may not occur naturally at most open-pit mine tailings, but they may occur in drainage from in-situ leaching U mining or from the processing of U ore. (*67*) Because a common strategy for immobilization of U is reduction to $UO_2$, understanding whether arsenate or similar anions such as phosphate or vanadate can limit reduction is important for the design of remediation strategies. (*183*, *184*) While the presence of stable U(VI) mineral phases may prevent U(VI) reduction, their formation may offer an alternative strategy for U immobilization. Further research into the influence of anions such as carbonate, phosphate, vanadate and arsenate is needed to better understand if U(VI) reduction by mackinawite is a significant process in all natural systems.

# CHAPTER 5

# SUMMARY

The research performed in this dissertation was meant to elucidate the redox chemistry of U and As that promotes or prevents mobilization of these elements in mine-impacted environments. The work presented here examines U and As chemistry in three different systems: (I) under field conditions at the North Cave Hills, to characterize reactions controlling the mobility at the site (Chapter 2); (II) in microbially stimulated laboratory systems with natural sediment, to determine how As and U behave in anoxic, microbially active systems similar to the conditions at the North Cave Hills and, later, under oxic conditions (Chapter 3); (III) in abiotic laboratory systems with mackinawite (FeS) to examine the reduction of U and As in a simplified system and to examine the formation of uranyl arsenate minerals and their reduction potential (Chapter 4). X-ray absorption spectroscopy was used in order to determine the solid-phase redox species present in all of the work presented here. This chapter summarizes the key findings and implications of the work in the previous three chapters and makes recommendations for continued research in the area of U and As redox chemistry.

Due to the previous detection of above background level concentrations of U and As in sediments and surface waters surrounding the North Cave Hills, the mechanisms controlling the transport of U and As from the tailings pile to the surrounding watershed were studied. Uranium was primarily transported by erosion at the site, based on decreasing concentrations in sediment with distance from the tailings. Sequential extractions and U XANES fitting indicate that U is immobilized in a near-source sedimentation pond both by prevention of sediment transport and by reduction of U(VI) to U(IV). In contrast to U, subsequent release of As to the watershed takes

place from the pond partially due to reductive dissolution of Fe oxy (hydr)oxides. However, As is immobilized by adsorption to clays and Fe oxy (hydr)oxides in oxic zones and by formation of As-sulfide mineral phases in anoxic zones down gradient, indicated by sequential extractions and As XANES fitting. This study indicates that As should be considered during remediation of uranium mine sites in order to prevent transport to public-use lands. While this work characterized the behavior of U and As specifically at the North Cave Hills, findings can be applied to other mine and mill tailings sites where both elements are present. The original intention of this research was to use U and As EXAFS to determine the specific forms of U and As present and determine if and how they are bound to one another or to Fe minerals in North Cave Hills sediments. Due to the low environmental concentrations of U and As present, high-quality EXAFS spectra could not be collected. Future work examining U and As redox chemistry at environmental concentrations should consider using micro-focused X-ray fluorescence spectroscopy (XRF) accompanied by micro-EXAFS in order to obtain high quality EXAFS spectra on selected high concentration U and As containing spots.

The seasonal variation in precipitation at the North Cave Hills inspired the laboratory-based experiments. By performing experiments in the lab using North Cave Hills sediments and media to mimic surface water composition, systems could be maintained under anoxic conditions and then later be exposed to air as would occur during the drying of an anoxic, waterlogged zone. In addition, we studied the behavior of U and As during biostimulation by three different common electron donors—acetate, lactate, and ethanol. U(VI) addition prevented sulfate reduction from occurring in batch systems, likely due to a toxicity effect on the stimulated microbes. U(VI) reduction also did not occur in these systems. Concentrations used in batch experiments were higher than would typically be found in natural environments, so the same

toxicity effect will likely not be observed under field conditions. In systems that originally contained no U(VI), the formation of mackinawite was observed, followed by the reduction of As(V) to As(III) and an As-sulfide mineral phase. When U(VI) was added to these bottles, reduction to nano-$UO_2$ was observed, indicating that mackinawite played a role in U reduction. Acetate was shown to be the electron donor that stimulated the most U(VI) reduction and ethanol was the electron donor that stimulated the most As(V) reduction. The results of these experiments indicate that biostimulation of a field site would result in mineralization of both U and As which would prevent further transport of both. While some re-release of U and As was observed upon exposure to air, much of the solid-phase U and As remained in their reduced forms. When mackinawite is formed during bioremediation, it can act as a strong electron donor and also can protect U and As from reoxidation. Although these studies indicate that U and As reduction can take place abiotically in the presence of biogenic mackinawite, we cannot rule out that direct microbial reduction was not also taking place. Further investigation in the microbial activity in these systems is necessary to understand why U(VI) limited microbial activity, whether direct U(VI) and As(V) reduction took place, and why different extents of reduction were observed in the presence of different electron donors. Characterization of the microbial communities in each treatment would help to answer these questions.

Many previous studies have examined U and As redox reactions in the presence of mackinawite, but the two elements have not been previously investigated together. Because many biostimulation studies both in the field and in the laboratory have observed mackinawite formation, understanding mackinawite interactions with U and As is important for the design of effective remediation strategies. In these experiments, As(V) was added to systems containing 47 μM and 470 μM U(VI) at concentrations ranging from 32 to 640 μM. Solid-phase speciation and

characterization of U and As were determined using XANES and EXAFS. In the absence of As(V), U(VI) was completely removed from solution and fully reduced to nano-uraninite ($UO_2$). U(VI) was also removed from the aqueous phase in the presence of As(V), but the reduction of U(VI) was limited at As(V) concentrations above 320 μM. The formation of the uranyl arsenate mineral trögerite, as observed by EXAFS, may change the reduction potential of uranyl, resulting in less overall U(VI) reduction when As(V) is present. The formation of uranyl arsenate aqueous complexes has not been observed in the environment, but uranyl arsenate minerals such as trögerite have been observed. Although these complexes have not been detected in environmental systems, the possibility of their formation must be considered in order to understand U and As behavior. Arsenate is a close analog for phosphate and one common remediation strategy for U is to add phosphate to systems in order to precipitate uranyl phosphate minerals. Because of the toxicity of As(V), the addition of As(V) for U remediation is not feasible, but understanding how As(V) effects U(VI) reduction will provide insight into the stability of both uranyl arsenate and uranyl phosphate minerals.

Despite the insight gained through the research described here, there is room for continued research in the areas of U and As redox chemistry. In order to better understand the mechanisms controlling U and As fate and transport in the field, further controlled laboratory experiments need to be conducted.

This is the first research into how thermodynamics of U(VI) and As(V) reduction change when they are present as a uranyl arsenate mineral. The system examined here involved four redox active elements (U, As, Fe, and S), but the system could be simplified. For example the reduction of uranyl arsenate minerals and aqueous complexes in the presence of aqueous sulfide or magnetite could be investigated. The microbial reduction of uranyl arsenate minerals by

sulfate reducing bacteria could also be investigated. While we used an excess of mackinawite in our systems, lowering the concentration of reducing agent would help to determine if the reduction of either U(VI) or As(V) is favored. In addition, surface precipitation of uranyl arsenate onto aluminum oxide has been studied, but the formation of uranyl arsenate surface complexes and precipitates on other common soil minerals such as Fe oxy(hydr)oxides has not been studied.

Many researchers are examining the formation of molecular U(IV) in the environment. The existence of molecular U(IV) is important because we previously believed that U(IV) only existed in mineral forms. The goal of most U remediation strategies is to immobilize U as $UO_2$, but this might not be successful if U can be reduced to a mobile form of U(IV). Recent work has shown that molecular U(IV) forms when phosphate groups are present in the form of biomass. Our work has not described the interactions between U(IV) and arsenate. Because of the important role that phosphate plays in molecular U(IV) formation, arsenate may have a similar effect in promoting molecular U(IV) formation. While molecular U(IV) was not observed in our work, most samples contained a mixture of U species and molecular U(IV) may have been difficult to detect if it were not the dominant species present.

REFERENCES


1. D. Langmuir, *Aqueous environmental geochemistry* (Prentice Hall, 1997).

2. S. R. Taylor, Abundance of chemical elements in the continental crust: a new table, *Geochem. Cosmochim. Acta* **28**, 1273–1285 (1964).

3. A. Abdelouas, Uranium mill tailings: geochemistry, mineralogy, and environmental impact, *Elements* **2**, 335 (2006).

4. M. Ginder-Vogel, C. S. Criddle, S. E. Fendorf, Thermodynamic constraints on the oxidation of biogenic UO2 by Fe (III)(hydr) oxides, *Environ. Sci. Technol.* **40**, 3544–3550 (2006).

5. A. Abdelouas, W. Lutze, E. Nuttall, Chemical reactions of uranium in ground water at a mill tailings site, *Journal of Contaminant Hydrology* **34**, 343–361 (1998).

6. G. Mudd, Critical review of acid in situ leach uranium mining: 1. USA and Australia, *Environmental Geology* **41**, 390–403 (2001).

7. D. Langmuir, Uranium solution-mineral equilibria at low temperatures with applications to sedimentary ore deposits, *Geochem. Cosmochim. Acta* **42**, 547–569 (1978).

8. W. Dong *et al.*, Influence of calcite and dissolved calcium on uranium (VI) sorption to a Hanford subsurface sediment, *Environ. Sci. Technol.* **39**, 7949–7955 (2005).

9. J. Wan *et al.*, Reoxidation of bioreduced uranium under reducing conditions, *Environ. Sci. Technol.* **39**, 6162–6169 (2005).

10. J. L. Jambor, J. E. Dutrizac, Occurrence and Constitution of Natural and Synthetic Ferrihydrite, a Widespread Iron Oxyhydroxide, *Science* **98**, 2549–2586 (1998).

11. C. Hsi, D. Langmuir, Adsorption of uranyl onto ferric oxyhydroxides: Application of the surface complexation site-binding model, *Geochem. Cosmochim. Acta* **49**, 1931–1941 (1985).

12. T. D. Waite, J. A. Davis, T. Payne, G. A. Waychunas, N. Xu, Uranium (VI) adsorption to ferrihydrite: Application of a surface complexation model, *Geochem. Cosmochim. Acta* **58**, 5465–5478 (1994).

13. E. Liger, L. Charlet, P. Van Cappellen, Surface catalysis of uranium (VI) reduction by iron (II), *Geochem. Cosmochim. Acta* **63**, 2939–2955 (1999).

14. T. Scott, G. Allen, P. Heard, M. Randell, Reduction of U (VI) to U (IV) on the surface of magnetite, *Geochem. Cosmochim. Acta* **69**, 5639–5646 (2005).

15. B. Hua, H. Xu, J. Terry, B. Deng, Kinetics of Uranium(VI) Reduction by Hydrogen

Sulfide in Anoxic Aqueous Systems, *Environ. Sci. Technol.* **40**, 4666–4671 (2006).

16. S. P. Hyun, J. A. Davis, K. Sun, K. F. Hayes, Uranium (VI) reduction by iron (II) monosulfide mackinawite, *Environ. Sci. Technol.* **46**, 3369–3376 (2012).

17. D. R. Lovley, E. Phillips, Reduction of uranium by Desulfovibrio desulfuricans, *Applied and Environmental Microbiology* **58**, 850 (1992).

18. D. R. Lovley, E. E. Roden, E. Phillips, J. Woodward, Enzymatic iron and uranium reduction by sulfate-reducing bacteria, *Marine Geology* **113**, 41–53 (1993).

19. J. D. Wall, L. R. Krumholz, Uranium reduction, *Annu. Rev. Microbiol.* **60**, 149–166 (2006).

20. J. R. Bargar, R. Bernier-Latmani, D. E. Giammar, B. M. Tebo, Biogenic Uraninite Nanoparticles and Their Importance for Uranium Remediation, *Elements* **4**, 407–412 (2008).

21. R. Bernier-Latmani *et al.*, Non-uraninite products of microbial U (VI) reduction, *Environ. Sci. Technol.* **44**, 9456–9462 (2010).

22. M. I. Boyanov *et al.*, Solution and Microbial Controls on the Formation of Reduced U(IV) Species, *Environ. Sci. Technol.* **45**, 8336–8344 (2011).

23. Y. Wang *et al.*, Mobile uranium(IV)-bearing colloids in a mining-impacted wetland, *Nature Communications* **4**, 1–9 (2013).

24. A. Singh, K.-U. Ulrich, D. E. Giammar, Impact of phosphate on U (VI) immobilization in the presence of goethite, *Geochem. Cosmochim. Acta* **74**, 6324–6343 (2010).

25. Y. Tang, R. J. Reeder, Enhanced Uranium Sorption on Aluminum Oxide Pretreated with Arsenate. Part I: Batch Uptake Behavior, *Environ. Sci. Technol.* **43**, 4446–4451 (2009).

26. A. Singh, J. G. Catalano, K.-U. Ulrich, D. E. Giammar, Molecular-Scale Structure of Uranium(VI) Immobilized with Goethite and Phosphate, *Environ. Sci. Technol.* **46**, 6594–6603 (2012).

27. W. H. Yu, C. M. Harvey, C. F. Harvey, Arsenic in groundwater in Bangladesh: A geostatistical and epidemiological framework for evaluating health effects and potential remedies, *Water Resources Research* **39** (2003).

28. H. K. Das *et al.*, Arsenic concentrations in rice, vegetables, and fish in Bangladesh: a preliminary study, *Environment International* **30**, 383–387 (2004).

29. S. Fendorf, P. S. Nico, B. D. Kocar, Y. Masue, K. J. Tufano, Arsenic chemistry in soils and sediments, *Developments in Soil Science* **34**, 357–378 (2010).

30. R. Donahue, M. J. Hendry, Geochemistry of arsenic in uranium mine mill tailings,

Saskatchewan, Canada, *Appl. Geochem.* **18**, 1733–1750 (2003).

31. P. A. O'day, Chemistry and mineralogy of arsenic, *Elements* **2**, 77 (2006).

32. R. A. Root *et al.*, Speciation and natural attenuation of arsenic and iron in a tidally influenced shallow aquifer, *Geochem. Cosmochim. Acta* **73**, 5528–5553 (2009).

33. E. A. Rochette, B. C. Bostick, G. Li, S. Fendorf, Kinetics of Arsenate Reduction by Dissolved Sulfide, *Environ. Sci. Technol.* **34**, 4714–4720 (2000).

34. T. J. Gallegos, Y.-S. Han, K. F. Hayes, Model Predictions of Realgar Precipitation by Reaction of As(III) with Synthetic Mackinawite Under Anoxic Conditions, *Environ. Sci. Technol.* **42**, 9338–9343 (2008).

35. S. G. Johnston *et al.*, Chemical Geology, *Chemical Geology* **334**, 9–24 (2012).

36. B. D. Kocar, T. Borch, S. Fendorf, Arsenic repartitioning during biogenic sulfidization and transformation of ferrihydrite, *Geochem. Cosmochim. Acta* **74**, 980–994 (2010).

37. S. Dixit, J. G. Hering, Comparison of Arsenic(V) and Arsenic(III) Sorption onto Iron Oxide Minerals: Implications for Arsenic Mobility, *Environ. Sci. Technol.* **37**, 4182–4189 (2003).

38. K. J. Tufano, C. Reyes, C. W. Saltikov, S. E. Fendorf, Reductive Processes Controlling Arsenic Retention: Revealing the Relative Importance of Iron and Arsenic Reduction, *Environ. Sci. Technol.* **42**, 8283–8289 (2008).

39. B. D. Kocar, M. J. Herbel, K. J. Tufano, S. E. Fendorf, Contrasting Effects of Dissimilatory Iron(III) and Arsenic(V) Reduction on Arsenic Retention and Transport, *Environ. Sci. Technol.* **40**, 6715–6721 (2006).

40. G. G. Kipp, J. J. Stone, L. D. Stetler, Arsenic and uranium transport in sediments near abandoned uranium mines in Harding County, South Dakota, *Appl. Geochem.* **24**, 2246–2255 (2009).

41. J. J. Stone, L. D. Stetler, A. Schwalm, Final Report: North Cave Hills Abandoned Uranium Mines Impact Investigation, *South Dakota School of Mines and Technology*, 1–217 (2007).

42. Agency for Toxic Substances and Disease Registry, *Toxicological Profile for Uranium* (U.S. Department of Health and Human Services, Public Health Service, Atlanta, GA, 2013), pp. 1–526.

43. J. Petrick, Monomethylarsonous Acid (MMAIII) Is More Toxic Than Arsenite in Chang Human Hepatocytes, *Toxicology and Applied Pharmacology* **163**, 203–207 (2000).

44. K. J. Tufano, S. E. Fendorf, Confounding impacts of iron reduction on arsenic retention, *Environ. Sci. Technol.* **42**, 4777 (2008).

45. V. K. Stucker, K. H. Williams, M. J. Robbins, J. F. Ranville, Arsenic geochemistry in a biostimulated aquifer: An aqueous speciation study, *Environ Toxicol Chem* **32**, 1216–1223 (2013).

46. R. Donahue, M. J. Hendry, P. Landine, Distribution of arsenic and nickel in uranium mill tailings, Rabbit Lake, Saskatchewan, Canada, *Appl. Geochem.* **15**, 1097–1119 (2000).

47. J. Essilfie-Dughan, M. J. Hendry, J. Warner, T. Kotzer, Arsenic and iron speciation in uranium mine tailings using X-ray absorption spectroscopy, *Appl. Geochem.* **28**, 11–18 (2013).

48. L. N. Larson, G. G. Kipp, H. V. Mott, J. J. Stone, Sediment pore-water interactions associated with arsenic and uranium transport from the North Cave Hills mining region, South Dakota, USA, *Appl. Geochem.* **27**, 879–891 (2012).

49. L. N. Larson, J. J. Stone, Sediment-bound Arsenic and Uranium Within the Bowman–Haley Reservoir, North Dakota, *Water Air Soil Pollut* **219**, 27–42 (2010).

50. G. Bernhard *et al.*, Uranyl (VI) carbonate complex formation: Validation of the Ca2UO2 (CO3) 3 (aq.) species, *Radiochim. Acta* **89**, 511 (2001).

51. B. D. Stewart, M. A. Mayes, S. Fendorf, Impact of Uranyl-Calcium-Carbonato Complexes on Uranium(VI) Adsorption to Synthetic and Natural Sediments, *Environ. Sci. Technol.* **44**, 928–934 (2010).

52. V. Sivaswamy *et al.*, Multiple Mechanisms of Uranium Immobilization by Cellulomonas sp Strain ES6, *Biotechnol Bioeng* **108**, 264–276 (2011).

53. J. O. Sharp *et al.*, Uranium speciation and stability after reductive immobilization in aquifer sediments, *Geochem. Cosmochim. Acta* **75**, 6497–6510 (2011).

54. T. Borch *et al.*, Biogeochemical Redox Processes and their Impact on Contaminant Dynamics, *Environ. Sci. Technol.* **44**, 15–23 (2010).

55. J. R. Bargar *et al.*, Uranium redox transition pathways in acetate-amended sediments, *Proc. Natl. Acad. Sci.* **110**, 4506–4511 (2013).

56. S. E. Fendorf, H. A. Michael, A. Van Geen, Spatial and Temporal Variations of Groundwater Arsenic in South and Southeast Asia, *Science* **328**, 1123–1127 (2010).

57. P. A. O'day, D. Vlassopoulos, R. Root, N. Rivera Jr, The influence of sulfur and iron on dissolved arsenic concentrations in the shallow subsurface under changing redox conditions, *Proc. Natl. Acad. Sci.* **101**, 13703 (2004).

58. P. M. Fox *et al.*, Abiotic U(VI) reduction by sorbed Fe(II) on natural sediments, *Geochem. Cosmochim. Acta* **117**, 266–282 (2013).

59. D. E. Latta, M. I. Boyanov, K. M. Kemner, E. J. O'Loughlin, M. M. Scherer, Abiotic reduction of uranium by Fe(II) in soil, *Appl. Geochem.* **27**, 1512–1524 (2012).

60. B. Hua, B. Deng, Reductive Immobilization of Uranium(VI) by Amorphous Iron Sulfide, *Environ. Sci. Technol.* **42**, 8703–8708 (2008).

61. H. Veeramani *et al.*, Abiotic reductive immobilization of U (VI) by biogenic mackinawite, *Environ. Sci. Technol.* **47**, 2361–2369 (2013).

62. D. R. Lovley, E. J. P. Phillips, Y. A. Gorby, E. R. Landa, Microbial reduction of uranium, *Nature* **350**, 413–416 (1991).

63. D. E. Cummings, F. Caccavo, S. Fendorf, R. F. Rosenzweig, Arsenic Mobilization by the Dissimilatory Fe(III)-Reducing Bacterium Shewanella algaBrY, *Environ. Sci. Technol.* **33**, 723–729 (1999).

64. R. Oremland, J. Stolz, The ecology of arsenic, *Science* **300**, 939 (2003).

65. W. R. Cullen, K. J. Reimer, Arsenic speciation in the environment, *Science* **89**, 713–764 (1989).

66. B. D. Kocar, S. E. Fendorf, Thermodynamic constraints on reductive reactions influencing the biogeochemistry of arsenic in soils and sediments, *Environ. Sci. Technol.* **43**, 4871–4877 (2009).

67. W. A. Gezahegne *et al.*, EXAFS and DFT Investigations of Uranyl Arsenate Complexes in Aqueous Solution, *Environ. Sci. Technol.* **46**, 2228–2233 (2012).

68. Y. Tang, R. J. Reeder, Uranyl and arsenate cosorption on aluminum oxide surface, *Geochem. Cosmochim. Acta* **73**, 2727–2743 (2009).

69. K. M. Campbell *et al.*, Geochemical, mineralogical and microbiological characteristics of sediment from a naturally reduced zone in a uranium-contaminated aquifer, *Appl. Geochem.* **27**, 1499–1511 (2012).

70. T. Ohnuki *et al.*, The formation of autunite (Ca(UO2)2(PO4)2nH2O) within the leached layer of dissolving apatite: incorporation mechanism of uranium by apatite, *Chemical Geology* **211**, 1–14 (2004).

71. K. R. Salome *et al.*, The role of anaerobic respiration in the immobilization of uranium through biomineralization of phosphate minerals, *Geochem. Cosmochim. Acta* **106**, 344–363 (2013).

72. B. J. Moldovan, D. T. Jiang, M. J. Hendry, Mineralogical Characterization of Arsenic in Uranium Mine Tailings Precipitated from Iron-Rich Hydrometallurgical Solutions, *Environ. Sci. Technol.* **37**, 873–879 (2003).

73. J. L. Domingo, Reproductive and developmental toxicity of natural and depleted

uranium: a review, *Reproductive Toxicology* **15**, 603–609 (2001).

74. E. S. Craft *et al.*, Depleted and Natural Uranium: Chemistry and Toxicological Effects, *Journal of Toxicology and Environmental Health, Part B* **7**, 297–317 (2004).

75. G. W. Kunze, J. B. Dixon, in *Methods of Soil Analysis: Part 1—Physical and Mineralogical Methods*, A. Klute, Ed. (Soil Science Society of America, 1986), pp. 91–100.

76. K. H. Tan, *Soil Sampling, Preparation, and Analysis* (Taylor & Francis Group, LLC, ed. 2, 2005).

77. L. J. Poppe, V. F. Paskevich, J. C. Hathaway, D. S. Blackwood, *A Laboratory Manual for X-Ray Powder Diffraction* (US Geological Survey, Woods Hole, MA, 2001).

78. L. D. Whittig, W. R. Allardice, in *Methods of Soil Analysis: Part 1: Physical and Mineralogical Methods*, A. Klute, Ed. (Soil Science Society of America, 1986), vol. 1, pp. 331–362.

79. W. Harris, G. N. White, in *Methods of Soil Analysis: Part 5—Mineralogical Methods*, A. L. Ulery, L. R. Drees, Eds. (Soil Science Society of America, Madison, WI, 2008), vol. 5, pp. 81–115.

80. W. Harris, G. N. White, X-ray diffraction techniques for soil mineral identification, *Methods of soil analysis, part*, 81–116 (2008).

81. P. N. Soltanpour, J. Benton Jones, S. M. Workman, in *Methods of Soil Analysis—Part 2: Chemical and Microbiological Properties*, A. L. Page, Ed. (Soil Science Society of America, 1982), vol. 2, pp. 55–57.

82. J.-H. Huang, R. Kretzschmar, Sequential extraction method for speciation of arsenate and arsenite in mineral soils, *Anal. Chem.* **82**, 5534–5540 (2010).

83. M. J. Beazley, R. J. Martinez, S. M. Webb, P. A. Sobecky, M. Taillefert, The effect of pH and natural microbial phosphatase activity on the speciation of uranium in subsurface soils, *Geochem. Cosmochim. Acta* **75**, 5648–5663 (2011).

84. A. Tessier, P. Campbell, M. Bisson, Sequential extraction procedure for the speciation of particulate trace metals, *Anal. Chem.* **51**, 844–851 (1979).

85. T. Borch, Y. Masue-Slowey, R. K. Kukkadapu, S. E. Fendorf, Phosphate Imposed Limitations on Biological Reduction and Alteration of Ferrihydrite, *Environ. Sci. Technol.* **41**, 166–172 (2007).

86. K. Amstaetter, T. Borch, P. Larese-Casanova, A. Kappler, Redox transformation of arsenic by Fe (II)-activated goethite (α-FeOOH), *Environ. Sci. Technol.* **44**, 102–108 (2010).

87. B. Ravel, M. Newville, ATHENA, ARTEMIS, HEPHAESTUS: data analysis for X-ray absorption spectroscopy using IFEFFIT, *Journal of synchrotron radiation* **12**, 537–541 (2005).

88. E. J. Schofield *et al.*, Structure of Biogenic Uraninite Produced by Shewanella oneidensisStrain MR-1, *Environ. Sci. Technol.* **42**, 7898–7904 (2008).

89. P. A. O'day, N. Rivera Jr, R. Root, S. A. Carroll, X-ray absorption spectroscopic study of Fe reference compounds for the analysis of natural sediments, *American Mineralogist* **89**, 572 (2004).

90. R. M. Cornell, U. Schwertmann, *The Iron Oxides* (Wiley-VCH, 2006).

91. J. J. Moran *et al.*, Laser ablation isotope ratio mass spectrometry for enhanced sensitivity and spatial resolution in stable isotope analysis, *Rapid Commun. Mass Spectrom.* **25**, 1282–1290 (2011).

92. J. K. Fredrickson *et al.*, Reduction of U (VI) in goethite (α-FeOOH) suspensions by a dissimilatory metal-reducing bacterium, *Geochem. Cosmochim. Acta* **64**, 3085–3098 (2000).

93. R. J. Reeder *et al.*, Coprecipitation of uranium (VI) with calcite: XAFS, micro-XAS, and luminescence characterization, *Geochem. Cosmochim. Acta* **65**, 3491–3503 (2001).

94. Z. Zheng, T. K. Tokunaga, J. Wan, Influence of Calcium Carbonate on U(VI) Sorption to Soils, *Environ. Sci. Technol.* **37**, 5603–5608 (2003).

95. J. D. C. Begg *et al.*, Bioreduction Behavior of U(VI) Sorbed to Sediments, *Geomicrobiology Journal* **28**, 160–171 (2011).

96. P. Smedley, D. Kinniburgh, A review of the source, behaviour and distribution of arsenic in natural waters, *Appl. Geochem.* **17**, 517–568 (2002).

97. B. A. Manning, S. Goldberg, Adsorption and Stability of Arsenic (III) at the Clay Mineral− Water Interface, *Environ. Sci. Technol.* **31**, 2005–2011 (1997).

98. M. F. Lengke, C. Sanpawanitchakit, R. N. Tempel, The Oxidation and Dissolution of Arsenic-Bearing Sulfides, *The Canadian Mineralogist* **47**, 593–613 (2009).

99. M. F. Lengke, R. N. Tempel, Reaction rates of natural orpiment oxidation at 25 to 40° C and pH 6.8 to 8.2 and comparison with amorphous As 2 S 3 oxidation, *Geochem. Cosmochim. Acta* **66**, 3281–3291 (2002).

100. D. K. Newman, T. J. Beveridge, F. Morel, Precipitation of Arsenic Trisulfide by Desulfotomaculum auripigmentum, *Applied and Environmental Microbiology* **63**, 2022–2028 (1997).

101. B. C. Bostick, Arsenite sorption on troilite (FeS) and pyrite (FeS2), *Geochem.*

*Cosmochim. Acta* **67**, 909–921 (2003).

102. S. Kelly, D. Hesterberg, B. Ravel, in *Methods of Soil Analysis: Part 5—Mineralogical Methods*, A. L. Ulery, L. R. Drees, Eds. (Soil Science Society of America, 2008), vol. 5, pp. 387–463.

103. H. H. Tabak, P. Lens, E. D. Hullebusch, W. Dejonghe, Developments in Bioremediation of Soils and Sediments Polluted with Metals and Radionuclides – 1. Microbial Processes and Mechanisms Affecting Bioremediation of Metal Contamination and Influencing Metal Toxicity and Transport, *Rev Environ Sci Biotechnol* **4**, 115–156 (2005).

104. D. R. Lovley, Y. A. Gorby, Enzymatic Uranium Precipitation, *Environ. Sci. Technol.* **26**, 205–207 (1992).

105. D. R. Lovley, E. J. Phillips, Reduction of uranium by Desulfovibrio desulfuricans, *Applied and Environmental Microbiology* **58**, 850 (1992).

106. R. B. Payne *et al.*, Interaction between uranium and the cytochrome c 3 of Desulfovibrio desulfuricans strain G20, *Archives of Microbiology* **181**, 398–406 (2004).

107. H. Beyenal *et al.*, Uranium Immobilization by Sulfate-Reducing Biofilms, *Environ. Sci. Technol.* **38**, 2067–2074 (2004).

108. E. J. O'Loughlin, S. D. Kelly, R. E. Cook, R. Csencsits, K. M. Kemner, Reduction of Uranium(VI) by Mixed Iron(II)/Iron(III) Hydroxide (Green Rust): Formation of $UO_2$ Nanoparticles, *Environ. Sci. Technol.* **37**, 721–727 (2003).

109. E. J. O'Loughlin, S. D. Kelly, K. M. Kemner, XAFS Investigation of the Interactions of $U^{VI}$ with Secondary Mineralization Products from the Bioreduction of $Fe^{III}$ Oxides, *Environ. Sci. Technol.* **44**, 1656–1661 (2010).

110. B. Jeon, B. A. Dempsey, W. D. Burgos, M. Barnett, E. E. Roden, Chemical Reduction of U (VI) by Fe (II) at the Solid− Water Interface Using Natural and Synthetic Fe (III) Oxides, *Environ. Sci. Technol.* **39**, 5642–5649 (2005).

111. J.-H. Jang, B. A. Dempsey, W. D. Burgos, Reduction of U(VI) by Fe(II) in the presence of hydrous ferric oxide and hematite: Effects of solid transformation, surface coverage, and humic acid, *Water research* **42**, 2269–2277 (2008).

112. S. Chakraborty *et al.*, U(VI) Sorption and Reduction by Fe(II) Sorbed on Montmorillonite, *Environ. Sci. Technol.* **44**, 3779–3785 (2010).

113. S. Regenspurg, D. Schild, T. Schäfer, F. Huber, M. E. Malmström, Removal of uranium(VI) from the aqueous phase by iron(II) minerals in presence of bicarbonate, *Appl. Geochem.* **24**, 1617–1625 (2009).

114. H. Veeramani *et al.*, Products of abiotic U(VI) reduction by biogenic magnetite and vivianite, *Geochem. Cosmochim. Acta* **75**, 2512–2528 (2011).

115. T. Behrends, P. Van Cappellen, Competition between enzymatic and abiotic reduction of uranium (VI) under iron reducing conditions, *Chemical Geology* **220**, 315–327 (2005).

116. P. Wersin *et al.*, Interaction between aqueous uranium (VI) and sulfide minerals: Spectroscopic evidence for sorption and reduction, *Geochem. Cosmochim. Acta* **58**, 2829–2843 (1994).

117. F. R. Livens *et al.*, X-ray absorption spectroscopy studies of reactions of technetium, uranium and neptunium with mackinawite, *Journal of Environmental Radioactivity* **74**, 211–219 (2004).

118. L. N. Moyes *et al.*, Uranium Uptake from Aqueous Solution by Interaction with Goethite, Lepidocrocite, Muscovite, and Mackinawite: An X-ray Absorption Spectroscopy Study, *Environ. Sci. Technol.* **34**, 1062–1068 (2000).

119. T. J. Gallegos, C. C. Fuller, S. M. Webb, W. Betterton, Uranium (VI) Interactions with Mackinawite in the Presence and Absence of Bicarbonate and Oxygen, *Environ. Sci. Technol.* **47**, 7357–7364 (2013).

120. D. E. Holmes, K. T. Finneran, R. A. O'Neil, D. R. Lovley, Enrichment of Members of the Family Geobacteraceae Associated with Stimulation of Dissimilatory Metal Reduction in Uranium-Contaminated Aquifer Sediments, *Applied and Environmental Microbiology* **68**, 2300–2306 (2002).

121. K. T. Finneran, M. E. Housewright, D. R. Lovley, Multiple influences of nitrate on uranium solubility during bioremediation of uranium‐contaminated subsurface sediments, *Environmental microbiology* **4**, 510–516 (2002).

122. K. T. Finneran, R. T. Anderson, K. P. Nevin, D. R. Lovley, Potential for bioremediation of uranium-contaminated aquifers with microbial U (VI) reduction, *Soil and Sediment Contamination: An International Journal* **11**, 339–357 (2002).

123. Y. Suzuki, S. D. Kelly, K. M. Kemner, J. F. Banfield, Microbial Populations Stimulated for Hexavalent Uranium Reduction in Uranium Mine Sediment, *Applied and Environmental Microbiology* **69**, 1337–1346 (2003).

124. E.-M. Burkhardt *et al.*, Impact of Biostimulated Redox Processes on Metal Dynamics in an Iron-Rich Creek Soil of a Former Uranium Mining Area, *Environ. Sci. Technol.* **44**, 177–183 (2010).

125. S. D. Kelly *et al.*, Uranium Transformations in Static Microcosms, *Environ. Sci. Technol.* **44**, 236–242 (2010).

126. B. J. Converse, T. Wu, R. H. Findlay, E. E. Roden, U(VI) Reduction in Sulfate-Reducing Subsurface Sediments Amended with Ethanol or Acetate, *Applied and Environmental Microbiology* **79**, 4173–4177 (2013).

127. J. Komlos, A. Peacock, R. K. Kukkadapu, P. R. Jaffe, Long-term dynamics of uranium

reduction/reoxidation under low sulfate conditions, *Geochem. Cosmochim. Acta* **72**, 3603–3615 (2008).

128. B. Gu *et al.*, Bioreduction of uranium in a contaminated soil column, *Environ. Sci. Technol.* **39**, 4841–4847 (2005).

129. J. Wan *et al.*, Effects of Organic Carbon Supply Rates on Uranium Mobility in a Previously Bioreduced Contaminated Sediment, *Environ. Sci. Technol.* **42**, 7573–7579 (2008).

130. W.-M. Wu *et al.*, Pilot-scale in situ bioremedation of uranium in a highly contaminated aquifer. 2. Reduction of U (VI) and geochemical control of U (VI) bioavailability, *Environ. Sci. Technol.* **40**, 3986–3995 (2006).

131. J. M. Senko, J. D. Istok, J. M. Suflita, L. R. Krumholz, In -Situ Evidence for Uranium Immobilization and Remobilization, *Environ. Sci. Technol.* **36**, 1491–1496 (2002).

132. R. T. Anderson *et al.*, Stimulating the In Situ Activity of Geobacter Species To Remove Uranium from the Groundwater of a Uranium-Contaminated Aquifer, *Applied and Environmental Microbiology* **69**, 5884–5891 (2003).

133. Y.-J. Chang *et al.*, Microbial Incorporation of 13C-Labeled Acetate at the Field Scale: Detection of Microbes Responsible for Reduction of U(VI), *Environ. Sci. Technol.* **39**, 9039–9048 (2005).

134. E. L. Brodie *et al.*, Application of a High-Density Oligonucleotide Microarray Approach To Study Bacterial Population Dynamics during Uranium Reduction and Reoxidation, *Applied and Environmental Microbiology* **72**, 6288–6298 (2006).

135. N. N. North *et al.*, Change in Bacterial Community Structure during In Situ Biostimulation of Subsurface Sediment Cocontaminated with Uranium and Nitrate, *Applied and Environmental Microbiology* **70**, 4911–4920 (2004).

136. C. Hwang *et al.*, Bacterial community succession during in situ uranium bioremediation: spatial similarities along controlled flow paths, *ISME J* **3**, 47–64 (2008).

137. Y. Liang *et al.*, Microbial Functional Gene Diversity with a Shift of Subsurface Redox Conditions during In Situ Uranium Reduction, *Applied and Environmental Microbiology* **78**, 2966–2972 (2012).

138. Y. Suzuki, S. D. Kelly, K. M. Kemner, J. F. Banfield, Radionuclide contamination: Nanometre-size products of uranium bioreduction, *Nature* **419**, 134 (2002).

139. T. Cheng, M. O. Barnett, E. E. Roden, J. Zhuang, Effects of phosphate on uranium (VI) adsorption to goethite-coated sand, *Environ. Sci. Technol.* **38**, 6059–6065 (2004).

140. Y. Tang, J. Mcdonald, R. J. Reeder, Enhanced Uranium Sorption on Aluminum Oxide Pretreated with Arsenate. Part II: Spectroscopic Studies, *Environ. Sci. Technol.* **43**,

4452–4458 (2009).

141. L. D. Troyer, J. J. Stone, T. Borch, Effect of biogeochemical redox processes on the fate and transport of As and U at an abandoned uranium mine site: an X-ray absorption spectroscopy study, *Environ. Chem.* **11**, 18–27 (2014).

142. E. Smith, W. Davison, J. Hamilton-Taylor, Methods for preparing synthetic freshwaters, *Water research* **36**, 1286–1296 (2002).

143. B. Jeon *et al.*, Microbial reduction of U (VI) at the solid− water interface, *Environ. Sci. Technol.* **38**, 5649–5655 (2004).

144. L. Stookey, Ferrozine---a new spectrophotometric reagent for iron, *Anal. Chem.* **42**, 779–781 (1970).

145. E. E. Roden, J. M. Zachara, Microbial reduction of crystalline iron (III) oxides: Influence of oxide surface area and potential for cell growth, *Environ. Sci. Technol.* **30**, 1618–1628 (1996).

146. M. Newville, IFEFFIT: interactive XAFS analysis and FEFF fitting, *Journal of synchrotron radiation* **8**, 322–324 (2001).

147. B. C. Bostick, thesis, STANFORD UNIVERSITY (2001).

148. B. C. Bostick, C. Chen, S. E. Fendorf, Arsenite retention mechanisms within estuarine sediments of Pescadero, CA, *Environ. Sci. Technol.* **38**, 3299–3304 (2004).

149. A. Tapia-Rodríguez, A. Luna-Velasco, J. A. Field, R. Sierra-Alvarez, Toxicity of Uranium to Microbial Communities in Anaerobic Biofilms, *Water Air Soil Pollut* **223**, 3859–3868 (2012).

150. A. Konopka, A. E. Plymale, D. A. Carvajal, X. Lin, J. P. Mckinley, Environmental Controls on the Activity of Aquifer Microbial Communities in the 300 Area of the Hanford Site, *Microb Ecol* **66**, 889–896 (2013).

151. S. C. Brooks *et al.*, Inhibition of bacterial U (VI) reduction by calcium, *Environ. Sci. Technol.* **37**, 1850–1858 (2003).

152. D. Rickard, G. W. Luther, Chemistry of Iron Sulfides, *Science* **107**, 514–562 (2007).

153. T. J. Gallegos, S. P. Hyun, K. F. Hayes, Spectroscopic Investigation of the Uptake of Arsenite from Solution by Synthetic Mackinawite, *Environ. Sci. Technol.* **41**, 7781–7786 (2007).

154. E. D. Burton, S. G. Johnston, B. Planer-Friedrich, Chemical Geology, *Chemical Geology* **343**, 12–24 (2013).

155. Y. Bi, K. F. Hayes, Nano-FeS inhibits UO2 reoxidation under varied oxic conditions,

*Environ. Sci. Technol.* **48**, 632–640 (2014).

156. Y. Arai, E. J. Elzinga, D. L. Sparks, X-ray absorption spectroscopic investigation of arsenite and arsenate adsorption at the aluminum oxide–water interface, *Journal of colloid and interface science* **235**, 80–88 (2001).

157. M. Rutsch, G. Geipel, V. Brendler, G. Bernhard, H. Nitsche, Interaction of uranium (VI) with arsenate (V) in aqueous solution studied time-resolved laser-induced fluorescence spectroscopy (TRMFS), *Radiochim. Acta* **86**, 135–141 (1999).

158. O. V. Nipruk, N. G. Chernorukov, Y. P. Pykhova, N. S. Godovanova, A. A. Eremina, State of uranyl phosphates and arsenates in aqueous solutions, *Radiochemistry* **53**, 483–490 (2011).

159. M. J. Beazley, R. J. Martinez, P. A. Sobecky, S. M. Webb, M. Taillefert, Nonreductive Biomineralization of Uranium(VI) Phosphate Via Microbial Phosphatase Activity in Anaerobic Conditions, *Geomicrobiology Journal* **26**, 431–441 (2009).

160. M. J. Beazley, R. J. Martinez, P. A. Sobecky, S. M. Webb, M. Taillefert, Uranium Biomineralization as a Result of Bacterial Phosphatase Activity: Insights from Bacterial Isolates from a Contaminated Subsurface, *Environ. Sci. Technol.* **41**, 5701–5707 (2007).

161. F. G. Simon, V. Biermann, B. Peplinski, Uranium removal from groundwater using hydroxyapatite, *Appl. Geochem.* **23**, 2137–2145 (2008).

162. C. C. Fuller, J. R. Bargar, J. A. Davis, M. J. Piana, Mechanisms of Uranium Interactions with Hydroxyapatite: Implications for Groundwater Remediation, *Environ. Sci. Technol.* **36**, 158–165 (2002).

163. A. E. Ray *et al.*, Evidence for multiple modes of uranium immobilization by an anaerobic bacterium, *Geochem. Cosmochim. Acta* **75**, 2684–2695 (2011).

164. X. Rui *et al.*, Bioreduction of Hydrogen Uranyl Phosphate: Mechanisms and U(IV) Products, *Environ. Sci. Technol.* **47**, 5668–5678 (2013).

165. T. V. Khijniak *et al.*, Reduction of Uranium(VI) Phosphate during Growth of the Thermophilic Bacterium Thermoterrabacterium ferrireducens, *Applied and Environmental Microbiology* **71**, 6423–6426 (2005).

166. W.-M. Wu *et al.*, In situ bioreduction of uranium (VI) to submicromolar levels and reoxidation by dissolved oxygen, *Environ. Sci. Technol.* **41**, 5716–5723 (2007).

167. D. Postma, R. Jakobsen, Redox zonation: Equilibrium constraints on the Fe (III)/SO 4-reduction interface, *Geochem. Cosmochim. Acta* **60**, 3169–3175 (1996).

168. R. A. Berner, Thermodynamic stability of sedimentary iron sulfides, *American Journal of Science* **265**, 773–785 (1967).

169. D. Rickard, Kinetics of FeS precipitation: Part 1. Competing reaction mechanisms, *Geochem. Cosmochim. Acta* **59**, 4367–4379 (1995).

170. R. T. Wilkin, H. L. Barnes, Pyrite formation by reactions of iron monosulfides with dissolved inorganic and organic sulfur species, *Geochem. Cosmochim. Acta* **60**, 4167–4179 (1996).

171. A. Abdelouas, W. Lutze, H. Nuttall, Oxidative dissolution of uraninite precipitated on Navajo sandstone, *Journal of Contaminant Hydrology* **36**, 353–375 (1999).

172. E. D. Burton, S. G. Johnston, R. T. Bush, Microbial sulfidogenesis in ferrihydrite-rich environments: Effects on iron mineralogy and arsenic mobility, *Geochem. Cosmochim. Acta* **75**, 3072–3087 (2011).

173. E. C. Butler, K. F. Hayes, Effects of solution composition and pH on the reductive dechlorination of hexachloroethane by iron sulfide, *Environ. Sci. Technol.* **32**, 1276–1284 (1998).

174. S. M. Webb, SIXPACK: a graphical user interface for XAS analysis using IFEFFIT, *Physica Scripta* **115**, 1011–1014 (2005).

175. M. Newville, S. A. Carroll, P. A. O'day, G. A. Waychunas, M. Ebert, A web-based library of XAFS data on model compounds, *Journal of synchrotron radiation* **6**, 276–277 (1999).

176. T. Ressler, WinXAS : A New Software Package not only for the Analysis of Energy-Dispersive XAS Data, *Journal of Physics IV France* **7**, 269–270 (1997).

177. S. I. Zabinsky, J. J. Rehr, A. Ankudinov, R. C. Albers, M. J. Eller, FEFF code for ab initio calculations of XAFS, *Physical Review B* **52**, 2995–3009 (1995).

178. M. Wolthers, L. Charlet, P. R. van Der Linde, D. Rickard, C. H. van Der Weijden, Surface chemistry of disordered mackinawite (FeS), *Geochimica et Cosmochimica Acta* **69**, 3469–3481 (2005).

179. H. Jeong, J. LEE, K. HAYES, Characterization of synthetic nanocrystalline mackinawite: Crystal structure, particle size, and specific surface area, *Geochem. Cosmochim. Acta* **72**, 493–505 (2008).

180. G. Geipel, G. Bernhard, V. Brendler, in *Uranium in the Aquatic Environment: proceedings of the International Conference [on] Uranium Mining and Hydrogeology III and the International Mine Water Association Symposium, Freiberg, Germany, 15-21 September 2002*, B. Merkel, B. Planer-Friedrich, C. Wolkersdorfer, I. M. W. A. Symposium, Eds. (Springer, 2002), p. 369.

181. X. Liu, R. H. Byrne, Rare earth and yttrium phosphate solubilities in aqueous solution, *Geochem. Cosmochim. Acta* **61**, 1625–1633 (1997).

182. M. F. Kirk, E. E. Roden, L. J. Crossey, A. J. Brealey, M. N. Spilde, Experimental analysis of arsenic precipitation during microbial sulfate and iron reduction in model aquifer sediment reactors, *Geochem. Cosmochim. Acta* **74**, 2538–2555 (2010).

183. T. K. Tokunaga, Y. Kim, J. Wan, L. Yang, Aqueous uranium (VI) concentrations controlled by calcium uranyl vanadate precipitates, *Environ. Sci. Technol.* **46**, 7471–7477 (2012).

184. T. K. Tokunaga, Y. Kim, J. Wan, Potential Remediation Approach for Uranium-Contaminated Groundwaters Through Potassium Uranyl Vanadate Precipitation, *Environ. Sci. Technol.* **43**, 5467–5471 (2009).

# APPENDIX A: IMPACT OF ORGANIC CARBON AND IRON BIOAVAILABILITY ON THE MAGNETIC SUSCEPTIBILITY OF SOILS

Available online at www.sciencedirect.com

ScienceDirect

Geochimica et Cosmochimica Acta 128 (2014) 44–57

Geochimica et Cosmochimica Acta

www.elsevier.com/locate/gca

# Impact of organic carbon and iron bioavailability on the magnetic susceptibility of soils

Katharina Porsch [a,1], Moti L. Rijal [b,2], Thomas Borch [c,d], Lyndsay D. Troyer [d], Sebastian Behrens [a], Florian Wehland [e,3], Erwin Appel [b], Andreas Kappler [a,*]

[a] *Geomicrobiology, Department of Geosciences, Center for Applied Geosciences, University of Tuebingen, Sigwartstrasse 10, 72076 Tuebingen, Germany*

[b] *Geophysics, Department of Geosciences, Center for Applied Geosciences, University of Tuebingen, Sigwartstrasse 10, 72076 Tuebingen, Germany*

[c] *Department of Soil and Crop Sciences, Colorado State University, Fort Collins, CO 80523, USA*

[d] *Department of Chemistry, Colorado State University, Fort Collins, CO 80523, USA*

[e] *Shell International Exploration and Production B.V., Postbus 60, 2280 AB Rijswijk, The Netherlands*

Received 20 October 2012; accepted in revised form 1 December 2013; Available online 11 December 2013

**Abstract**

Microorganisms are known to couple the degradation of hydrocarbons to Fe(III) reduction leading to the dissolution and (trans)formation of Fe minerals including ferro(i)magnetic Fe minerals such as magnetite. The screening of soil magnetic properties, in particular magnetic susceptibility (MS), has the potential to assist in locating and assessing hydrocarbon (e.g. gasoline) contamination in the environment. In order to evaluate this, it must be understood how changes in soil geochemistry and hydrocarbon input impact MS. To this end, we incubated microcosms with soils from six different field sites anoxically and followed the changes in soil MS. In parallel we simulated hydrocarbon (i.e., gasoline) contamination in the same soils under anoxic conditions. We found that in microbially active microcosms both with or without added gasoline, average changes in MS of $6.9 \pm 2.6\%$ occurred, whereas in sterile controls the changes were less than 2.5% demonstrating that microbial metabolism played a major role in the (trans)formation of ferro(i)magnetic minerals. The microcosms reached stable MS values after a few weeks to months in four out of the six soils showing an increase in MS while in two soils the MS decreased over time. After stable MS values were reached, further addition of labile organic carbon (i.e., lactate/acetate) did not lead to further changes in MS, but the addition of Fe(III) oxyhydroxides (ferrihydrite) led to increases in MS suggesting that the changes in MS were limited by bioavailable Fe and not by bioavailable organic carbon. In the control experiments without carbon amendment, we observed that natural organic matter was mobilized from the soil matrix by water or microbial growth medium (0.33-0.47 mL/g field moist soil) added to the microcosms, and that this mobilized organic matter also stimulated microbial Fe metabolism and thus also led to a microbially driven change in MS. This study shows that changes in MS after an increase of the amount of bioavailable organic carbon can occur in a variety of soils. It also suggests that whether MS increases or decreases depends on the initial MS of the soil and the extent of the MS change seems to depend upon the amount of bioavailable Fe(III).


* Corresponding author. Tel.: +49 7071 2974992; fax: +49 7071 295059.
*E-mail address:* andreas.kappler@uni-tuebingen.de (A. Kappler).
[1] Current address: UFZ – Helmholtz Centre for Environmental Research, Department of Bioenergy, Permoserstrasse 15, 04318 Leipzig, Germany
[2] Current address: Central Department of Geology, Institute of Science and Technology, Tribhuvan University, Kathmandu, Nepal
[3] Current address: European Patent Office, Bayerstrasse 115, 80335 Munich, Germany

0016-7037/$ - see front matter © 2013 Elsevier Ltd. All rights reserved.
http://dx.doi.org/10.1016/j.gca.2013.12.001

## 1. INTRODUCTION

Crude oil and its products such as gasoline and diesel fuel are used worldwide. Soil and sediment contamination by these compounds represents a severe environmental threat (Readman et al., 1992; Masak et al., 2003; Zachara et al., 2004; Mendelssohn et al., 2012). For effective remediation of such sites, the contamination must be located and the spatial extent of the affected area assessed. Soil samples are usually taken from the potentially contaminated area and analyzed in the laboratory, however, this is time consuming and cost intensive. Therefore, rapid and inexpensive methods for assessment of hydrocarbon contamination in the field are necessary.

Measurement of soil magnetic susceptibility (MS) has been used to localize anthropogenic heavy metals in soils based on the fact that heavy metals and magnetic phases (mostly magnetite) are emitted from identical sources (combustion processes, steel industries, mining activities, traffic) and have similar transport pathways into and in the environment (Petrovský and Ellwood, 1999). Since MS can be measured within seconds in the field, this parameter can be used for fast and cost effective surveys of large areas. MS describes how strong a substance is magnetized in an external magnetic field. Diamagnetic materials (e.g. quartz, water) have a small negative MS, whereas paramagnetic minerals (e.g. siderite, ferrihydrite) and antiferromagnetic minerals with spin-canting (hematite) or defect moments (goethite) have a small positive MS. Ferromagnetic elements (e.g. metallic Fe) and ferrimagnetic minerals (e.g. magnetite, maghemite, greigite) have a very high or moderately high (e.g. pyrrhotite) positive MS (Dunlop and Özdemir, 1997). For simplicity the term ferro(i)magnetic minerals is used in this study and refers to ferrimagnetic minerals and antiferromagnetic minerals with spin-canting or defect moments. Although crude oil and its products such as gasoline have a low or even negative MS (Ivakhnenko and Potter, 2004), the measurement of soil MS has also the potential to serve as a proxy for the presence of hydrocarbons.

Ferro(i)magnetic phases are known to form in oil as secondary products during oil biodegradation (McCabe et al., 1987). Additionally, crude oil components like n-alkanes and polycyclic aromatic hydrocarbons can be degraded by soil microorganisms (Hamamura et al., 2006; Borch et al., 2010) including different Fe(III)-reducing microorganisms (Lovley et al., 1989; Lovley and Anderson, 2000). Fe(III)-reducers were shown to be able to reduce poorly crystalline ferrihydrite as well as more crystalline Fe(III) minerals such as goethite, hematite, and magnetite (for reviews see Kappler and Straub, 2005; Weber et al., 2006; Konhauser et al., 2011). Depending on the geochemical conditions present during Fe(III) reduction (e.g. pH, presence of carbonate, sulfide and phosphate) and depending on the Fe mineral transformation pathway (reductive dissolution, dissolution-reprecipitation or solid-state conversion), different Fe-phases can form. Ferrihydrite was shown for example to be converted into Fe(II)-carbonate, -sulfide, -phosphate or goethite as well as mixed Fe(II)-Fe(III) minerals such as magnetite or green rusts (Roden and Zachara, 1996; Fredrickson et al., 1998; Hansel et al., 2005; Borch et al., 2007; Piepenbrock et al., 2011; Amstaetter et al., 2012). In turn, Fe(II) can be oxidized by anaerobic and aerobic Fe(II)-oxidizing microorganisms (Kappler and Straub, 2005; Weber et al., 2006; Konhauser et al., 2011) which can also lead to the formation of magnetite (Chaudhuri et al., 2001; Jiao et al., 2005; Dippon et al., 2012) or green rust (Pantke et al., 2012).

Since some Fe(III)-reducers are able to metabolize hydrocarbons, the input of hydrocarbons into soils has a direct influence on microbial Fe(III) reduction and indirectly (via Fe(II) formation) on microbial Fe(II) oxidation. Additionally, hydrocarbons, especially lipophilic ones, are toxic for many microorganisms due to their interaction with microbial membranes (Sikkema et al., 1995) and thus hydrocarbon input into soils can also decrease microbial activity including Fe-metabolizing microorganisms. Therefore, hydrocarbon input may lead to changes in soil MS by changing Fe mineralogy including ferro(i)magnetic minerals. As a consequence, similar to heavy metal contamination hydrocarbon contamination may also be localized rapidly by screening soil MS in the presumably contaminated area in comparison to MS values at uncontaminated reference sites.

Only a few studies have tried to correlate the amount of hydrocarbons in soils with soil MS (see references in Schumacher, 1996). Guzman et al. (2011) and Aldana et al. (2011), studied the magnetic signature of oil fields from Venezuela and identified magnetite and Fe-sulfides (e.g. greigite) as the main magnetic phases causing increased MS values in oil wells. In two recent field studies, we also observed increased MS values in hydrocarbon contaminated soils (Rijal et al., 2010, 2012). However, no detailed studies exist that answer the key questions whether microbial activity is involved in the changes of soil MS after hydrocarbon input and how the changes in MS are influenced by the geochemical conditions of the soil. Therefore, we incubated soils from different field sites anoxically in laboratory microcosm experiments, simulated hydrocarbon contamination, and followed the change of soil MS over time. The objectives of this study were (i) to determine the importance of microbial processes for changes in MS and (ii) to determine the influence of geochemical conditions, including the amount of bioavailable organic carbon and bioavailable Fe, on the extent and temporal development of the changes in MS.

## 2. METHODS

### 2.1. Field sites, soil sampling and soil pre-treatment

Soil samples from six different field sites were collected. The field sites were chosen due to their minimal anthropogenic influence especially regarding combustion pollution that is known to release ferro(i)magnetic particles. The first five sampling sites Holzgerlingen (HG), Waldenbuch (Wabu), Fraeulinsberg (FB), Allemendwald (AW) (all four grassland) and Schoenbuch (Sbu) (forest) are located in Southwest Germany. At the grassland sites the top ~20 cm of soil was sampled including the sward, whereas the forest soil Sbu was sampled without leaf litter. During

a field study (Rijal et al., 2012), a sixth soil sample was collected in the Haenigsen area (Northeast of Hanover, Northern Germany), a region where crude oil is leaking naturally to the surface. For the microcosm experiments presented here a sample was taken in this region from an uncontaminated surface soil of farmland (Hclean). Large organic particles (e.g. plant matter) were removed from the soils either with tweezers (HG, Wabu, FB, AW, Hclean) or by pressing the field moist soil through a 2 mm sieve (Sbu). Soils were stored for up to four months in plastic bags at 4 °C in the dark before use. Soil stored at 4 °C that did not receive any amendments is named "original soil" in the following text.

### 2.2. Experimental setup of microcosms

In order to determine the processes influencing soil MS after addition of organic carbon, three microcosm experiments with six soils and three different carbon amendments (no carbon, lactate and acetate, and gasoline) were set up in 60 mL glass bottles under anoxic conditions (Table 1). Six different soils were used to determine if the geochemistry of soils had an influence on the rate or extent of MS change. Setups without carbon amendment served as a negative control to quantify the change of soil MS by the incubation of the soil alone. Gasoline (95 octane) containing a diverse mixture of aliphatic and aromatic hydrocarbons was added as model compound representing a hydrocarbon contamination arising from spills. Bottles with lactate/acetate addition served as control for setups containing easily biodegradable organics.

In order to determine the impact of microbial activity for the changes in soil MS, two sets of microcosms were set up, one with sterile soil and one with non-sterile soil with at least two replicates per setup. For setups with sterile soil, the soil was autoclaved (121 °C, 25 min, 1 bar). All solutions added to the soils were sterile and anoxic.

Either microbial growth medium (for composition see Straub et al., 2005) or high-purity water (to determine if the nutrients present in the medium had an influence on the MS changes) was added to the autoclaved and non-autoclaved soil (5–7 mL to 15–21 g of soil; see Table 1). The medium was buffered at pH 7 with 20 mM sodium bicarbonate. The headspace of the bottles was exchanged with $N_2$:$CO_2$ (90:10) to obtain anoxic conditions. Microcosms with three different carbon amendments were set up: (i) no carbon source added, (ii) lactate/acetate (each 15 mmol/L; referring to the volume of added microbial growth medium or water), and (iii) unleaded gasoline (3.60 μL/g field moist soil) obtained from a gasoline station. The lactate/acetate concentrations were chosen based on a previous study that indicated stimulation of Fe(III) reduction at these concentrations (Porsch et al., 2010). Bottles were closed with viton stoppers. Microcosms were homogenized directly after preparation and weekly thereafter by shaking for a few seconds on a vortexer. The microcosms were incubated at 28 °C in the dark. MS was measured weekly, until the MS was constant, then every other week.

In order to examine whether carbon or Fe limitation was responsible for cessation of changes in MS, selected microcosms were used for two additional experiments (Table 1). Since only two to four replicate bottles were available per setup, different soils were chosen for these two experiments. The importance of carbon limitation for the cessation of changes in MS, was determined by adding lactate/acetate (both 15 mmol/L, referring to the volume of added microbial growth medium) again to the corresponding setups of soils HG and Wabu (experiment I) after 14.5 weeks of incubation. In order to determine if bioavailable Fe(III) limitation led to cessation of changes in MS, microcosms with soil Hclean containing medium and no additional carbon (experiment II) were amended with ferrihydrite after 51 weeks of incubation. Soil Hclean was selected as this soil had the lowest total Fe ($Fe_{tot}$) concentration as determined by XRF (see below). Ferrihydrite was chosen since it is considered to be a source of bioavailable Fe(III) and magnetite is one of the possible products of its reduction (Porsch et al., 2010). 2 mL of a 0.5 M ferrihydrite suspension (synthesized according to Raven et al., 1998) was added to half of the parallel experiments in each setup. In order to follow changes in Fe mineralogy during incubation in more detail, sub-samples of sterile and microbial active microcosms without carbon amendment and with lactate/acetate addition with soil Sbu were analyzed by Mössbauer and EXAFS spectroscopy (see below) (Table 1, experiment III).

After incubation, one microcosm from each setup and experiment was opened under oxic conditions and sampled immediately for the quantification of Fe(II) and $Fe_{tot}$ in the different Fe fractions (i.e., adsorbed plus Fe carbonates, poorly crystalline Fe, and crystalline Fe) and for the analysis of dissolved organic carbon, dissolved inorganic carbon, and organic acids.

### 2.3. Analytical methods

#### *2.3.1. Soil analysis*

The water content of the original soils was determined by drying the soil at 105 °C (Blume et al., 2000). The soil pH was measured 24 h after addition of 0.01 M $CaCl_2$ solution (Blume et al., 2000). All soils were finely ground and dried at 105 °C prior to the following analyses: Total organic carbon and total nitrogen was determined with a CN analyzer (Vario EL, Elementar, Germany) after carbonate removal with 1 M HCl. The $CaCO_3$ content was quantified by mixing soil with 1 M HCl and determining the consumed HCl by titration with 1 M NaOH. The total Fe and total sulfur content of the soils was quantified by X-ray fluorescence analysis (Bruker AXS S4 Pioneer X-ray spectrometer, Bruker AXS GmbH, Germany). Fe extractions from two sub-samples of the soil before and after incubation were performed according to Moeslund et al. (1994) and Roden and Zachara (1996) with a soil:extractant ratio (w:v) of 1:50. Prior to extraction, microcosms with soils FB, AW and Sbu were centrifuged (10 min, 2000 rpm) and the supernatant was removed for dissolved carbon and organic acid analyses (see below). The first sub-sample of soil was extracted with Na-acetate (pH 5) for 24 h and the second sub-sample with

Table 1
Experimental setup of microcosm experiments. Three microcosm experiments (I–III) with six soils were set up. The microcosms consisted of two sets: one with autoclaved (sterile setups) and one with non-autoclaved soil (microbially active setups). Either microbial growth medium or high-purity water was added as liquid. Microcosms were either not amended with organic carbon or amended with lactate/acetate or with gasoline.

| Soil | Microcosm experiment/ replicates per setup | Measuring time (before + after 2nd C or Fe addition) [weeks] | Ratio Soil [g]:Liquid [mL] | Carbon source added to sets of sterile and microbially active microcosms | | | | | |
|---|---|---|---|---|---|---|---|---|---|
| | | | | No carbon | | Lactate/acetate (15 mM each)[a] | | Gasoline (3.6 µL/g field moist soil) | |
| | | | | Medium | Water | Medium | Water | Medium | Water |
| HG | I/2 | 11 + 10 | 15:5 | x | | x, 2nd C[b] | | x | |
| Wabu | I/2 | 11 + 10 | 15:5 | x | | x, 2nd C[b] | | x | |
| FB | II/4 | 46 | 15:7 | x | x | | | x | |
| AW | II/4 | 46 | 15:7 | x | x | | | x | |
| Hclean | II/4 | 46 + 73 | 15:7 | x, Fe[c] | x | | | x, Fe[c] | |
| Sbu | III/4 | 48 | 21:7 | | x, MB + EXAFS[d] | | x, MB + EXAFS[d] | | x |

[a] 15 mM final concentration in the microcosms referring to the volume of added liquid.
[b] After 14.5 weeks (MS values of microcosms were stable) lactate/acetate was added a second time.
[c] After 51 weeks (MS values of microcosms were stable) 2 mL of 0.5 M ferrihydrite suspension were added to two replicates per setup.
[d] Soil Fe mineralogy was analyzed after incubation by Mössbauer and EXAFS spectroscopy.

0.5 M HCl for 1 h, both under oxic conditions at room temperature on a shaker. For soil Sbu a third sub-sample was extracted with 1 M HCl at 70 °C under oxic conditions in a water bath for 24 h (Porsch and Kappler, 2011). From all extracts 1.8 mL were centrifuged (15 min, 20,817*g*) to remove soil particles. Fe(II) and $Fe_{tot}$ of the supernatant were quantified by the ferrozine assay (Stookey, 1970) in microtiter plates as described by Hegler et al. (2008). The properties of the original soils are given in Table 2.

### 2.3.2. Magnetic susceptibility measurements

Low-field MS of the microcosms was measured as described in Porsch et al. (2010). In order to determine the mass specific MS of the original soil samples, 5–10 sub-samples of each soil were packed in 10 $cm^3$ plastic containers and the results of the volume specific MS were divided by the overall density of the contents of the container. The extent of MS change in soil microcosms was calculated as the % difference between the initial MS value and the final MS value which was calculated as average of the last four to five measured MS data points during the plateau phase.

### 2.3.3. Dissolved carbon and organic acid analysis

Microcosm bottles with soils FB, AW and Sbu were centrifuged (10 min, 2000 rpm) and the supernatants were frozen and stored in sterile plastic cups at −28 °C until analysis of dissolved organic and inorganic carbon, and organic acids. For analysis, the supernatant was thawed and remaining soil particles were removed either by centrifugation (soils FB and AW, 10 min at 20,817*g*) or by centrifugation and filtration (soil Sbu, centrifugation for 10 min at 5000*g* followed by filtration with a 0.22 µm mixed cellulose ester filter). Dissolved organic and inorganic carbon (DOC, DIC) contents were determined using a carbon analyzer (high TOC, Elementar, Germany). Organic acids (acetate, butyrate, formate, lactate, and propionate) were quantified by HPLC using a diode array detector (absorption at 210 nm) and a refractive index detector. The acids were separated on a Bio-Rad Aminex HPX-87H Ion Exclusion Column (300 * 7.8 mm) with two pre-columns, a Bio-Rad Micro guard Cation H Cartridge and a Dionex IonPac NG1 Guard column (2 * 50 mm). 5 mM $H_2SO_4$ was used as eluent (0.6 mL/min). The column heater temperature was 60 °C.

### 2.3.4. Mineral analysis by Mössbauer and extended x-ray absorption fine structure (EXAFS) spectroscopy

Initial attempts to separate magnetic mineral particles from the soil by magnetic separation failed (data not shown), probably due to their small size, coatings of the magnetic particles with organics or associations with non-magnetic mineral particles. Therefore, minerals were analyzed directly from soil samples.

Preparation of samples from microcosms for Mössbauer spectroscopic analysis was done anoxically in a glovebox (100% $N_2$), whereas the original soil was prepared under oxic conditions. Soil samples were sealed between two layers of Kapton tape. Mössbauer spectra were recorded at room temperature for up to 19 days and analyzed as described by Hohmann et al. (2010).

To prepare samples for EXAFS, microcosms of soil Sbu were opened in a glovebox (100% $N_2$) and a sub-sample of the soil was dried at ambient temperature and finely ground in an agate mortar. Ground samples were packed in Teflon sample holders for XAS analyses and sealed with Kapton tape to prevent oxidation. The structural environment of Fe was determined using EXAFS spectroscopy at the Stanford Synchrotron Radiation Lightsource (SSRL) on beamlines 11-2 (26-pole wiggler) and 4-1 (20 pole wiggler). The storage ring was operated at 3.0 GeV and at currents between 60 and 100 mA. The Fe EXAFS analytical procedures used here were similar to those described previously by Borch et al. (2007). Energy selection was accomplished

Table 2
Selected properties of original soils used for microcosms experiments.

| Soil properties | HG | Wabu | FB | AW | Sbu | Hclean |
|---|---|---|---|---|---|---|
| pH[a] | 5.4[c] | 7.1[c] | 5.2 ± 0.0 | 3.6[b] ± 0.0 | 7.0 ± 0.0 | 4.8 ± 0.0 |
| Water content [wt.%][b,d] | 32 ± 0 | 40 ± 0 | 23 ± 1 | 30 ± 1 | 48 ± 0 | 15 ± 1 |
| $CaCO_3$ [wt.%][a,d] | 4.7 ± 0.7 | 1.5 ± 0.0 | 1.2 ± 0.2 | 0.2 ± 0.2 | 12.0 ± 1.0 | 0.2 ± 0.2 |
| TOC [wt.%][a,d] | 2.8 ± 0.0 | 4.1 ± 0.1 | 3.3 ± 0.2 | 4.6 ± 0.3 | 3.5 ± 0.1 | 2.0 ± 0.2 |
| $N_{total}$ [wt.%][a,d] | 0.3 ± 0.0 | 0.4 ± 0.0 | 0.3 ± 0.0 | 0.3 ± 0.0 | 0.2 ± 0.0 | 0.1 ± 0.0 |
| $Fe_{total}$ 0.5 M HCl [wt.%][b,d] | 0.1 ± 0.0 | 0.1 ± 0.0 | 0.1 ± 0.0 | 0.2 ± 0.0 | 0.2 ± 0.0 | 0.1 ± 0.0 |
| $Fe_{total}$ XRF [wt.%][a,d,e] | 3.8 ± 0.0 | 2.2 ± 0.0 | 2.1 ± 0.1 | 2.0 ± 0.0 | 2.6 ± 0.0 | 0.6 ± 0.0 |
| $S_{total}$ XRF [ppm][a,d,e] | 778 ± 120 | 1083 ± 51 | n.d.[f] | n.d. | 850 ± 2 | n.d. |
| *Mass specific magnetic susceptibility (MS) [$10^{-8}$ $m^3/kg$][b]* | | | | | | |
| MS Average | 19.9 ± 1.4 | 17.3 ± 5.3 | 27.1 ± 0.6 | 45.5 ± 4.7 | 13.9 ± 1.3 | 11.6 ± 0.5 |
| MS Minimum | 17.7 | 13.5 | 26.4 | 39.7 | 12.3 | 11.0 |
| MS Maximum | 21.3 | 26.7 | 27.8 | 51.1 | 16.1 | 12.3 |

[a] Average of duplicates ± difference to the minimum and maximum.
[b] Average of three or more replicates ± standard deviation.
[c] single measurement.
[d] wt.% and ppm refers to 105 °C dried soil.
[e] XRF = X-ray fluorescence analysis.
[f] Not determined.

with a Si (220) monochromator and spectra were recorded by fluorescent X-ray production using a Lytle-detector. A set of Fe reference compounds was used for linear combination $k^3$-weightened EXAFS spectral fitting using the SIXPACK interface to IFEFIT (Webb, 2005). Linear combinations of the reference compounds were optimized and the only variable parameters were the fractions of each reference compound (see Fig. EA1 of the Electronic Annex for one example of linear combination fitting). Reference compounds were chosen based on their likelihood of being present in the soil or being a reaction product and were included in the fit only if they contributed 5% or more. The detection limit for minor constituents is approximately 5 mol.%. Mössbauer spectroscopy, with a detection limit of approximately 5 wt.%, was used to constrain EXAFS analysis as described earlier by Borch et al. (2007).

### 2.4. Quantification of Fe(III)-reducing microorganisms

Anaerobic Fe(III)-reducing microorganisms of the original soil Sbu were quantified by the most probable number (MPN) method as described in Emmerich et al. (2012) with the following changes: the soil was diluted in 1:10 dilution series with the microbial growth medium, the electron donor mix contained 5 mM Na-acetate, 5 mM Na-lactate, 10 mM Na-formate, 2 mM Na-propionate and 2 mM Na-butyrate, and the MPN plates were incubated for 18 weeks.

### 2.5. Statistical analysis

A one sample *t*-test was used for setups with gasoline amendment and for setups without additional carbon for which there were more than two replicates (Table 1) to determine if the MS of each microbially active setup as well as each sterile setup changed significantly over time. The setups for which this test was conducted, as well as the data used for the tests, are shown in Table EA1 of the Electronic Annex. The Pearson correlation coefficient *r* for linear correlations between MS dependent parameters (maximum extent of MS change, absolute value of the maximum extent of MS change, time within stable MS values were reached (Fig. 1)) and the soil properties (Table 2) was determined for all microbially active microcosms of all six soils without carbon amendment and with gasoline addition (Table EA2 of the Electronic Annex). The setup of soil AW without carbon amendment was excluded from these calculations due to its extreme decrease in MS in comparison to the other soils (Fig. 1). All tests and calculations were performed with the software package PASW statistics 17.0 from SPSS Inc. (Chicago, USA).

## 3. RESULTS

In order to determine the importance of microbial activity and geochemical conditions on the extent and temporal development of changes in soil MS in presence and absence of hydrocarbons, microcosms with six different soils and three different treatments (no carbon addition, addition of lactate/acetate or addition of gasoline) were set up (Table 1).

### 3.1. Microbial processes involved in changes of soil MS

#### *3.1.1. Changes in MS of sterile vs. microbially active soil microcosms*

The MS of microbially active soil microcosms with soils Hclean, Sbu, FB and AW without additional carbon or with gasoline amendment changed significantly during incubation with the exception of microcosms with soil FB amended with gasoline (Fig. 1, Table EA1 of the Electronic Annex). In contrast, for five out of eight sterile microcosms containing the same soils no significant changes in MS were observed (Fig. 1, Table EA1 of the Electronic Annex). The extent of MS change of the microbially active microcosms

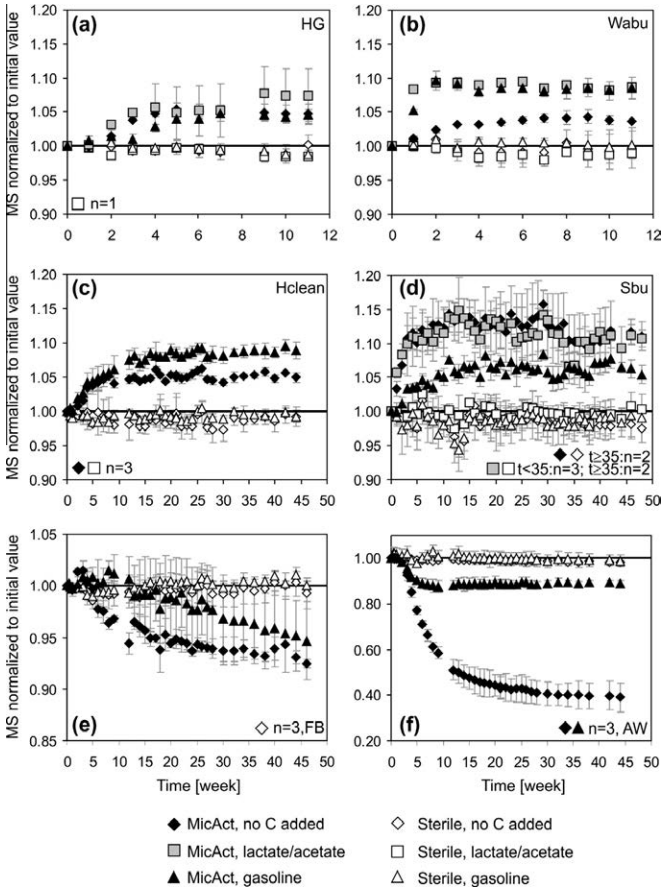


Fig. 1. Changes of magnetic susceptibility (MS) over time of microbially active (MicAct) and sterile soil microcosms either without carbon amendment (no C), amended with 15 mM lactate/acetate or amended with 3.6 μL gasoline/g field moist soil. Lactate/acetate was only added to soils HG, Wabu and Sbu. High-purity water was added to microcosms with soil Sbu. Microbial growth medium was added to all other microcosms. The MS values measured at each time point were normalized to the MS values measured directly after setting up the microcosms (time $t = 0$). Solid horizontal lines indicate MS without any change over time. Note the different scales of the axes. Results are means of two ($n = 2$, a and b) or four ($n = 4$, c–f) replicates, except those noted in the graphs. One replicate of sterile and microbially active setups of soil Sbu without carbon amendment and with lactate/acetate were harvested in week 35 for EXAFS measurements. Bars bracket the range of duplicates or indicate the standard deviation of three and four replicates.

varied between $4.0 \pm 0.4\%$ (soil Wabu, no carbon added) and $11.3 \pm 3.2\%$ (soil Sbu, no carbon added). In one particular microbially active setup (soil AW without any carbon amendment), MS decreased by $60.3 \pm 6.0\%$. On average (excluding the very high change of >60% observed with soil AW) the MS of all microbially active setups, including those with lactate/acetate amendment, changed by $7.3 \pm 2.4\%$. The change in MS of all sterile microcosms varied between $0.6 \pm 0.3\%$ (soil FB, gasoline) and $2.4 \pm 0.9\%$ (soil AW, gasoline) with an average change of $1.4 \pm 0.6\%$.

Whether MS of the non-sterile microcosms increased or decreased over time was dependent upon the soil used (but not upon the carbon source) (Fig. 1). Microcosms with soils HG, Wabu, Hclean and Sbu showed increases in MS, whereas soils FB and AW showed decreases in MS. Furthermore, the time needed until stable MS values were reached also mainly depended on the soil and only to a small extent on the added carbon source. Microcosms with soil Wabu and carbon amendment reached stable MS values within two weeks, whereas microcosms with soil FB

required around 30 weeks for stabilization. The reasons for the different time span until MS stabilizes are probably related to specific properties of the different soils such as soil composition, geochemistry, and microbial community structure.

*3.1.2. Cell numbers of Fe-metabolizing microorganisms in soil Sbu*

Differences of MS and Fe mineralogy (see Section 3.2.1.) observed between sterile and microbially active microcosms with soil Sbu suggest the activity of Fe(III)-reducing microorganisms. MPN quantification of Fe(III)-reducers in the original soil Sbu yielded $2.1 * 10^5$ cells/g dry soil (95% confidence interval: $8.3 * 10^4$–$5.5 * 10^5$ cells/g dry soil).

### 3.2. Geochemical parameters affecting changes in soil MS

*3.2.1. Fe mineralogy changes in soil microcosms*

In order to verify that MS changes in our microcosms were caused by changes in soil Fe mineralogy, we extracted three different Fe fractions from sterile and microbially active soils after incubation. Fig. 2 shows the Fe extraction data of microcosms with soil Sbu (Fig. 1d). The other soils were analyzed as well and showed comparable results (data not shown).

The amount of $Fe_{tot}$ extractable with 1 M HCl at 70 °C (crystalline Fe minerals) was similar for the original soil Sbu and for soil Sbu incubated for approximately 1 year in sterile and microbially active microcosms (Fig. 2b), showing that the $Fe_{tot}$ content was similar in all bottles. The total amount of Fe extractable with Na-acetate (adsorbed Fe and Fe carbonates) and 0.5 M HCl (poorly crystalline Fe minerals) was similar for the sterile and the original soil indicating no major changes in mineralogy during sterilization and incubation of the sterilized soil. In contrast, in the microbially active setups, especially those without carbon amendment and those with lactate/acetate addition, $Fe_{tot}$ extracted by Na-acetate and 0.5 M HCl was much higher (Fig. 2a) indicating changes in the different Fe pools caused by microbial activity. Among all sterile setups as well as among all microbially active setups, the Fe(II):$Fe_{tot}$ ratio of the 0.5 M HCl and 1 M HCl fraction, respectively, was very similar, independent of the carbon treatment. The percentage of total Fe present as Fe(II) as determined in the 0.5 M HCl extract was 14.3% in the original soil, 57.5 ± 2.7% on average in the sterile setups, and 97.4 ± 2.4% on average in the microbially active setups. In the 1 M HCl fraction, the percentage of total Fe present as Fe(II) in the sterile setups (69.2 ± 8.2%) was similar to the percentage in the original soil (69.7%), whereas in microbially active setups the Fe(II) content was approximately 20% higher (90.1 ± 2.4%).

The Fe extraction data indicate a difference in soil Fe mineralogy and Fe redox states in microbial active microcosms in comparison to the sterile microcosms (Fig. 2). In order to identify the Fe minerals that were (trans)formed in the soils during incubation, we performed Mössbauer and EXAFS spectroscopy analysis of the original soil Sbu and of soil Sbu from sterile and microbially active microcosms without carbon amendment, and with lactate/acetate addition after several months of incubation. Confirming the Fe extraction data, Mössbauer spectroscopy revealed that the original soil Sbu and soil Sbu from the two sterile setups contained more Fe(III) phases (82–92%, percentages refer to the relative absorption of γ-rays by $Fe_{tot}$) than the microbially active setups without carbon amendment (71%) or lactate/acetate addition (65%) (Table 3, Fig. 3). The main fraction of Fe(III) in the original soil and all four setups was a paramagnetic Fe(III) phase which might have been ferrihydrite, nano-goethite, lepidocrocite, Fe(III) in clays or Fe(III) associated with humic substances. Additionally, hematite (<10%) was identified in the original soil and in the microbially active setup with lactate/acetate (Fig. 3b). The amount of Fe(II) phases detected by Mössbauer spectroscopy varied between 29% and 35% in the microbially active setups, whereas it was between 12% and 19% in the sterile setups and only 8% in the original soil. In the microbially active setups, Fe(II) was present as siderite and an associated Fe(II) phase represented in the spectrum by an extra Fe(II) doublet occurring together with siderite (Fig. 3b). A similar spectral feature was also detected when siderite was chemically synthesized in our lab by mixing dissolved $Fe^{2+}$ with an $HCO_3^-$ solution at pH 8 and 25 °C (data not shown). Its identity is so far unknown, however,

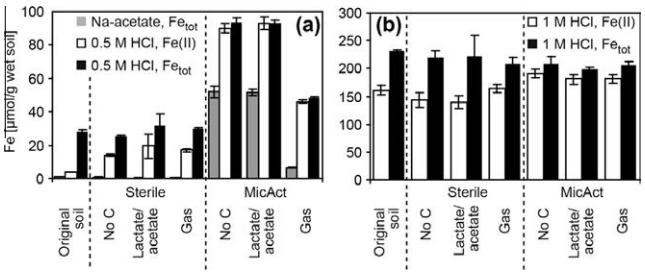


Fig. 2. (a) $Fe_{tot}$ extracted with Na-acetate, Fe(II) and $Fe_{tot}$ extracted with 0.5 M HCl from original soil Sbu and from sterile and microbially active (MicAct) microcosms with soil Sbu after 48 weeks of incubation without additional carbon (No C), with 15 mM lactate/acetate or with 3.6 µL gasoline/g field moist soil (Gas). (b) Fe(II) and $Fe_{tot}$ extracted with 1 M HCl (70 °C) from the same soil samples as in (a). Results are means of triplicate measurements of one bottle per setup or of the original soil, except for the original soil which was extracted with 1 M HCl only in duplicates. Bars indicate the range of duplicates or the standard deviation of triplicates.

Table 3
Relative abundance and fitting data of different Fe phases determined by Mössbauer spectroscopy in the original soil Sbu and in soil Sbu from sterile and microbially active (MicAct) microcosms without additional carbon or with 15 mM lactate/acetate after 9-23 months of incubation. Fitting errors are given in parentheses.

| Sample (incubation time [weeks]) | Reduced $\chi^2$ of fit | Fe phases | Abundance[f] [%] | CS[f] [mm/s] | QS[f] [mm/s] | H[f] [T] |
|---|---|---|---|---|---|---|
| Original soil | 3.14 | Paramagnetic Fe(III)[a] | 83 (±0.3) | 0.36 (<0.01) | 0.64 (<0.01) | – |
| | | Hematite | 9 (±0.07) | 0.37 * | −0.20 * | 51.3* |
| | | Fe(II) in silicates[b] | 8 (±0.4) | 1.08 (±0.01) | 2.73 (±0.02) | – |
| Sterile microcosm, no carbon (99) | 0.56 | Paramagnetic Fe(III)[a] | 82 (±2.1) | 0.36 * | 0.60 (±0.03) | – |
| | | Fe(II) in silicates[b] | 12 (±1.5) | 1.14 * | 2.67 * | – |
| | | Fe(II) in silicates[b] | 7 (±1.6) | 1.10 * | 1.94 * | – |
| Sterile microcosm, lactate/acetate (93) | 0.88 | Paramagnetic Fe(III)[a] | 88 (±1.7) | 0.35 * | 0.65 * | – |
| | | Unknown Fe(II) phase 1[c] | 12 (±1.7) | 1.31 (±0.07) | 2.33 (±1.4) | – |
| MicAct microcosm, no carbon (62.5) | 1.35 | Paramagnetic Fe(III)[a] | 71 (±1.2) | 0.35 * | 0.63 * | – |
| | | Hematite | n.d.[e] | – | – | – |
| | | Unknown Fe(II) phase 2[d] | 13 (±0.9) | 1.21 * | 2.49 * | – |
| | | Siderite | 16 (±0.9) | 1.20 * | 1.80 * | – |
| MicAct microcosm, lactate/acetate (40) | 1.29 | Paramagnetic Fe(III)[a] | 59 (±0.73) | 0.31 (±0.01) | 0.65 (±0.02) | – |
| | | Hematite | 6 (±0.12) | 0.38 * | −0.20 * | 51.2* |
| | | Unknown Fe(II) phase 2[d] | 18 (±0.64) | 1.21 * | 2.49 * | – |
| | | Siderite | 17(±0.73) | 1.23 * | 1.80 * | – |

[a] Paramagnetic Fe(III) might be ferrihydrite, nano-goethite, lepidocrocite, Fe(III) in clays, Fe(III) associated with humic substances or a mix of these.
[b] Silicates are probably phyllosilicates such as clays and micas. Differences in the modeling parameters indicate Fe(II) present either in different silicates or in different sites of one silicate.
[c] Maybe a mixture of siderite and unknown Fe(II) phase 2.
[d] Unknown Fe(II) phase associated with siderite.
[e] Hematite could not be modeled, since the signal to noise ratio was too low.
[f] Abundance [%] = absorption of γ-ray [%]. CS = center shift, QS = quadrupol splitting, H = hyperfine field.
* Model parameter fixed during fitting.

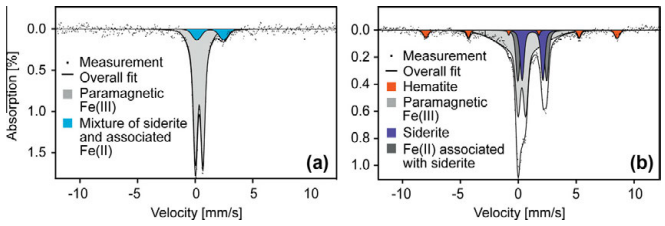


Fig. 3. Mössbauer spectra collected at room temperature of soil Sbu from (a) sterile and (b) microbially active microcosms with 15 mM lactate/acetate amendment after 93 and 40 weeks of incubation, respectively. Fitting parameters are given in Table 3.

based on the broadness of the signals, its crystallinity is similar to that of siderite. In the original soil and in sterile soil without carbon amendment, Fe(II) was present as ferrosilicates. The Fe(II) phase present in the sterile setup with lactate/acetate is unknown.

EXAFS analyses of soil Sbu from microcosms confirmed the results of Fe extraction and Mössbauer spectroscopy and showed that the Fe composition of the original soil was similar to the sterile setups regarding all Fe-containing phases identified by EXAFS (data not shown). Additionally, the EXAFS analyses showed that in microbially active setups without carbon addition or with lactate/acetate addition (Fig. EA1 of the Electronic Annex), the fraction of the Fe(III) minerals goethite and hematite decreased and the Fe(II)-bearing mineral siderite was formed (Table 4). The amount of Fe present as Fe(III) minerals in sterile setups decreased in microbially active setups by around 10 mol.%, which is less than the amount of Fe found as Fe(II) in siderite (14 mol.%) in the microbially active setups. However, the main fraction of Fe (71-74 mol.%) identified by EXAFS in sterile and microbially active setups was present in augite- and ferro-smectite-like minerals and likely in association with humic substances.

Table 4
Relative amounts of Fe phases (in % on a per mol basis) resulting from linear combination fits of $k^3$-weighted EXAFS spectra (the data were fit to $k = 11$[a] and the detection limit is approximately 5 mol.% Fe). The table gives the data for sterile and microbially active (MicAct) microcosms of soil Sbu without carbon amendment (no C) and with addition of 15 mM lactate/acetate (lac/ac). Dashes indicate Fe phases which were not detected due to their low concentration or absence. As an example, the linear combination fitting for the lactate/acetate-amended, microbially active sample is displayed in Fig. EA1 of the Electronic Annex.

| Sample | Goethite [mol.% Fe] | Hematite [mol.% Fe] | Siderite [mol.% Fe] | Augite [mol.% Fe] | Ferro-Smectite [mol.% Fe] | Fe-HS[d] [mol.% Fe] | Reduced $\chi^2$ of fit |
|---|---|---|---|---|---|---|---|
| Sterile, no C[b] | 20 | 5 | – | 28 | 15 | 31 | 0.026 |
| Sterile, lac/ac[b] | 20 | 6 | – | 28 | 14 | 31 | 0.037 |
| MicAct, no C[c] | 16 | – | 14 | 19 | 6 | 46 | 0.031 |
| MicAct, lac/ac[b] | 15 | – | 14 | 38 | - | 33 | 0.021 |

[a] Data fit to $k = 14$ did not change the overall results.
[b] Measured at beamline 11-2 at the Stanford Synchrotron Radiation Lightsource.
[c] Measured at beamline 4-1 at the Stanford Synchrotron Radiation Lightsource 4 months later than samples labeled with (b).
[d] Fe associated with humic substances (HS).

*3.2.2. Mobilization of organic carbon from soils*

The MS of most microbially active setups without carbon amendment changed to a similar or even larger extent than that of setups with carbon amendment (Fig. 1). Since microcosms of soils AW, FB and Hclean amended with growth medium showed a similar change in MS compared to microcosms of the same soils amended only with water (Fig. EA2 of the Electronic Annex), we believe that neither carbon amendment nor the trace metals and vitamins in the medium were the key parameters causing MS changes. Instead, this suggests that the addition of liquid – independent of whether it was pure water or medium – mobilized organic carbon (natural organic matter) from the soil that drove metabolic processes and MS changes in all microbially active setups. In order to determine which dissolved carbon sources were available in the microcosms, the concentrations of organic acids (lactate, formate, acetate, and propionate) and dissolved inorganic (DIC) and organic (DOC) carbon in the liquid phase of microcosms with soil Sbu after 48 weeks of incubation were quantified (Fig. 4). The concentrations of the four different organic acids were similar in all sterile setups of soil Sbu, except in setups amended with lactate/acetate which resulted in higher lactate and acetate concentrations (Fig. 4a). In contrast, no organic acids besides small amounts of lactate (<2.5 mM) were detected in the microbially active setups of soil Sbu without carbon amendment, and in the setups with lactate/acetate addition. In the microbially active setups with gasoline, the lactate and formate concentrations were also low (<1.2 mM) but the acetate (37.4 mM) and propionate (8.2 mM) concentrations were higher than in all other sterile and microbially active setups.

The DIC in all sterile microcosms of soil Sbu was <0.1 g/L whereas in microbially active ones the DIC was higher (0.1–0.4 g/L) indicating microbial mineralization of organic carbon (Fig. 4b). The DOC in sterile setups without carbon addition and with gasoline was similar (~2 g/L) indicating the low solubility of the gasoline hydrocarbons, whereas in the sterile setup with lactate/acetate the DOC was 0.6 g/L higher than in setups without carbon addition. The DOC content in microbially active setups without carbon amendment and in setups with lactate/acetate addition was lower (both 0.3 g/L) than in setups amended with gasoline (1.9 g/L).

*3.2.3. Influence of organic carbon and Fe bioavailability on changes in MS of soil microcosms*

All microbially active soil microcosms with and without carbon addition reached stable MS values after a few weeks to several months (Fig. 1). This suggests that the soils reached a stable state and no further Fe mineral transformation occurred after that time. In order to determine whether the amount of bioavailable organic carbon was limiting the mineral transformation, we added lactate and acetate a second time to the respective setups of soils HG and Wabu (Table 1). Lactate and acetate were chosen, since the first addition of these compounds led to a similar or even higher change in MS than the addition of gasoline (Fig. 1). The carbon sources were added after 14.5 weeks of incubation at which time the MS values had stabilized (Fig. 1). In the following 10 weeks, the MS values of both the sterile and microbially active setups changed in all but one setup by less than 2.0% (data not shown), indicating that the amount of bioavailable carbon was probably not a primary limiting factor for ferro(i)magnetic mineral transformation.

In order to determine if bioavailable Fe(III) limitation in the soils led to cessation of changes in MS, ferrihydrite was added to microcosms with soil Hclean after 51 weeks of incubation when MS did not show further change (Table 1, Fig. 1). Ferrihydrite addition to soil Hclean led to an immediate increase in MS of 10.6–20.1% when measured directly after its addition (Fig. 5). In the following 73 weeks, MS in microbially active microcosms further increased by $5.4 \pm 3.4\%$ (no carbon addition) and $13.4 \pm 1.6\%$ (gasoline addition), respectively. From these MS values we can estimate that about 1% and 2% of the ferrihydrite has been converted into magnetite (calculation not shown). In the corresponding sterile setups the increase within the 73 weeks was only minor ($2.4 \pm 1.2\%$ and $0.8 \pm 0.0\%$).

*3.2.4. Influences of soil properties on soil MS changes*

In order to determine if soil properties had an influence on changes in MS, linear correlation analyses between the

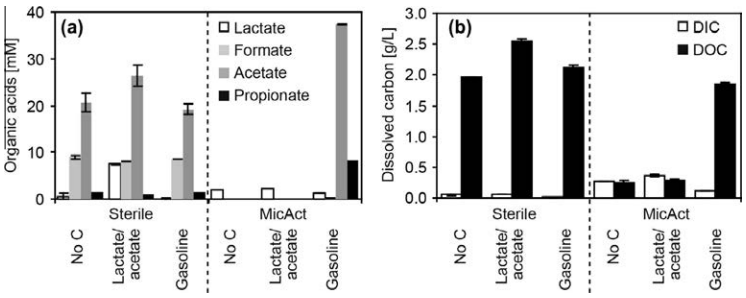


Fig. 4. (a) Concentration of short chain fatty acids lactate, formate, acetate and propionate and (b) dissolved inorganic (DIC) and dissolved organic carbon (DOC) in the water in soil Sbu microcosms after 48 weeks of incubation. Shown are data from sterile and microbially active (MicAct) microcosms without carbon addition (no C), with 15 mM lactate/acetate or with 3.6 μL gasoline/g field moist soil. Results are means of duplicate measurements of one bottle per setup. Propionate was measured only once. Bars bracket the range of duplicates.

MS dependent parameters of the microcosms (extent of MS change, absolute value of the extent of MS change, time required to reach stable MS values, Fig. 1) and the soil properties (Table 2) were performed. Since significant changes in MS occurred mainly in microbially active microcosms (Table EA1 of the Electronic Annex), only these setups were used for the analysis. Furthermore, only setups without carbon amendment and with gasoline addition were considered, since lactate/acetate was added to only three soils. As the MS of microbially active soil AW without carbon amendment decreased by >60% in contrast to the other microbially active microcosms (average MS change $7.3 \pm 2.4\%$, Fig. 1), this setup was considered an exception and was also excluded from the calculations.

The MS dependent parameters of the microcosms were not linearly correlated with most of the soil parameters tested (Table EA2 of the Electronic Annex). There may be several reasons for the lack of a strong correlation. Either the correlation between the parameters was not linear, the relevant soil parameters were not tested, or the sample number (five to six) was too small to observe any correlation. However, our analysis revealed a significant positive correlation between the absolute value of the extent of MS change and the $Fe_{tot}$ extractable with 0.5 M HCl for the microbially active microcosms without carbon amendment (Pearson correlation coefficient 0.959, 2-tailed significance 0.010) (Table EA2 of the Electronic Annex). The $Fe_{tot}$ fraction extractable with 0.5 M HCl is considered to be the "bioavailable" Fe fraction. Hence, the results suggest that the higher the concentration of the bioavailable Fe fraction in a soil is, the higher the change in MS. For microbially active microcosms amended with gasoline, a linear correlation was neither observed between the absolute value of the extent of MS change and the $Fe_{tot}$ extractable with 0.5 M HCl nor between the extent of MS change (including positive and negative MS values) and the $Fe_{tot}$ extractable with 0.5 M HCl. However, a significant negative linear correlation between the extent of MS change and the initial mass specific MS of the soil was found (Pearson correlation coefficient −0.957, 2-tailed significance 0.003) (Table EA2 of the Electronic Annex). This suggests, that in soils with a low MS, ferro(i)magnetic minerals are formed, whereas in soils with a relatively high MS, ferro(i)magnetic minerals are transformed.

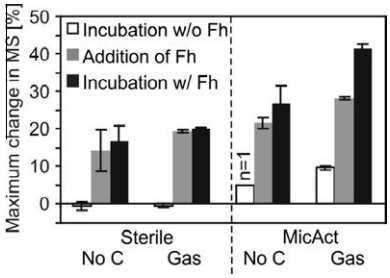


Fig. 5. Changes in magnetic susceptibility (MS) of sterile and microbially active (MicAct) microcosms with soil Hclean without carbon addition (No C) or with gasoline addition (Gas, 3.6 μL/g field moist soil) within 46 weeks of incubation (□, Fig. 1c). After 51 weeks 2 mL of a 0.5 M ferrihydrite suspension (Fh) was added to the microcosms leading to an immediate increase in MS (■) and to a slower MS increase in the following 73 weeks of incubation (■). All values are given in % relative to the MS values measured directly after setting up the microcosms. Results are means of duplicates, except those marked in the figure ($n = 1$). Bars bracket the range of duplicates.

## 4. DISCUSSION

Magnetic susceptibility measurements of microcosms with six different sterile and microbially active soils showed that during anoxic incubation of the soils microbially mediated processes were predominantly responsible for changes in the MS. Furthermore, the results indicated that besides microbial activity the bioavailable Fe and organic carbon content as well as the initial mass specific MS were the main factors controlling the changes in MS of the soil microcosms. In the following sections, we therefore first discuss how microorganisms potentially have been involved in the

(trans)formation of magnetite, a ferro(i)magnetic mineral, and of non-ferro(i)magnetic Fe-containing minerals in the microcosms. Secondly, we describe how the mobilization of bioavailable soil organic carbon or the addition of bioavailable carbon (e.g. gasoline) may have influenced the changes of soil MS in the microcosms indirectly by influencing the Fe(III)-reducing microorganisms.

### 4.1. Microbial (trans)formation of Fe-containing soil minerals

#### *4.1.1. (Trans)formation of ferro(i)magnetic minerals*

The increase and decrease in MS of the soil microcosms (Fig. 1) indicated the formation and transformation of ferro(i)magnetic minerals. Statistical analysis suggested that in microcosms without additional carbon amendment the extent of the increase or decrease in MS depended on the amount of bioavailable Fe in the soil (Table EA2 of the Electronic Annex). This hypothesis is supported by the experiment in which ferrihydrite was added as an easily reducible and thus as bioavailable Fe(III) source to microcosms after they had reached stable MS values (Fig. 5). The ferrihydrite addition to the microbially active microcosms led to further changes in the MS over time, indicating that either the ferrihydrite served as precipitation site for magnetite by a reaction of the ferrihydrite with $Fe^{2+}$ present in the soil and/or that the ferrihydrite itself was reduced. For microbially active microcosms amended with gasoline, the statistical analysis (Table EA2 of the Electronic Annex) suggested, that in soils with a low mass specific MS, ferro(i)magnetic minerals are formed, whereas in soils with a relatively high mass specific MS, ferro(i)magnetic minerals are transformed.

The most important ferro(i)magnetic minerals in soils are the mixed-valent Fe mineral magnetite ($Fe_3O_4$) and the Fe(III) oxide maghemite ($\gamma$-$Fe_2O_3$) (Mullins, 1977). In sulfur-rich environments also the ferro(i)magnetic minerals greigite ($Fe_3S_4$) and pyrrhotite ($Fe_7S_8$) may form (Farina et al., 1990; Stanjek et al., 1994). Since the total sulfur content of the soils was low (<1100 ppm in comparison to 6000–38,000 ppm $Fe_{tot}$, Table 2) and since both EXAFS and Mössbauer spectroscopy did not provide evidence for the presence of Fe-sulfide minerals, (trans)formation of greigite or pyrrhotite did probably not contribute considerably to the change of MS of the soil microcosms.

Microbially controlled formation of magnetite and greigite inside cells is known from magnetotactic bacteria (Blakemore, 1975). Since other studies showed that the cell numbers of magnetotactic bacteria in soils were too low to contribute significantly to the soil magnetic properties (Fassbinder et al., 1990; Dearing et al., 1996), we assume that their contribution to the changes in MS of our microcosms was also minor.

In contrast, ferro(i)magnetic Fe minerals can be produced in large amounts extracellularly by secondary mineral formation during microbial Fe(III) reduction under anoxic conditions. Magnetite formation was observed, for example, during microbial reduction of ferrihydrite (Lovley et al., 1987) and hematite (Behrends and Van Cappellen, 2007). Ferrihydrite, hematite and goethite are common Fe minerals in soils (Cornell and Schwertmann, 2003) and we identified these Fe(III) phases by Mössbauer spectroscopy and/or EXAFS measurements in the original soil Sbu (no amendments, stored at 4 °C) that also contained Fe(III)-reducing bacteria (see Section 3.1.2.). However, although MS measurements of microbially active soil Sbu indicated an increase in ferro(i)magnetic minerals (e.g. magnetite, Fig. 1d), such minerals were neither detected by Mössbauer spectroscopy nor by EXAFS, probably due to their low content in the soil. For identification and quantification of a certain Fe mineral in soils by Mössbauer spectroscopy or EXAFS, the Fe present in this respective Fe mineral must represent at least 5–10 wt.% of the total Fe content in the sample. In contrast, MS measurements are more sensitive. An increase in the initial soil Fe content of soil FB by addition of magnetite by less than 3 wt.% (corresponding to less than 0.1 wt.% magnetite in the soil) led to an increase in the soil MS by more than 100% (Fig. EA3 of the Electronic Annex).

In contrast to setups with soils HG, Wabu, Hclean and Sbu where MS increased over time, a decline of the MS over time was observed in setups with soils FB and AW indicating a microbially mediated decrease in the ferro(i)magnetic mineral content, e.g. magnetite, in the soils. Magnetite can serve also as electron acceptor for Fe(III)-reducing microorganisms (Kostka and Nealson, 1995; Brown et al., 1997) and microbial Fe(III) reduction could potentially have led to the transformation of ferro(i)magnetic minerals in our anoxic microcosms.

#### *4.1.2. (Trans)formation of non-ferro(i)magnetic Fe-containing minerals*

Besides magnetite, non-ferro(i)magnetic Fe minerals can form during microbial Fe(III) reduction. Depending on geochemical conditions such as the presence of anions, mineral nucleation sites and humic substances and depending on the Fe(III) reduction rates, the formation of dissolved $Fe^{2+}$, goethite, green rust, vivianite, or siderite has been reported (for reviews see Konhauser, 1998; Fortin and Langley, 2005). Mössbauer and EXAFS spectroscopy revealed that microbially active soil Sbu contained more siderite than the sterile and the original soil Sbu. The carbonate necessary for the siderite formation might originate from the soil Sbu itself (it showed the highest carbonate content of all soils, Table 2) or from microbial degradation of organic matter. Microbial $CO_2$ production was indicated by a higher DIC content in microbially active soil Sbu in comparison to the sterile soil (Fig. 4b).

Both Mössbauer and EXAFS spectroscopy of soil Sbu microcosms revealed that part of the Fe was also present in silicates, augite-like and ferro-smectite-like phases and in association with humic substances (Tables 3 and 4). These Fe phases are typical soil constituents (Cornell and Schwertmann, 2003) and are also non-ferro(i)magnetic. Fe-containing minerals which are non-ferro(i)magnetic have only a small positive MS. However, when the concentration of ferro(i)magnetic minerals in a soil is low, these minerals can contribute considerably to the soil MS (Mullins, 1977).

### 4.2. Influences of organic carbon sources on microbially induced soil MS changes

#### *4.2.1. Mobilized soil organic carbon as substrate for microorganisms*

Analysis of the water and microbial growth medium added to soil Sbu revealed that organic compounds including organic acids were mobilized from the soil matrix (Fig. 4). DOC represents an important source of bioavailable carbon in soils (Marschner and Kalbitz, 2003). The mobilized natural organic matter was partly consumed in microbially active microcosms leading to a change in soil MS comparable to setups amended with a carbon source (Fig. 1). The fact that the microbial (trans)formation of ferro(i)magnetic minerals was not limited by the availability of organic carbon was supported by the experiment in which a second amendment of lactate/acetate to microcosms with soils HG and Wabu did not lead to a further change in MS (data not shown).

#### *4.2.2. Gasoline as organic carbon source*

In all microbially active microcosms, the addition of gasoline led to changes in MS within the first five weeks (Fig. 1), indicating that gasoline was not toxic for all soil microorganisms and that at least some of them remained active and caused changes in MS. Previous studies showed that microbial communities in uncontaminated soils could adapt to added hydrocarbons such as crude oil and gasoline and were able to partly degrade them (Bundy et al., 2002; Hamamura et al., 2006). The microbial degradation of hydrocarbons can be directly coupled to the reduction of Fe(III) (Lovley et al., 1989; Lovley and Anderson, 2000). Additionally, nitrate-reducers, sulfate-reducers and methanogens are able to degrade hydrocarbons under anoxic conditions (Grbić-Galić and Vogel, 1987; Kuhn et al., 1988; Rueter et al., 1994) and the metabolic products (e.g. sulfide or nitrite) can react abiotically with Fe(III) and Fe(II) and thus influence the soil Fe mineralogy (Moraghan and Buresh, 1977; dos Santos Afonso and Stumm, 1992; Klueglein and Kappler, 2013).

The changes in MS and the formation of acetate and propionate in the microbially active setup of soil Sbu amended with gasoline suggest that the microorganisms were indeed active and have degraded at least part of the added gasoline (Cozzarelli et al., 1994). However, the smaller changes in MS (Fig. 1) and the lower content of 0.5 M extractable Fe(II) (Fig. 2a) compared to microbially active setups of soil Sbu without carbon addition indicate that the transformation of Fe minerals in soil Sbu was less pronounced in the presence of gasoline than without gasoline. This suggests that gasoline had an inhibiting effect on the microbial (trans)formation of ferro(i)magnetic minerals in this soil. Nevertheless, in some soils the change in MS was similar (HG, FB) or even larger (Wabu, Hclean) in setups with gasoline than without carbon amendment (Fig. 1). These results suggest that the microorganisms were well adapted to the presence of hydrocarbons.

## 5. CONCLUSIONS

The motivation for our study was the idea that soil magnetic susceptibility measurements as a fast screening of soil magnetic properties can be used to localize hydrocarbon contamination in the field. However, this study suggests that hydrocarbon addition is not the only factor driving changes in soil MS. The major findings of the present soil microcosm study were that (i) changes in soil MS were mainly microbially mediated, (ii) the MS of the soils started to change within the first few weeks of incubation, (iii) the extent of the MS change depended on the bioavailable Fe content of the soils, (iv) the MS value of the original soils determined whether the MS increased or decreased during incubation, and (v) mobilization of natural organic matter from the soil by addition of water also led to a change in MS similar to setups with hydrocarbon contamination. Although the changes in MS were only around 4–11% for most soil microcosms, the high sensitivity of MS analysis allowed their detection with high accuracy. In contrast, Mössbauer and EXAFS spectroscopy analysis are less sensitive to small changes in soil ferro(i)magnetic mineral content and are more time and labor intensive.

## ACKNOWLEDGEMENTS

This work was funded by the Deutsche Forschungsgemeinschaft (DFG), and partly also by Shell International Exploration and Production B.V. under the Contract No. 4600003533 within the Gamechanger programme as well as by a National Science Foundation (NSF) CAREER Award (EAR 0847683) to Thomas Borch. Portions of this research were carried out at the Stanford Synchrotron Radiation Lightsource, a national user facility operated by Stanford University on behalf of the US Department of Energy, Office of Basic Energy Sciences. We also thank Ellen Struve for help during soil and liquid analyses and Philip Larese-Casanova and Urs Dippon for Mössbauer spectroscopy and data analyses.

## APPENDIX A. SUPPLEMENTARY DATA

Supplementary data associated with this article can be found, in the online version, at http://dx.doi.org/10.1016/j.gca.2013.12.001.

## REFERENCES

Aldana M., Costanzo-Alvarez V., Gomez L., Gonzalez C., Diaz M., Silva P. and Rada M. (2011) Identification of magnetic minerals related to hydrocarbon authigenesis in venezuelan oil fields using an alternative decomposition of isothermal remanence curves. *Stud. Geophys. Geod.* **55**, 343–358.

Amstaetter K., Borch T. and Kappler A. (2012) Influence of humic acid imposed changes of ferrihydrite aggregation on microbial Fe(III) reduction. *Geochim. Cosmochim. Acta* **85**, 326–341.

Behrends T. and Van Cappellen P. (2007) Transformation of hematite into magnetite during dissimilatory iron reduction – conditions and mechanisms. *Geomicrobiol. J.* **24**, 403–416.

Blakemore R. (1975) Magnetotactic bacteria. *Science* **190**, 377–379.

Blume H.-P., Deller B., Leschber R., Paetz A. and Wilke B.-M. (2000) *Handbuch der Bodenuntersuchung: Terminologie, Verfahrensvorschriften und Datenblätter – Physikalische, chemische, biologische Untersuchungsverfahren – Gesetzliche Regelwerke*. Wiley-VCH, Weinheim.

Borch T., Masue Y., Kukkadapu R. K. and Fendorf S. (2007) Phosphate imposed limitations on biological reduction and alteration of ferrihydrite. *Environ. Sci. Technol.* **41**, 166–172.

Borch T., Kretzschmar R., Kappler A., Cappellen P. V., Ginder-Vogel M., Voegelin A. and Campbell K. (2010) Biogeochemical redox processes and their impact on contaminant dynamics. *Environ. Sci. Technol.* **44**, 15–23.

Brown D. A., Sherriff B. L. and Sawicki J. A. (1997) Microbial transformation of magnetite to hematite. *Geochim. Cosmochim. Acta* **61**, 3341–3348.

Bundy J. G., Paton G. I. and Campbell C. D. (2002) Microbial communities in different soil types do not converge after diesel contamination. *J. Appl. Microbiol.* **92**, 276–288.

Chaudhuri S. K., Lack J. G. and Coates J. D. (2001) Biogenic magnetite formation through anaerobic biooxidation of Fe(II). *Appl. Environ. Microbiol.* **67**, 2844–2848.

Cornell R. M. and Schwertmann U. (2003) *The Iron Oxides, Structure, Properties, Reactions, Occurences and Uses*. Wiley-VCH, Weinheim.

Cozzarelli I. M., Baedecker M. J., Eganhouse R. P. and Goerlitz D. F. (1994) The geochemical evolution of low-molecular-weight organic acids derived from the degradation of petroleum contaminants in groundwater. *Geochim. Cosmochim. Acta* **58**, 863–877.

Dearing J. A., Hay K. L., Baban S. M. J., Huddleston A. S., Wellington E. M. H. and Loveland P. J. (1996) Magnetic susceptibility of soil: an evaluation of conflicting theories using a national data set. *Geophys. J. Int.* **127**, 728–734.

Dippon U., Pantke C., Porsch K., Larese-Casanova P. and Kappler A. (2012) Potential function of added minerals as nucleation sites and effect of humic substances on mineral formation by the nitrate-reducing Fe(II)-oxidizer *Acidovorax* sp BoFeN1. *Environ. Sci. Technol.* **46**, 6556–6565.

dos Santos Afonso. M. and Stumm W. (1992) Reductive dissolution of iron(III) (hydr)oxides by hydrogen sulfide. *Langmuir* **8**, 1671–1675.

Dunlop D. J. and Özdemir Ö. (1997) *Rock Magnetism: Fundamentals and Frontiers*. Cambridge University Press, Cambridge.

Emmerich M., Bhansali A., Losekann-Behrens T., Schroder C., Kappler A. and Behrens S. (2012) Abundance, distribution, and activity of Fe(II)-oxidizing and Fe(III)-reducing microorganisms in hypersaline sediments of lake Kasin, Southern Russia. *Appl. Environ. Microbiol.* **78**, 4386–4399.

Farina M., Esquivel D. M. S. and Debarros H. (1990) Magnetic iron-sulphur crystals from a magnetotactic microorganism. *Nature* **343**, 256–258.

Fassbinder J. W. E., Stanjek H. and Vali H. (1990) Occurence of magnetic bacteria in soil. *Nature* **343**, 161–163.

Fortin D. and Langley S. (2005) Formation and occurence of biogenic iron-rich minerals. *Earth Sci. Rev.* **72**, 1–19.

Fredrickson J. K., Zachara J. M., Kennedy D. W., Dong H., Onstott T. C., Hinman N. W. and Li S.-M. (1998) Biogenic iron mineralization accompanying the dissimilatory reduction of hydrous ferric oxide by a groundwater bacterium. *Geochim. Cosmochim. Acta* **62**, 3239–3257.

Grbić-Galić D. and Vogel T. M. (1987) Transformation of toluene and benzene by mixed methanogenic cultures. *Appl. Environ. Microbiol.* **53**, 254–260.

Guzman O., Costanzo-Alvarez V., Aldana M. and Diaz M. (2011) Study of magnetic contrasts applied to hydrocarbon exploration in the Maturin Sub-Basin (Eastern Venezuela). *Stud. Geophys. Geod.* **55**, 359–376.

Hamamura N., Olson S. H., Ward D. M. and Inskeep W. P. (2006) Microbial population dynamics associated with crude-oil biodegradation in diverse soils. *Appl. Environ. Microbiol.* **72**, 6316–6324.

Hansel C. M., Benner S. G. and Fendorf S. (2005) Competing Fe(II)-induced mineralization pathways of ferrihydrite. *Environ. Sci. Technol.* **39**, 7147–7153.

Hegler F., Posth N. R., Jiang J. and Kappler A. (2008) Physiology of phototrophic iron(II)-oxidizing bacteria: implications for modern and ancient environments. *FEMS Microbiol. Ecol.* **66**, 250–260.

Hohmann C., Winkler E., Morin G. and Kappler A. (2010) Anaerobic Fe(II)-oxidizing bacteria show As resistance and immobilize As during Fe(III) mineral precipitation. *Environ. Sci. Technol.* **44**, 94–101.

Ivakhnenko O. P. and Potter D. K. (2004) Magnetic susceptibility of petroleum reservoir fluids. *Phys. Chem. Earth* **29**, 899–907.

Jiao Y. Y. Q., Kappler A., Croal L. R. and Newman D. K. (2005) Isolation and characterization of a genetically tractable photo autotrophic Fe(II)-oxidizing bacterium, *Rhodopseudomonas palustris* strain TIE-1. *Appl. Environ. Microbiol.* **71**, 4487–4496.

Kappler A. and Straub K. L. (2005) Geomicrobiological cycling of iron. *Rev. Mineral. Geochem.* **59**, 85–108.

Klueglein N. and Kappler A. (2013) Abiotic oxidation of Fe(II) by reactive nitrogen species in cultures of the nitrate-reducing Fe(II)-oxidizer *Acidovorax* sp. BoFeN1 – questioning the existence of enzymatic Fe(II) oxidation. *Geobiology* **11**, 180–190.

Konhauser K. O., Kappler A. and Roden E. E. (2011) Iron in microbial metabolisms. *Elements* **7**, 89–93.

Konhauser K. O. (1998) Diversity of bacterial iron mineralization. *Earth Sci. Rev.* **43**, 91–121.

Kostka J. E. and Nealson K. H. (1995) Dissolution and reduction of magnetite by bacteria. *Environ. Sci. Technol.* **29**, 2535–2540.

Kuhn E. P., Zeyer J., Eicher P. and Schwarzenbach R. P. (1988) Anaerobic degradation of alkylated benzenes in denitrifying laboratory aquifer columns. *Appl. Environ. Microbiol.* **54**, 490–496.

Lovley D. R. and Anderson R. T. (2000) Influence of dissimilatory metal reduction on fate of organic and metal contaminants in the subsurface. *Hydrogeol. J.* **8**, 77–88.

Lovley D. R., Stolz, Jr., J. F., Nord G. L. and Phillips E. J. P. (1987) Anaerobic production of magnetite by a dissimilatory iron-reducing microorganism. *Nature* **330**, 252–254.

Lovley D. R., Baedecker M. J., Lonergan D. J., Cozzarelli I. M., Phillips E. J. P. and Siegel D. I. (1989) Oxidation of aromatic contaminants coupled to microbial iron reduction. *Nature* **339**, 297–300.

Marschner B. and Kalbitz K. (2003) Controls of bioavailability and biodegradability of dissolved organic matter in soils. *Geoderma* **113**, 211–235.

Masak J., Machackova J., Siglova M., Cejkova A. and Jirku V. (2003) Capacity of the bioremediation technology for clean-up of soil and groundwater contaminated with petroleum hydrocarbons. *J. Environ. Sci. Health A Toxic Hazard. Subst. Environ. Eng.* **A38**, 2447–2452.

McCabe C., Sassen R. and Saffer B. (1987) Occurence of secondary magnetite within biodegraded oil. *Geology* **15**, 7–10.

Mendelssohn I. A., Andersen G. L., Baltz D. M., Caffey R. H., Carman K. R., Fleeger J. W., Joye S. B., Lin Q. X., Maltby E., Overton E. B. and Rozas L. P. (2012) Oil impacts on coastal wetlands: Implications for the Mississippi river delta ecosystem after the deepwater horizon oil spill. *Bioscience* **62**, 562–574.

Moeslund L., Thamdrup B. and Jørgensen B. B. (1994) Sulfur and iron cycling in a coastal sediment: radiotracer studies and seasonal dynamics. *Biogeochemistry* **27**, 129–152.

Moraghan J. T. and Buresh R. J. (1977) Chemical reduction of nitrite and nitrous-oxide by ferrous iron. *Soil Sci. Soc. Am. J.* **41**, 47–50.

Mullins C. E. (1977) Magnetic susceptibility of soil and its significance in soil science – a review. *J. Soil Sci.* **28**, 223–246.

Pantke C., Obst M., Benzerara K., Morin G., Ona-Nguema G., Dippon U. and Kappler A. (2012) Green rust formation during Fe(II) oxidation by the nitrate-reducing *Acidovorax* sp strain BoFeN1. *Environ. Sci. Technol.* **46**, 1439–1446.

Petrovský E. and Ellwood B. B. (1999) Magnetic monitoring of air-, land- and water-pollution. In *Quarternary Climates, Environments and Magnetism* (eds. B. A. Maher and R. Thompson). Cambridge University Press, Cambridge, pp. 279–322.

Piepenbrock A., Dippon U., Porsch K., Appel E. and Kappler A. (2011) Dependence of microbial magnetite formation on humic substance and ferrihydrite concentrations. *Geochim. Cosmochim. Acta* **75**, 6844–6858.

Porsch K. and Kappler A. (2011) $Fe^{II}$ oxidation by molecular $O_2$ during HCl extraction. *Environ. Chem.* **8**, 190–197.

Porsch K., Dippon U., Rijal M. L., Appel E. and Kappler A. (2010) In-situ magnetic susceptibility measurements as a tool to follow geomicrobiological transformation of Fe minerals. *Environ. Sci. Technol.* **44**, 3846–3852.

Raven K. P., Jain A. and Loeppert R. H. (1998) Arsenite and arsenate adsorption on ferrihydrite: kinetics, equilibrium, and adsorption envelopes. *Environ. Sci. Technol.* **32**, 344–349.

Readman J. W., Fowler S. W., Villeneuve J. P., Cattini C., Oregioni B. and Mee L. D. (1992) Oil and combustion-product contamination of the Gulf marine environment following the war. *Nature* **358**, 662–665.

Rijal M. L., Appel E., Petrovsky E. and Blaha U. (2010) Change of magnetic properties due to fluctuations of hydrocarbon contaminated groundwater in unconsolidated sediments. *Environ. Pollut.* **158**, 1756–1762.

Rijal M. L., Porsch K., Kappler A. and Appel E. (2012) Magnetic signatures of hydrocarbon-contaminated soils and sediments at the former oil-field Hänigsen, Germany. *Stud. Geophys. Geod.* **56**, 889–908.

Roden E. E. and Zachara J. M. (1996) Microbial reduction of crystalline iron(III) oxides: influence of oxide surface area and potential for cell growth. *Environ. Sci. Technol.* **30**, 1618–1628.

Rueter P., Rabus R., Wilkes H., Aeckersberg F., Rainey F. A., Jannasch H. W. and Widdel F. (1994) Anaerobic oxidation of hydrocarbons in crude oil by new types of sulphate-reducing bacteria. *Nature* **372**, 455–458.

Schumacher D. (1996) Hydrocarbon-induced alteration of soils and sediments. In *Hydrocarbon Migration and its Near-Surface Expression* (eds. D. Schumacher and M. A. Abrams). AAPG, pp. 71–89.

Sikkema J., Debont J. A. M. and Poolman B. (1995) Mechanisms of membrane toxicity of hydrocarbons. *Microbiol. Rev.* **59**, 201–222.

Stanjek H., Fassbinder J. W. E., Vali H., Wägele H. and Graf W. (1994) Evidence of biogenic greigite (ferrimagnetic $Fe_3S_4$) in soil. *Eur. J. Soil Sci.* **45**, 97–103.

Stookey L. L. (1970) Ferrozine – a new spectrophotometric reagent for iron. *Anal. Chem.* **42**, 779–781.

Straub K. L., Kappler A. and Schink B. (2005) Enrichment and isolation of ferric-iron- and humic-acid-reducing bacteria. *Methods Enzymol.* **397**, 58–77.

Webb S. M. (2005) SIXPack a graphical user interface for XAS analysis using IFEFFIT. *Phys. Scr.* **T115**, 1011–1014.

Weber K. A., Achenbach L. A. and Coates J. D. (2006) Microorganisms pumping iron: anaerobic microbial iron oxidation and reduction. *Nat. Rev. Microbiol.* **4**, 752–764.

Zachara J. M., Kukkadapu R. K., Gassman P. L., Dohnalkova A., Fredrickson J. K. and Anderson T. (2004) Biogeochemical transformation of Fe minerals in a petroleum-contaminated aquifer. *Geochim. Cosmochim. Acta* **68**, 1791–1805.

*Associate editor:* Jon Chorover

# APPENDIX B: SCHWERTMANNITE AND Fe OXIDES FORMED BY BIOLOGICAL LOW-pH Fe(II) OXIDATION VERSUS ABIOTIC NEUTRALIZATION: IMPACT ON TRACE METAL SEQUESTRATION

Available online at www.sciencedirect.com

SciVerse ScienceDirect

Geochimica et Cosmochimica Acta 76 (2012) 29–44

Geochimica et Cosmochimica Acta

www.elsevier.com/locate/gca

# Schwertmannite and Fe oxides formed by biological low-pH Fe(II) oxidation versus abiotic neutralization: Impact on trace metal sequestration

William D. Burgos [a,*], Thomas Borch [b,c], Lyndsay D. Troyer [c], Fubo Luan [a], Lance N. Larson [a], Juliana F. Brown [a], Janna Lambson [d], Masayuki Shimizu [b]

[a] Department of Civil and Environmental Engineering, The Pennsylvania State University, University Park, PA 16802, United States
[b] Department of Chemistry, Colorado State University, Fort Collins, CO 80523-1872, United States
[c] Department of Soil and Crop Sciences, Colorado State University, Fort Collins, CO 80523-1170, United States
[d] Department of Biology, Washington University in St. Louis, St. Louis, MO 63105, United States

Received 3 May 2011; accepted in revised form 6 October 2011; available online 20 October 2011

**Abstract**

Three low-pH coal mine drainage (CMD) sites in central Pennsylvania were studied to determine similarities in sediment composition, mineralogy, and morphology. Water from one site was used in discontinuous titration/neutralization experiments to produce Fe(III) minerals by abiotic oxidative hydrolysis for comparison with the field precipitates that were produced by biological low-pH Fe(II) oxidation. Even though the hydrology and concentration of dissolved metals of the CMD varied considerably between the three field sites, the mineralogy of the three iron mounds was very similar. Schwertmannite was the predominant mineral precipitated at low-pH (2.5–4.0) along with lesser amounts of goethite. Trace metals such as Zn, Ni and Co were only detected at μmol/g concentrations in the field sediments, and no metals (other than Fe) were removed from the CMD at any of the field sites. Metal cations were not lost from solution in the field because of unfavorable electrostatic attraction to the iron mound minerals. Ferrihydrite was the predominant mineral formed by abiotic neutralization (pH 4.4–8.4, 4 d aging) with lesser amounts of schwertmannite and goethite. In contrast to low-pH precipitation, substantial metal removal occurred in the neutralized CMD. Al was likely removed as hydrobasaluminite and $Al(OH)_3$, and as a co-precipitate into schwertmannite or ferrihydrite. Zn, Ni and Co were likely removed via adsorption onto and co-precipitation into the freshly formed Fe and Al solids. Mn was likely removed by co-precipitation and, at the highest final pH values, as a Mn oxide. Biological low-pH Fe(II) oxidation can be cost-effectively used to pretreat CMD and remove Fe and acidity prior to conventional neutralization techniques. A further benefit is that solids formed under these conditions may be of industrial value because they do not contain trace metal or metalloid contaminants.


## 1. INTRODUCTION

Pennsylvania is currently the fourth largest coal producing state in the United States and has produced more than 25% of the total coal mined in the US during the past 200 years (USGS, 2008). These practices, though, have left their mark on the environment. Coal mine drainage (CMD) is a severe environmental threat to much of the Appalachian region of the US. Commonly referred to as acid mine drainage (AMD), CMD is marked by high concentrations of Fe and acidity. More than 10,000 km of streams in the Appalachian region are contaminated by AMD, with greater than 2000 km of those in Pennsylvania (Herlihy et al.,

* Corresponding author.
*E-mail addresses:* WDB3@engr.psu.edu, wdb3@psu.edu (W.D. Burgos).

0016-7037/$ - see front matter © 2011 Elsevier Ltd. All rights reserved.
doi:10.1016/j.gca.2011.10.015

1990). The cost of reclamation of contaminated watersheds in Pennsylvania alone is estimated between $5 and $15 billion (USGS, 2008).

Fe(III)-containing precipitates, often referred to as "yellowboy", are found at CMD sites coating rocks and streambeds. In certain settings where AMD springs emerge with elevated concentrations of Fe(II), biological low-pH Fe(II) oxidation produces terraced mounds of Fe(III) minerals that can be meters thick (DeSa et al., 2010). Most of these phases are amorphous; however, schwertmannite ($Fe_8O_8(OH)_x(SO_4)_y$; $x = 8 - 2y$, $1 < y < 1.75$), appears to be the predominant phase for low-pH water with high concentrations of sulfate while goethite can also be present in minor amounts (Bigham et al., 1990, 1996; Acero et al., 2006). Schwertmannite is metastable with respect to goethite and is often found on fresh depositional surfaces of AMD sites while goethite is found to increase with depth (Acero et al., 2006; Kumpulainen et al., 2007; Burton et al., 2008; Peretyazhko et al., 2009). The stability of schwertmannite can be enhanced by elevated concentrations of silica, phosphorus, and natural organic matter (Collins et al., 2010).

In order to offset the high costs associated with CMD treatment, it may be possible to collect the large amounts of Fe(III) precipitates at CMD sites for industrial reuse. Hedin et al. (1994) showed that Fe(III) precipitates formed at circumneutral pH and collected at CMD sites were similar to those mined for use as pigments. Since these pigments may be used in products such as cosmetics and ceramic serving ware, the incorporation of trace metals in the Fe(III) mineral is a potential concern. Due to kinetic limitations on abiotic Fe(II) oxidation at low pH, it is widely believed that acidophilic Fe(II)-oxidizing microorganisms are responsible for the majority of Fe(II) oxidation and subsequent precipitation of Fe(III) at AMD sites (Lane et al., 1992; Johnson et al., 2005; Senko et al., 2008). It is likely that the mineralogy and elemental composition of biogenic precipitates formed at low-pH CMD sites differ from those formed as a result of abiotic precipitation after neutralization of CMD.

There has been a great deal of research on the characterization of schwertmannite precipitation at low-pH and ferrihydrite precipitation at circumneutral-pH, as well as the conversion of schwertmannite to goethite (Bigham et al., 1996; Schwertmann and Carlson, 2005; Acero et al., 2006; Burton et al., 2008). However, little research has compared the incorporation of trace metal cations during low-pH biologically mediated precipitation to abiotic precipitation at higher pH. This is an important consideration for the remediation of heavy metal-laden AMD and industrial reuse of Fe(III) precipitates. The objectives of this study were to identify the mineral phases present and the extent of trace metal incorporation into precipitates formed in the field via low-pH Fe(II) oxidation at three AMD sites as compared to precipitates formed in the laboratory via abiotic neutralization at pH 4.38–8.35. The neutralization experiments were designed to mimic geochemical conditions encountered during alkali addition in a conventional AMD active treatment system.

## 2. MATERIALS AND METHODS

### 2.1. Site descriptions

Three CMD sites in western Pennsylvania were included in the current study: Lower Red Eyes in Somerset County, PA; Fridays-2 in Clearfield County, PA; and, Hughes Borehole in Cambria County, PA (Fig. 1). Physical characteristics and water chemistry for each site are provided in Table 1 and site schematics are provided in the Electronic Annex (Figs. EA-1–EA-3). Lower Red Eyes is a low flow (<1 L/s) CMD artesian spring that emerges within the Prince Gallitzin State Forest near Windber, PA (40° 14′ 25″ N; 78° 44′ 49″ W). The CMD is believed to originate from a nearby surface mine operated from the 1970s into the 2000s, and located along the Clarion, Brookville, and Kittanning coal seams. The CMD flows downstream across a spectacular series of iron terraces and pools (Fig. 1a) before eventually seeping back into the ground (150 m downstream of spring). This site is unique to the other two field sites in that the CMD is never hydrologically captured by a larger receiving stream, establishing a more extensive geochemical gradient. The CMD at this site is characterized by higher acidity, dissolved metals, and sulfate as compared to the other two field sites (Table 1).

Fridays-2 is the smaller of two CMD discharges (2.3 L/s) that drain the underground Fridays Mine complex. Fridays Mine is located in Hollywood, PA (41° 14′ 34″ N; 78° 32′ 28″ W) along the Kittanning coal seam and was first mined in the late 1800s (PA DEP, 2006). Fridays-2 emerges as an artesian spring at a collapsed mine entry, and flows 5–15 m over an iron mound before discharging to an unnamed tributary of Bennett Branch. The CMD flows over the mound as shallow (ca. 1 cm) sheet flow, and drops over a ca. 1 m tall terrace before immediately joining the tributary. The tall terrace contains unique stalactite-like Fe precipitates (Fig. 1d). Because of the higher flow rate and shorter path length across the iron mound, leading to a much shorter hydraulic residence time, the extent of Fe(II) oxidation at Fridays-2 is much less as compared to Lower Red Eyes (Table 1 and Fig. 2).

Hughes Borehole is a high flow (63 L/s) artesian spring that was purposefully drilled to drain a very large underground mine complex (2900 ha) near Portage, PA (40° 24′ 31″ N; 78° 39′ 17″ W) (DeSa et al., 2010). The CMD emerges near, and later flows into, the Little Conemaugh River. The CMD emergence is surrounded by a 0.61 ha iron mound that is up to 2 m deep. The CMD flows across the iron mound through relatively deep channels (ca. 0.6 m deep; captures most of the flow from the borehole) and as shallow sheet flow (ca. 1 cm deep) before discharging off the iron mound ca. 60 m downstream of the borehole.

### 2.2. Field sampling

Sampling locations were established as a function of distance downstream of each source along a single flow path that conveyed the majority of the water across each iron mound. Sediments were collected at different downstream distances to obtain solids that had formed under varying


Fig. 1. Field photographs of the AMD sites. Upstream view of pool and terraces at Lower Red Eyes (a). Upstream view of iron mound at Fridays-2 with large ledge in the bottom left corner (b). Downstream view of scoured channels on the iron mound at Hughes Borehole (c). Detail view of the large ledge at Fridays-2 where samples H1 and H4 were collected – note 50 mL tube (d).

geochemical conditions. Sediments were collected from areas of relatively fast and slow water velocities to obtain solids that been deposited under varying hydrological conditions. Sediments were collected from terraces, pools, and microterracettes to obtain solids from unique depositional *facies* (Fouke et al., 2000; Brown et al., 2010). Six to twelve sediment samples were collected from each site to capture any variances caused by these geochemical, hydrological, and geomorphological differences. Sediments were collected from the top 2 cm of the iron mounds, transported on ice, and stored under atmospheric conditions at 4 °C until analysis.

Two core samples (designated as H1 and H4) were collected horizontally into the vertical face of the tall terrace (ca. 6 cm penetration depth) that marked one edge of the iron mound at Fridays-2 (Fig. 1b and d). Photographs of the collected sediment cores are included in the Electronic Annex (Fig. EA-4). Location H1 was collected from the terrace directly below the primary flowpath from the borehole, while H4 was collected from the terrace ca. 1 m to the right/downhill of H1. The soil cores were plugged with rubber stoppers and immediately stored in an airtight, $N_2$-flushed ammunition box, and then kept at 4 °C. The box was opened in an anaerobic chamber (95:5% $N_2$:$H_2$) and the soil cores were divided into three sections, each approximately 2 cm long, and dried in the chamber prior to analysis.

Dissolved oxygen (DO) was measured using an Oakton DO 300 Series field meter; temperature, pH, and oxidation–reduction potential (ORP) were measured with Beckman Φ265 pH/Temp/mV meters; and conductivity was measured using an Oakton CON 400 series field meter. Filtered (0.45 μm) water samples were preserved in the field with HCl (for dissolved Fe(II) analysis) or $HNO_3$ (for dissolved metals analysis by inductively coupled plasma-atomic emission spectroscopy, ICP-AES). Samples for sulfate analysis were neither filtered nor acidified. All water samples were transported on ice and stored at 4 °C until analysis.

### 2.3. Laboratory abiotic neutralization experiments

Water was collected from the emergent Lower Red Eyes spring by completely submerging 10 L high density polyethylene (HDPE) plastic containers ca. 10 cm below the water surface. DO was below detection (<0.5 μM), pH was 4, and ORP was 225 mV at both times of collection (July 2009, October 2010). Containers were filled underwater with no headspace, capped underwater, and then stored on ice during transport. The water was then filtered (0.45 μm) and stored in another plastic container with no headspace at 4 °C. No attempt was made to maintain anoxic conditions after filtration.

The filtered Lower Red Eyes water was used in discontinuous titration/neutralization experiments to produce Fe(III) precipitates via abiotic reactions at a number of elevated pH values. The theoretical total acidity of the Lower Red Eyes water was calculated based on pH and measured concentrations of dissolved Fe(II), Fe(III), Mn, and Al according to Kirby and Cravotta (2005), and found to equal 28.3 meq/L. Four acid-washed HDPE plastic bottles were filled with 250 mL of Lower Red Eyes water. NaOH was titrated into Lower Red Eyes water in aliquots equivalent to ¼ of the theoretical total acidity of the water, until the pH of the system reached pH 8.3. This amounted to first adding 17.8 mL of 0.10 N NaOH to each bottle of Lower Red Eyes water (i.e., to complete 25% of the neutralization). The bottles were stirred to maintain a small vortex

Table 1
Water chemistry of the emergent springs at Lower Red Eyes, Fridays-2, and Hughes Borehole.

| | Lower Red Eyes | Fridays-2 | Hughes Borehole |
|---|---|---|---|
| Flow (L/s) | 0.4 | 2.3 | 20–125 |
| Temp. (°C) | 9.4 ± 0.7 | 9.8 ± 0.1 | 12.7 ± 0.6 |
| | $N = 7$ | $N = 4$ | $N = 30$ |
| DO (μM) | <0.5 | 11.3 ± 13.4 | 34.4 ± 25.0 |
| | $N = 2$ | $N = 4$ | $N = 21$ |
| Conductivity (mS/cm) | 4.36 ± 0.16 | 0.772 ± 0.001 | 1.08 ± 0.1 |
| | $N = 7$ | $N = 2$ | $N = 23$ |
| pH | 4.04 ± 0.25 | 4.1 ± 0.2 | 3.96 ± 0.25 |
| | $N = 7$ | $N = 4$ | $N = 29$ |
| Dissolved total Fe[a] (μM) | 9620 ± 387 | 865 ± 105 | 1590 ± 6 |
| | $N = 5$ | $N = 4$ | $N = 7$ |
| Dissolved Fe(II)[a] (μM) | 9720 ± 326 | 840 ± 108 | 1790 ± 312 |
| | $N = 5$ | $N = 5$ | $N = 25$ |
| Al (μM) | 1590 ± 43 | 741 ± 89 | 304 ± 14 |
| | $N = 3$ | $N = 6$ | $N = 7$ |
| Mn (μM) | 2060 ± 53 | 24 ± 2 | 44 ± 0.4 |
| | $N = 3$ | $N = 6$ | $N = 7$ |
| Co (μM) | 2060 ± 53 | n.a. | 3.22 ± 0.17 |
| | $N = 3$ | | $N = 7$ |
| Ni (μM) | 138 ± 83 | n.a. | 6.82 ± 0.17 |
| | $N = 3$ | | $N = 7$ |
| Zn (μM) | 199 ± 23 | n.a. | 4.13 ± 0.15 |
| | $N = 3$ | | $N = 7$ |
| As (μM) | <0.67 | n.a. | <0.13 |
| | $N = 3$ | | $N = 7$ |
| $SO_4^{2-}$ (μM) | 31,170 ± 3833 | 3410 ± 770 | 5970 ± 660 |
| | $N = 12$ | $N = 4$ | $N = 5$ |
| Acidity(mM $CaCO_3$/L) | 14.2 ± 0.05 | 2.07 ± 0.05 | 2.3 ± 0.05 |
| | $N = 2$ | $N = 4$ | $N = 7$ |
| Si (μM) | 423 ± 5.1 | 792 ± 143 | 630 ± 8.5 |
| | $N = 2$ | $N = 4$ | $N = 7$ |
| TOC (μM) | 91.7 | 167 ± 100 | 72.5 ± 18 |
| | | $N = 3$ | $N = 3$ |
| $PO_4^{3-}$ (μM) | 5.3 ± 0.7 | n.a. | 6.2 ± 3.2 |
| | $N = 3$ | | $N = 3$ |

[a] Dissolved total Fe measured by ICP-AES, dissolved total Fe(II) measured by ferrozine.

and purged continuously with compressed air for 1 h, and then refrigerated overnight. The following day, the bottles were removed from the refrigerator to come to room temperature, the pH was measured in the overlying water in all four bottles, and one bottle was returned to the refrigerator (pH 5.18). For the remaining three bottles, another 17.8 mL of 0.10 N NaOH was added to each bottle and identical procedures were followed over the next three days to produce suspensions equivalent to 50 (pH 5.36), 75 (pH 6.21), and 100% neutralization (pH 8.34). One day after the 100% neutralization suspension was produced; all of the suspensions were transferred to centrifuge tubes and centrifuged at 8000 rpm for 10 min. Supernatant samples were collected and preserved with $HNO_3$ for dissolved metals analysis by ICP-AES, and concentrations were calculated to account for sample dilution with NaOH. Pelletized precipitates were rinsed once with distilled–deionized water, and air-dried for SEM analysis or dried under nitrogen for XRD analysis.

This experiment was repeated with the October 2010 water to generate solids for Fe K-edge EXAFS analysis. During this repeat experiment pH and ORP were monitored continuously over the four days allowed for precipitates to form. ORP was measured after calibrating with a freshly prepared +228 mV Zobel standard solution. Suspensions were mixed and bubbled with air continuously, and maintained at room temperature (22–25 °C) over the four days. For suspensions with NaOH added equivalent to 25%, 50%, 75% and 100% neutralization, final pH values were 4.38, 4.40, 7.03 and 8.35, respectively. An additional sample was prepared where NaOH was added equivalent to 100% neutralization in one single aliquot (71.2 mL 0.1 N NaOH to 250 mL of Lower Red Eyes water). The final pH for this suspension was 8.13. Supernatant and solid samples were prepared as described above.

### 2.4. Analytical methods

Dissolved metal concentrations were analyzed on a Perkin-Elmer Optima 5300 ICP-AES. Dissolved Fe(II) concentrations were measured by ferrozine. Field sediments and laboratory precipitates were sieved (<1-mm) and ground into fine powders. The composition of metal oxides was determined for field sediments via ICP-AES, after lithium

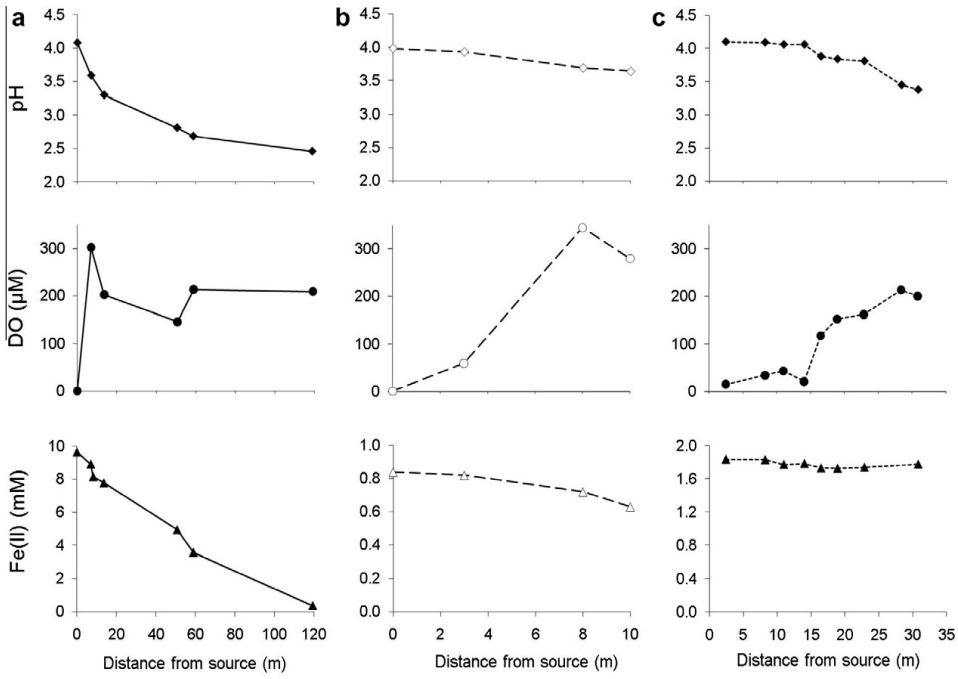


Fig. 2. Water chemistry trends for Lower Red Eyes (July 2009) (a), Fridays-2 (July 2006) (b), and Hughes Borehole (August 2007) (c).

metaborate fusion at 1000 °C. Laboratory precipitates produced from Lower Red Eyes water and field samples collected from the Lower Red Eyes iron mound were dissolved in ammonium oxalate (28 g/L ammonium oxalate + 15 g/L oxalic acid, pH ~2.7) and 6 N HCl, respectively, to operationally distinguish poorly crystalline iron oxides (schwertmannite and ferrihydrite) from less soluble crystalline iron oxides (goethite) (Peretyazhko et al., 2009). Fifty mg dried solids were reacted with 50 mL of each reagent for 1 h, then centrifuged and supernatant samples were preserved with $HNO_3$ prior to analysis by ICP-AES.

Sediment samples were prepared for scanning electron microscopy (SEM) following procedures described by Zhang et al. (2007). Samples were preserved in the field with 2.5% glutaraldehyde and prepared for imaging with a series of ethanol dehydrations followed by critical point drying. Dried samples were mounted onto carbon SEM stubs and imaged on an FEI Quanta 200 environmental SEM under low vacuum. Higher magnification images were collected using a Jeol JSM-6700F field emission SEM with a working distance of 3 mm.

Powder X-ray diffraction patterns were collected using a Rigaku D/Max Rapid II X-ray diffractometer (XRD) with a Mo X-ray tube and a 0.3 mm collimator. Intensities were measured with the omega axis fixed at 0° and phi axis oscillation between −20° and +20° with a 10 min exposure time. Data was integrated from 0° to 360° with a step size of 0.02 using AreaMax software and all data analysis was performed using Jade 7 software.

Dry samples for X-ray absorption spectroscopic analyses were diluted with boron nitride and packed in Teflon sample holders and sealed with a Kapton polyimide film to prevent oxidation while minimizing X-ray absorption. The structural environment of Fe was determined using extended X-ray absorption fine structure (EXAFS) spectroscopy at the Stanford Synchrotron Radiation Lightsource (SSRL). Data were collected for the Fridays-2 samples on beamline 10-2 (26-pole wiggler). The storage ring was operated at 3.0 GeV and at currents between 60 and 100 mA. Data for the abiotic precipitation samples were collected on beamline 4-3 (20-pole wiggler). The storage ring was operated at 3.0 GeV at a current of 300 mA. The Fe EXAFS analytical procedures used here were similar to those described previously (Borch et al., 2006; Jacquat et al., 2009; Moberly et al., 2009). Energy selection was accomplished with a Si (1 1 1) monochromator and spectra were recorded in X-ray transmission mode using ion chambers. A set of Fe reference compounds was used to perform linear combination (LC) $k^3$-weighted EXAFS spectral fitting using the SIXPACK interface to IFEFFIT (Webb, 2005). Principal component analysis was performed on sample spectra to estimate the number of reference compounds required for LC fitting. Fe EXAFS reference spectra for ferrihydrite, schwertmannite and goethite are included in the Electronic Annex (Fig. EA-5). The appropriate Fe reference

spectra were identified using target transformation (TT) testing. Based on the SPOIL value from TT testing, preliminary LC fitting, appearance in XRD patterns, and their likelihood of formation based on reaction path modeling; schwertmannite, goethite and ferrihydrite were specifically selected as reference compounds. The SPOIL values for schwertmannite and ferrihydrite were greatly different from each other, which implies that these reference spectra are different from each other (Fig. EA-5). Reference compounds were included in the fit only if they contributed more than 5% mol/mol, equivalent to our detection limit for minor constituents (Hansel et al., 2003). Linear combinations of the reference compounds were optimized and the only variable parameters were the mole fractions of each reference compound.

## 3. RESULTS

### 3.1. AMD chemistry

The three field sites we studied all contained iron mounds that formed via biological low-pH Fe(II) oxidation (Fig. 1), while the water chemistry (Table 1), geochemical gradients (Fig. 2), and hydrodynamics across the iron mounds varied considerably. The importance of biological Fe(II) oxidation was confirmed through a series of laboratory experiments using live and sterilized sediments from Lower Red Eyes (Brown et al., 2010), Fridays-2 (Lucas, 2008) and Hughes Borehole (DeSa et al., 2010). Lower Red Eyes had the highest concentrations of metals, acidity, and sulfate, the lowest flow rate, and the longest residence time across its iron mound (Table 1). The influx and saturation of DO, and decreases in pH, dissolved Fe(II) and dissolved Fe are consistent with biologically-mediated low-pH Fe(II) oxidation and Fe(III) hydrolysis and precipitation (Fig. 2a). Fridays-2 had the lowest concentration of Fe(II), acidity, and sulfate, an intermediate flow rate, and likely the shortest residence time across its iron terrace. Hughes Borehole had intermediate concentrations of Fe(II), acidity, and sulfate, an extremely high flow rate, and variable residence times across its iron mound because of a combination of flow along scoured channels or across shallow microterracettes. Even though dissolved Fe(II) and dissolved total Fe concentrations did not drop dramatically across the Hughes Borehole iron mound (Fig. 2c), Fe precipitation over the past several decades has produced mound sediments 1–2 m deep.

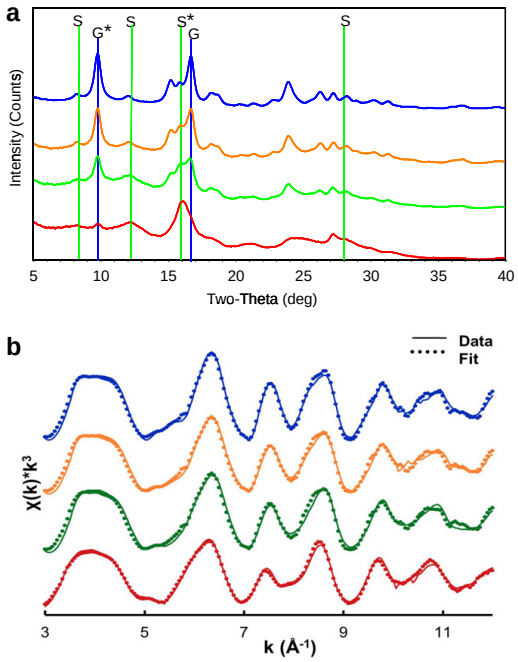


Fig. 3. X-ray diffraction patterns (a) and Fe K-edge EXAFS spectra (b) from field samples collected from Fridays-2. Samples were collected 10 m downstream of emergent AMD spring from the vertical face of a large ledge. Core samples (6 cm penetration depth) were collected horizontally into the ledge face at two locations, H1 and H4. H1 was directly below the primary flowpath while H4 was 1 m to the right/downhill of H1. Patterns are arranged top to bottom, respectively, for samples with highest to lowest goethite contents and are in identical order in (a) and (b). Top pattern from H1 0–2 cm depth, 2nd pattern from H1 4–6 cm depth, 3rd pattern from H4 0–2 cm depth, and bottom pattern from H4 4–6 cm depth. In (a) G = goethite, S = schwertmannite, and ∗ designates peak with greatest intensity in reference pattern. Details for fits of the Fe K-edge EXAFS spectra in (b) are provided in Table 2.

### 3.2. Mineralogy of natural sediments produced via biological low-pH Fe(II) oxidation

Iron precipitates varied across these sites with respect to their physical features and morphology. For example, at Lower Red Eyes, the iron mound was classified into unique depositional *facies* such as terraces, pools, and microterracettes (Fouke et al., 2000; Brown et al., 2010). Terraces consisted of vertical drops greater than 5 cm, pools with diameters of 1–2 m contained quiescent water, and microterracettes consisted of vertical drops less than 2 cm. At Fridays-2, the predominant depositional *facie* was microterracettes, but there was one tall terrace (1 m) that the CMD ran over before entering the adjacent unnamed tributary. At Hughes Borehole, the predominant depositional *facie* was microterracettes, however, the majority of the CMD was conveyed along deep (0.5 m), narrow (1 m wide) scoured channels. We found that schwertmannite was the predominant mineral across these iron mounds while goethite was found in smaller amounts (Figs. 3 and 4).

Based on comparisons of XRD patterns and LC fitting of Fe K-edge EXAFS spectra (Fig. 3 and Table 2), we qualitatively ranked the goethite content of all of the sediments based on the XRD peak intensity at 9.73° two theta. From this we then arranged all of the XRD patterns from each site (6–12) in order of highest to lowest goethite content. In Figs. 3a and 4 we selected four patterns from each site that captured the whole range of schwertmannite-to-goethite ratios observed for each site. We found that there were no observable systematic trends in iron mineralogy with respect to location on the iron mound (i.e., along a geochemical gradient), or with respect to the sample location's water velocity (i.e., across a hydrodynamic gradient), or with respect to the depositional *facies* where the sediments were formed. No mineralogical phases other than schwertmannite and goethite were detected at any field site. SEM analysis of all field samples also revealed a predominance of spherical particles (1–2 μm diameter) with a "hedgehog" morphology characteristic of schwertmannite (Fig. 5a–d). The average Fe/S molar ratio in the Lower Red Eyes sediments was $5.42 \pm 0.83$ ($n = 4$) (based on HCl digestions, Table 3), corresponding to a schwertmannite stoichiometry of $Fe_8O_8(OH)_5(SO_4)_{1.5}$ (with reported values of $1 < SO_4 < 1.75$).

Based on LC fitting of Fe K-edge EXAFS spectra, goethite decreased with horizontal distance into the tall terrace at Fridays-2 (Fig. 3b and Table 2). The surface section of sample H1 (0–2 cm horizontal penetration into the vertical

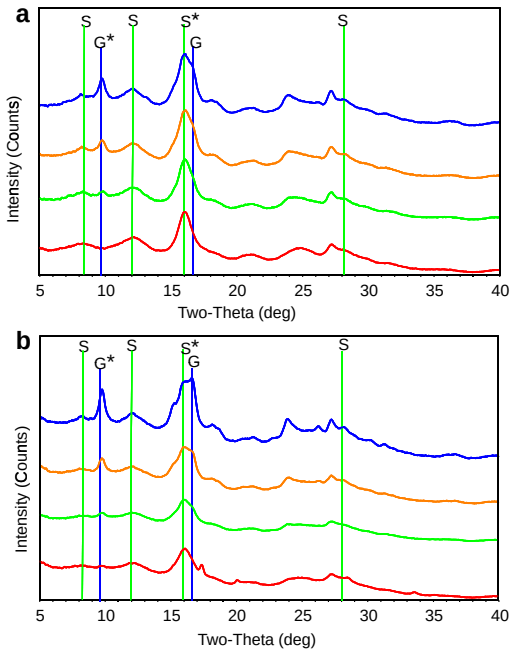


Fig. 4. X-ray diffraction patterns from samples collected from Lower Red Eyes (a) and Hughes Borehole (b). In both panels, patterns are arranged top to bottom, respectively, for samples with highest to lowest goethite contents. (a) Top pattern from pool *facies* 59 m downstream of Lower Red Eyes spring, 2nd pattern from terrace 62 m downstream, 3rd pattern from terrace 52 m downstream, and bottom pattern from pool 14 m downstream. (b) Top pattern from the main scoured channel 8 m downstream of Hughes Borehole, 2nd pattern from terrace *facies* 60 m downstream, 3rd pattern from microterracette 31 m downstream, and bottom pattern from pool 55 m downstream. G = goethite, S = schwertmannite, and ∗ designates peak with greatest intensity in reference pattern.

Table 2
Mineralogical composition of samples based on linear combination fitting of Fe K-edge EXAFS spectra. Field samples were collected from Fridays-2 (H1, H4) and solids were formed in the laboratory via abiotic neutralization/precipitation from Lower Red Eyes water. Precision of fits is ca. 5 mol%.

| Sample | Schwertmannite mol% Fe | Goethite mol% Fe | Ferrihydrite mol% Fe | Red. $\chi^2$ |
|---|---|---|---|---|
| H1 0–2 cm depth | 44.6 | 55.4 | – | 0.08 |
| H1 4–6 cm depth | 55.7 | 44.3 | – | 0.08 |
| H4 0–2 cm depth | 58.9 | 41.1 | – | 0.11 |
| H4 4–6 cm depth | 68.3 | 31.7 | – | 0.17 |
| Abiotic precipitate pH 4.38 | 38.1 | 16.8 | 45.1 | 0.19 |
| Abiotic precipitate pH 4.40 | 33.2 | 17.1 | 49.7 | 0.11 |
| Abiotic precipitate pH 7.03 | 30.2 | 10.0 | 59.8 | 0.10 |
| Abiotic precipitate pH 8.13 | 20.5 | 10.1 | 69.4 | 0.16 |
| Abiotic precipitate pH 8.35 | 21.9 | 7.0 | 71.1 | 0.11 |

terrace face) consisted of 45% schwertmannite, 55% goethite, while the deeper section (4–6 cm horizontal penetration) consisted of 56% schwertmannite and 44% goethite (all estimates ±5%). A similar difference along the horizontal penetration depth into the terrace was found in sample H4. The first 0–2 cm into the ledge was composed of 59% schwertmannite and 41% goethite, while the sample 4–6 cm into the ledge was composed of 68% schwertmannite and 32% goethite. Because schwertmannite is metastable with respect to goethite, sample locations with high schwertmannite-to-goethite ratios should reflect conditions that stabilize schwertmannite. The Lower Red Eyes AMD contained the highest sulfate concentration which should favor the stabilization of schwertmannite, while the Fridays-2 AMD contained the lowest sulfate concentration which could favor the conversion of schwertmannite to goethite. In addition to sulfate, silica, phosphorus and dissolved organic carbon (DOC) have been shown to stabilize schwertmannite with respect to Fe(II)-catalyzed conversion to goethite (Jones et al., 2009). At these three sites, dissolved Si concentrations ranged from 420 to 790 μM, dissolved phosphate concentrations were around 5–6 μM (but less downstream of the springs), and DOC concentrations ranged from 70 to 170 μM (Table 1). Jones et al. (2009) showed that 1 mM dissolved Si completely stabilized schwertmannite while 25 mg/L Suwannee River fulvic acid (equivalent to ca. 1 mM DOC) partially stabilized schwertmannite. We speculate that Si concentrations below 1 mM, rather than P or DOC, stabilized schwertmannite at our field sites.

### 3.3. Mineralogy from abiotic precipitation experiments

Discontinuous titration/neutralization experiments were conducted with Lower Red Eyes water to produce solids that formed at elevated pH values (pH 4.4–8.4) as compared to field conditions (emergent pH 4.0 declined to pH 2.5; Fig. 1a). Our motivation for conducting these experiments was to examine trace metal partitioning under relatively high pH conditions encountered in AMD active treatment systems as compared to natural low-pH iron mound sediments. We conducted these experiments on two different occasions with water collected in July 2009 and October 2010, however, the water chemistry of the emergent Lower Red Eyes spring was essentially identical. In our first experiment, the discontinuous titration process yielded precipitates that formed at final pH values of 5.18, 5.36, 6.21, and 8.34. After the first aliquot of NaOH was added (day 0), an orange precipitate formed and its color remained unchanged for the whole 4 d reaction period (final pH 5.18). After the second aliquot of NaOH was added (day 1), a dark green precipitate formed initially but then became orange after 1 h (final pH 5.36). After the third aliquot of NaOH was added (day 2) a green precipitate formed initially but then became orange-brown (final pH 6.21). After the fourth and final aliquot of NaOH was added (day 3), an orange precipitate formed and its color remained unchanged for the remainder of the reaction period (final pH 8.34).

During our second experiment we continuously monitored the pH and ORP of the suspensions during the whole 4 d reaction period (Fig. 6). In this repeat experiment, the discontinuous titration process yielded precipitates that formed at final pH values of 4.38, 4.40, 7.03, and 8.35. In contrast to the first experiment where we mixed and aerated the suspensions for 1 h after NaOH addition and then stored the suspension at 4 °C until the next day, in this repeat experiment we continuously mixed and aerated the suspensions so that we could continuously monitor pH and ORP. Continuous aeration promoted greater Fe(II) oxidation in the first two suspensions (i.e., one and two additions of NaOH), and the subsequent precipitation of more Fe(III) decreased the final pH values to 4.38 and 4.40 (as compared to final pH values of 5.18 and 5.36 in the first experiment). Continuous monitoring of pH and ORP in these suspensions clearly showed that the geochemical conditions varied much more than just the differences between the initial and final conditions. For example, while we designated the first suspension as "abiotic precipitate pH 4.38", over its 4 d reaction period the suspension pH varied from pH 3.72 to 5.89 and the ORP varied from –9 to +300 mV (Fig. 6a). In the first 10 min (inset in Fig. 6a), the pH increased quickly because of the instantaneous dosing of NaOH while the ORP decreased because the initial oxidation rate of Fe(II) exceeded the mass transfer rate of $O_2$. The subsequent decrease in pH was caused by hydrolysis of the Fe(III) that had been produced while the subsequent increase in ORP demonstrated that the mass transfer rate of $O_2$ began to exceed the oxidation rate of Fe(II). Similarly, for the suspension that was discontinuously dosed with four aliquots of NaOH and designated

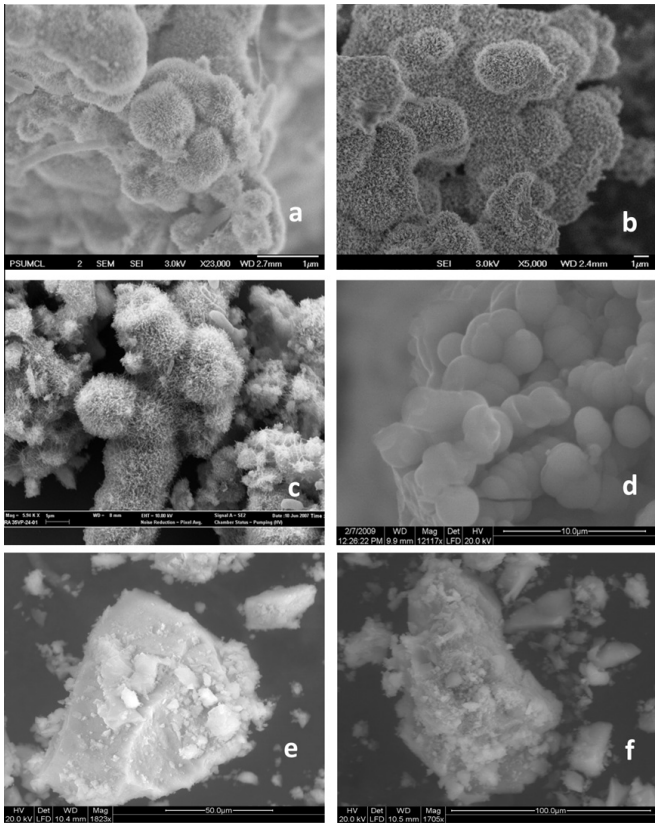


Fig. 5. SEM images of representative samples from: Lower Red Eyes at the AMD source (a); Lower Red Eyes at a downstream pool (b); Fridays-2 (c); Hughes Borehole (d); and solids formed in the lab from Lower Red Eyes water via abiotic neutralization/precipitation at final pH 4.38 (e) and final pH 8.13 (f).

as "abiotic precipitate pH 8.35", over its 4 d reaction period the suspension pH varied from pH 3.72 to 9.38 while its ORP varied from –100 to +300 mV (Fig. 6b). These large changes in pH and pe (i.e., ORP) span mineral stability fields of schwertmannite, goethite and ferrihydrite. In other words, all of these minerals could have potentially formed as the water chemistry evolved over the different reaction periods (e.g., as reaction path "trajectories" plotted on a pe-pH diagrams; Figs. EA-6 and EA-7 in the Electronic Annex; generated using Geochemists Workbench and the water chemistry of Lower Red Eyes in Table 1).

Based on XRD patterns (Fig. 7a) and LC fitting of the Fe K-edge EXAFS spectra (Fig. 7b and Table 2), a combination of schwertmannite, goethite, and ferrihydrite were identified in all of the precipitates formed via abiotic neutralization. We found that abiotic precipitates formed at pH 4.38 contained 38% schwertmannite, 17% goethite, and 45% ferrihydrite, similar to LC fitting results for the solids formed at pH 4.40. As the final pH of the abiotic precipitates increased, the mole fractions of schwertmannite and goethite decreased while the fraction of ferrihydrite increased. Abiotic precipitates formed at pH 8.35 contained 22% schwertmannite, 7% goethite, and 71% ferrihydrite. SEM analysis of the neutralized precipitates revealed distinctly different particle morphologies (Fig. 5e and f) as compared to field samples (Fig. 5a–d). Instead of spheres with a hedgehog texture, neutralized precipitates appeared as laths fused into much larger particles. Characteristic dimensions of these laths were difficult to generalize from these SEM micrographs. This altered morphology was similar to observations reported by Acero et al. (2006) coincident with schwertmannite transformation into goethite in aging experiments (353 d) where the pH decreased from pH 3.07 to 1.74.

Higher amounts of schwertmannite at pH 4.38 and 4.40 were consistent with higher solid-phase S/Fe ratios measured in these precipitates as compared to precipitates formed at pH > 7 (Table 3). It is important to note that

Table 3
Metal content of solids formed via abiotic neutralization/precipitation in the laboratory, and for sediments collected from Lower Red Eyes and Hughes Borehole. Solids were dissolved in 6 N HCl and ammonium oxalate.

| Sample ID | $Fe_{HCl}$ (mmol/g) | $Fe_{ox}$ (mmol/g) | $S_{HCl}$ (mmol/g) | $S_{ox}$ (mmol/g) | $Al_{HCl}$ (μmol/g) | $Al_{ox}$ (μmol/g) | $Mn_{HCl}$ (μmol/g) | $Mn_{ox}$ (μmol/g) | $Co_{HCl}$ (μmol/g) | $Co_{ox}$ (μmol/g) | $Ni_{HCl}$ (μmol/g) | $Ni_{ox}$ (μmol/g) | $Si_{HCl}$ (μmol/g) | $Si_{ox}$ (μmol/g) | $Zn_{HCl}$ (μmol/g) | $Zn_{ox}$ (μmol/g) |
|---|---|---|---|---|---|---|---|---|---|---|---|---|---|---|---|---|
| Abiotic precipitate pH 4.38 | 6.06 | 4.19 | 1.73 | 1.23 | 3380 | 2380 | 3 | 1.6 | 5 | 3.7 | 14 | 11 | 159 | 81 | 30 | 22 |
| Abiotic precipitate pH 4.40 | 6.15 | 5.12 | 1.01 | 0.96 | 1380 | 1200 | 2 | 1.9 | 3 | 3.0 | 13 | 11 | 114 | 75 | 34 | 30 |
| Abiotic precipitate pH 7.03 | 6.80 | 6.36 | 0.57 | 0.53 | 1180 | 1080 | 141 | 140 | 37 | 36 | 61 | 59 | 288 | 260 | 150 | 144 |
| Abiotic precipitate pH 8.13 | 5.55 | 5.58 | 0.37 | 0.35 | 950 | 930 | 1160 | 1150 | 42 | 42 | 55 | 56 | 255 | 235 | 124 | 125 |
| Abiotic precipitate pH 8.35 | 5.76 | 5.22 | 0.33 | 0.35 | 1010 | 990 | 1260 | 1250 | 44 | 44 | 59 | 59 | 269 | 233 | 132 | 127 |
| Lower Red Eyes upper pool[a] | 7.89 | 0.42 | 1.72 | 0.03 | 29 | 2.6 | 2.3 | 0.4 | 1.9 | 0.00 | 0.78 | 0.10 | 41.8 | 2.0 | 0.95 | 3.8 |
| Lower Red Eyes upper terrace[a] | 8.55 | 1.27 | 1.78 | 0.41 | 22 | 2.7 | 2.3 | 1.1 | 2.3 | 0.03 | 1.2 | 0.12 | 46.7 | 5.0 | 2.1 | 0.8 |
| Lower Red Eyes lower pool[a] | 7.43 | 0.73 | 1.22 | 0.26 | 14 | 3.9 | 1.9 | 1.1 | 0.21 | 0.02 | 0.16 | 0.12 | 26.7 | 4.2 | 1.2 | 0.8 |
| Lower Red Eyes lower terrace[a] | 8.56 | 1.15 | 1.39 | 0.42 | 10 | 1.5 | 1.8 | 1.1 | 2.4 | 0.04 | 2.2 | 0.12 | 50.8 | 4.1 | 3.5 | 1.4 |

[a] Lower Red Eyes sediment sampling locations refer to depositional *facies* where samples were collected. Upper terrace and pool sediments were collected 27 m downstream from the emergent AMD spring, lower terrace and pool sediments were collected 60 m downstream, emergent pool was collected 0 m downstream, and top terrace was collected 11 m downstream.

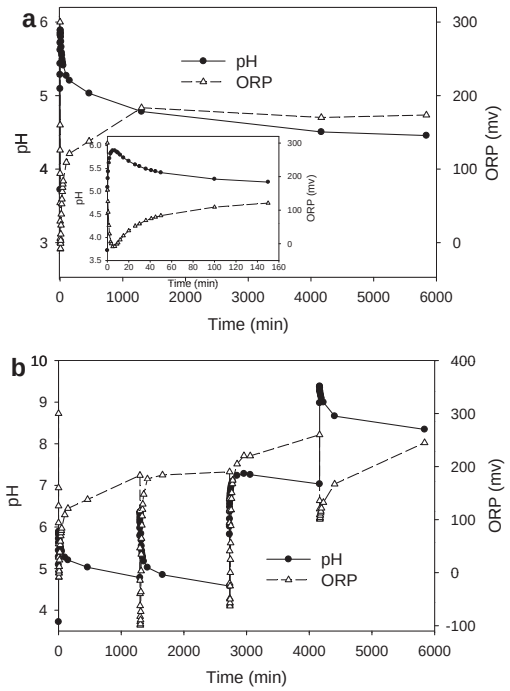


Fig. 6. Kinetics of pH and oxidation–reduction potential (ORP) changes in Lower Red Eyes water during abiotic neutralization/precipitation experiments. Results shown after addition of one aliquot of NaOH that yielded a final suspension of pH 4.38 (a). Inset in (a) details initial kinetics. Results shown for complete discontinuous neutralization where four aliquots of NaOH were added over four days and yielded a final suspension of pH 8.35 (b). Note that ORP values are relative to a +228 mV Zobel solution.

we did rinse these solids with distilled–deionized water before drying and digesting. Sulfate and other weakly adsorbed elements were likely removed to some unquantified extent by this water rinsing. Based on solid-phase Fe and S concentrations measured in ammonium oxalate and HCl digestions, the crystalline mineral fraction was highest for the precipitates formed at pH 4.38 and 4.40 (Table 3), consistent with higher estimated fractions of goethite for these samples (based on Fe EXAFS LC fitting; Table 2). For precipitates formed above pH 7, concentrations of Fe and S measured in the oxalate and HCl digestions were near equal, consistent with higher proportions of poorly crystalline minerals (i.e., schwertmannite and ferrihydrite). In contrast, S and Fe concentrations measured in the field sediments were much higher in the HCl digestions as compared to the oxalate digestions (Table 3). XRD peaks from field sediments (Figs. 3a and 4) could have been broadened by nanocrystalline phases (i.e., short-range ordered phases resistant to oxalate dissolution) of schwertmannite and goethite thereby confounding our operational distinction of crystalline versus poorly crystalline phases for certain samples.

The mineralogy of the abiotic precipitates formed from Lower Red Eyes water clearly differed from the natural sediments collected from Lower Red Eyes (compare Fig. 4a with 7a), and clearly differed from the natural sediments collected from Fridays-2 (Table 2). The large fraction of ferrihydrite found in the abiotic precipitates formed at high pH is consistent with other studies (Bigham et al., 1996; Murad and Rojik, 2003). The formation of ferrihydrite over a more crystalline phase such as goethite or lepidocrocite could be promoted by dissolved species in the Lower Red Eyes water. For example, the presence of Si or Al favors the formation of ferrihydrite over lepidocrocite during oxidative hydrolysis of Fe(II) (Schwertmann and Thalmann, 1976; Taylor and Schwertmann, 1978). Both of these elements were present at high concentrations in the Lower Red Eyes water (Table 1), where Al was 1590 μM (Al/Fe(II) = 0.16) and Si was 423 μM (Si/Fe(II) = 0.04).

The incorporation of Al and Fe into the abiotic precipitates was confirmed by measuring the loss from solution of these elements from the supernatant of the neutralized suspensions (R-hand portions of Fig. 8). In the abiotic experiments, at final pH values of 4.38 and 4.40, Al ($C_i = 1.6$ mM) was removed to a greater relative extent ($C_{\text{final pH}}/C_i = 0.083$–$0.22$; i.e., 91.7–88% removal) as compared to Fe ($C_i = 8.9$ mM; $C_{\text{final pH}}/C_i = 0.29$–$0.67$). At fi-

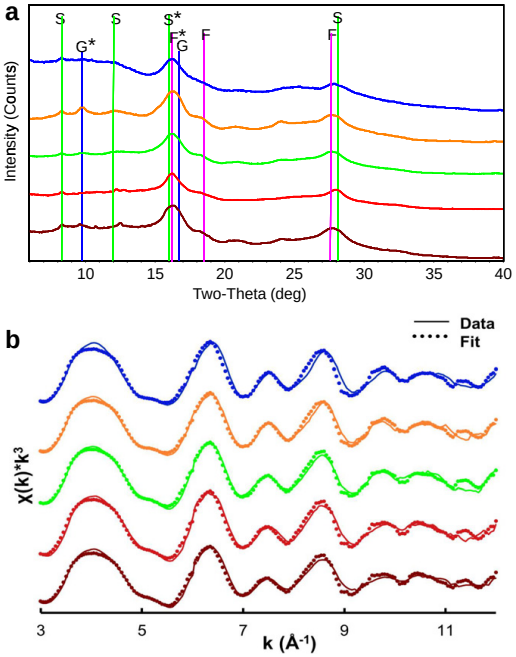


Fig. 7. X-ray diffraction patterns (a) and Fe K-edge EXAFS spectra (b) from solids formed in the lab from Lower Red Eyes water via abiotic neutralization/precipitation. Patterns are arranged top to bottom, respectively, for samples with lowest to highest final pH values and are in identical order in (a) and (b). Top pattern from pH 4.38 suspension, 2nd pattern from pH 4.40 suspension, 3rd pattern from pH 7.03 suspension, 4th pattern from pH 8.13 suspension, and bottom pattern from pH 8.35 suspension. In (a) F = ferrihydrite, G = goethite, S = schwertmannite, and ∗ designates peak with greatest intensity in reference pattern. Details for fits of the Fe K-edge EXAFS spectra in (b) are provided in Table 2.

nal pH values >7, dissolved Fe and Al concentrations were always <50 μg/L.

We include dissolved metal concentrations as a function of pH on the iron mound in the L-hand portions of Fig. 8 to compare metal loss from solution in the field with the abiotic precipitates formed in the laboratory. In this unconventional plot, the dashed vertical line represents the emergent CMD spring, while points to the left represent sample sites further downstream of the CMD spring (where pH values continue to decline due to greater biological Fe(II) oxidation and Fe(III) hydrolysis) and points to the right represent laboratory samples with more NaOH addition. No metals other than Fe were removed across the Lower Red Eyes iron mound (L-hand portions of Fig. 8). Metal cations were not lost from surface waters in the field because of unfavorable electrostatic attraction to the iron mound minerals (i.e., schwertmannite). The pH of the surface waters decreased from ca. pH 4.0 to 2.5 across the iron mounds. The pH of zero point of charge ($pH_{zpc}$) of schwertmannite has been reported to be 7.2 (Johnson et al., 2005), thus metal cations would not be strongly attracted to the surface of schwertmannite at the low pH values found in the field. This result is consistent with other related field studies (Sidenko and Sherriff, 2005; Nagano et al., 2011).

Zinc, nickel and cobalt were the trace metals detected at the highest concentrations in the emergent AMD spring at Lower Red Eyes (Table 1). The removal of these metals from solution via NaOH addition was similar to the behavior of Fe and Al. At final pH values of 4.38–4.40, Ni was removed to a greater extent ($C_i = 233$ μM; $C_{final\ pH}/C_i = 0.33$–$0.37$) as compared to Zn ($C_i = 199$ μM; $C_{final\ pH}/C_i = 0.84$–$0.98$), and as compared to Co ($C_i = 70$ μM; $C_{final\ pH}/C_i = 0.95$–$1.0$). At final pH values >5, $C_{final\ pH}/C_i$ ratios were $0.042 \pm 0.030$ for Ni ($n = 7$), $0.015 \pm 0.013$ for Zn, and $0.10 \pm 0.10$ ($n = 7$) for Co. Greater removal of these metals at pH values >5 was confirmed based on corresponding increased solid-phase concentrations (Table 3). Based on oxalate and HCl digestions, the majority of these trace metals were associated with poorly crystalline minerals, especially for solids formed above pH 7.

## 4. DISCUSSION

The remediation of CMD focuses primarily on the removal of metals and acidity. Active CMD treatment refers to the continuous addition of chemicals and collection of metal precipitates. The most common active treatment processes are aeration and alkali addition to neutralize acidity

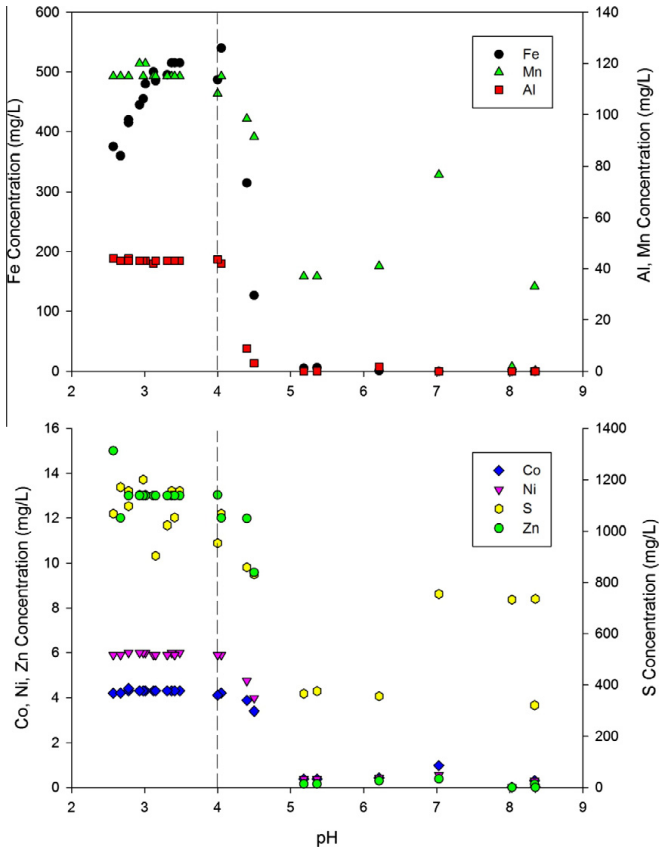


Fig. 8. Concentrations of dissolved elements in Lower Red Eyes water plotted as a function of pH. The dashed line indicates conditions at the emergent AMD spring. Left of the dashed line corresponds to field conditions downstream of the spring. Right of the dashed line corresponds to abiotic neutralization/precipitation in the laboratory. Note secondary axes for certain elements.

and promote rapid oxidation of $Fe^{2+}$ and precipitation of $Fe^{3+}$, $Al^{3+}$ and other metal contaminants. Depending on alkali dosing conditions, effective removal of Mn via oxidative hydrolysis of $Mn^{2+}$ may or may not occur. Sodium hydroxide and calcium oxide are the most commonly used neutralizing agents for CMD active treatment. Alkali dosing is targeted to slightly exceed the total load (flow $*$ concentration) of hot peroxide acidity of the influent CMD and results in abrupt geochemical changes. For example, it is not uncommon to see blue-green Fe(II)-rich and/or $Fe(OH)_2$(s)-containing water immediately downstream of the alkali dosing location. Even with settling ponds open to the atmosphere, the oxygen demand caused by high Fe(II) concentrations can allow reducing conditions to persist for some time. As aeration continues, the blue-green water eventually converts to an orange-red color indicative of Fe(III)-rich and/or $Fe(OH)_3$(s)-containing water. We describe these field observations because our laboratory neutralization experiments essentially mimicked geochemical conditions encountered during CMD active treatment.

A number of studies have examined the stability of Fe precipitates formed in AMD and the corresponding controls on trace metals and metalloids. A portion of these studies began their experiments with minerals pre-formed in the field and/or via laboratory synthesis and monitored phase transformations and metal release/uptake as a function of time or as a function of solution chemistry (Bigham et al., 1996; Jönsson et al., 2005; Kumpulainen et al., 2008; Paikaray and Peiffer, 2010). At pH 2.5–4.0 goethite is often the sole transformation product of schwertmannite, while at pH >4.5–6.0 ferrihydrite and goethite are both produced (Bigham et al., 1996; Sánchez-España et al., 2011). Schwertmannite transformation to goethite is slow, often requiring hundreds of days, but conflicting results have been reported regarding the effect of pH. Two studies have reported that transformation to goethite was faster at high pH as com-

pared to low pH (Regenspurg et al., 2004; Jönsson et al., 2005; Schwertmann and Carlson, 2005), while one study reported that transformation was faster at low pH (Kumpulainen et al., 2008). These conflicting reports are likely caused by differing concentrations of constituents that can stabilize schwertmannite (e.g., Si, P, TOC – Jones et al., 2009; $SO_4$ – Knorr and Blodau, 2007) and/or Fe speciation that can control the importance of Fe(II)-induced conversion of schwertmannite (Burton et al., 2008).

Another group of studies more similar to our laboratory experiments involved using metal-rich solutions that abruptly became supersaturated due to aeration (Johnston et al., 2011) or neutralization (Lee et al., 2002; Sánchez-España et al., 2011) and then were monitored for phase transformations and release/uptake of metals and metalloids. Under these conditions trace metals can be removed from solution via (i) adsorption onto freshly formed mineral surface(s), (ii) co-precipitation into the mineral structure(s), and/or (iii) precipitation as "discrete" trace metal solid phases (e.g., $Me(OH)_x(s)$). The partitioning of adsorbed or co-precipitated trace metals can be subsequently affected by any phase transformation of the initial precipitate (e.g., schwertmannite) into secondary products (e.g., goethite). These studies have also focused on arsenic because it is a key contaminant of concern in the Iberian Pyrite Belt (Sánchez-España et al., 2011) and in Australian coastal lowland acid sulfate soils (Johnston et al., 2011). Arsenic, however, is not an important contaminant in Appalachian CMD. For example, in one survey of 156 CMD sources in Pennsylvania, the median As concentration was 0 μg/L (no detection limit reported; Watzlaf et al., 2002). In another survey of 99 CMD sources in the bituminous coal mining region of Pennsylvania (same as current study), the median As concentration was 2.0 μg/L (Cravotta, 2008).

Instead of arsenic, Fe, Al, Mn and acidity are the primary contaminants of concern in CMD. Active treatment using aeration and NaOH addition was clearly effective in removing Fe and Al (and Mn at highest pH values) from Lower Red Eyes water (Fig. 8). Based on reaction path modeling for Fe, schwertmannite would precipitate at pH >4.5 and ferrihydrite would precipitate at pH >6.2 if goethite precipitation was suppressed within the model (Electronic Annex, Fig. EA-6). If goethite precipitation was not suppressed, then it became thermodynamically stable throughout the entire pe-pH range over schwertmannite and ferrihydrite, indicating that all three Fe(III) minerals could form under these geochemical conditions. The simultaneous occurrence of schwertmannite, ferrihydrite, goethite and lepidocrocite (near pH 5.5) was observed in similar AMD titrations (Jönsson et al., 2006). Based on Fe EXAFS (Table 2), schwertmannite, goethite and ferrihydrite were all present in the abiotic precipitates, including those collected at final pH values >4.5. We speculate that both schwertmannite and ferrihydrite were the initial Fe phases to nucleate in these suspensions (Bigham et al., 1996; Schwertmann and Carlson, 2005) while goethite formed as a secondary product from schwertmannite (Regenspurg et al., 2004; Burton et al., 2008).

Based on reaction path modeling for Al, hydrobasaluminite ($Al_4(SO_4)(OH)_{10} \cdot 15H_2O$) would precipitate near pH 4.0 and was predicted to be the predominant solid Al phase throughout the entire pe-pH range of our experiments if $Al(OH)_3$ precipitation was suppressed in the model (Electronic Annex, Fig. EA-7). Inclusion of basaluminite instead of hydrobasaluminite yielded similar model predictions but we chose hydrobasaluminite because no dehydration to basaluminite would be expected to occur in these fresh, fully hydrated suspensions. If $Al(OH)_3$ precipitation was not suppressed, then it became predominant throughout the entire pe-pH range over hydrobasaluminite indicating that both hydrobasaluminite and $Al(OH)_3$ could form in our experiments. In Australian coastal lowland acid sulfate soils, a combination of basaluminite and amorphous $Al(OH)_3$ were found to control dissolved $Al^{3+}$ concentrations between pH 3–7 (Jones et al., 2011). In Pennsylvanian coal mine drainage, a combination of amorphous $Al(OH)_3$ and a poorly crystalline aluminum hydroxysulfate were found to control dissolved $Al^{3+}$ concentrations above pH 5 (Pu et al., 2010). In our experiments, Al was detected in the abiotic precipitates by SEM-EDS but we were unable to resolve whether the Al signal originated from morphologically unique particles (i.e., as Al solids vs. co-precipitated with Fe solids). However, because Al solids were predicted to form at pH values lower than when Fe solids were first predicted to form, Al was likely removed both as hydrobasaluminite (especially at low pH), amorphous $Al(OH)_3$, and/or as a co-precipitate into schwertmannite or ferrihydrite. It was unclear whether jurbanite (Al(OH)-$SO_4$) formed in our neutralization experiments, however, suppression of jurbanite substantially increased the accuracy of our reaction path modeling. In contrast to field sediments collected from Lower Red Eyes, Al concentrations were two to three orders of magnitude higher in the abiotic precipitates (Table 3).

Reaction path modeling for Zn, Ni and Co showed that these trace metals would not be removed from solution as their corresponding $Me(OH)_2(s)$ phases at the pH values that we observed for their removal. Therefore, adsorption to or co-precipitation in schwertmannite, ferrihydrite, and hydrobasaluminite were the predominant trace metal removal mechanisms in our experiments. This interpretation is supported by the results from the oxalate and HCl digestions, where the majority of trace metals were associated with poorly crystalline minerals (Table 3). Similar results have been reported by Lee et al. (2002) using AMD generated from the mining of massive sulfide ore deposits in eastern Tennessee. Using one fully oxidized, Fe-rich AMD sample (pH 2, 12 mM Fe, 21 mM $SO_4^{2-}$) that was similar to Lower Red Eyes CMD, they found that Fe was removed from solution at pH >3, Al was removed at pH >5, and Mn was removed at pH >8. The removal of Cd, Co, Cu, Pb and Zn occurred fairly sharply over different pH ranges for each metal but complete removal of all metals did not occur until pH >8. In the current study, we found that removal of Fe, Al, Co, Ni and Zn all occurred fairly sharply and somewhat simultaneously at pH >5 (Fig. 8). As noted above, removal of metal cations (except Fe) did not occur in the field be-

cause of limited sorption at pH <4 (Sidenko and Sherriff, 2005; Nagano et al., 2011).

Biological low-pH Fe(II) oxidation could be a very useful pre-treatment step in the remediation of AMD. Fe and acidity loads could be decreased before conventional active or passive treatment processes, thereby decreasing the size and cost of these units. Removal of any iron and acidity before passive treatment limestone beds will improve performance by decreasing limestone armoring, decreasing hydraulic clogging by Fe precipitates, and decreasing the acidity load. Removal of any iron and acidity before active treatment via neutralization will reduce costs by decreasing alkali chemical requirements and decreasing Fe sludge production. Furthermore, in portions of the Appalachian coal mining region where As or other anionic contaminants such as Se are present at only exceptional low concentrations, the Fe(III) precipitates should be essentially free of trace metal and metalloid contaminants. The mineral composition of iron mounds produced by low-pH Fe(II) oxidation of Appalachian CMD appeared to be similar at all of the field sites we studied both spatially across any one site and comparatively between any two sites. Based on metal oxide contents measured after lithium metaborate fusion (Electronic Annex, Table EA-1), $Fe_2O_3$ contents of 50–67% approached values of Fe ore bodies (Hedin, 2003). Because of their high Fe content, mineralogical purity and absence of trace contaminants, these iron mound sediments could prove to be of considerable economic value (Janneck et al., 2010).

Iron mounds and low-pH Fe(II) oxidation are often underappreciated by watershed professionals responsible for designing AMD remediation systems. In many cases significant amounts of Fe and associated acidity are naturally and passively removed by these mounds. Assuming that we can better understand the biogeochemistry of this process, we should be able to exploit and engineer it for even greater treatment. Water discharged from these mounds would still have to be neutralized to remove acidity and trace metals but the iron and acidity loads going into downstream systems could be dramatically reduced. If the iron mound sediments were periodically collected and sold for some industrial purpose (e.g., anion adsorbents, pigments, ceramics) then any profit could be invested back into additional AMD treatment systems. Future research will hopefully develop the economic and environmental sustainability of these efforts.

## ACKNOWLEDGMENTS

This work was supported by the National Science Foundation (NSF) under Grant No. CHE-0431328, by the Pennsylvania Department of Environmental Protection, Bureau of Abandoned Mine Reclamation, by the Office of Surface Mining under Cooperative Agreement S11AC20005, and by an NSF CAREER Award (EAR 0847683) to Thomas Borch. Janna Lambson was supported by NSF EAR 0525503 (REU Supplement) to Jenn L. Macalady. Portions of this research were carried out at the Stanford Synchrotron Radiation Lightsource (SSRL), a national user facility operated by Stanford University on behalf of the U.S. Department of Energy, Office of Basic Energy Sciences. We thank Brent Means from the US Office of Surface Mining, and Malcolm Crittenden from the Pennsylvania Department of Environmental Protection for directing us to the Lower Red Eyes site. We thank the associate editor and three anonymous reviewers for the helpful suggestions to improve this work.

## APPENDIX A. SUPPLEMENTARY DATA

Supplementary data associated with this article can be found, in the online version, at doi:10.1016/j.gca.2011.10.015.

## REFERENCES

Acero P., Ayora C., Torrentó C. and Nieto J.-M. (2006) The behavior of trace elements during schwertmannite precipitation and subsequent transformation into goethite and jarosite. *Geochim. Cosmochim. Acta* **70**, 4130–4139.

Bigham J. M., Schwertmann U., Carlson L. and Murad E. (1990) A poorly crystallized oxyhydroxysulfate of iron formed by bacterial oxidation of Fe(II) in acid mine waters. *Geochim. Cosmochim. Acta* **54**, 2743–2758.

Bigham J. M., Schwertmann U., Traina S. J., Winland R. L. and Wolf M. (1996) Schwertmannite and the chemical modeling of iron in acid sulfate waters. *Geochim. Cosmochim. Acta* **60**, 2111–2121.

Borch T., Masue Y., Kukkadapu R. K. and Fendorf S. (2006) Phosphate imposed limitations on biological reduction and alteration of ferrihydrite. *Environ. Sci. Technol.* **41**, 166–172.

Brown J. F., Jones D. S., Mills D. B., Macalady J. L. and Burgos W. D. (2010) Application of a depositional *facies* model to an acid mine drainage site. *Appl. Environ. Microbiol.*. AEM.01550–01510.

Burton E. D., Bush R. T., Sullivan L. A. and Mitchell D. R. G. (2008) Schwertmannite transformation to goethite via the Fe(II) pathway: reaction rates and implications for iron-sulfide formation. *Geochim. Cosmochim. Acta* **72**, 4551–4564.

Collins R. N., Jones A. M. and Waite T. D. (2010) Schwertmannite stability in acidified coastal environments. *Geochim. Cosmochim. Acta* **74**, 482–496.

Cravotta C. A. (2008) Dissolved metals and associated constituents in abandoned coal-mine discharges, Pennsylvania, USA. Part 1: constituent quantities and correlations. *Appl. Geochem.* **23**, 166–202.

DeSa T., Brown J. and Burgos W. (2010) Laboratory and field-scale evaluation of low-pH Fe(II) oxidation at Hughes Borehole, Portage, Pennsylvania. *Mine Water Environ.* **29**, 239–247.

Fouke B. W., Farmer J. D., Des Marais D. J., Pratt L., Sturchio N. C., Burns P. C. and Discipulo M. K. (2000) Depositional *facies* and aqueous-solid geochemistry of travertine-depositing hot springs (Angel Terrace, Mammoth Hot Springs, Yellowstone National Park, USA). *J. Sediment. Res.* **70**, 565–585.

Hansel C. M., Benner S. G., Neiss J., Dohnalkova A., Kukkadapu R. K. and Fendorf S. (2003) Secondary mineralization pathways induced by dissimilatory iron reduction of ferrihydrite under advective flow. *Geochim. Cosmochim. Acta* **67**, 2977–2992.

Hedin R. S., Watzlaf G. R. and Nairn R. W. (1994) Passive treatment of acid mine drainage with limestone. *J. Environ. Qual.* **23**, 1338–1345.

Hedin R. S. (2003) Recovery of marketable iron oxide from mine drainage in the USA. *Land Contam. Reclaminat.* **11**, 93–97.

Herlihy A., Kaufmann P., Mitch M. and Brown D. (1990) Regional estimates of acid mine drainage impact on streams

in the mid-atlantic and Southeastern United States. *Water Air Soil Pollut.* **50**, 91–107.

Jacquat O., Voegelin A. and Kretzschmar R. (2009) Soil properties controlling Zn speciation and fractionation in contaminated soils. *Geochim. Cosmochim. Acta* **73**, 5256–5272.

Janneck E., Arnold I., Koch T., Meyer J., Burghardt D. and Ehinger S. (2010) Microbial synthesis of schwertmannite from lignite mine water and its utilization for removal of arsenic from mine waters and for production of iron pigments. Mine Water and Innovative Thinking, Sydney, NS.

Johnson D. B., Okibe N. and Hallberg K. B. (2005) Differentiation and identification of iron-oxidizing acidophilic bacteria using cultivation techniques and amplified ribosomal DNA restriction enzyme analysis. *J. Microbiol. Methods* **60**, 299–313.

Johnston S. G., Keene A. F., Burton E. D., Bush R. T. and Sullivan L. A. (2011) Iron and arsenic cycling in intertidal surface sediments during wetland remediation. *Environ. Sci. Technol.* **45**, 2179–2185.

Jones A. M., Collins R. N., Rose J. and Waite T. D. (2009) The effect of silica and natural organic matter on the Fe(II)-catalysed transformation and reactivity of Fe(III) minerals. *Geochim. Cosmochim. Acta* **73**, 4409–4422.

Jones A. M., Collins R. N. and Waite T. D. (2011) Mineral species control of aluminum solubility in sulfate-rich acidic waters. *Geochim. Cosmochim. Acta* **75**, 965–977.

Jönsson J., Persson P., Sjöberg S. and Lövgren L. (2005) Schwertmannite precipitated from acid mine drainage: phase transformation, sulphate release and surface properties. *Appl. Geochem.* **20**, 179–191.

Jönsson J., Jönsson J. and Lövgren L. (2006) Precipitation of secondary Fe(III) minerals from acid mine drainage. *Appl. Geochem.* **21**, 437–445.

Kirby C. S. and Cravotta Iii C. A. (2005) Net alkalinity and net acidity 1: theoretical considerations. *Appl. Geochem.* **20**, 1920–1940.

Knorr K.-H. and Blodau C. (2007) Controls on schwertmannite transformation rates and products. *Appl. Geochem.* **22**, 2006–2015.

Kumpulainen S., Carlson L. and Räisänen M.-L. (2007) Seasonal variations of ochreous precipitates in mine effluents in Finland. *Appl. Geochem.* **22**, 760–777.

Kumpulainen S., Raisanen M.-L., Von Der Kammer F. and Hofmann T. (2008) Ageing of synthetic and natural schwertmannites at pH 2–8. *Clay Mineral.* **43**, 437–448.

Lane D. J., Harrison, Jr., A. P., Stahl D., Pace B., Giovannoni S. J., Olsen G. J. and Pace N. R. (1992) Evolutionary relationships among sulfur- and iron-oxidizing eubacteria. *J. Bacteriol.* **174**, 269–278.

Lee G., Bigham J. M. and Faure G. (2002) Removal of trace metals by coprecipitation with Fe, Al and Mn from natural waters contaminated with acid mine drainage in the Ducktown Mining District, Tennessee. *Appl. Geochem.* **17**, 569–581.

Lucas M. A. (2008) The comparison of two acid mine drainage sites in central Pennsylvania: field site characterizations and batch reactor experiments. M. S. Thesis, The Pennsylvania State Univ., University Park, PA, USA, pp. 172.

Moberly J., Borch T., Sani R., Spycher N., Şengör S., Ginn T. and Peyton B. (2009) Heavy metal–mineral associations in Coeur d'Alene river sediments: a synchrotron-based analysis. *Water Air Soil Pollut.* **201**, 195–208.

Murad E. and Rojik P. (2003) Iron-rich precipitates in a mine drainage environment: influence of pH on mineralogy. *Am. Mineral.* **88**, 1915–1918.

Nagano T., Yanase N., Hanzawa Y., Takada M., Mitamura H., Sato T. and Naganawa H. (2011) Evaluation of the affinity of some toxic elements to schwertmannite in natural streams contaminated with acid mine drainage. *Water Air Soil Pollut.* **216**, 153–166.

Paikaray S. and Peiffer S. (2010) Dissolution kinetics of sulfate from schwertmannite under variable pH conditions. *Mine Water Environ.* **29**, 263–269.

Pennsylvania Department of Environmental Protection (PA DEP). (2006) The Development of a Mine Drainage Restoration Plan for Bennett Branch, Sinnemahoning Creek: Clearfield, Elk, and Cameron Counties, Pennsylvania.

Peretyazhko T., Zachara J. M., Boily J. F., Xia Y., Gassman P. L., Arey B. W. and Burgos W. D. (2009) Mineralogical transformations controlling acid mine drainage chemistry. *Chem. Geol.* **262**, 169–178.

Pu X., Vazquez O., Monnell J. D. and Neufeld R. D. (2010) Speciation of aluminum precipitates from acid rock discharges in Central Pennsylvania. *Environ. Eng. Sci.* **27**, 169–180.

Regenspurg S., Brand A. and Peiffer S. (2004) Formation and stability of schwertmannite in acidic mining lakes. *Geochim. Cosmochim. Acta* **68**, 1185–1197.

Sánchez-España J., Yusta I. and Diez-Ercilla M. (2011) Schwertmannite and hydrobasaluminite: a re-evaluation of their solubility and control on the iron and aluminium concentration in acidic pit lakes. *Appl. Geochem.* **26**, 1752–1774.

Schwertmann U. and Thalmann H. (1976) The influence of [Fe(II)], [Si], and pH on the formation of lepidocrocite and ferrihydrite during oxidation of aqueous $FeCl_2$ solutions. *Clay Mineral.* **11**, 189–200.

Schwertmann U. and Carlson L. (2005) The pH-dependent transformation of schwertmannite to goethite at 25 °C. *Clay Mineral.* **40**, 63–66.

Sidenko N. V. and Sherriff B. L. (2005) The attenuation of Ni, Zn and Cu, by secondary Fe phases of different crystallinity from surface and ground water of two sulfide mine tailings in Manitoba, Canada. *Appl. Geochem.* **20**, 1180–1194.

Senko J. M., Wanjugi P., Lucas M., Bruns M. A. and Burgos W. D. (2008) Characterization of Fe(II) oxidizing bacterial activities and communities at two acidic Appalachian coalmine drainage-impacted sites. *ISME J.* **2**, 1134–1145.

Taylor R. M. and Schwertmann U. (1978) The influence of aluminum on iron oxides: Part 1. The influence of Al on Fe oxide formation from the Fe(II) system. *Clays Clay Miner.* **26**, 373–383.

United States Geological Survey (USGS). (2008) Coal mine drainage projects in Pennsylvania. US Geological Survey. <http://pa.water.usgs.gov/projects/energy/amd/> (accessed May 2, 2011).

Watzlaf G. R., Schroeder K. T., Kleinmann R. L. P., Kairies C. L. and Nairn R. W. (2002) *The Passive Treatment of Coal Mine Drainage*. American Society of Mining and Reclamation, Lexington, Kentucky.

Webb S. M. (2005) SIXpack: a graphical user interface for XAS analysis using IFEFFIT. *Phys. Scr.* **2005**, 1011.

Zhang G., Dong H., Kim J. and Eberl D. D. (2007) Microbial reduction of structural $Fe^{3+}$ in nontronite by a thermophilic bacterium and its role in promoting the smectite to illite reaction. *Am. Mineral.* **92**, 1411–1419.

*Associate editor:* Donald L. Sparks